



The use of 1050nm OCT to identify changes in optic nerve head pathophysiology in glaucoma

A thesis submitted to Cardiff University for the degree of
Doctor of Philosophy

Bethany Esther Frost

School of Optometry and Vision Sciences,
Cardiff University

September 2015

Acknowledgements

Firstly I would like to thank my supervisors, Dr Julie Albon and Prof Rachel North, for their constant help, support and guidance throughout this PhD.

Thank you to the College of Optometrists, for their financial support, without them this work would not have been possible. Additional thanks are given for the travel bursary that allowed me to present some of this work at ARVO.

Thank you to Dr Katie Mortlock, for her support and friendship throughout my time in Cardiff, and for help with this project.

Thank you to all the friends and office mates I've had during my PhD, particularly everyone in Room 2.11. It would have been a lot harder without you. Thank you to Sue, Judith and Leanne, for always being there when things weren't going quite right and for being calm with helpful advice.

Finally, Chris, thank you for being there.

Abstract

Glaucoma is a progressive optic neuropathy that causes irreversible vision loss and is the second leading cause of blindness worldwide. Glaucoma is characterised by loss of retinal ganglion cells (RGC) and the proposed site of primary damage is the lamina cribrosa (LC), where RGC axonal transport is disrupted causing subsequent RGC damage and eventual cell death. Current detection for primary open angle glaucoma (POAG) is based upon clinical measures such as intraocular pressure (IOP), visual field loss and changes to the optic nerve head (ONH). However, for there to be an indication that there is a problem using these measures, often RGC damage has already occurred. Therefore it is crucial to determine ocular parameters that alter in the earliest stage of disease, prior to vision loss occurring.

In this thesis optical coherence tomography (OCT) was used to assess the optic nerve heads and maculae of control eyes and eyes with preperimetric, early and advanced glaucoma in order to characterise changes that could potentially be used as biomarkers for the earliest stages of the disease. A custom built 1050 nm research OCT was used to acquire datasets from the macula and optic nerve heads of eyes glaucomatous and control eyes *in vivo*. Analysis of the inner retinal layers at the macula was performed to indirectly assess RGC integrity. At the ONH the prelamina and LC volume and regional depth and thicknesses were investigated. Additionally, nerve fibre layer and Bruch's membrane parameters were assessed. Finally, LC beam coherence and orientation were probed in order to determine whether regional or glaucomatous changes could be detected at the LC connective tissue microstructure.

Prelamina depth and thickness was shown to be an indicator of early and preperimetric glaucoma ($p < 0.01$), although the volume of the prelamina did not change with increasing stage of glaucoma ($p > 0.01$). Border nerve fibre layer revealed significant thinning in early glaucoma compared to control, and the superior peripapillary nerve fibre layer was thinner in preperimetric glaucoma than control. The ratio of inner plexiform layer (IPL) : ganglion cell layer (GCL) showed significant differences between control eyes and preperimetric glaucoma, and as such has potential to be a useful biomarker for indicating the earliest stages of disease. Both the GCL and IPL were thinner in early glaucoma than control ($p < 0.01$), a hypothesis that cell body shrinkage and death occurs in preperimetric glaucoma and dendritic loss occurs in early glaucoma, when vision loss is first apparent, is suggested. Additionally, LC beams showed greater coherence in the superior and inferior poles than the temporal region, indicating that the shows regional variation but that further research is required to characterise changes.

In conclusion, 1050 nm OCT was used to probe microstructural parameters of the optic nerve head *in vivo* to characterise changes that could be used as a potential biomarker for early glaucoma. ONH and retinal parameters have been identified that, with further research, may be used to differentiate between control eyes and those with preperimetric and early glaucoma. These have the potential to help identify those ONHs at risk of glaucoma damage.

Table of contents

Declaration	ii
Acknowledgements	iii
Abstract	ix
Table of contents	iv
List of figures	xvi
List of tables	xxiv
1 Introduction	2
<i>1.1 The structure of the optic nerve head</i>	2
1.1.1 Prelamina	3
1.1.2 Lamina cribrosa	4
1.1.3 Postlaminar Optic Nerve	6
<i>1.2 The structure of the retina</i>	7
<i>1.3 The aging optic nerve head</i>	8
1.3.1 Aging of the optic nerve	8
<i>1.4 Glaucoma</i>	9
1.4.1 The role of intraocular pressure in glaucoma	11
1.4.2 Visual field loss in glaucoma	11
1.4.3 Optic nerve head changes in glaucoma	12
1.4.3.1 Changes to the Lamina Cribrosa in Glaucoma	13
1.4.4 Damage to the retina in glaucoma	14
1.4.5 Theories of glaucoma	15
1.4.6 Mechanical theory of glaucomatous damage	16
1.4.7 Vascular insult and involvement in glaucomatous damage	18

1.4.8	Glaucoma detection in vivo.....	19
1.5	<i>Optical Coherence Tomography</i>	20
1.5.1	Theory of optical coherence tomography.....	20
1.5.2	Types of OCT Device	21
1.5.2.1	Time Domain OCT.....	22
1.5.2.2	Spectral Domain OCT	22
1.5.3	The wavelength of the OCT source and its effect on ocular imaging.....	23
1.5.4	Recent development to improve OCT imaging.....	24
1.6	<i>The use of OCT to assess and monitor the eye during glaucoma</i>	26
1.6.1	OCT to image the ONH	26
1.6.2	The use of OCT to measure macula parameters in glaucoma.....	27
1.7	<i>Hypothesis and aims of this study</i>	28
2	Methods	31
2.1	<i>Ethics</i>	31
2.2	<i>Participant recruitment</i>	31
2.3	<i>Data acquisition</i>	32
2.3.1	Clinical assessments	32
2.3.2	Optical Coherence Tomography	33
2.4	<i>Data processing</i>	34
2.4.1	Flow chart of stages of data and image processing	34
2.4.2	Spectral OCT data processing	35
2.4.3	Image processing	36
2.4.4	Image scaling and pixel calibration.....	39
2.4.4.1	Transverse pixel calibration	39
2.4.4.2	Transverse scaling according to axial length	41
2.4.4.3	Axial pixel calibration	41

2.4.5	Scaling according to calculated pixel values.....	42
2.4.6	Criteria for classification of optic nerve heads and maculae into stages of glaucoma..	42
2.4.7	Orientation of the OCT datasets.....	43
2.5	<i>Analysis of the inner retinal layers in glaucomatous and healthy eyes</i>	44
2.5.1	Manual image segmentation	44
2.5.2	Classification of eyes according to stage of glaucoma	45
2.5.3	Colour-coded thickness maps.....	45
2.5.4	Regional analysis of retinal layer thickness and volume.....	46
2.5.5	Repeatability of retinal segmentation technique	47
2.6	<i>Analysis of the optic nerve head in aging and glaucoma in 2D OCT images</i>	49
2.6.1	Repeatability of 2D optic nerve head measurement technique	54
2.7	<i>3D volumetric measurements of the optic nerve head in glaucomatous and healthy subject</i>	55
2.8	<i>Microstructural analysis of the lamina cribrosa in healthy and glaucoma eyes</i>	61
2.9	<i>Statistical analysis</i>	63
2.9.1	Model structure	64
2.9.2	Model optimisation	65
2.9.3	Model assumptions	66
2.9.4	Model interpretation	66
3	Analysis of the inner retinal layers in glaucomatous and healthy eyes	69
3.1	<i>Introduction</i>	69
3.2	<i>Aim of study</i>	70
3.3	<i>Experimental Design</i>	70
3.3.1	Participants	70
3.3.2	Clinical assessments	71
3.3.3	OCT data and image processing.....	71
3.3.4	Glaucoma classification	72

3.3.5	Generation of colour-coded thickness maps of inner retinal layers.....	72
3.3.6	Regional analysis of retinal layer thickness and volume.....	73
3.3.7	Statistical analysis	73
3.4	<i>Results</i>	74
3.4.1	Colour coded thickness maps of the inner retinal layers for control and glaucoma	74
3.4.2	Quantitative thickness and volume measurements of inner retinal layers.....	76
3.4.3	Comparative analysis of macula thickness and volume of regions at equal eccentricity from the fovea in each disease stage categories	76
3.4.4	Ganglion cell complex thickness and volume in control and different staged glaucoma macula	79
3.4.4.1	Comparative analysis of regional ganglion cell complex thickness	79
3.4.4.2	Inter-stage differences in ganglion cell complex volume	81
3.4.5	Inter stage differences in macula nerve fibre layer thickness and volume	81
3.4.5.1	Comparative analysis of regional macula nerve fibre layer thickness.....	81
3.4.5.2	Inter-stage differences in macula nerve fibre layer volume.....	83
3.4.6	Inter stage differences in ganglion cell layer thickness and volume	86
3.4.6.1	Comparative analysis of regional ganglion cell layer thickness	86
3.4.7	Inner plexiform layer thickness and volume in different glaucoma disease stages	89
3.4.7.1	Comparative analysis of regional inner plexiform layer thickness	89
3.4.7.2	Inter-stage differences in inner plexiform layer volume	91
3.4.8	Differences in the ratio of inner plexiform layer to macula nerve fibre layer in control and increased stages of glaucoma.....	91
3.4.9	Differences in the ratio of inner plexiform layer to ganglion cell layer in control and increased glaucoma stages.....	94
3.4.10	Summary of results.....	96
3.5	<i>Discussion</i>	96
3.5.1	Limitations of study	103
3.5.2	Conclusion.....	104

4	Analysis of age related changes in <i>in vivo</i> human optic nerve head microstructure.	106
4.1	Introduction.....	106
4.1.1	Aims of the study.....	107
4.2	Experimental design.....	108
4.2.1	Participants	108
4.2.2	Clinical assessments	108
4.2.3	Optical coherence tomography	108
4.2.4	2D Image analysis of optic nerve head microstructure	109
4.2.5	Statistical analysis	109
4.3	Results.....	110
4.3.1	The effect of age and other ocular parameters on Bruch’s membrane opening diameter.....	110
4.3.1.1	Quantification of Bruch’s membrane opening diameter.....	111
4.3.1.2	Multivariate analysis of Bruch’s membrane opening diameter	112
4.3.1.3	The effect of age on Bruch’s membrane opening diameter	113
4.3.1.4	Other factors that contribute to explain membrane opening diameter	113
4.3.2	The effect of age and other ocular parameters on the peripapillary and border nerve fibre layer thickness	115
4.3.2.1	Quantification of nerve fibre layer parameters.....	115
4.3.2.2	Univariate analysis of nerve fibre layer parameters	116
4.3.2.3	Multivariate analysis of nerve fibre layer parameters.....	116
4.3.2.4	The effect of age on nerve fibre layer parameters	116
4.3.2.5	The effect of other ocular parameters on the nerve fibre layer	120
4.3.3	The effect of age and other ocular parameters on the prelamina.....	121
4.3.3.1	Quantification of prelamina parameters	122
4.3.3.2	Univariate analysis of prelamina measurements	123
4.3.3.3	Multivariate analysis of prelamina measurements	125

4.3.3.4	The effect of age on prelamina parameters	125
4.3.3.5	The effect of other ocular parameters on the prelamina	128
4.3.4	The effect of age and other ocular parameters on the lamina cribrosa	129
4.3.4.1	Quantification of lamina cribrosa parameters.....	130
4.3.4.2	Univariate analysis of lamina cribrosa parameters	131
4.3.4.3	Multivariate analysis of lamina cribrosa parameters.....	133
4.3.4.4	The effect of age on lamina cribrosa parameters	137
4.3.4.5	The effect of other ocular parameters on the lamina cribrosa.....	138
4.3.5	Summary of results	139
4.4	<i>Discussion</i>	140
4.4.1	The effect of age on Bruch’s membrane opening diameter.....	142
4.4.2	The effect of age on the nerve fibre layer thickness	143
4.4.3	The effect of age and ocular parameters on the prelamina.....	144
4.4.4	The effect of age on the lamina cribrosa	147
4.4.5	Axial length.....	150
4.4.6	Limitations of the study	150
4.4.7	Conclusion.....	151
5	2D optic nerve head parameters as a function of glaucoma.....	153
5.1	<i>Introduction</i>	153
5.1.1	Aims of chapter.....	154
5.2	<i>Experimental design</i>	154
5.2.1	Subjects	154
5.2.2	Clinical assessments	155
5.2.3	2D Image analysis of optic nerve head microstructure	155
5.2.4	Statistical analysis	156
5.3	<i>Results</i>	157

5.3.1	BMO diameter as a of glaucoma disease stage.....	157
5.3.1.1	Changes in Bruch’s membrane opening diameter as a function of visual field progression.....	158
5.3.1.2	Quantitative analysis of Bruch’s membrane opening diameter for different glaucoma disease stage.....	159
5.3.1.3	Multivariate analysis of Bruch’s membrane opening diameter for different glaucoma disease stage.....	159
5.3.1.4	The effect of glaucoma on Bruch’s membrane opening diameter	162
5.3.2	Changes in peripapillary and border nerve fibre layer thickness as a function of glaucoma.....	162
5.3.2.1	Changes in nerve fibre layer thickness as a function of visual field loss.....	163
5.3.2.2	Quantitative analysis of nerve fibre layer parameters for stages of glaucoma.....	163
5.3.2.3	Multivariate analysis of nerve fibre layer parameters in glaucomatous eyes	164
5.3.2.4	The effect of stage of glaucoma on peripapillary and border nerve fibre layer thickness..	166
5.3.3	The effect of glaucoma and other ocular parameters on the prelamina.....	172
5.3.3.1	Changes in prelamina parameters as a function of visual field progression	172
5.3.3.2	Quantitative analysis of prelamina parameters as a function of glaucoma stage.....	173
5.3.3.3	Multivariate analysis of prelamina parameters in glaucomatous eyes	173
5.3.3.4	The effect of stage of glaucoma on prelamina depth	178
5.3.4	The effect of glaucoma and other ocular parameters on the lamina cribrosa.....	182
5.3.4.1	Changes in lamina cribrosa parameters as a function of visual field progression	183
5.3.4.2	Quantitative analysis of lamina cribrosa for stages of glaucomatous progression.....	185
5.3.4.3	Multivariate analysis of lamina cribrosa parameters in glaucomatous eyes.....	186
5.3.4.4	The effect of stage of glaucoma on the lamina cribrosa	191
5.3.4.5	The effect of stage of glaucoma on lamina cribrosa thickness	193
5.3.5	Summary of results	196
5.4	<i>Discussion</i>	198
5.4.1	The effect of glaucoma and other ocular parameters on Bruch’s membrane opening diameter.....	198

5.4.2	The effect of glaucoma and other ocular parameters on the peripapillary and border nerve fibre layer	199
5.4.3	The effect of glaucoma and other ocular parameters on the prelamina.....	203
5.4.4	The effect of glaucoma and other ocular parameters on the lamina cribrosa.....	207
5.4.5	Limitations of study	213
5.4.6	Conclusion.....	215
6	3D volumetric measurements of the optic nerve head in glaucomatous and healthy subjects	217
6.1	<i>Introduction</i>	217
6.1.1	Aims of study	218
6.2	<i>Experimental design</i>	218
6.2.1	Participants	218
6.2.2	Clinical assessments	219
6.2.3	Optical coherence tomography	219
6.2.4	3D image analysis of optic nerve head structure.....	219
6.2.5	Statistical analysis	221
6.3	<i>Results</i>	221
6.3.1	Changes in Bruch’s membrane opening area as a function of glaucoma disease stage.....	221
6.3.2	Changes in the volume of the optic cup as a function of glaucoma disease stage	222
6.3.3	Changes in the volume of the prelamina below Bruch’s membrane as a function of glaucoma disease stage	223
6.3.4	Changes in the volume of the lamina cribrosa as a function of glaucoma disease stage.....	224
6.3.5	Summary of key findings	225
6.4	<i>Discussion</i>	225

6.4.1	Limitations of study	226
6.4.2	Conclusion.....	227
7	Microstructural analysis of the lamina cribrosa in healthy and glaucomatous eyes	229
7.1	<i>Introduction</i>	229
7.1.1	Aims of study	230
7.2	<i>Experimental design</i>	230
7.2.1	Participant demographics	230
7.2.2	Clinical assessments	231
7.2.3	Optical coherence tomography datasets and image processing	231
7.2.4	Statistical analysis	233
7.3	<i>Results</i>	234
7.3.1	Visualisation of lamina cribrosa (LC) beam orientation and coherence in control and glaucoma.....	234
7.3.2	Regional differences within the lamina cribrosa beam orientation in control and glaucoma.....	237
7.3.3	Regional differences within the lamina cribrosa beam coherence	237
7.3.4	Differences within lamina cribrosa beam orientation at increasing depth.....	239
7.3.5	Differences in lamina cribrosa beam coherence with increasing depth in the optic nerve head in control and glaucoma.....	240
7.3.6	Differences in lamina cribrosa beam orientation at different stages of glaucoma.....	242
7.3.7	Differences in lamina cribrosa beam coherence between control and each stage of glaucoma.....	243
7.3.8	Summary of significant results.....	243
7.4	<i>Discussion</i>	244
7.4.1	Limitations of study	246

8 Discussion	250
8.1 Conclusion.....	261
8.2 Future work.....	262
9 Bibliography.....	265
Appendix 1: Examples of participant consent form and information	287
<i>Example consent form for participants in the study.....</i>	<i>287</i>
<i>Example participant information sheet.....</i>	<i>288</i>
Appendix II: Regional thickness and volume of the inner retinal layers	293
<i>Regional volume of inner retinal layers for control and each stage of glaucoma</i>	<i>293</i>
<i>Regional thickness of inner retinal layers for control and each stage of glaucoma</i>	<i>294</i>
<i>Regional inner plexiform layer : macula nerve fibre layer and inner plexiform layer : ganglion cell layer ratios</i>	<i>295</i>
Appendix III: Regional differences in the inner retinal layers in glaucoma	296
<i>Differences in thickness of the ganglion cell complex between control and glaucoma</i>	<i>296</i>
<i>Differences in volume of the ganglion cell complex between control and glaucoma</i>	<i>297</i>
<i>Differences in thickness of the macula nerve fibre layer between control and glaucoma</i>	<i>298</i>
<i>Differences in thickness of the ganglion cell layer between control and glaucoma.....</i>	<i>299</i>
<i>Differences in volume of the ganglion cell layer between control and glaucoma.....</i>	<i>300</i>
<i>Differences in thickness of the inner plexiform layer between control and glaucoma</i>	<i>301</i>
<i>Differences in volume of the inner plexiform layer between control and glaucoma</i>	<i>302</i>
<i>Differences in inner plexiform layer : ganglion cell layer ratio between control and glaucoma</i>	<i>303</i>

Differences in volume of the macula nerve fibre layer between control and glaucoma 304

*Differences in inner plexiform layer : macula nerve fibre layer ratio between control and
glaucoma 304*

Appendix IV: Published abstracts and conferences 305

Oral presentations 305

Poster presentations 305

List of figures

1 Introduction

Figure 1.1: Schematic diagram of the human optic nerve head, where pink indicates astrocytes and blue indicates connective tissue.	4
Figure 1.2: Overview of the structure of the human retina	8
Figure 1.3: Features of healthy and glaucomatous optic nerve heads.....	13
Figure 1.4: Schematic diagram describing the mechanisms by which optic nerve head biomechanics may result in retinal ganglion cell death in glaucoma.	17
Figure 1.5: The effects of scleral biomechanics on the ONH.....	18
Figure 1.6: Schematic diagram of a generic optical coherence tomography (OCT) device.....	21
Figure 1.7: OCT image of the macula acquired using conventional technique and enhanced depth imaging with a Spectralis OCT.....	25

2 Methods

Figure 2.1: Flow chart showing data processing stages prior to measurements.	35
Figure 2.2: (a) Histograms of pixel intensities were normally distributed initially. (b) The lower limit was set to the centre of the histogram and upper limit to the edge of the curve then (c) the pixels were automatically redistributed over this range.	36
Figure 2.3: OCT images of the macula and optic nerve head before and after brightness and contrast adjustment.....	37
Figure 2.4: Macula and optic nerve head images before and after filtering to improve visibility of retinal and ONH structures.....	39
Figure 2.5: Schematic diagram of eye showing the measurements required to calculate the transverse pixel scaling.....	40

Figure 2.6: Processed OCT images of the macula and optic nerve head prior to and afterscaling using the modified Littmann equation.....	42
Figure 2.7: The correct orientation of the images was ensured by comparing a maximum intensity projection of the OCT dataset to the corresponding fundus photograph and flipping or rotating the OCT dataset as required.	43
Figure 2.8: Macula OCT b-scan with segmentation of the macular nerve fibre layer (mNFL), ganglion cell layer (GCL) and inner plexiform layer (IPL).....	45
Figure 2.9: Bland-Altman plots to assess agreement between repeated measures of the mean thickness for ganglion cell complex (GCC), macular nerve fibre layer (mNFL), ganglion cell layer (GCL) and inner plexiform layer (IPL).....	47
Figure 2.10: Retinal thickness maps were divided into 13 regions centred on the fovea.....	48
Figure 2.11: 3D OCT image stacks were averaged using maximum intensity projections (MIP) of the optic nerve head (ONH)	50
Figure 2.12: (a) A 45° radial reslice starting at the temporal side of the disc was used to create four radial B-scans in the (b) temporal-nasal, (c) superior temporal-inferior nasal, (d) superior-inferior, and (e) superior nasal-inferior temporal planes.....	51
Figure 2.13: (a) Schematic diagram and (b) fundus photograph of a left optic nerve	51
Figure 2.14: (a) Bruch's membrane opening (BMO) diameter in red. The distance from BMO to (b) the prelamina depth, (c) anterior lamina cribrosa (LC) depth and (d) posterior LC depth was measured	53
Figure 2.15: Schematic diagram of prelamina measurements above and below BMO	54
Figure 2.16: Bland-Altman plots to assess agreement between repeated measures for Bruch's membrane opening (BMO) in the temporal-nasal plane, and prelamina depth (PreL), anterior lamina cribrosa depth (AnL) and posterior lamina cribrosa depth (PostL) in the central region.....	55
Figure 2.17: (a) An <i>enface</i> view of the optic nerve head (ONH) in the left eye of a myopic 65 year old male with glaucoma.....	57

Figure 2.18: The volume of the optic cup (C) was subtracted from the volume of the area between the anterior LC surface and BMO..... 58

Figure 2.19: (a) An oblique radial slice of the ONH in the left eye of a myopic 65 year old male with glaucoma.....59

Figure 2.20: (a) An oblique radial slice of the ONH in the left eye of a myopic 65 year old male with glaucoma..... 60

Figure 2.21: (a) Schematic diagram of division of optic nerve head (ONH) regions of a left eye, with nasal side of the ONH greyed out as the measurements were discarded due to vascular shadowing. (b) Fundus photo of optic nerve head with (c) grid overlay showing regional division. 62

3 Analysis of the inner retinal layers in glaucomatous and healthy eyes

Figure 3.1: (a) Retinal thickness maps subdivisions: 13 regions centred on the fovea. R..... 75

Figure 3.2: Colour-coded thickness maps of ganglion cell complex (GCC), macula nerve fibre layer (mNFL), ganglion cell layer (GCL) and inner plexiform layer (IPL), with the visual field plot (VF) for eyes at different of glaucoma..... 76

Figure 3.3: Differences in macula nerve fibre layer (mNFL) and ganglion cell layer (GCL) thickness (thick) and volume (vol) at regions of equal eccentricity from the fovea. 77

Figure 3.4: Differences in advanced glaucoma maculae ganglion cell layer (GCL), inner plexiform layer (IPL) and macular nerve fibre layer (mNFL) thickness (thick) and volume (vol) at corresponding hemizones and inner-hemizones..... 78

Figure 3.5: Differences in macular nerve fibre layer (mNFL) and ganglion cell layer (GCL) volume (vol) at corresponding quadrants and inner-quadrants. 79

Figure 3.6: Regional ganglion cell complex (GCC) thickness for each control and each stage of glaucoma progression, and inter-stage regional and total area differences..... 80

Figure 3.7: Regional ganglion cell complex (GCC) volume for each control and each stage of glaucoma progression, and inter-stage regional and total area differences 82

Figure 3.8: Regional macula nerve fibre layer (mNFL) thickness for each control and each stage of glaucoma progression, and inter-stage regional and total area differences.....84

Figure 3.9: Regional macula nerve fibre layer (mNFL) volume for each control and each stage of glaucoma progression, and inter-stage regional and total area differences.....85

Figure 3.10: Regional ganglion cell layer (GCL) thickness for each control and each stage of glaucoma progression, and inter-stage regional and total area differences.87

Figure 3.11: Regional ganglion cell layer (GCL) volume for each control and each stage of glaucoma progression, and inter-stage regional and total area differences.88

Figure 3.12: Regional inner plexiform layer (IPL) thickness for each control and each stage of glaucoma progression, and inter-stage regional and total area differences.....90

Figure 3.13: Regional inner plexiform layer (IPL) volume for each control and each stage of glaucoma progression, and inter-stage regional and total area differences..92

Figure 3.14: Regional inner plexiform layer : macula nerve fibre layer (IPL:mNFL) ratio for each control and each stage of glaucoma progression, and inter-stage regional and total area differences93

Figure 3.15: Regional inner plexiform layer : ganglion cell layer (IPL:GCL) ratio for each control and each stage of glaucoma progression, and inter-stage regional and total area differences.95

Figure 3.16: Changes in the ganglion cell layer (GCL) and inner plexiform layer (IPL) were identified between control and increasing stages of glaucoma.102

Figure 3.17: Comparison of (a) ETDRS grid and (b) the grid used to divide the macula into 13 regions in the present study.104

4 Analysis of age related changes in *in vivo* human optic nerve head microstructure

Figure 4.1: Schematic diagram of Bruch's membrane opening (BMO) diameter across the optic disc, and demonstrated on example images from old and young ONH datasets.111

Figure 4.2: Bruch’s membrane opening (BMO) diameter for each region of the optic nerve head, and horizontal:vertical BMO diameter, plotted against age.	112
Figure 4.3: Schematic diagram of peripapillary nerve fibre layer (pNFL)	115
Figure 4.4: Regions of peripapillary nerve fibre layer (pNFL) and border nerve fibre layer (bNFL) that were affected by age, using general linear models.	116
Figure 4.5: Peripapillary nerve fibre layer (pNFL) and border nerve fibre layer (bNFL) thickness as a function of age.	117
Figure 4.6: Schematic diagram of prelamina depth and prelamina thickness, shown in red, and example images from old and young optic nerve heads	122
Figure 4.7: Prelamina depth and prelamina thickness plotted against age, for each region of the optic nerve head.	124
Figure 4.8: Optic nerve head regions where prelamina depth	125
Figure 4.9: Mean deviation (MD) in visual field, plotted against age, and mean spherical refraction plotted against axial length.....	129
Figure 4.10: Schematic diagram of measurements of (a) anterior lamina cribrosa (LC) depth, (b) posterior LC depth, and (c) LC thickness.....	130
Figure 4.11: Anterior and posterior lamina cribrosa (LC) depth as a function of age for each region of the optic nerve head.....	132
Figure 4.12: Lamina cribrosa (LC) thickness as a function of age for each region of the optic nerve head.	133
Figure 4.13: Regions of the anterior lamina cribrosa depth (Ant LC), posterior lamina cribrosa depth (Post LC), and lamina cribrosa thickness (LC thick) that were affected as a function of age, using general linear models (GLM).....	137
Figure 4.14: Regions of the optic nerve head that were affected as a function of age, using general linear models (GLM).....	141

5. 2D optic nerve head parameters as a function of glaucoma

Figure 5.1: Diagram of the Bruch's membrane opening (BMO) diameter across the optic disc on a schematic and OCT images from each stage of glaucoma	158
Figure 5.3: The association between mean spherical refractive error and axial length.	160
Figure 5.4: a) Regional Bruch's membrane opening (BMO) diameter and b) Horizontal:vertical BMO diameter ratio for each stage of glaucoma (G).....	162
Figure 5.5: Diagram of measurements of peripapillary nerve fibre layer (pNFL), measured at a distance 1.7mm from the centre of the optic disc, and border NFL (bNFL), measured above Bruch's membrane opening (BMO), on a schematic and OCT images from each stage of glaucoma..	163
Figure 5.6: Peripapillary nerve fibre layer (pNFL) and border nerve fibre layer (bNFL) thickness as a function of visual field loss for each region.	165
Figure 5.7: a) Peripapillary nerve fibre layer and b) Border NFL thickness for each glaucoma (G) stage	169
Figure 5.8: Regional changes in peripapillary nerve fibre layer (pNFL) and border nerve fibre layer (bNFL) as a function of glaucoma (G) stage detected using linear mixed-effects models and subsequent posthoc analysis (Tukey).	171
Figure 5.9: Diagram of measurements of (a) prelamina depth and (b) thickness on a schematic and OCT images from each stage of glaucoma, on a superior-inferior slice.	172
Figure 5.10: a) Prelamina (PreL) depth and b) PreL thickness as a function of visual field loss for each region. x-axis is reversed so greater visual field loss is further along the x-axis.	174
Figure 5.11: Mean prelamina depth and thickness for each glaucoma (G) stage.	179
Figure 5.12: Regions of the optic nerve head where prelamina depth was affected by stage of glaucoma, using linear mixed-effects models and subsequent pairwise comparisons.....	181
Figure 5.13: Diagram of measurements of (a) anterior and (b) posterior lamina cribrosa (LC) depth on a schematic and OCT images from each stage of glaucoma.....	182

Figure 5.14: Diagram of measurements of lamina cribrosa (LC) thickness on a schematic and OCT images from each stage of glaucoma,183

Figure 5.15: Anterior and posterior lamina cribrosa (LC) depth as a function of visual field loss for each region.....184

Figure 5.16: Lamina cribrosa (LC) thickness as a function of visual field loss for each region.185

Figure 5.17: Regional anterior and posterior lamina cribrosa (LC) depth for each glaucoma (G) stage192

Figure 5.18: Regions of the optic nerve head where posterior lamina cribrosa depth was affected by stage of glaucoma, using linear mixed-effects models and subsequent pairwise comparisons.....194

Figure 5.19: Lamina cribrosa (LC) thickness for each region of the ONH for glaucoma (G) stage, and regions of the LC that were affected by glaucoma using linear mixed effects models (LMM).195

Figure 5.20: Regions of the optic nerve head that were affected by *stage of glaucoma*, using linear mixed-effects models (LMM).....197

Figure 5.21: Comparison of minimum rim width (MRW, shown in green) and peripapillary nerve fibre layer (pNFL) and border nerve fibre layer (bNFL) measurements demonstrated in red dashed lines, both in relation to Bruch’s membrane opening202

Figure 5.22: (a) Schematic diagram and (b) fundus photograph of a left optic nerve, with a grid superimposed demonstrating the location of prelamina and lamina cribrosa measurements (blue), border nerve fibre layer (bNFL, cyan) and peripapillary nerve fibre layer (pNFL, green).207

Figure 5.23: Schematic diagram of how deformation of the sclera and lamina cribrosa (LC), may be related.....209

6. 3D volumetric measurements of the optic nerve head in glaucomatous and healthy subjects

Figure 6.1: (a) An oblique radial slice of the ONH in the left eye of a myopic 65 year old male with glaucoma.....220

Figure 6.2: Bruch’s membrane opening (BMO) area for each stage of glaucoma. 222

Figure 6.3: Cup volume for each stage of glaucoma..... 223

Figure 6.4: Prelamina volume for each stage of glaucoma..... 224

Figure 6.5: Lamina cribrosa (LC) volume for each stage of glaucoma. 224

7. Microstructural analysis of the lamina cribrosa in healthy and glaucomatous eyes

Figure 7.1: Schematic diagram of division of optic nerve head (ONH) regions of a left eye, with nasal side of the ONH in greyscale as the measurements were discarded due to vascular shadowing 232

Figure 7.2: Colour code used to represent dominant orientation of LC beams in the OCT datasets. 232

Figure 7.3: Examples of colour coded maps of lamina cribrosa (LC) beam orientation and coherence with increasing depth into the LC for control, early glaucoma and advanced glaucoma 235

Figure 7.4: Summary of differences in regional lamina cribrosa (LC) beam coherence in the optic nerve head (ONH). 239

Figure 7.5: Regional lamina cribrosa (LC) beam orientation and change in orientation for each stage of glaucoma with increasing depth into the LC. 240

Figure 7.6: Regional lamina cribrosa (LC) beam coherence and change in coherence for each stage of glaucoma with increasing depth into the LC. 241

Figure 7.7: Regional differences in lamina cribrosa (LC) beam coherence with increasing depth in the optic nerve head were observed in eyes with advanced glaucoma..... 241

Figure 7.8: Regional lamina cribrosa (LC) beam orientation and difference in orientation for each stage of glaucoma, with outliers represented by black spots. 243

8. Discussion

Figure 8.1: Regions of the optic nerve head that were affected as a function of age, using general linear models (GLM)..... 254

Figure 8.2: Difference between control and preperimetric glaucoma (PG) and early glaucoma (EG) using linear mixed-effects models (LMM).257

Figure 8.3: Schematic diagram of how deformation of the sclera and lamina cribrosa (LC), may be related. For a compliant sclera, and increase in IOP induces scleral deformation which increases the size of the scleral canal and pulls the LC taut, resulting in a decrease in LC depth..... 258

Figure 8.4: Schematic diagram of possible scleral canal expansion in glaucoma. Pink indicate the measured volume of the prelamina in (a) control and (b) glaucoma eyes.....260

Figure 8.5: Summary of differences in regional lamina cribrosa (LC) beam coherence in the optic nerve head (ONH) 261

Appendix II

Figure 0.1:Regional volume of inner retinal layers for each stage of glaucoma.293

Figure 0.2: Regional mean thickness of inner retinal layers for each stage of glaucoma. 294

Figure 0.3: Regional ratio of inner plexiform layer (IPL) : macula nerve fibre layer (mNFL) and IPL : ganglion cell layer (GCL) for each stage of glaucoma.. 295

Appendix III

Figure 0.1: Differences in ganglion cell complex (GCC) thickness between control (C) and preperimetric glaucoma (PG), early glaucoma (EG) and advanced glaucoma (AG) 296

Figure 0.2: Differences in ganglion cell complex (GCC) volume between control (C) and preperimetric glaucoma (PG), early glaucoma (EG) and advanced glaucoma (AG). 297

Figure 0.3: Differences in macula nerve fibre layer (mNFL) thickness between control (C) and preperimetric glaucoma (PG), early glaucoma (EG) and advanced glaucoma (AG). 298

Figure 0.4: Differences in ganglion cell layer (GCL) thickness between control (C) and preperimetric glaucoma (PG), early glaucoma (EG) and advanced glaucoma (AG). 299

Figure 0.5: Differences in ganglion cell layer (GCL) volume between control (C) and preperimetric glaucoma (PG), early glaucoma (EG) and m advanced glaucoma (AG).300

Figure 0.6: Differences in inner plexiform layer (IPL) thickness between control (C) and preperimetric glaucoma (PG), early glaucoma (EG) and advanced glaucoma (AG).301

Figure 0.7: Differences in inner plexiform layer (IPL) volume between control (C) and preperimetric glaucoma (PG), early glaucoma (EG) and advanced glaucoma (AG).302

Figure 0.8: Differences in inner plexiform layer : ganglion cell layer (IPL:GCL) ratio between control (C) and preperimetric glaucoma (PG), early glaucoma (EG) and advanced glaucoma (AG).....303

List of tables

2 Methods

Table 2.1: Inclusion criteria for study participants.	33
Table 2.2: Classification of glaucoma staging,	43
Table 2.3: Lamina cribrosa slice number and corresponding depth into LC.....	61

3 Analysis of the inner retinal layers in glaucomatous and healthy eyes

Table 3.1: Demographics for control and glaucomatous subjects.	96
---	----

4 Analysis of age related changes in *in vivo* human optic nerve head microstructure

Table 4.1: Participant demographics.	108
Table 4.2: Mean of each Bruch's membrane opening (BMO) diameter for each ONH region.....	111
Table 4.3: General linear models for Bruch's membrane opening (BMO) diameter for each direction within the optic nerve head.....	114
Table 4.4: Mean of each nerve fibre layer parameter	115
Table 4.5: General linear models for peripapillary nerve fibre layer (pNFL) thickness	118
Table 4.6: General linear models for border nerve fibre layer (bnFL) thickness,.....	119
Table 4.7: Mean of each regional optic nerve head parameter.	123
Table 4.8: General linear models for prelamina (PreL) depth for each optic nerve head region.....	126
Table 4.9: General linear models for prelamina (PreL) thicknes	127
Table 4.10: Mean of each regional optic nerve head parameter.	131
Table 4.11: General linear models for anterior lamina cribrosa depth (Ant LC)	134
Table 4.12: General linear models for posterior lamina cribrosa depth (Post LC)	135
Table 4.13: General linear models for lamina cribrosa thickness (LC thick),.....	136

Table 4.14: Independent variables included in the optimised general linear model to explain variance in Bruch’s membrane opening diameter	143
Table 4.15: Independent variables included in the optimised general linear model to explain variance in nerve fibre layer parameters.	144
Table 4.16: Independent variables included in the optimised general linear model to explain variance in prelamina parameters.	147
Table 4.17: Independent variables included in the optimised general linear model to explain variance in regional lamina cribrosa parameters.	149

5. 2D optic nerve head parameters as a function of glaucoma

Table 5.1: Participant demographics for those eyes included in the study.....	154
Table 5.2: Mean of each regional Bruch’s membrane opening (BMO) diameter for each stage of glaucoma.....	159
Table 5.3: Linear mixed-effects model for Bruch’s membrane opening (BMO) diameter for each direction within the optic nerve head.	161
Table 5.4: Mean of each regional nerve fibre layer (NFL) parameter for each stage of glaucoma....	164
Table 5.5: Linear mixed-effects models for peripapillary nerve fibre layer (pNFL) thickness	168
Table 5.7: Mean of each regional prelamina parameter for each stage of glaucoma.....	173
Table 5.8: Linear mixed-effects model (LMM) for prelamina depth (PreL depth) for each optic nerve head region.	175
Table 5.9: Linear mixed-effects model (LMM) for prelamina thickness (PreL thick).....	176
Table 5.10: Mean of each lamina cribrosa (LC) parameter for each stage of glaucoma.....	186
Table 5.11: Linear mixed-effects models for anterior LC (Ant LC) depth	187
Table 5.12: Linear mixed-effects models for posterior LC (Post LC) depth	188
Table 5.13: Linear mixed-effects models for lamina cribrosa thickness (LC thick).....	189

Table 5.14: Independent variables included in the linear mixed-effects model to explain variance in regional Bruch’s membrane opening (BMO) parameters.	199
Table 5.15: Independent variables included in the linear mixed-effects model to explain variance in regional peripapillary nerve fibre layer (pNFL) and border nerve fibre layer (bNFL) parameters.	201
Table 5.16: Independent variables included in the linear mixed-effects model to explain variance in regional prelamina (PreL) depth and thickness parameters.	205
Table 5.17: Independent variables included in the linear mixed-effects model to explain variance in regional lamina cribrosa (LC) parameters.....	213

6. 3D volumetric measurements of the optic nerve head in glaucomatous and healthy subjects

Table 6.1: Demographics for the eyes included in the present study	218
Table 6.2:Quantification of optic nerve head parameters in 3D	221

7. Microstructural analysis of the lamina cribrosa in healthy and glaucomatous eyes

Table 7.1: Demographics for the eyes included in the present study.	231
Table 7.2: Dominant lamina cribrosa (LC) beam orientation for each optic nerve head (ONH) region at each depth in the ONH	236
Table 7.3: Lamina cribrosa (LC) beam coherence for each optic nerve head (ONH) region at each depth in the ONH	237

Abbreviations

A	angle of scan
ACD	anterior chamber depth
AG	advanced glaucoma
Ant LC	anterior LC depth
APON	acquired pit of the optic nerve
AxL	axial length
BM	Bruch's membrane
BMO	Bruch's membrane opening
bNFL	border nerve fibre layer
C	control
CCT	central corneal thickness
CD	cup-to-disc (ratio)
CRA	central retinal artery
CRV	central retinal vein
D	dioptries
dB	decibels
EDI	enhanced depth imaging
EG	early glaucoma
ETDRS	Early Treatment Diabetic Retinopathy Study
FD-OCT	Fourier domain optical coherence tomography
G	glaucoma
GCC	ganglion cell complex
GCL	ganglion cell layer
GLM	general linear model

GLMM	generalised linear mixed-effects model
HRT	Heidelberg Retinal Tomography
H : V	horizontal : vertical ratio
INL	inner nuclear layer
I	inferior
IN	inferior-nasal
IOP	intraocular pressure
IPL	inner plexiform layer
IPL : GCL	ratio of inner plexiform layer to ganglion cell layer
IPL : mNFL	ratio of inner plexiform layer to macula nerve fibre layer
IT	inferior-temporal
LC	lamina cribrosa
LGN	lateral geniculate nucleus
LMM	linear mixed-effects model
LUT	look up table
MD	mean deviation on visual fields
MG	moderate glaucoma
MIP	maximum intensity projection
mm	millimetres
mmHG	millimetres of mercury
mNFL	macula nerve fibre layer
MS	mean spherical refraction
n	number
N	nasal
NFL	nerve fibre layer
NHS	National Health Service

NICE	National Institute for Health and Care Excellence
nm	nanometres
NRR	neuroretinal rim
NTG	normal tension glaucoma
OCT	optical coherence tomography
ON	optic nerve
ONH	optic nerve head
p	constant for the machine used when scaling an image
PAGC	primary angle closure glaucoma
PG	preperimetric glaucoma
pNFL	peripapillary nerve fibre layer
POAG	primary open angle glaucoma
Post LC	posterior LC depth
PreL	prelamina
q	axial length – 1.82
r	distance between stationary point and retina/radius of the eye
R	region
RGC	retinal ganglion cell
RPE	retinal pigment epithelium
s	(number of pixels * transverse pixel calibration) / 1000
S	superior
SC	scleral canal
SD	standard deviation
SD-OCT	spectral domain optical coherence tomography
SEM	scanning electron microscopy
SN	superior-nasal

SS-OCT	swept source optical coherence tomography
ST	superior-temporal
t	true size of an image
T	temporal
TD-OCT	time domain optical coherence tomography
BF	visual fields
μm	micrometres
2D	two dimensional
3D	three dimensional

Chapter 1:

Introduction

1 Introduction

Glaucoma is a progressive optic neuropathy and is the second leading cause of blindness worldwide, affecting around 60 million people (Quigley and Broman 2006; Quigley 2011). The primary site of ocular damage in glaucoma has been proposed to be the lamina cribrosa in the optic nerve (Minckler et al. 1976; Quigley et al. 1981; Quigley et al. 1983; Bellezza et al. 2003), though there is also significant damage to the retina as part of the disease process (Tan et al. 2008; Tan et al. 2009; de A Moura et al. 2012; Niles et al. 2012; Hood et al. 2014). Previously, examination of the lamina cribrosa and individual retinal layers has not been possible *in vivo*, but the development and subsequent advancements in optical coherence tomography (OCT), especially enhanced depth imaging and long wavelength OCT, has enabled the imaging of deeper structures within the human eye *in vivo*, including the lamina cribrosa (Keane et al. 2009; Lee et al. 2011; Park and Ritch 2011; Park et al. 2012).

1.1 The structure of the optic nerve head

When viewed anteriorly, i.e. in the *enface* orientation, the human optic nerve head (ONH) is typically oval shaped. The mean vertical diameter in a Caucasian population is 1.88 mm and mean horizontal diameter 1.70 mm (Quigley et al. 1990). The optic disc is the portion of the optic nerve that is visible when looking through the pupil into the eye; the average optic disc is around 2.38 mm², and it is generally accepted that there are no significant difference in area between males and females (Sekhar et al. 2001; Hermann et al. 2004; Sihota et al. 2005).

The cup-to-disc (CD) ratio is used to indicate the diameter of the optic cup expressed as fraction of the diameter of the optic disc, measured horizontally and vertically. In healthy eyes the average vertical CD ratio is 0.34 (Jonas et al. 1988b). Asymmetry of 0.2 or more between the two eyes can be an indication of glaucomatous development. Afro-Caribbean patients have larger CD ratios than

Caucasian patients (0.35 and 0.24 respectively, Beck et al. 1987). Important to note is that different viewing techniques, such as slit lamp fundoscopy, Heidelberg Retinal Tomography (HRT) and stereoscopic photography, can give significantly different measurements for the same discs (Durmus et al. 2009), likely due to the difference in internal optics of the different viewing modalities.

Retinal ganglion cell (RGC) axons run from cell body in the retina to the optic nerve head. There are roughly 1.2 million RGC axons in the eye (Anderson et al. 1967), each with a mean diameter $1.18\mu\text{m}$ (Jonas et al. 1992), and these axons come together to become the optic nerve.

The optic nerve head (ONH) can be anatomically divided into three structurally distinct regions: the prelamina, lamina cribrosa (LC) and the postlaminar optic nerve (Figure 1.1). Basic organisation of RGC axons is the same in all three regions: the axons are collected into bundles (fascicles) of several thousand, each surrounded by ensheathing tissue that differs from region to region.

1.1.1 Prelamina

The prelamina region represents the optic nerve head proper, and is the region of the optic nerve head that is commonly assessed during routine ophthalmic examination. 80-95% of the region consists of neural tissue (Wilczek 1947). Astrocytes form thin sheets around the blood vessels in these regions (Oyama et al. 2006). The optic nerve head is separated from the vitreous by a thin layer of astrocytes called the internal limiting membrane of Elschnig, which is continuous with the internal limiting membrane of the retina (Hogan et al. 1971)

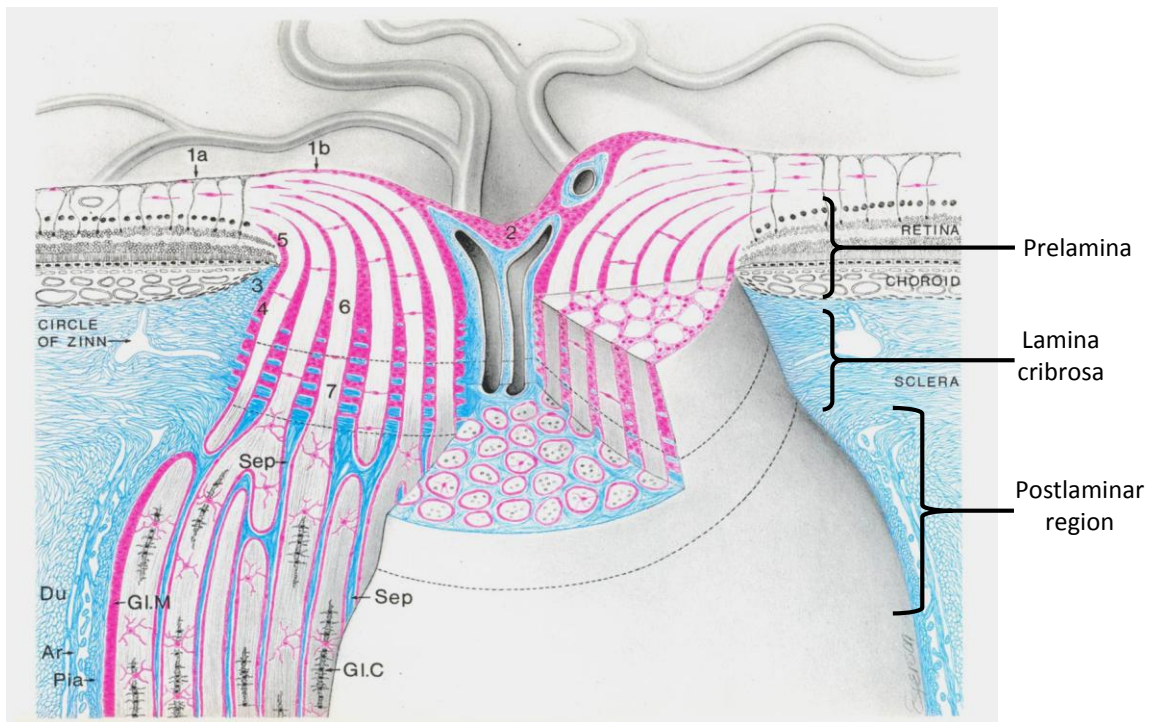


Figure 1.1: Schematic diagram of the human optic nerve head, where pink indicates astrocytes and blue indicates connective tissue. Lamina cribrosa is shown between dotted lines. Adapted from Anderson (1969)

1.1.2 Lamina cribrosa

The lamina cribrosa (LC) is a thin sieve-like structure located at the level of the sclera, which offers structural support to the RGC axons leaving the eye to form the optic nerve. It is made up of 10-11 cribriform sheets (Quigley et al. 1983), that are a network of collagen fibrils and elastic fibres that separates the RGC axons into bundles (Hernandez 1989, Morrison et al. 1990, Albon et al. 1995, Albon et al. 2000; Oyama et al. 2006). The RGC axon bundles pass through the pores formed by these connective tissue beams.

There are substantial amounts of collagen types I and III in the lamina cribrosa (Hernandez et al. 1986; Morrison et al. 1989; Albon et al. 1995; Albon et al. 2000). Collagen fibrils interspersed with elastin make up the core of the LC beams (Albon et al. 1995; Albon et al. 2000) and ultrastructurally resemble those found in sclera (Quigley et al. 1991; Hernandez 1992). The elastin appears as discrete fibres intermingled with collagen fibrils, rather than solid structures occupying entire beam

(Morrison et al. 1989). It is likely that the recoil properties of elastic fibres work with the collagen fibrils to cushion responses of the lamina cribrosa to changes in intraocular pressure (IOP). Thus the lamina cribrosa provides mechanical support for RGC axons as they pass from a relatively high pressure in the eye to a relatively low pressure in the retrobulbar cerebrospinal space (Downs et al. 2008). Astrocytes form glial columns that line axonal bundles (Hernandez et al. 1986; Oyama et al. 2006).

There is a greater density of connective tissue in the nasal and temporal areas of the LC than in the superior and inferior; and nasal more than temporal (Quigley and Addicks 1981; Radius and Gonzales 1981) The superior and inferior LC contains larger pores and then the nasal and temporal regions (Quigley and Addicks 1981). In glaucoma the superior and inferior-nasal regions of the optic nerve head are affected preferentially, and this is thought to be a consequence of these areas of the LC having less connective tissue i.e. less protection and therefore increased axon susceptibility to damage by elevated IOP (Gaasterland et al. 1978).

The LC has been shown to be thinner in healthy eyes with longer axial length (Ren et al. 2009), although there is significant difference in LC thickness measurements using *in vivo* and *in vitro* methods. Jonas and Holbach (2005) used histological techniques to determine a healthy LC thickness of $378 \pm 118 \mu\text{m}$, and in a different study (Kotecha et al. 2006) measured the thickness to be between $345 \mu\text{m}$ and $556 \mu\text{m}$ (average of $451 \mu\text{m}$). An OCT study has reported the healthy *in vivo* LC thickness to be $245.80 \pm 69.31 \mu\text{m}$ (Lee et al. 2011), and the group suggest that the difference between thickness measurements *in vivo* and those previously published for *ex vivo* were likely due to histological processing leading to tissue shrinkage, warping and/or swelling in the *ex vivo* samples.

The connective tissue beams of the LC form pores, through which RGC axons exit the eye. Pores vary in size, with larger pores at the superior and inferior poles where RGC axons originating in the

superior and inferior retina pass through the LC. In an *ex vivo* study Ivers et al. (2011) reported the mean pore area in the healthy human to be $1713 \pm 1413 \mu\text{m}^2$, range 154 to $6637 \mu\text{m}^2$. More pores are reported at the posterior LC surface than the anterior surface, with anterior pores larger than posterior (Ogden et al. 1988). This is consistent with Quigley and Addicks (1981), Ogden et al. (1988) and Albon et al. (2007) who demonstrated that pores divide as they travel down through the LC, contributing to organisation of RGC axon bundles for higher cortical processing.

1.1.3 Postlaminar Optic Nerve

The postlaminar ON is the area of optic nerve immediately behind the LC. In humans, axons become myelinated from the postlaminar ON to the terminal nuclei in the brain, but myelination does not usually extend past the LC into the retina. However, it has been shown that in approximately 1% of the population myelination of the retinal nerve fibres occurs, and that it is bilateral in 7.7% of these cases (Tarabishy et al. 2007).

The meninges that surround the brain also surround the optic nerve extending towards the posterior LC. The pia mater is the innermost, then arachnoid, and the dura mater outermost. A layer of glial cells lie between the pia mater and outermost axon bundles (Fujita et al. 2000). Connective tissue in the postlaminar ON forms septae that run in the same direction as the RGC axons. The collagen fibres have been found to be continuous with those in the pia mater (Oyama et al. 2006) and lie longitudinally along the optic nerve to provide tensile strength to optic nerve bundles. Of interest is that LC insertion into the pia mater has been proposed to alter with age and glaucoma (Sigal et al. 2010). Astrocytes in the postlaminar region are stellate in shape in the centre of nerve bundles (Oyama et al. 2006).

1.2 The structure of the retina

The retina is a multi-layered, light sensitive tissue lining the inner surface of the eye (Figure 1.2). It is the site of transformation of light energy into a neural signal, and contains the first three cells in the visual pathway, namely the photoreceptor, bipolar and ganglion cells. Simply, when light enters the eye, photoreceptor cells transform photons of light into a neural signal through phototransduction. The signal is passed to bipolar cells in the mid-retina, then to retinal ganglion cells (RGCs). Retinal ganglion cells pass the signal from the retina to the brain. The RGC cell bodies are located in the ganglion cell layer (GCL), and their dendrites are in the inner plexiform layer (IPL), where they synapse with both bipolar and amacrine cells. The RGC axons form the nerve fibre layer (NFL) as they cross the retina to exit the eye at the optic nerve head (Hildebrand and Fielder 2011).

There are up to 20 types of RGC in the human retina, although the most prominent are midget ganglion cells, that receive input from midget bipolar cells and as such have a small dendritic tree; and parasol ganglion cells, that have much larger dendritic spread. The midget and parasol cells project to the parvocellular and magnocellular layers of the lateral geniculate nucleus (LGN) respectively (Callaway 2005) and together account for around 80% of the ganglion cell population (Hildebrand and Fielder 2011).

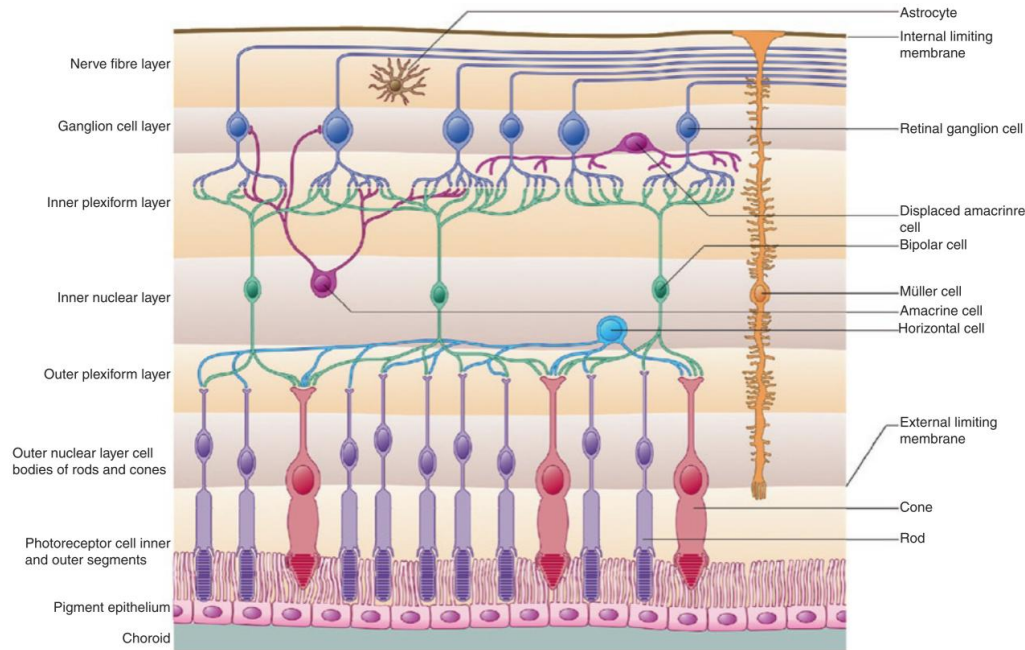


Figure 1.2: Overview of the structure of the human retina. Taken from Hildebrand and Fielder (2011).

1.3 The aging optic nerve head

1.3.1 Aging of the optic nerve

In the aging optic nerve there has been shown to be enlargement of the optic cup (Bengtsson 1980; Carpel and Engstrom 1981), i.e. an increase in optic cup diameter and optic cup area, with a subsequent increase in cup-to-disc (CD) ratio (Healey et al. 1997; Klein et al. 2006; Sung et al. 2009). Garway-Heath et al. (1997) also revealed larger cupping with aging, alongside a decrease in the area of the neuroretinal rim (NRR), predicted at 0.28% decrease in NRR/year. The decrease in NRR agrees with studies from Tsai et al. (1992) and is likely due to a decrease in nerve fibre count with increasing age (Dolman et al. 1980; Balazsi et al. 1984; Jonas et al. 1990). Indeed, the loss of RGC axons with increasing age is well reported (Johnson et al. 1987; Mikelberg et al. 1989; Jonas et al. 1990; Jonas et al. 1992), with one histological study reporting a decrease of around 5600 axons/year (Balazsi et al. 1984). However, Dolman et al. (1980) showed a trend for axon count decreasing with age that became more noticeable in those aged over 60 years. Repka and Quigley (1989), in a

histological study, reported a 6% axon loss over 75 years in human eyes, however this was not statistically significant.

An increase in LC thickness has been shown with increasing age by Kotecha et al. (2006), who also showed an age-related thickening of the LC beams. The latter is likely due to the age-related increase in connective tissue components of the lamina cribrosa (Hernandez et al. 1987; Hernandez et al. 1989; Morrison et al. 1989; Albon et al. 1995; Albon et al. 2000). This is consistent with the reports that the proportion of the LC that is occupied by pores decreases with age, causing a subsequent change in the ratio of pore : inter pore tissue (Ogden et al. 1988).

The increase in the amount of connective tissue in the LC with increasing age is accompanied by a change in the ratio of collagen type I : collagen type III (Albon et al. 1995). Collagen type I fibrils are larger and less flexible than collagen type III (Silver et al. 2002) and may contribute to changes in the biomechanical behaviour of the LC with increasing age, i.e. the LC becomes stiffer and less resilient (Albon, et al. 2000). This could influence the susceptibility of an eye to RGC axon damage from increased IOP and contribute to the age-related increase in susceptibility to glaucoma. Similarly, the posterior sclera has been shown to become less compliant with increasing age (Grytz et al. 2012), which is thought to have an effect of the amount of strain experienced by both the LC and the peripapillary sclera, which in turn is likely to increase the susceptibility of an eye to glaucomatous damage (Downs et al. 2008; Campbell et al. 2014).

1.4 Glaucoma

Glaucoma is characterised by retinal ganglion cell (RGC) loss that results in optic nerve damage and permanent visual field loss. Population based surveys indicate that around one in 40 adults over the age of 40 has glaucoma with loss of visual function (Quigley 2011), and prevalence increases from 2% in adults over 40 years to 7% in adults over 75 years. Clinical detection and management of

glaucoma is primarily based on three clinical measures: intraocular pressure (IOP), examination of the visual field, and the appearance of the optic nerve head (Anderson 2006). An increase in CD ratio can represent an early glaucomatous change, and as RGC axon loss increases the cupping of the optic disc increases (Kokotas et al. 2012). There is currently no known cure for glaucoma and vision loss is irreversible, and as such, current treatment mechanisms revolve around decreasing IOP to prevent disease progression and further damage to vision (Heijl et al. 2002; Feiner and Piltz-Seymour 2003; Leske et al. 2003). Females account for 59% of all glaucoma; specifically, 55% of primary open angle glaucoma (POAG) and 70% of primary angle closure glaucoma (PACG; Quigley and Broman 2006).

Glaucoma can be either primary or secondary; primary glaucoma is that which occurs as the primary disease, i.e. it is not caused by any other pathology, and secondary glaucoma occurs as a consequence of another pathology, e.g. rubeosis irides, whereby neovascularisation of the iris causes blockage of the trabecular meshwork and subsequent neovascular glaucoma. Similarly, there are two forms of primary glaucoma. Primary open angle glaucoma (POAG) accounts for around 74% of glaucoma worldwide (Quigley and Broman 2006). The disease is slow progressing, usually bilateral but often asymmetrical, and on average there is half as much damage in the better eye than the worse eye (Broman et al. 2008). The mean age of onset is 60 years, and the frequency of glaucoma increases with age (Quigley 2011).

Primary angle closure glaucoma (PACG) is a chronic disorder where the anterior chamber angle becomes blocked, limiting aqueous outflow via the trabecular meshwork. Worldwide, a third of all glaucoma is PACG (Quigley and Broman 2006), and there is significantly higher prevalence in East Asian countries. Optic disc and visual field changes are similar in POAG and PACG, although upon first clinical presentation patients with PACG tend to have greater levels of visual loss, particularly if the PACG is asymptomatic (Ang et al. 2004).

1.4.1 The role of intraocular pressure in glaucoma

Intraocular pressure (IOP) is determined by the rate of aqueous secretion and rate of aqueous outflow. In the healthy eye, aqueous humour is secreted from the ciliary epithelium and flows from the posterior chamber through the pupil and into the anterior chamber, where it exits the eye via either the trabecular meshwork or the uveoscleral pathway. 90% of aqueous outflow is via the trabecular meshwork, whereby aqueous flows through the trabeculae into Schlemm's canal and is drained by episcleral vessels. This process is pressure-sensitive, therefore increased pressure results in increased outflow. The remaining 10% of aqueous outflow is via the uveoscleral pathway, whereby aqueous flows across the ciliary body into the suprachoroidal space where it is drained by venous circulation in the ciliary body, choroid and sclera, and a small proportion is drained through the iris. In POAG there is higher resistance to aqueous outflow via the trabecular meshwork (Johnson et al. 2002), which leads to an increase in IOP and subsequent damage to RGCs.

According to NICE Guidelines (2009) which govern best practice for clinicians working in the UK, intraocular pressure of a healthy eye is below 21 mmHg and ocular hypertension is defined as IOP over 21mmHg. However, only 10% of patients with IOP 22 mmHg or above have glaucoma (Tielsch et al. 1991), and up to a third of patients with POAG did not initially present with raised IOP (Klein et al. 1992). IOP undergoes diurnal variation, and tends to be higher in the morning, lower in the afternoon and evening. In a healthy eye the IOP could change by up to 4 mmHg throughout the day, although a larger change may be observed in glaucomatous and hypertensive eyes (S. Fan et al. 2011).

1.4.2 Visual field loss in glaucoma

A characteristic feature of glaucomatous nerve damage is the pattern and progression of the visual field defect. The earliest loss typically appears as an isolated paracentral scotoma in the arcuate area between 5° and 25° from fixation, then becomes larger within the arcuate area, touching the

horizontal raphe nasal to fixation then joining to the blind spot. The central 5° and temporal visual field are usually preserved until late in the disease (Quigley and Addicks 1981).

Although a retinal nerve fibre defect causes a change in the visual field, it can take several years before glaucomatous damage is identified using perimetry alone, as 35% of the RGC axons can be lost before a visual field defect is detected (Kerrigan-Baumrind et al. 2000). It has also been demonstrated that 86% of patients with an abnormal visual field result revert back to normal on repetition of the test (Keltner et al. 2000), so it is apparent that supplementary methods should be used for glaucoma monitoring and progression.

1.4.3 Optic nerve head changes in glaucoma

Glaucoma causes a progressive enlargement of the optic cup in the ONH due to loss of RGC axons that make up the majority of neuroretinal rim tissue, often prior to detectable visual field loss. The glaucomatous damage exceeds the physiological cupping that is present before the onset of raised IOP, meaning glaucomatous cupping is usually larger than physiological cupping. Clinically, the neuroretinal rim is assessed for thickness, symmetry, colour and the presence of notching, and the optic disc is assessed for any enlargement of cup or vascular changes e.g. bayonetting of blood vessels or disc haemorrhages (Drance 1989; Jonas et al. 1993; Jonas et al. 1999). It is reported that as the LC moves posteriorly during the glaucomatous disease process (Yang et al. 2011), anterior capillaries, present in the ONH and collagenous sheets of the lamina cribrosa, would stretch if they were to maintain connections in the peripapillary retina. Some vessels may rupture under such tension, therefore a disc haemorrhage would be a direct result of distortion of the ONH (Drance 1989; Kim et al. 2010).

1.4.3.1 Changes to the Lamina Cribrosa in Glaucoma

The anterior surface of the LC is typically a shallow depression. In glaucoma, the cupping of the optic nerve head becomes deeper than in a healthy eye, due to RGC axonal loss (therefore less prelaminar tissue), as well as posterior displacement of the anterior LC surface. This displacement forms a 'w' shape from superior to inferior (Quigley and Addicks 1981; Quigley et al. 1983), as seen in Figure 1.3.

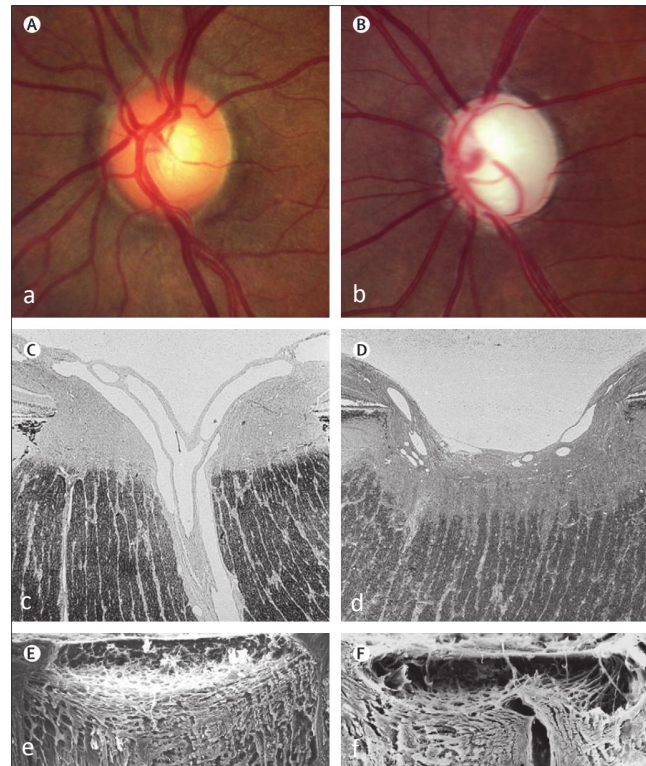


Figure 1.3: Features of healthy (left) and glaucomatous (right) optic nerve heads (ONH). (a) The cup of the optic disc is a small central pale area, whereas (b) the cup is excavated in glaucoma. (c) The typical histological image appearance of the ONH shows prelaminar tissue loss in glaucoma (d). (e) Connective tissues of the ONH showing the lamina cribrosa (LC) and (f) the LC becomes bowed backwards forming a 'w' shape. Taken from Quigley (2011).

The LC has been shown to be significantly thinner in glaucomatous eyes compared to healthy eyes in both histological studies (Jonas and Hayreh 2009; Ren et al. 2009; Jonas et al. 2012) and *in vivo* (Lee et al. 2012; Park et al. 2012). In a scanning electron microscopy (SEM) study, the healthy LC was reported to be around 240 μm in healthy eyes, decreasing to 140 μm in glaucomatous subjects (Quigley et al. 1983). One OCT study measured the healthy LC *in vivo* to have central thickness of around 350 μm , decreasing to around 240 μm in eyes with POAG and 175 μm in eyes with normal

tension glaucoma (NTG; Park et al. 2012), whereas another (Inoue et al. 2009) showed the mean LC thickness for subjects with ocular hypertension to be 245 μm , decreasing to 130 μm in advanced glaucoma. As previously stated, the difference in thickness measurements between *in vivo* and *ex vivo* measurements has been suggested to be due to tissue processing techniques used in histological studies, causing tissue shrinkage and/or warping.

Additional to posterior displacement of the LC during the glaucomatous disease process, there have also been reports of lateral extension. The LC surface was shown to remain covered by astrocytes that also filled the empty spaces left in pores by loss of nerve fibres. It was suggested that glial activation during glaucomatous neurodegeneration leads to an upregulation of extracellular matrix synthesis (Hernandez et al. 1989; Hernandez 2000) and that the astrocytes were migrating into LC pores (Tezel et al. 2004).

In glaucoma, those eyes that have normal or minimally damaged visual fields have a predominance of small round pores at the anterior LC surface; however, with increasing visual field loss the proportion of elongated pores increases (Susanna 1983; Miller and Quigley 1988). This is consistent with a recent *in vivo* characterisation of LC pores (Nadler et al. 2014). The LC pores are thought to elongate as the connective tissue fibres that form the LC stretch under the increased IOP in glaucoma.

1.4.4 Damage to the retina in glaucoma

Arguably, the regions of most importance when considering glaucoma are those layers that consist of the retinal ganglion cells, i.e. the retinal nerve fibre layer, ganglion cell layer and inner plexiform layer. The nerve fibre layer becomes thinner during the glaucomatous process as the RGC axons are damaged (Anton et al. 2007), both peripapillary and at the macula. The NFL drop out may be diffuse or localised. Localised damage is characterised by slit defects in NFL that become larger as the

glaucomatous damage progresses (Pieroth et al. 1999). One *in vivo* OCT study has found the mNFL thickness in healthy eyes to be $96.1 \pm 9.7 \mu\text{m}$, in POAG eyes $79.0 \pm 8.7 \mu\text{m}$, and in NTG eyes $79.2 \pm 9.0 \mu\text{m}$ (Park et al. 2012).

Areas of NFL thinning in early glaucoma may occur out of proportion to visual field loss or cupping, however, in advanced glaucoma NFL thinning around the optic disc is correlated with neuroretinal rim loss and corresponding visual field defects (Pieroth et al. 1999). In one study, Sommer et al. (1991) found that 60% of subjects with glaucomatous visual field loss had nerve fibre layer defects 6 years before any field loss occurred. It has therefore been suggested that evaluation of the nerve fibre layer should be used alongside ONH assessment to more accurately diagnose glaucoma (Deleon-Ortega et al. 2006) or be used as a screening tool for early glaucoma (Parikh et al. 2007).

1.4.5 Theories of glaucoma

There are many theories as to how glaucomatous damage may arise and these have previously been reviewed (Sigal and Ethier 2009; Burgoyne 2011; Chrysostomou et al. 2013; Downs 2015) and are indicated below in Figure 1.4. However, since glaucoma is a multifactorial disease, there are likely many interactions between these mechanisms. Below the mechanical and vascular theories are explored in more detail – but this by no means suggests that these are solely responsible for glaucomatous damage seen in the optic nerve head or retina as disease progresses. Additionally, there is evidence to suggest that retinal ganglion cells undergo dendritic remodelling in response to glaucoma (Weber et al. 1998; Morgan et al. 2006; Liu et al. 2010), with later changes in the axon and cell body.

1.4.6 Mechanical theory of glaucomatous damage

The LC has been identified as one of the primary sites of damage to RGC axons in glaucoma where it is thought that raised IOP results in deformation of the LC with shearing of individual cribriform plates in relation to one another (Quigley et al. 1981; Radius and Gonzales 1981; Quigley et al. 1983; Kotecha et al. 2006). It is thought that the deformation of the cribrosal plates may cause compression, extension or shearing of axons within the LC leading to axonal damage directly or as a result of blocked axonal transport (Minckler 1986).

High IOP generates mechanical stress (force/cross sectional area) and strain (physical deformation of tissue), leading to changes in microarchitecture and progressive damage to adjacent axons (Kiumehr et al. 2012). IOP exerts a uniform force on the inner eye but regional variation in the LC microarchitecture may lead to local mechanical stress and strain, correlated with local LC density. IOP related deformations cause yield and failure of anterior LC beams, so the load is transferred to adjacent beams, causing a cascade of damage leading to glaucomatous cupping (Downs et al. 2011).

The superior and inferior poles of the LC typically contain larger pores and less connective tissue than the temporal and nasal (Quigley and Addicks 1981; Miller and Quigley 1988), and the inferior and inferior-nasal have lower collagen density compared to other regions (Quigley et al. 1991). It is concluded that the LC is more vulnerable to focal damage in these regions, as more focal damage is found in here compared to elsewhere (Kiumehr et al. 2012). Focal LC defects show corresponding visual field defects due to localised RGC axon drop out, and some discs show deep excavations (acquired pits of the optic nerve; APONs) at the vertical poles (Quigley and Addicks 1981).

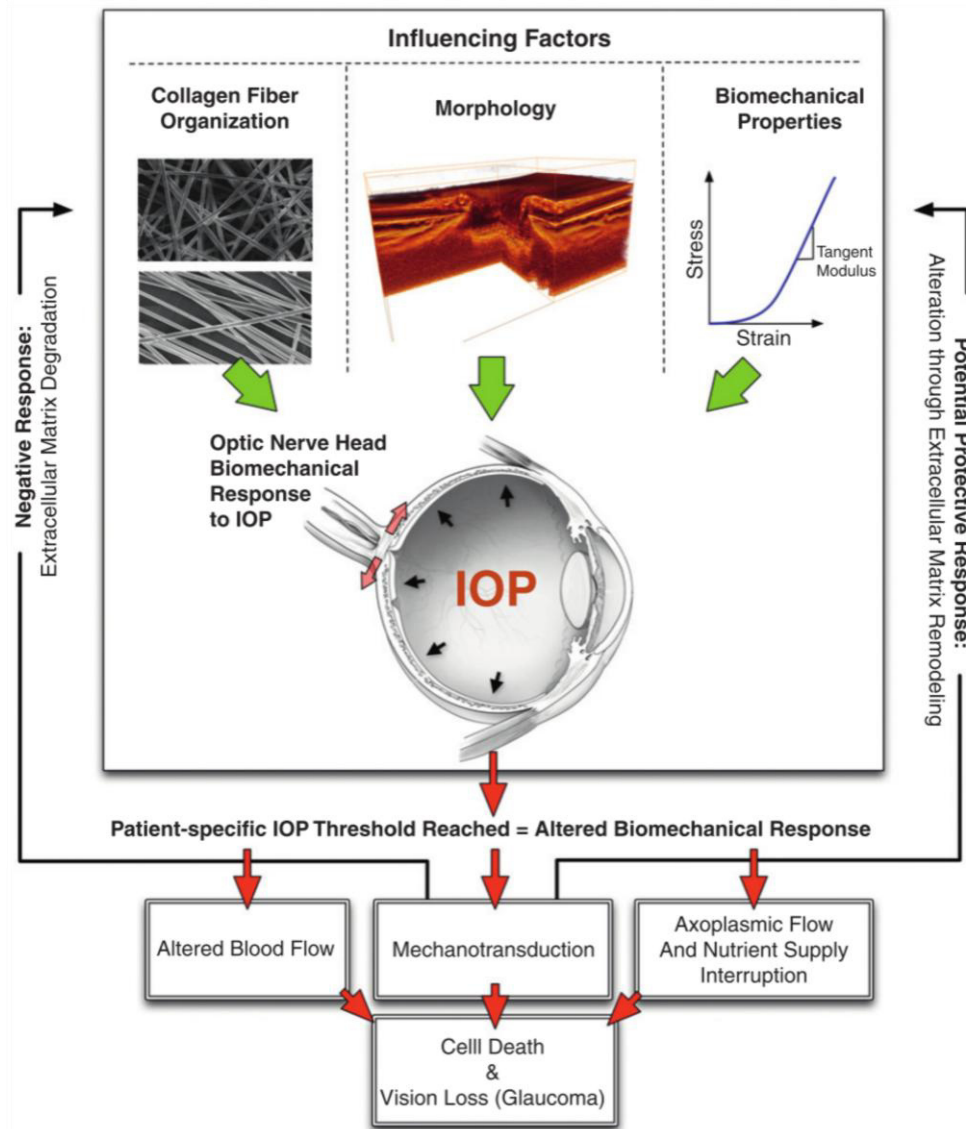


Figure 1.4: Schematic diagram describing the mechanisms by which optic nerve head biomechanics may result in retinal ganglion cell death in glaucoma. 'Mechanotransduction' refers to the conversion of mechanical stimuli to chemical signals at a cellular level. Taken from Strouthidis and Girard (2013).

The superior and inferior poles of the LC typically contain larger pores and less connective tissue than the temporal and nasal (Quigley and Addicks 1981; Miller and Quigley 1988), and the inferior and inferior-nasal have lower collagen density compared to other regions (Quigley et al. 1991). It is concluded that the LC is more vulnerable to focal damage in these regions, as more focal damage is found in here compared to elsewhere (Kiumehr et al. 2012). Focal LC defects show corresponding visual field defects due to localised RGC axon drop out, and some discs show deep excavations (APONs) at the vertical poles (Quigley and Addicks 1981).

It has been suggested that axons passing through large pores are more at risk of being damaged by elevated IOP, and that pores elongate as glaucomatous optic nerve damage increases. Miller and Quigley (1988) concluded that axonal resistance to damage must decrease as glaucomatous atrophy worsens, and that RGC axons lose their resistance to elevated IOP either as a direct consequence of the decrease in connective tissue density at ONH, perhaps by direct mechanical forces disrupting metabolic transport processes, or because of associated changes in other parameters, such as reduced nutrition from compromised blood vessels.

Another theory relates to the peripapillary scleral wall. The thickness of the scleral wall has been found to be susceptible to acute rises in IOP. If the sclera is compliant then it deforms under an increase in IOP and pulls the LC taut. If the sclera is stiff then the increased IOP deforms the sclera, pushing it backwards (Bellezza et al. 2001; Sigal et al. 2005; Norman et al. 2010; Sigal et al. 2011). This is demonstrated below (Figure 1.5).

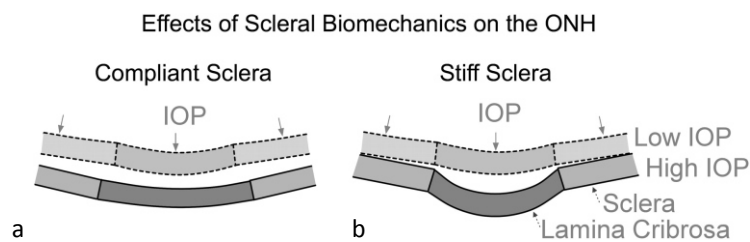


Figure 1.5: The effects of scleral biomechanics on the ONH. (a) If the sclera is compliant then it deforms under an increase in intraocular pressure (IOP), pulling the lamina cribrosa (LC) taut. (b) If the sclera is stiff then it does not change under an increase in IOP and the LC is pushed backwards. Taken from Sigal et al. (2011)

1.4.7 Vascular insult and involvement in glaucomatous damage

The vascular theory for glaucomatous deformation of the LC suggests that the blood supply to the LC is impaired, an effect either associated with or independent of increased IOP. The blood supply within ONH supplies oxygen and nutrients and removes waste products, and disruption to this supply will inevitably cause harm. Evidence suggests a correlation between vascular insult (particularly ischaemia and hypoxia) within the ONH and development of glaucoma (Osborne et al.

2001; Piltz-Seymour et al. 2001). Ischaemia deprives surrounding tissues of oxygen and nutrients. It is suggested that the ganglion cell mitochondria are affected by the ischaemia, i.e. the lack of optimum blood supply causes oxidative stress and results in the ganglion cells being more susceptible to damage (Osborne and Del Olmo-Aguado 2013).

The mechanism for glaucomatous damage to the LC remains unclear. Whether an IOP affects the vasculature surrounding the ONH first, or whether mechanical damage occurs to RGCs and the LC first, thus causing problems in blood supply and nutrient diffusion throughout the ONH, or another mechanism contributes is the focus of current and future research. Changes in LC connective tissue could be caused by stress on the LC relating to IOP, affecting blood supply and nutrient diffusion to RGC axons before any structural damage and changes can be seen (Burgoyne et al. 2005; Downs et al. 2008). Additionally, activation of LC cells and astrocytes in response to stress and/or damage and connective tissue remodelling (Downs et al. 2011) further complicates our understanding.

1.4.8 Glaucoma detection *in vivo*

The detection and management of glaucoma is primarily based on three clinical measures: IOP, examination of the visual field and the appearance of the optic nerve head (Anderson 2006). However, only 10% of patients with IOP 22mmHg or above have glaucoma (Tielsch et al. 1991), and up to a third of patients with glaucoma did not have raised IOP initially (Klein et al. 1992). Indeed, it can take several years before glaucomatous damage to the visual field damage is detected by perimetry (Quigley et al. 1989; Quigley et al. 1992). Assessing the CD ratio is limited because a change indicates that a loss in RGC axons has already occurred. It has been proposed that *in vivo* assessment of the ONH and particularly the LC can aid the understanding of structural changes in the eye due to glaucoma (Inoue et al. 2009).

1.5 Optical Coherence Tomography

The advent of Optical Coherence Tomography (OCT) an *in-vivo* imaging technique that provides high-resolution cross sectional images of the internal microstructure of living tissue (Schmitt 1999), including the human optic nerve head and LC, makes such *in vivo* assessment a potential reality. OCT was first developed by Huang et al. in 1991 as a non-invasive biological imaging technique, and by the mid-1990's was being used to study glaucoma and retinal disease (Hee et al. 1995; Schuman et al. 1995). OCT imaging is analogous to ultrasound, but measures the back-reflection of infrared light rather than of sound (Brezinski 2006). OCT has the advantage of not requiring direct contact with tissue as ultrasound does (Gupta et al. 2004), but as light is highly scattered or absorbed within most biological tissues imaging is constrained to tissues that are optically accessible (Puliafito et al. 1999; Unterhuber et al. 2005). Typical OCT imaging depth is approximately 1-2 mm, but in the eye the majority of tissue is essentially transparent so the retina can be imaged despite an average axial length of approximately 24 mm (Kodach et al. 2010).

1.5.1 Theory of optical coherence tomography

In OCT, a broadband light source is used to illuminate an interferometer. The interferometer splits the broadband light source into two beams: reference and sample. The sample beam focuses through both the scanning optics of the system and an objective lens towards a point below the surface of the tissue to be imaged (the sample). The reference beam is reflected back through the optical system by a reference mirror.

Within the sample, light is reflected back from the boundaries between structures and is scattered differently by tissues with different optical properties. The reflected light from both the reference mirror and the sample is then recombined. If the wavelengths of the two beams match, interference occurs and this interference is measured by an interferometer. This allows an image of reflected light from the sample to be created (Schmitt 1999; Gupta et al. 2004), which from a single point is

called an a-scan. As the OCT device scans a sample, individual a-scans are combined to form b-scans (slices), the equivalent to a line of a-scans. Individual b-scans can be combined to form 3D volumes (sometimes known as c-scans). A schematic diagram of a generic OCT system is shown below (Figure 1.6).

The centre wavelength of the OCT light source dictates the depth of penetration into a tissue sample, and its bandwidth dictates axial resolution. Traditionally, a centre wavelength in the 820 nm range and bandwidth of 25 nm are used for ocular imaging, giving structural detail to a resolution of 8-10 μm (Gabriele et al. 2010). Broader bandwidth light sources were later used in OCT systems to improve axial resolution (Drexler et al. 1999).

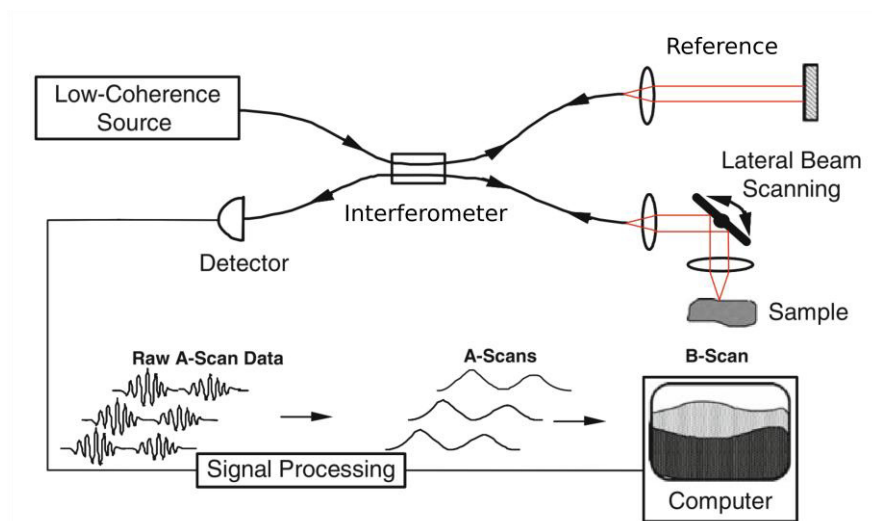


Figure 1.6: Schematic diagram of a generic optical coherence tomography (OCT) device. Light from the low coherence source is split to a sample and a reference arm. The light that is reflected back is recombined the interference measured by the detector. The signal is then processed to form a-scans, which are combined to form 2D b-scans. Adapted from Izatt and Choma (2008).

1.5.2 Types of OCT Device

There are two main types of OCT device that work in different ways: time domain OCT, and Fourier domain OCT.

1.5.2.1 Time Domain OCT

The first commercially available OCT device was a time domain OCT (TD-OCT), Stratus (Zeiss Meditec). In TD-OCT the resolution of the images is produced as a function of time (Han and Jaffe 2009); a reflectivity profile (a-scan) is built by a reference mirror physically scanning over a coherence length to collect backscattered light from various depths within a sample (Choma et al. 2003). The reference arm of the system oscillates back and forth to achieve real time imaging, so the potential resolution and clarity of the image is limited by the speed of the mechanical movement (Gabriele et al. 2010). As the scan speed for TD-OCT is limited, the resultant images can be prone to eye movement-related artefacts.

1.5.2.2 Fourier Domain OCT

Fourier domain OCT (FD-OCT) differs from TD-OCT in that it does not require mechanical movement of the reference mirror. There are two types of FD-OCT:

Spectral domain OCT (SD-OCT): uses a broadband light source and achieves spectral discrimination using a dispersive spectrometer (Wojtkowski et al. 2002) i.e. the light source in SD-OCT uses a dispersive element to create different optical frequencies. The backscattered light from the sample combines with reflected light from a stationary reference arm, and is collected by a spectrometer (as opposed to the photodetector used in TD-OCT). The interference spectrum is then processed using Fourier transformation to obtain the magnitude and echo time delay of light (the a-scan). The reflected light from the entire depth of a sample at a given point is detected simultaneously, without requiring a moving reference arm. This enables significantly faster scanning speeds (Kagemann et al. 2008; Forte et al. 2009; Gabriele et al. 2010) and higher axial resolution (Keane et al. 2009), compared to TD-OCT.

Swept source OCT (SS-OCT): works by rapidly tuning a narrowband source through a broad optical bandwidth, allowing greater scan speed and less attenuation of light. A new commercially available swept source OCT (Topcon DRI OCT Triton, Topcon, Netherlands) has swept-source technology combined with a long wavelength at 1050 nm, allowing for imaging of deeper ocular structures such as the lamina cribrosa and the choroid (Agawa et al. 2011).

1.5.3 The wavelength of the OCT source and its effect on ocular imaging

Commercial OCT instruments tend to utilise light sources with wavelength in the range of approximately 830 nm. The eye is essentially transparent in 800 nm wavelength range, meaning there is minimal optical attenuation and scattering of light, therefore the ~800 nm wavelength allows imaging of the eye's anterior segment and retina, in the absence of any ocular opacity.

However, if the retinal pigment epithelium (RPE) is healthy and intact there is limited visualisation of the choroid with 800 nm range wavelength OCT devices. If the RPE is damaged or atrophied in a particular region then the 800 nm range OCT instrument may be able to image part of the choroid or sclera in that area. This is due to the high concentration of melanin in the RPE, which is highly scattering and absorbs light. Light absorption in melanin is strongly wavelength dependant, and in the 600-1200 nm range absorption is shown to decrease with increasing wavelength, as does the general scattering of light in biological tissue (Povazay et al. 2003; Unterhuber et al. 2005).

Therefore, logically, using a light source with wavelength longer than 800 nm should improve the visualisation of features in the choroid. However, one confounding factor is that the eye consists of around 90% water, and water absorption also increases with higher wavelength, which means the light beam from the OCT will be strongly attenuated at higher wavelengths.

Fortunately, water has zero-dispersion point at around 1000 nm (also called the water window). There is minimum dispersion at this wavelength of light so the axial resolution stays constant over a reasonable depth. Wang et al. (2003) found with a 1000 nm light source that a laboratory-based OCT can maintain high resolution to larger depth range than with an 800 nm source, and can eliminate the influence of depth-dependant dispersion of water in tissue. Additionally, the water absorption profile has a local minimum at around 1060 nm (Hammer et al. 1995) so the signal is not as strongly attenuated with that wavelength.

Povazay et al. (2007) showed that the performance of an ~800 nm OCT system was significantly affected by light scattering induced by cataract, but that with a 1050 nm device the scattering was noticeably less. This is due to the reduced light scatter by tissue at longer wavelengths of light. They and others (Esmaeelpour et al. 2010) concluded the 1050 nm wavelength OCT device enabled visualisation of the deeper structures in the presence of lens opacities better than the 800 nm range OCT could. This is of particular relevance clinically as cataracts are predominantly age-related, and age is a major risk factor for glaucoma.

1.5.4 Recent developments in OCT imaging

Conventional OCT has a limited ability to image deep structures in the posterior segment because of a depth-dependant decrease in sensitivity and scattering of light by melanin and by blood vessels (Spaide et al. 2008). Enhanced depth imaging (EDI) OCT improves image quality of deeper structures of the outer retina, choroid, sclera (Park and Ritch 2011) and in the deep ONH tissue (Lee et al. 2012) when compared to traditional imaging techniques. EDI images are obtained by focussing the OCT device on the retina in the conventional way then moving the device closer to the eye to move the reference plane more posterior. An inverted image is created with the inner portion of retina facing downwards (Park et al. 2012) and the deeper structures closer to zero depth (at the top of the OCT device screen). 100 OCT scans are averaged to provides better detail for deeper structures (Figure

1.7), and EDI of the lamina cribrosa, peripapillary sclera and choroid can help evaluate glaucomatous neuropathy and its relationship to structures of the optic nerve complex (Park et al. 2012). **EDI is a technique exclusive to Spectralis OCT devices (Heidelberg Engineering, Heidelberg, Germany); however, inverting the OCT image during acquisition on other OCT instruments as described above is still shown to improve visualisation of deeper ocular structures.**

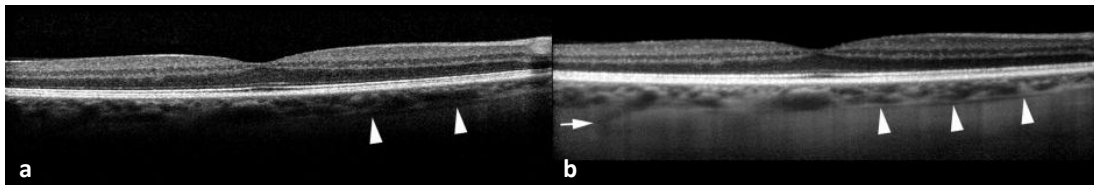


Figure 1.7: OCT image of the macula acquired using (a) conventional technique and (b) enhanced depth imaging (EDI), with a Spectralis OCT. The EDI image has been flipped vertically for comparison with the conventional method. White arrows emphasise the improvement in the detail of the choroid. Copied from Spaide et al. (2008)

Another advancement in OCT is adaptive optics, whereby a deformable mirror is used within the optical system to compensate for wavefront distortions. The transverse resolution of an OCT image is limited by the size of the beam of light focussed on the retina, and as such, optical aberrations can occur as light passes through the different media of the eye (Folio et al. 2012). Using adaptive optics the transverse resolution of the device can be reduced allowing better resolution of small ocular features (Zawadzki et al. 2005; Zhang et al. 2005). Indeed, an adaptive optics OCT system has been used to measure LC beam thickness and pore diameter *in vivo* (Nadler et al. 2014).

Typically there are four arterial and four venous branches originating in the ONH, arranged into two superior and two inferior branches of the central retinal artery (CRA) and central retinal vein (CRV; Hayreh 2001) and these can cause significant shadows in OCT images, due. Post-image processing techniques have been able to improve imaging of the LC, such as algorithms to improve contrast and compensate for light attenuation in OCT image, improving visibility of deep LC structures and in some cases removing vascular shadows from blood vessels (Girard et al. 2011; Mari et al. 2013; Girard et al. 2015).

Typically OCT devices are table-mounted; however, recently devices have been developed which allow mobile ocular imaging by utilising a handheld probe (Envisu C-class system, Bioptigen, Morrisville, USA) or scanning head (iVue, Optovue Inc., Fremont, USA; Keane and Sadda 2014). These have uses in paediatric and neonatal eye care (Anwar et al. 2014; Avery et al. 2014a; Avery et al. 2014b; Tong et al. 2014) as well as in animal research (Fenolland et al. 2013), which is of particular benefit in analysis of glaucoma models.

Finally, further recent developments in OCT have enabled optical coherence angiography (OCA), whereby maps of retinal and choroidal vasculature are created using high-speed sequential OCT a- or b-scans at a consistent retinal location then assessing the differences in the scans that occur due to blood flow (Choi et al. 2013). Retinal blood flow can be analysed using Doppler OCA, by comparing changes in vessel diameter, orientation and position in subsequent retinal images (Makita et al. 2008). The visualisation of retinal blood vessels has been shown to be comparable to fluorescein angiography at the macula (Zeimer et al. 2015), and *better* than fluorescein angiography in visualising the radial peripapillary capillary network (Spaide et al. 2015). At the optic disc itself it has been shown that in a healthy eye there is a dense microvascular network visible using OCA, whereas in glaucomatous eyes this network is visibly attenuated (Jia et al. 2014), and is less dense in advanced glaucoma than in early or moderate disease (Zhu et al. 2015; Lévêque et al. 2016).

1.6 The use of OCT to assess and monitor the eye during glaucoma

1.6.1 OCT to image the ONH

The advent of commercial OCT machines and EDI allowed the deeper structures of the ONH to be evaluated *in vivo*, particularly the anterior surface of the LC (Park and Ritch 2011). Subsequently, 2D (Lee et al. 2011) and 3D (Lee et al. 2012) analysis techniques are now being developed to analyse these images. OCT data has been shown to be comparable with histological analysis in a monkey eye

(Strouthidis et al. 2009; Strouthidis et al. 2010). OCT can also detect LC thickness differences between normal and glaucomatous eyes (Park et al. 2012) and focal defects in the LC (Kiumehr et al. 2012). The anterior surface of the LC can be examined and pores can be visualised (Inoue et al. 2009; Sigal et al. 2010) and measured (Ivers et al. 2011; Nadler et al. 2014), though as yet no group has been able to visualise pores at the posterior LC surface.

1.6.2 The use of OCT to measure macula parameters in glaucoma

Glaucoma primarily affects the retinal ganglion cells, and as such, OCT can be used to measure the retinal layers that comprise the ganglion cell axons, cell bodies and dendrites. Retinal nerve fibre layer thickness gives a measure of RGC axon layer. Thinner than average superior and inferior NFL thickness measurements at baseline, alone or in conjunction with clinical and demographic factors (age, IOP, central corneal thickness, stereophoto assessment) predicts the development of repeatable visual field damage and/or progressive glaucomatous optic neuropathy (Lalezary et al. 2006). With the advancement of commercial OCT machines NFL thickness can be monitored easily in a clinical setting, and the inbuilt software on some commercial machines has the capability to automatically distinguish glaucomatous eyes from non-glaucoma, even at the early stages of the disease (Mwanza et al. 2011). In the same way, the ganglion cell complex, consisting of the NFL, GCL and IPL combined has been shown to have value in detecting early and preperimetric glaucoma (Arintawati et al. 2013). However, as yet, there is no published data describing the diagnostic potential of the IPL and the GCL independently.

1.7 Hypothesis and aims of this study

Glaucoma is the second leading cause of irreversible blindness worldwide, affecting around one in 40 adults over 40 years (Quigley 2011). There is no cure for glaucoma, so current treatment aims to halt disease progression in order to prevent further vision loss. Previous work has shown that, although the lamina cribrosa is thought to be the primary site of RGC axonal damage in glaucoma (Quigley et al. 1983), the macula is also affected (Mwanza et al. 2011). With the advances in OCT we now have the ability to thoroughly investigate structural changes in the retina and optic nerve head as a result of glaucoma, and attempt to use the changes that are discovered as a marker for early disease. If we can detect and diagnose glaucoma at the earliest stages then we are in a better position to treat before any vision loss occurs. As such, the aim of this thesis is to characterise structural changes in the ONH and macula in order to identify biomarkers for the earliest stages of glaucomatous disease.

The hypothesis of this thesis is that OCT imaging can be used to characterise alterations in retinal and/or ONH structures, and in doing so identify factors that i) can be used to determine early disease such that therapy can begin prior to substantial vision loss, and ii) may be critical in determining ONHs that are predisposed to glaucomatous optic neuropathy.

The specific aims for this thesis are:

- To quantify regional thickness and volume measurements of the inner retinal layers (i.e. the mNFL, GCL and IPL) in 3D OCT image datasets of maculae measured at different disease stages of glaucoma severity, in order to identify a measure of RGC integrity that can be used as a biomarker of early stage glaucomatous damage.
- To identify if ONH microstructural parameters alter with age, as age is a major risk factor for glaucoma, and if changes are present to identify whether they are region specific.

- To identify those microstructural changes that occur in the ONH at different glaucoma disease stages, i.e. preperimetric, early, moderate and advanced glaucoma, and subsequently determine those factors that best explain the observed changes.
- To quantify and identify 3D changes in volume of the optic cup, prelamina and lamina cribrosa, and in the area of BMO, in different stages of glaucoma.
- To investigate if regional and depth-related differences in LC beam orientation and coherence occurred between healthy and glaucomatous eyes.

Chapter 2: Methods

2 Methods

2.1 Ethics

Ethical approval was received from the School of Optometry and Vision Sciences Research Ethics Committee, Cardiff University, UK for recruitment of staff and students, and from the South East Wales Research Ethics Committee, UK for recruiting NHS patients for this research project.

All participants were recruited in accordance with the tenets of the Declaration of Helsinki and informed consent was obtained prior to participation in the study. Example participant information and consent forms are shown in Appendix I.

2.2 Participant recruitment

Thirty-three participants (aged 70.34 ± 9.97 years) with glaucoma were recruited from Professor JE Morgan's glaucoma clinic at the University Hospital of Wales, Cardiff, UK. Twenty-one controls (55.97 ± 9.69 years) were recruited from within staff, postgraduate students and friends at the School of Optometry and Vision Sciences, Cardiff University. Twenty-eight participants aged 18-30 years (mean 21.89 ± 2.99 years) were recruited from students at the School of Optometry and Vision Sciences, Cardiff University. For the macula study (Chapter 3), OCT images from an additional thirty-one participants (22 with glaucoma, aged 62 ± 10.60 years; and 9 control, aged 65.36 ± 11.76 years) were included. These OCT datasets were acquired by Dr KE Mortlock for a previous study. Where possible, both eyes from each participant were used for this research

2.3 Data acquisition

2.3.1 Clinical assessments

Each participant was first asked a brief medical history focussing predominantly on ocular history (and glaucoma, if present), as well as general health and any prescription medications. Exclusion criteria at this stage included pregnancy, epilepsy, non-glaucomatous ocular pathology (not including mild cataracts) or systemic pathology with significant ocular complications, e.g. diabetes.

LogMAR visual acuity, and refractive state, using a KR-7500 autorefractor (Topcon Europe Medical B.V., Netherlands), was determined for each eye. For inclusion, participants were required to have a mean refractive error of less than ± 6.00 dioptres (D), with less than 3.00 D cylinder, to ensure no bias on optic nerve head parameters due to axial myopia, and in order to allow accurate focussing of the OCT device. Participants then underwent a slit-lamp anterior eye exam to assess the health of the anterior eye and ensure the absence of significant corneal or lenticular opacities that would limit the quality of subsequently acquired image data. The anterior chamber angle was then graded using the Van Herrick technique in order to ensure that glaucomatous participants had open anterior chamber angles (i.e. open angle glaucoma rather than narrow-angle glaucoma), and to reduce the risk of angle closure during dilation.

For anaesthesia, 0.5% proxymetacaine hydrochloride was instilled in each eye and triplicate IOP readings were recorded following Goldmann applanation tonometry (Haag Streight AG, Switzerland). Visual fields were assessed using SITA 24-2 fast threshold visual field test (Humphrey Field Analyser, Carl Zeiss Meditec Inc, Germany), in order to obtain mean deviation (MD) values. Axial eye length was measured using an IOLmaster (Carl Zeiss Meditec Inc, Germany). Ocular biometry, including central corneal thickness and anterior chamber depth, were determined using a Pentacam (Oculus Optikgeräte GmbH, Germany). 1.0% tropicamide was used to dilate the pupils, and fundus photos were acquired using a Topcon 3DOCT-1000 (Topcon Medical Systems, USA).

A summary of inclusion criteria for these studies is shown below (Table 2.1).

Criteria	Details
Ocular health	<ul style="list-style-type: none"> No non-glaucomatous ocular pathology Mild cataract (lens opacities) included providing the view of the posterior pole was not restricted
General health	<ul style="list-style-type: none"> No systemic pathology that had ocular complications (e.g. diabetes) No pregnancy or epilepsy
Refractive error	<ul style="list-style-type: none"> Within ± 6.00 D mean spherical error Less than 3.00 D cylindrical error
Additional criteria for control participants	
IOP	<ul style="list-style-type: none"> ≤ 21 mmHg average from three consecutive readings measured using Goldmann tonometry
Visual fields	<ul style="list-style-type: none"> No visual field defect, as described by (Hodapp et al. 1993)
Visual acuity	<ul style="list-style-type: none"> 0.1 logMAR acuity or better

Table 2.1: Inclusion criteria for study participants.

2.3.2 Optical Coherence Tomography

Images were acquired using a purpose-built, laboratory-based spectral domain optical coherence tomography (SD-OCT) instrument with a 1050 nm (70 nm bandwidth) light source (1-M-ASE-HPE-S, NP Photonics, Tuscan, US) operating at 47,000 a-scans/second, allowing for acquisition time of a 512 x 512 scan of around 6 seconds. The beam diameter of the system was 1.5 mm, and the optical power at the cornea was 1.8 mW. The spectrometer within the OCT was grating-based with a Goodrich SU-LDH-1.7 camera. Three-dimensional volumetric datasets of the optic nerve head (ONH) and macula of each eye were acquired, consisting of 512 x 512 a-scans, 1024 points/a-scan, providing axial resolution of ~ 5 μm in tissue (assuming a grouped refractive index of 1.4) and maximum transverse resolution of ~ 17.5 μm .

Participants were directed to focus on a central fixation target for macula imaging, and a peripheral target for optic nerve head imaging. Macula scans were acquired using the traditional imaging modality, with the retina closest to the zero-delay, in order to provide optimal definition of the inner

retinal layers. ONH scans were acquired vertically inverted, allowing for better definition of the deeper ONH structures.

Scan size was dependent on date of acquisition, as sight modifications to the OCT device were performed partway through recruitment. For the glaucomatous cohort and corresponding controls, 20° scans were acquired of the macula, and both 10° and 20° scans of the ONH. For the young control ONH data and glaucoma macula data 18.7° scans the ONH were performed.

2.4 Data processing

2.4.1 Flow chart of stages of data and image processing

A summary of the stages involved in processing the initial raw data into final images prior to performing measurements is shown below in Figure 2.1.



Figure 2.1: Flow chart showing data processing stages prior to measurements.

2.4.2 Spectral OCT data processing

OCT spectral data were acquired and saved in .FD1 format, then processed into image files using a custom-written MATLAB program (FDProcessing v1.0). This program converted the spectral data into 16 bit TIFF images.

2.4.3 Image processing

Initially, datasets were imported into ImageJ (version 1.47n; NIH, USA, <http://imagej.nih.gov.ij>). The 16 bit images were converted into 8 bit images in order to allow brightness and contrast adjustment and also reduce file size. The brightness and contrast of each image was altered according to the histogram of pixel intensities; the pixel intensities were initially normally distributed (Figure 2.2a). The lower pixel limit of was set at the central peak of the histogram and the upper limit was set to the edge of the curve (Figure 2.2b). The pixels values were then automatically redistributed across this range (Figure 2.2c), thus improving contrast between retinal layers or ONH structures (Figure 2.3).

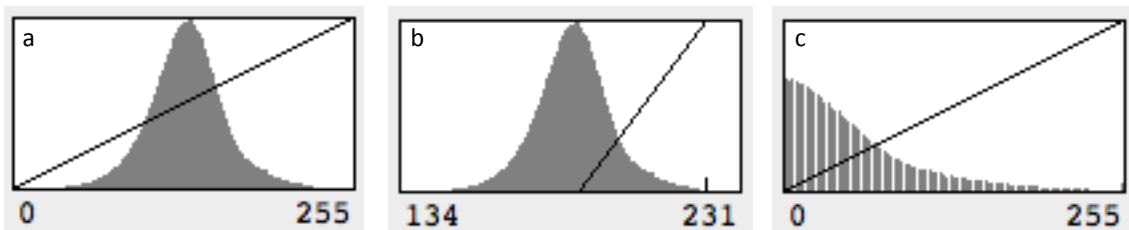


Figure 2.2: (a) Histograms of pixel intensities were normally distributed initially. (b) The lower limit was set to the centre of the histogram and upper limit to the edge of the curve then (c) the pixels were automatically redistributed over this range.

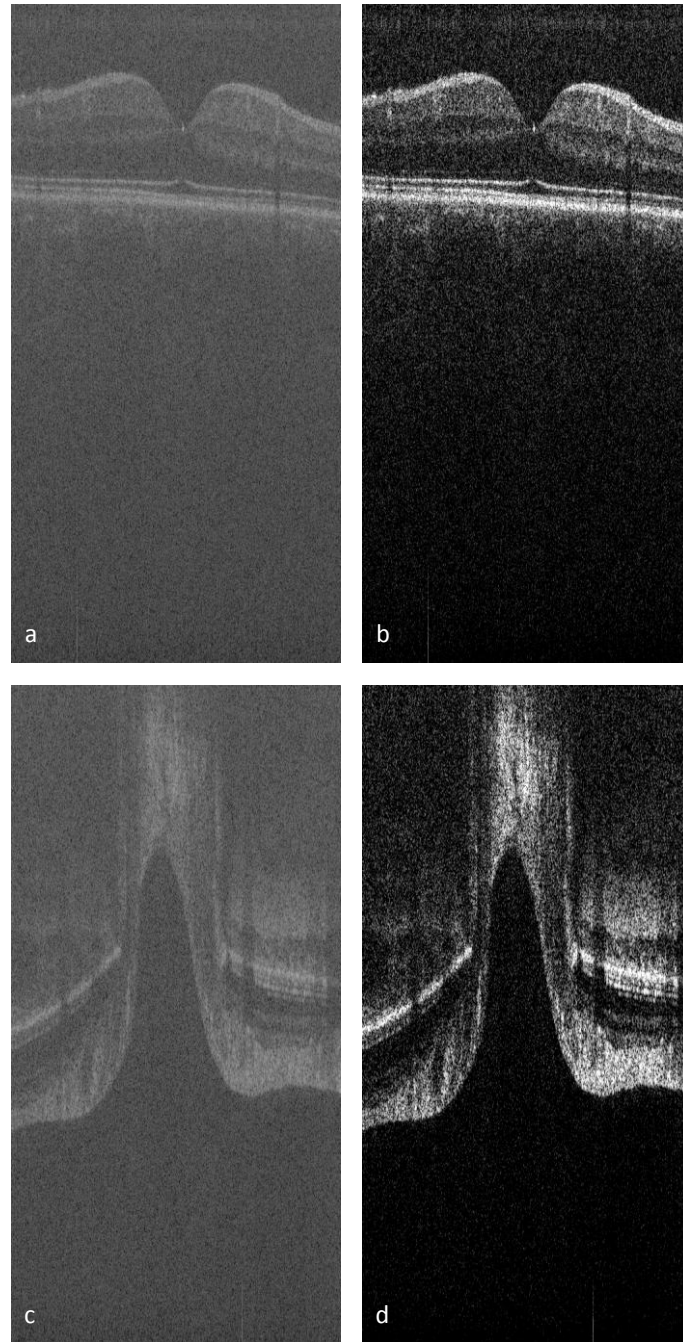


Figure 2.3: OCT images of the macula (above) and optic nerve head (below) (a, c) before and after (b, d) brightness and contrast adjustment. Note improved visibility of retinal layers and ONH structures in b and d. Datasets are were not scaled correctly at this stage.

Image data stacks were then cropped to remove either excess vitreous or areas of signal loss.

‘Stackreg’, an ImageJ plugin (P Thevenaz, Biomedical Imaging Group, Swiss Federal Institute of Technology), was used to align tomograms, and small eye movements or blinks, where present,

kernel in the lateral direction. These filter combinations had previously been deemed optimal for data acquired on this research OCT device. A demonstration of pre- and post- filtered images is shown below (Figure 2.4).

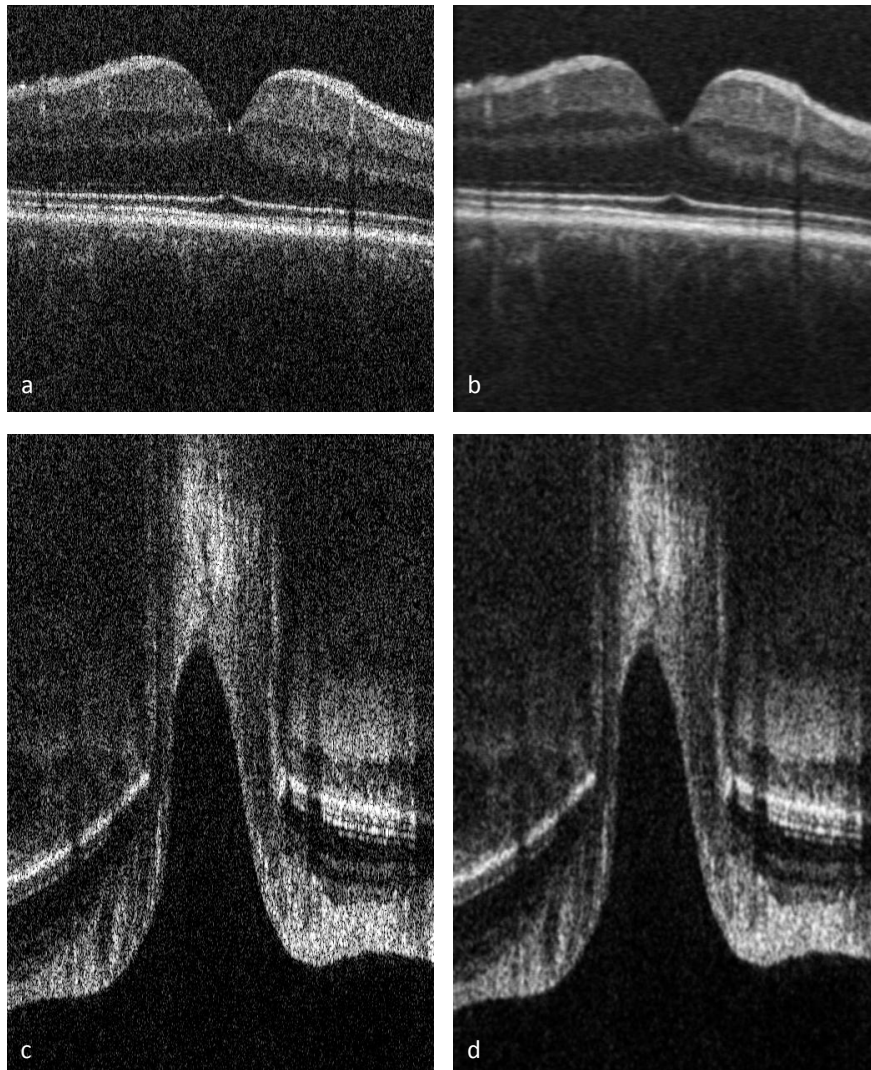


Figure 2.4: Macula (above) and optic nerve head (ONH, below) images before (a and c) and after (b and d) filtering to improve visibility of retinal and ONH structures. Note the OCT datasets were not scaled correctly at this stage.

2.4.4 Image scaling and pixel calibration

2.4.4.1 Transverse pixel calibration

Image datasets from the OCT device were not scaled correctly after image acquisition, due to the interferometric properties of OCT that produce a decoupling of the transverse and axial resolution.

The OCT device produced a collimated beam that was focussed on the posterior eye in order for a clear image to be produced. Therefore the transverse scaling of an image is dependent on the optics of the eye being imaged. The calculation of transverse pixel calibration requires knowledge of the angle of the scan (A) and the distance between the stationary point of the eye and the retina (r ; see Figure 2.5). The stationary point is the point in the eye at which a beam of light passing through, in this case the OCT beam has equal angle to the angle on the retina.

The stationary point is close to the centre of curvature of the retina, so the calculation for the circumference of a circle, $2\pi r$, can be used to find the scan size on the retina using:

$$\begin{aligned}\text{Scan size on retina} &= \text{fraction of circumference covered by angle } A \\ &= 2\pi r (A / 360)\end{aligned}$$

The transverse pixel calibration can then be calculated using the formula:

$$\text{Transverse pixel calibration} = (2\pi r (A / 360)) / n$$

Where:

n = number of pixels in the scan

A = scan angle

r = radius of the eye, or the distance from the stationary point to the retina.

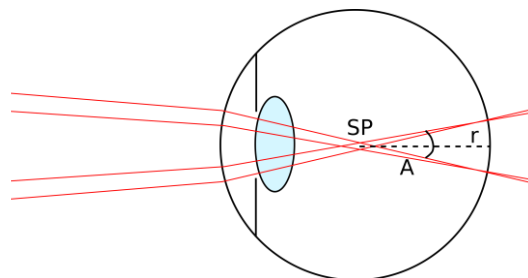


Figure 2.5: Schematic diagram of eye showing the measurements required to calculate the transverse pixel scaling. SP = stationary point of the eye, A = scan angle, r = distance from SP to the retina.

The stationary point is not constant in each participant because axial eye length varies, and there are currently no devices to measure the stationary point to retina distance. If the eye is considered as a

simple thin lens, where all refraction occurs at a single point in the eye's principle plane, then r can be calculated using the formula:

$$r = (\text{axial length} - 1.6)/1.4$$

where 1.4 is the grouped refractive index of the eye and 1.6 is the distance from the cornea to the principle plane (based on the Gullstrand model of the eye).

2.4.4.2 Transverse scaling according to axial length

When taking measurements in the transverse direction on OCT images the transverse pixel calibration was corrected for axial length of each eye using the modified Littmann equation BRE2 (Bennett et al. 1994), based on improvements from Littmann's (1988) original calculations for measuring the true size of retinal features. The BRE2 formula is:

$$t = p * q * s$$

where:

t = the true size of an image

p = a constant for the machine used (for our research OCT device this value is 3.382)

q = axial length – 1.82

s = (number of pixels * transverse pixel calibration)/1000

The transverse pixel calibration was determined using the calculations described above. The average transverse pixel calibration for a 20° OCT scan was 10-12 μm /pixel.

2.4.4.3 Axial pixel calibration

The axial pixel calibration of the OCT device was not affected by the optical properties of the participant eye so was a fixed number for all participants. This was calculated by imaging an object of known size using the OCT device then measuring the image size in pixels. The image size in μm was divided by the number of pixels resulting in the axial scaling of the OCT device in air, which was

found to be $2.578 \mu\text{m}/\text{pixel}$. This was then divided by the refractive index of the eye, which was taken to be 1.4, in order to calculate the pixel calibration for ocular OCT images. The axial scaling of the OCT images was therefore $1.84 \mu\text{m}/\text{pixel}$.

2.4.5 Scaling according to calculated pixel values

After data acquisition and initial processing the transverse and axial pixel calibrations were input into the OCT image files in ImageJ in order to scale the images correctly. Example images of a macula and ONH OCT scan before and after image scaling according to the above parameters is shown below (Figure 2.6).

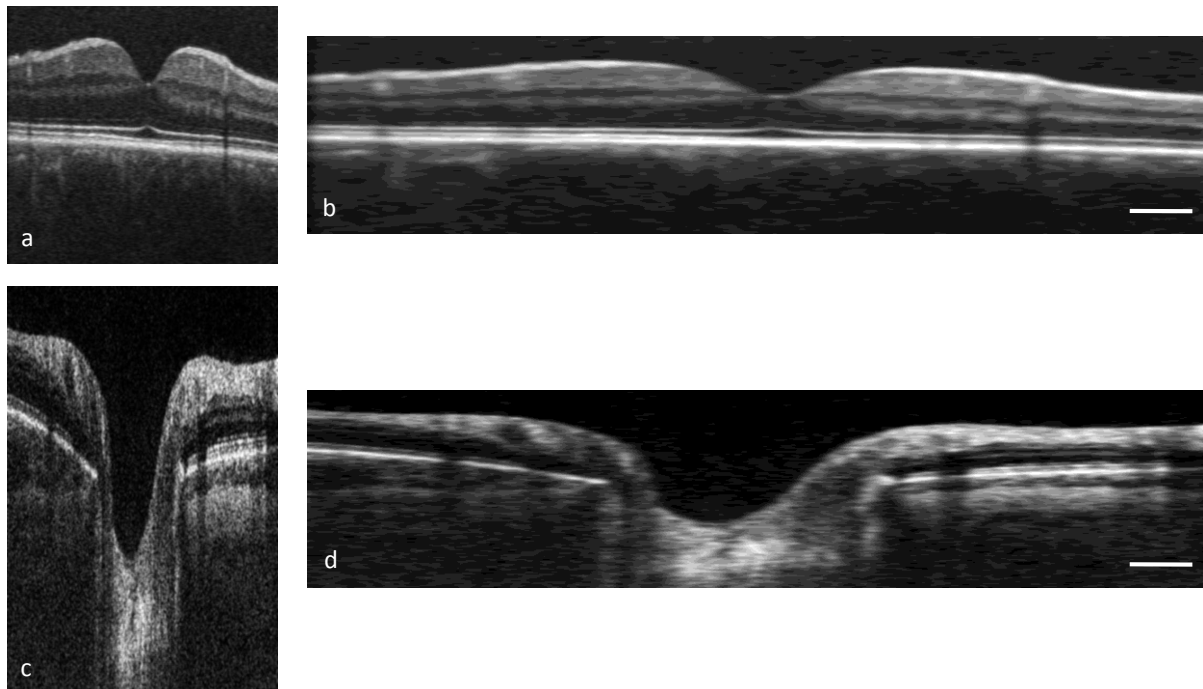


Figure 2.6: Processed OCT images of the macula (above) and optic nerve head (ONH, below) prior to (a and c) and after (b and d) scaling using the modified Littmann equation. Note ONH images have been flipped vertically. Scale bars = $500 \mu\text{m}$

2.4.6 Criteria for classification of optic nerve heads and maculae into stages of glaucoma

Participant eyes were grouped into glaucoma stages based on optic nerve head appearance, IOP and visual field loss using a criteria adapted from Hodapp et al. (1993). The criteria are provided in Table

2.2. Where a participant had one eye with glaucoma and one without, the eye without was considered ‘suspect glaucoma’ and excluded from analysis. Group classification was performed after all image measurements had been taken, so that the examiner was masked as to the health status of the eye during analysis.

Classification of glaucomatous disease	Features
Control	<ul style="list-style-type: none"> • No diagnosis of glaucoma • No other ocular pathology • No visual field defect • IOP \leq21 mmHg
Preperimetric (PG)	<ul style="list-style-type: none"> • No visual field defect detected • Positive glaucoma diagnosis from a consultant ophthalmologist based on either ONH damage or progression from a lower baseline IOP
Early (EG)	<ul style="list-style-type: none"> • MD less than -6.00 dB • Less than 25% of the points (18) are depressed below 5% level and less than 10 points are depressed below 1% level on pattern deviation plot • All points in central 5° have sensitivity of at least 15 dB
Advanced (AG)	<ul style="list-style-type: none"> • MD less than -12.00 dB • More than 25% of the points (18) are depressed below 5% level and less than 10 points are depressed below 1% level on pattern deviation plot • No points in the central 5° have a sensitivity of 0 dB

Table 2.2: Classification of glaucoma staging, adapted from Hodapp et al. (1993).

2.4.7 Orientation of the OCT datasets

To ensure correct orientation of datasets maximum intensity projections (MIP) of the OCT images were compared to fundus photographs and flipped or rotated as necessary (Figure 2.7).

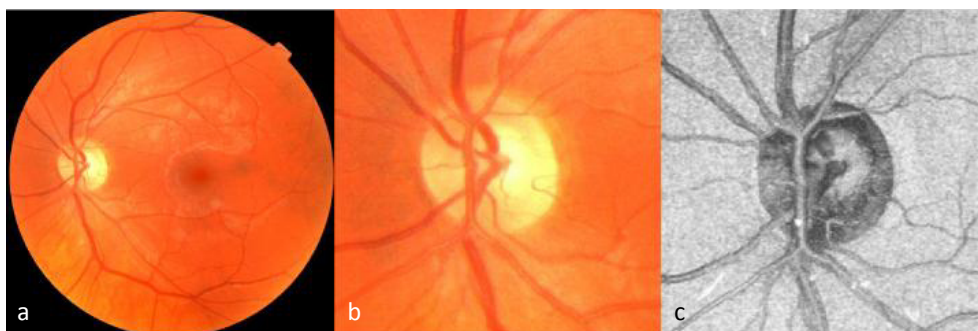


Figure 2.7: The correct orientation of the images was ensured by comparing a maximum intensity projection of the OCT dataset (c) to the corresponding fundus photograph (a and b) and flipping or rotating the OCT dataset as required.

2.5 Analysis of the inner retinal layers in glaucomatous and healthy eyes

The following methods were used in the study 'Analysis of the inner retinal layers in glaucomatous and healthy eyes' (Chapter 3). The aim of the chapter was to investigate regional differences in the thickness and volume of the macular nerve fibre layer (mNFL), inner plexiform layer (IPL), ganglion cell layer (GCL) and ganglion cell complex (GCC) in control eyes and those with glaucoma.

2.5.1 Manual image segmentation

OCT datasets were masked as the their glaucoma classification during segmentation. The central image of each macula image stack was determined by examining the dataset in ImageJ to identify the deepest point of the foveal pit. Every four b-scans were block-averaged either side of the foveal pit using a custom MATLAB-based software in order to enable better visualisation of the retinal layers.

The look up table (LUT) for each image was then inverted to further improve visibility between retinal layers and the inner retinal layers were delineated using `Manseg_Anylayer` version 1.0 (F Rakebrant, Cardiff University), a custom-written MATLAB-based software. This software was used to manually mark along the top of the mNFL, and the boundaries between mNFL-GCL, GCL-IPL, and IPL-inner nuclear layer (INL) allowing for the segmentation of the mNFL, GCL and IPL in each averaged b-scan (Figure 2.8).

Segmentation criteria were that: the surface of the blood vessels above the mNFL would be segmented exactly, in order to mimic edge detection algorithms in commercial devices; and for other retinal boundaries a line was extrapolated through the blood vessels.

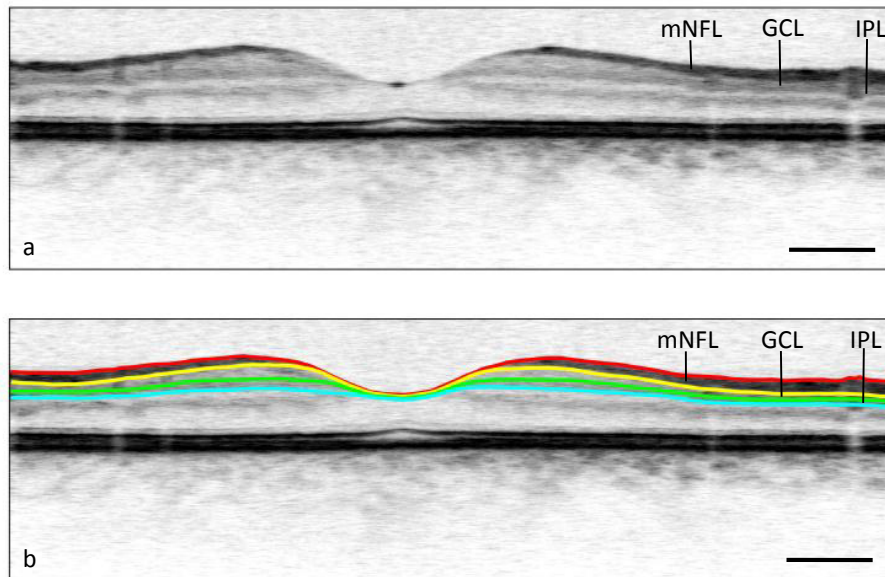


Figure 2.8: (a) Macula OCT b-scan with (b) segmentation of the macular nerve fibre layer (mNFL), ganglion cell layer (GCL) and inner plexiform layer (IPL). Scale bar = 500 μm .

2.5.2 Classification of eyes according to stage of glaucoma

After segmentation, eyes were classified into stage of glaucoma, as described in section 2.4.6.

2.5.3 Colour-coded thickness maps

A custom-written MATLAB program (F Rakebrant, Cardiff University) was used to create colour-coded thickness maps of the mNFL, GCL, IPL and GCC, by calculating the difference between two segmented boundaries at each point and converting this value to microns, according to the calculations described in section 2.4.4.

Images were displayed with a graduated colour scale, with thicker regions displayed in red and thinner regions in blue. Colour maps for each dataset were compared to the corresponding visual field plot. All the datasets were arranged in order of increasing mean deviation of visual fields (i.e. increasing visual field loss) in order to identify trends in visual field loss and equivalent regions of retinal thinning.

2.5.4 Regional analysis of retinal layer thickness and volume

The colour coded thickness maps were then subdivided into 13 regions in order to examine regional differences. To this purpose, a grid consisting of 13 regions was placed over the thickness maps centred on the fovea. The grid split the macula into the central 1.5° and concentric rings at 2.5°, 5.5° and 8.6° eccentricity, with two divisions along the superior-inferior and temporal-nasal planes to split the macula into quadrants (see Figure 2.10a). The grid was manually placed over the fovea, using the (x,y) co-ordinates of both the original and averaged TIFF image file in ImageJ, and then correspondence was visually checked on the thickness maps. The mean thickness and volume of each retinal layer was calculated for each individual region (R) by computing the distance between the two segmentation lines for each retinal layer, while the GCC was calculated from the mNFL and the IPL-INL boundary line, as a measure of the mNFL, IPL and GCL combined.

Thickness and volume were calculated for each individual region to examine changes with increasing glaucoma stage for mNFL, GCL, IPL and GCC. The IPL:mNFL and IPL:GCL thickness ratios were also calculated for each region in each retinal layer. Regions within a ring of equal eccentricity from the fovea (i.e. inner, middle and outer macula) were compared to each other (see Figure 2.10b, c and d) for the GCC, mNFL, GCL and IPL for each stage of glaucomatous progression in order to determine whether damage occurred primarily in a specific area.

The individual regions were also grouped to form:

- Full-quadrants (e.g. R1, 5 and 9 grouped to form inferior-nasal, Figure 2.10e)
- Inner-quadrants (R5 and 9 grouped to form inner inferior-nasal, Figure 2.10f)
- Full- superior and inferior (R1, 2, 5, 6, 9 and 10 to form inferior, Figure 2.10g)
- Inner- superior and inferior (R5, 6, 9 and 10 to form inner-inferior, Figure 2.10h)

2.5.5 Repeatability of retinal segmentation technique

To assess reproducibility of the technique, ten datasets were selected at random for segmentation by both the main examiner (BF) and an outside observer experienced in the technique. The thickness for each of the three retinal layers (mNFL, GCL and IPL) and the GCC were then calculated. Bland-Altman plots were created to assess agreement between two observers for each retinal layer thickness. The reproducibility results for each of the retinal layers assessed are shown in Figure 2.9. Using this method, the repeated measures were statistically similar and within the 95% confidence intervals therefore the technique is repeatable.

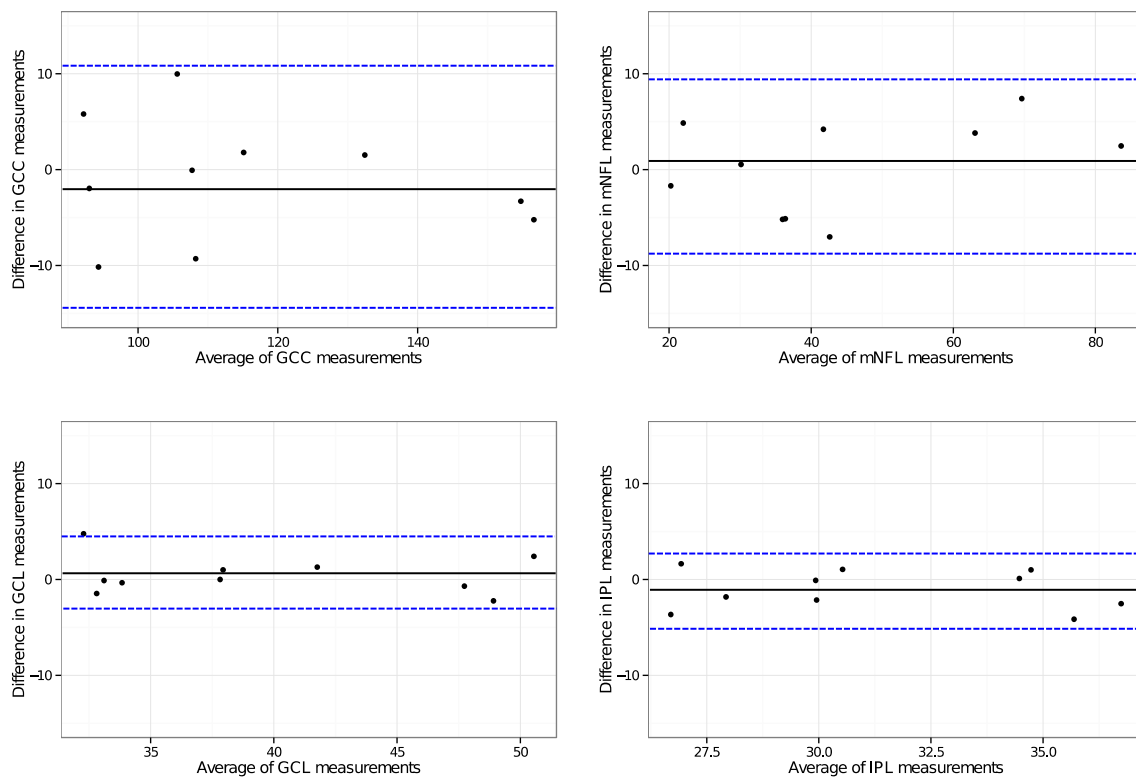


Figure 2.9: Bland-Altman plots to assess agreement between repeated measures of the mean thickness for ganglion cell complex (GCC), macular nerve fibre layer (mNFL), ganglion cell layer (GCL) and inner plexiform layer (IPL). Black line indicates mean difference between two measurements, blue lines indicate mean \pm 2 standard deviations.

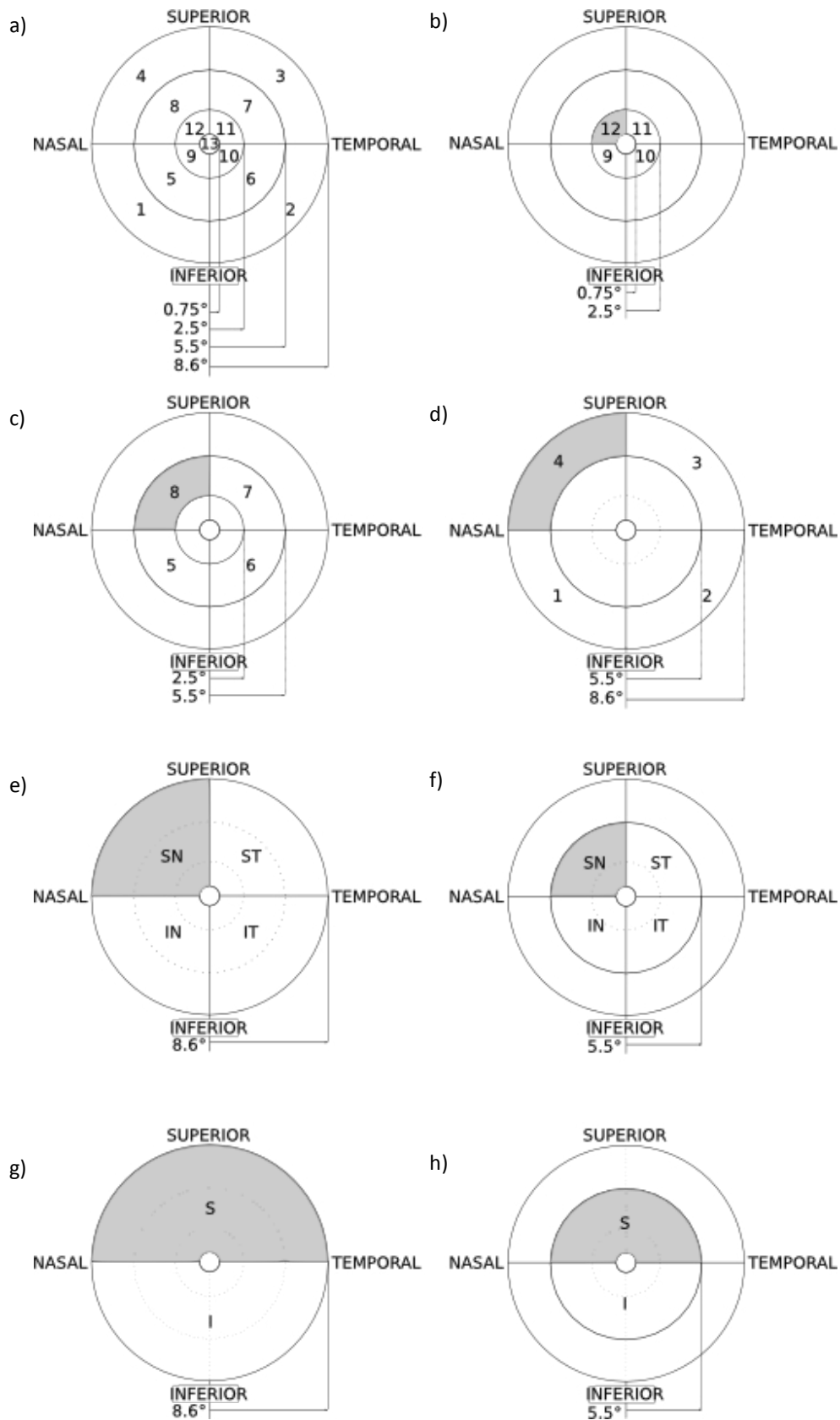


Figure 2.10: (a) Retinal thickness maps were divided into 13 regions centred on the fovea. Regions of equal eccentricity from the fovea were compared for (b) inner (0.75° - 2.5°); (c) middle (3.5° - 5.5°); and (d) outer areas (5.5° - 8.6°). Regions were grouped to form (e) quadrants (superior-nasal shaded); (f) inner-quadrants (inner- superior-nasal shaded); (g) hemizones (superior shaded); and (h) inner-hemizones (inner-superior shaded).

2.6 Analysis of the optic nerve head in aging and glaucoma in 2D OCT images

The following methods were used in the studies ‘Analysis of age related changes in *in vivo* human optic nerve head microstructure’ (Chapter 4) and ‘2D optic nerve head parameters as a function of glaucoma progression’ (Chapter 4). The aim of these chapters was to characterise regional differences in the prelamina and lamina cribrosa thickness and depth from Bruch’s membrane opening (BMO), as well as nerve fibre layer thickness, with respect to aging (Chapter 4) and glaucoma (Chapter 5).

Analysis in 2D images were performed on 18.7° (young) or 20° (for older controls and glaucoma data) 1050 nm OCT datasets centred on the ONH, taken with the choroid closest to the zero delay (i.e. enhanced depth imaging). To determine the centre of each ONH, the image stacks were ‘flattened’ into a maximum intensity projection in the *enface* plane (Figure 2.11a), and the edge of the ONH was demarcated using the polygon selection tool in ImageJ (Figure 2.11b). The centroid of the ONH outline was determined. A horizontal line 3600 μm long was then placed starting at the temporal side of the disc with the middle through the centroid of the ONH on the 3D image stack (i.e. through the patient’s temporal-nasal plane, Figure 2.11c). This line was used as a reference to create a 45° radial reslice through the ONH (Figure 2.11d), resulting in four 2D b-scan images that showed the temporal (T) –nasal (N) plane, superior (S) – inferior (I) plane, and the two diagonals ST-IN and SN-IT (Figure 2.12). A ‘T’ was drawn in the top corner of the temporal-nasal plane for reference. The look up table (LUT) of each image stack was inverted to improve discrimination between the ONH structure boundaries.

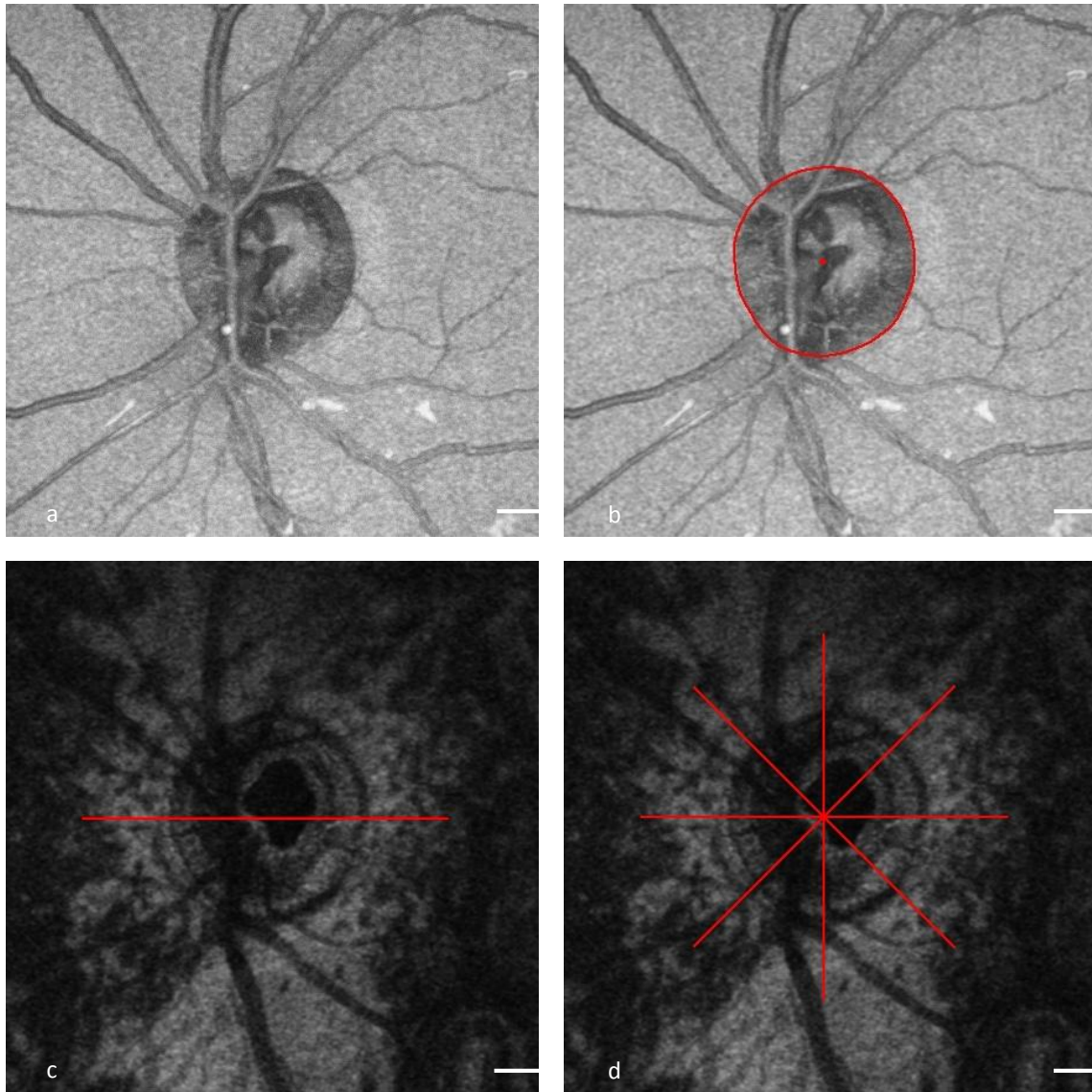


Figure 2.11: (a) 3D OCT image stacks were averaged using maximum intensity projections (MIP) of the optic nerve head (ONH). (b) The edge of the optic disc was demarcated and the centroid located. (c) A horizontal line 3600 μm long was placed through the ONH on the 3D OCT dataset, through the centroid. (d) A radial grid at 45° intervals starting at the baseline was used to create four radial b-scans. Scale bar = 500 μm

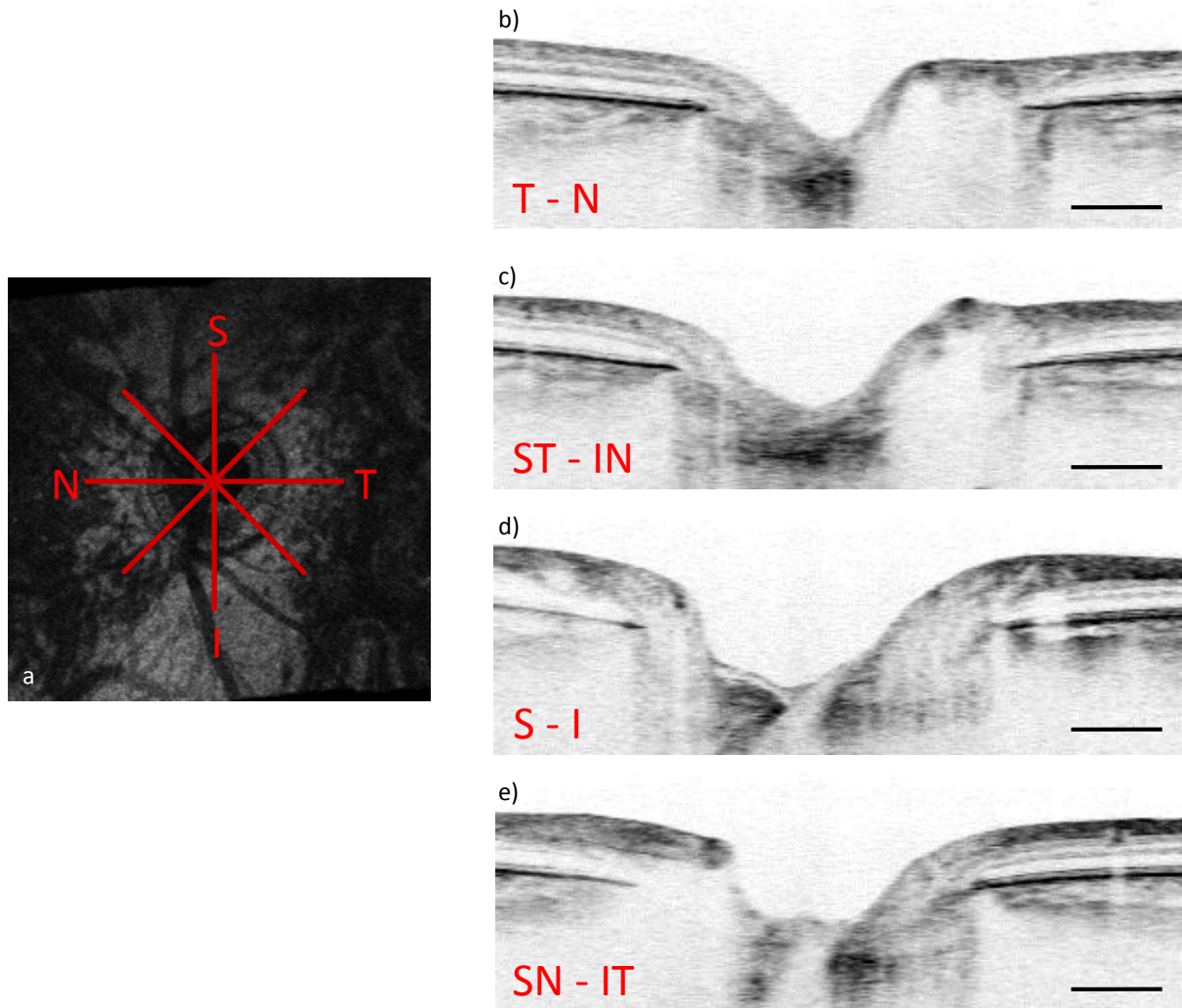


Figure 2.12: (a) A 45° radial reslice starting at the temporal side of the disc was used to create four radial B-scans in the (b) temporal-nasal, (c) superior temporal-inferior nasal, (d) superior-inferior, and (e) superior nasal-inferior temporal planes. Scale bar = 500 μm

Measurements were performed at the locations shown in Figure 2.13.

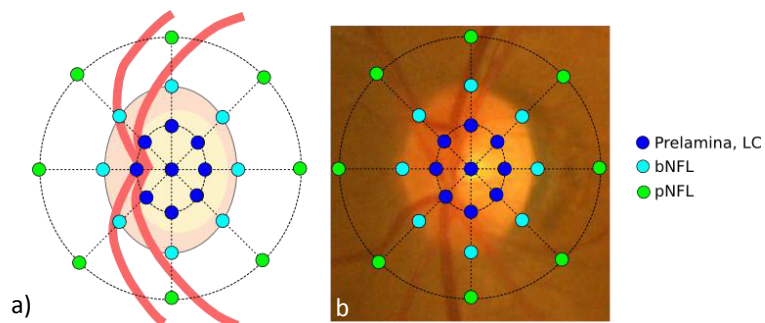


Figure 2.13: (a) Schematic diagram and (b) fundus photograph of a left optic nerve, with a grid superimposed demonstrating the location of prelamina and lamina cribrosa (LC) measurements (blue), border nerve fibre layer (bNFL, cyan) and peripapillary nerve fibre layer (pNFL, green).

On each radial b-scan, two terminations of Bruch's membrane at the edge of the ONH, i.e. Bruch's membrane opening (BMO), were determined and the (x,y) coordinates on the image noted. A line from either side of BMO was drawn using ImageJ and the length was measured (Figure 2.14a). The (x,y) coordinates of each side of BMO were used to calculate the midpoint and two quartiles of the BMO line. At each of these points, the distance was measured from BMO to the anterior prelamina surface to calculate prelamina depth (Figure 2.14b); to the posterior prelamina/anterior lamina cribrosa (LC) surface to calculate anterior LC depth (Figure 2.14c); and to the posterior LC surface to calculate posterior LC depth (Figure 2.14d). Additionally, the vertical distance from each BMO endpoint to the prelamina surface directly above it, i.e. the retinal nerve fibre layer thickness at BMO (border nerve fibre layer, bNFL; Figure 2.14g), was measured, as well as the peripapillary nerve fibre layer (pNFL, Figure 2.14g) at a point 1.7 mm from the centre of BMO. This was to mimic the equivalent measurement that can be acquired on some commercial OCT devices.

In some cases the prelamina depth was above the BMO reference plane. In these instances, the distance from BMO to the prelamina surface was recorded as a measurement with a negative value, whereas the distances below BMO were given a positive value (see Figure 2.15). This allowed the prelamina thickness to be calculated at each point by subtracting prelamina depth from anterior LC depth. In the same way, the LC thickness could be calculated by subtracting the anterior LC depth from posterior LC depth (Figure 2.15).

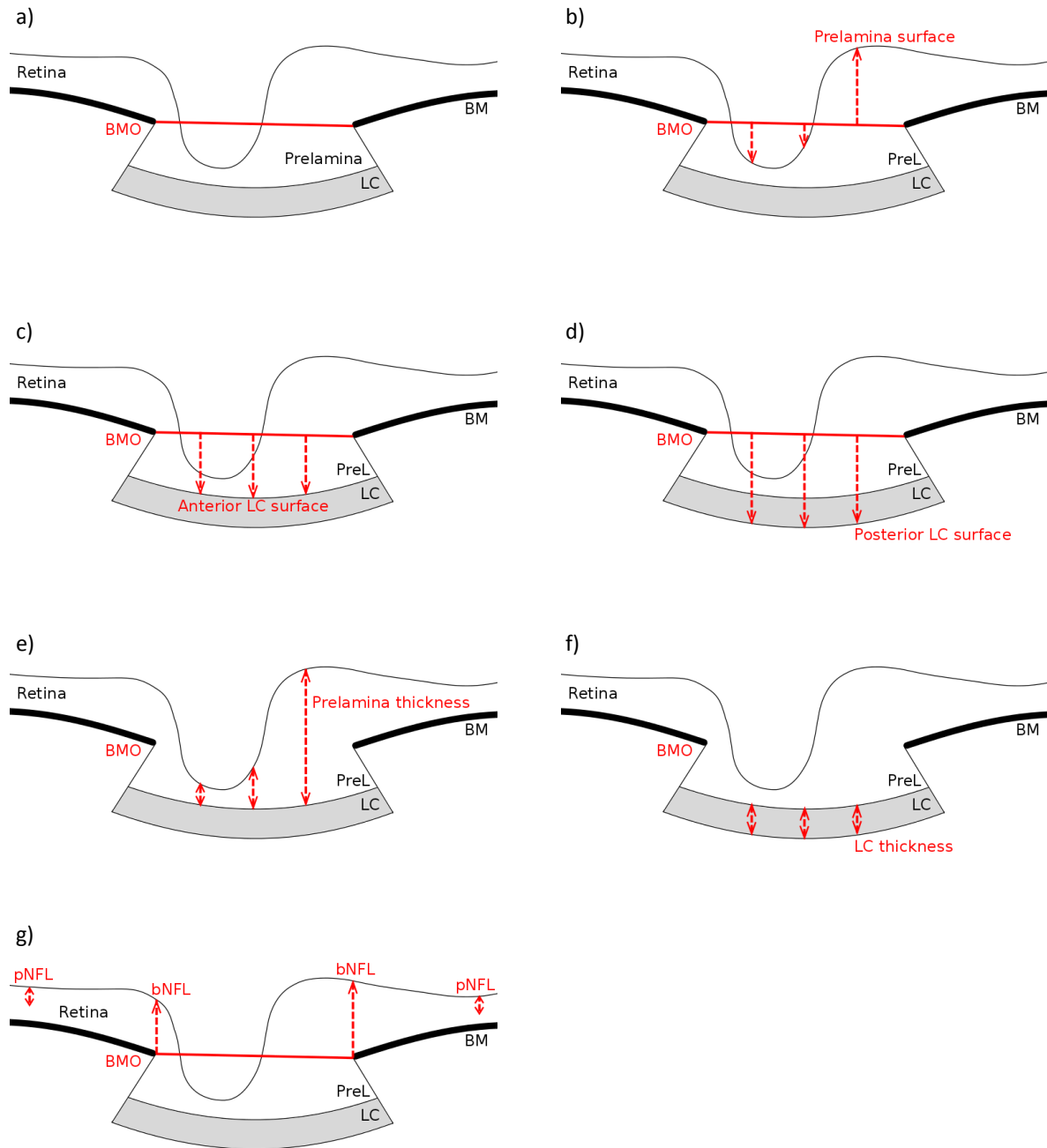


Figure 2.14: (a) Bruch's membrane opening (BMO) diameter in red. The distance from BMO to (b) the prelaminar depth, (c) anterior lamina cribrosa (LC) depth and (d) posterior LC depth was measured and the midpoint of BMO and at the two quartiles (for mid-periphery). This allowed the calculation of (e) prelaminar thickness and (f) LC thickness. (g) Nerve fibre layer thickness was measured at BMO (bNFL) and at 1.7mm from the centre of the optic disc (pNFL).

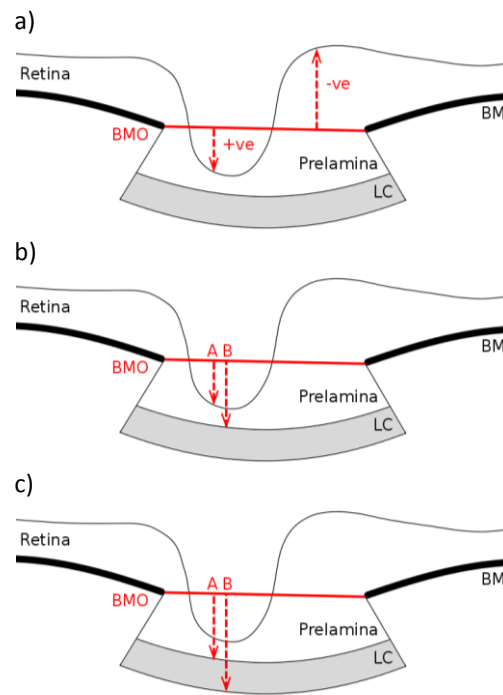


Figure 2.15: Schematic diagram of prelamina measurements above and below BMO (top). Prelamina thickness (middle) and lamina cribrosa thickness (below) could be calculated by subtracting the anterior surface depth (A) from posterior surface depth (B). BM = Bruch's membrane, BMO = Bruch's membrane opening, LC = lamina cribrosa.

2.6.1 Repeatability of 2D optic nerve head measurement technique

To investigate repeatability of the 2D technique ten datasets were selected at random and measured, then masked and measured a second time by the same examiner. BMO in the superior-inferior plane, central prelamina depth, anterior and posterior depth, were calculated. Bland-Altman plots were used to assess agreement between results. The plots are shown in Figure 2.16.

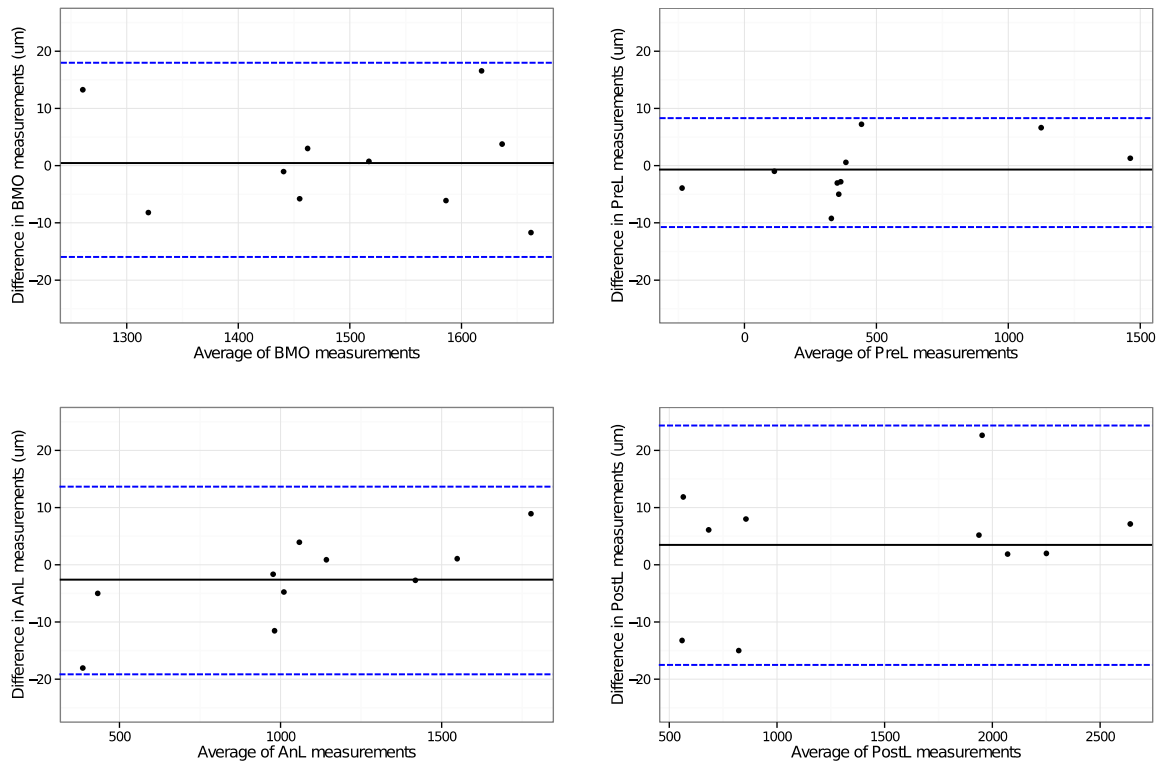


Figure 2.16: Bland-Altman plots to assess agreement between repeated measures for Bruch's membrane opening (BMO) in the temporal-nasal plane, and prelamina depth (PreL), anterior lamina cribrosa depth (AnL) and posterior lamina cribrosa depth (PostL) in the central region. Black line indicates mean difference between two measurements, blue lines indicate mean \pm 2 standard deviations.

2.7 3D volumetric measurements of the optic nerve head in glaucomatous and healthy subjects

The following methods were used in the chapter '3D volumetric measurements of the optic nerve head in glaucomatous and healthy subjects' (Chapter 6). The aim of this chapter was to quantify Bruch's membrane opening (BMO) as a 3D surface, and quantify cup volume, prelamina volume, and lamina cribrosa volume in healthy and glaucomatous eyes.

The 3D analyses were performed on 20° optic nerve head OCT datasets. The datasets were imported into Amira (version 5.4.0; Visage Imaging, Pro Medicus, Australia) and the correct pixel calibration (as calculated in section 2.4.4) was input. A landmark was placed at the centre of the ONH based on visual examination of the enface view (Figure 2.17a). A radial slice was selected through this central

point, and two landmarks were placed at BMO on either side of the ONH (Figure 2.17b). The radial slice was then rotated by 15° around the central point and additional landmarks placed at BMO (Figure 2.17c). This was repeated until the BMO was segmented around the entire ONH (Figure 2.17d). The OCT tomograms were then hidden, leaving just the landmarks (Figure 2.17e), which were subsequently joined together to generate a surface using the PointWrap tool (Figure 2.17f-h). The area of this surface was then measured as a representation of optic disc size.

The BMO surface was then superimposed over the OCT tomograms (Figure 2.17h, Figure 2.19a), and landmarks were placed along the boundary between the BMO surface and the optic cup, i.e. the anterior prelamina surface (Figure 2.19b). The radial slice was then rotated by 15° around the central point and placement of the landmarks was repeated. This process was repeated until the entire optic cup was demarcated (Figure 2.19c-d). The landmarks were joined using the Pointwrap tool to recreate the volume of the optic cup (Figure 2.19e-h). This surface was used to calculate the volume of the cup below BMO.

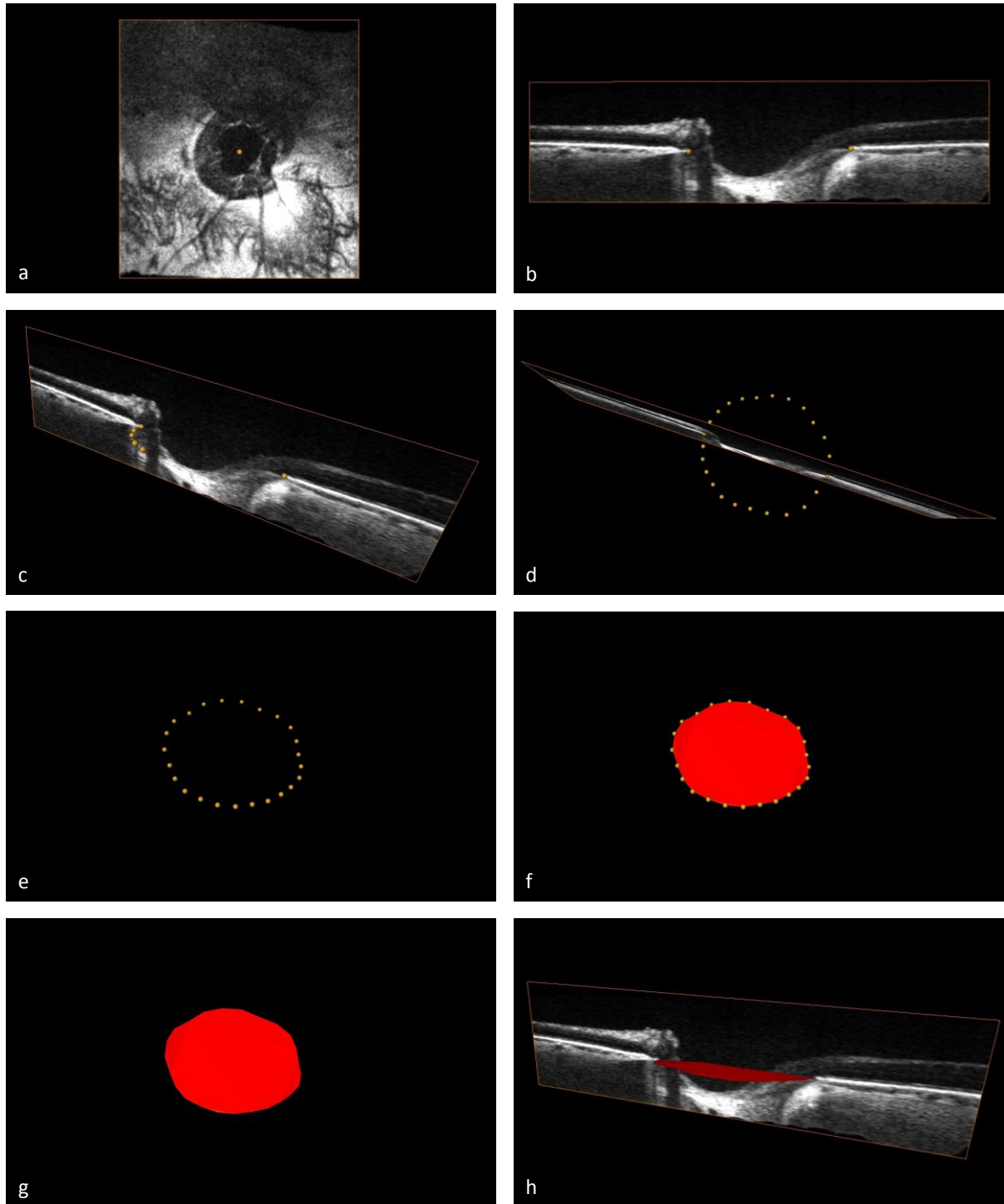


Figure 2.17: (a) An *enface* view of the optic nerve head (ONH) in the left eye of a myopic 65 year old male with glaucoma. A landmark is placed at the centre of the optic disc. (b) A radial slice through the 3D dataset with landmarks denoting either side of Bruch's membrane opening (BMO). (c) The radial slice was rotated at 15° intervals and BMO was marked on each side until (d, e) the entire BMO was demonstrated. (f) The landmarks were joined to create a 3D surface demonstrating BMO. (g) The landmarks were hidden from the edge of BMO. (h) BMO surface superimposed over a radial slice of the OCT tomogram.

The landmarks and surface used to measure the optic cup were hidden, and the BMO surface was superimposed back over the original OCT dataset. Landmarks were placed along the boundary of the anterior LC surface and the BMO surface (Figure 2.20) using the same technique until the entire prelamina was segmented. Pointwrap was used to recreate the region encompassed by BMO and the anterior LC surface, and the volume was calculated. Subsequently, the volume of the optic cup below BMO was subtracted from this value in order to determine the volume of the prelamina below BMO (Figure 2.18). Additionally, the lamina cribrosa volume was calculated where it was visible. This was performed by placing landmarks along the anterior and posterior LC surface at 15° intervals, as described previously. The LC was recreated using Pointwrap, and the volume was calculated.

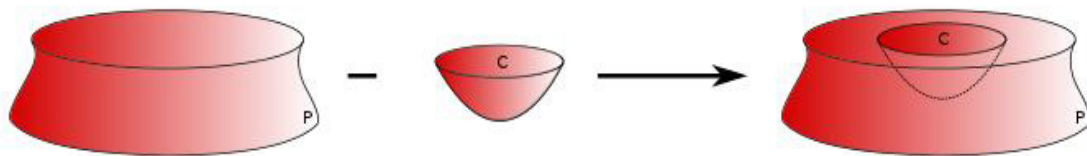


Figure 2.18: The volume of the optic cup (C) was subtracted from the volume of the area between the anterior LC surface and BMO (P), in order to calculate the volume of the prelamina below BMO.

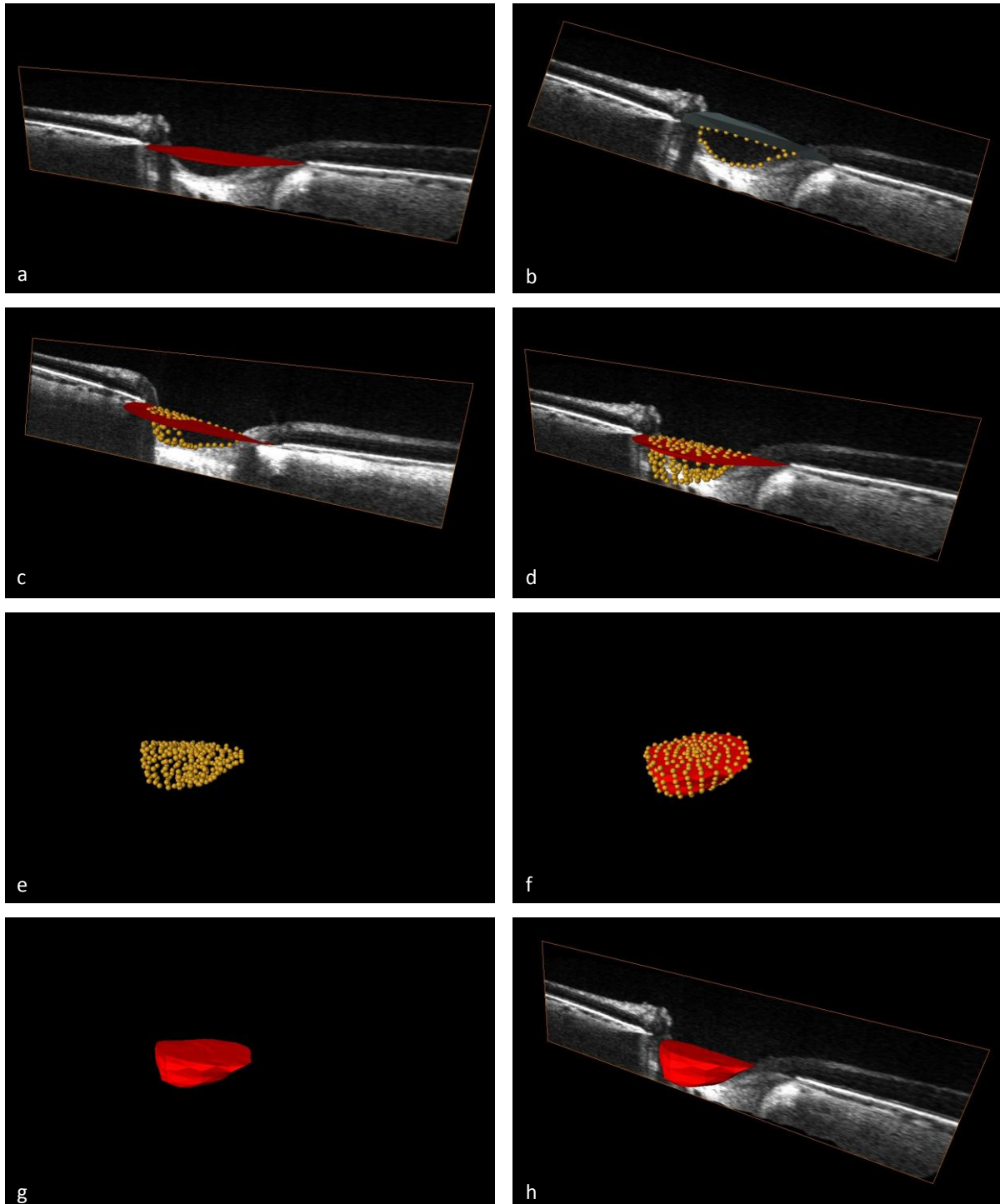


Figure 2.19: (a) An oblique radial slice of the ONH in the left eye of a myopic 65 year old male with glaucoma. The BMO surface is superimposed over the B-scan. (b) Landmarks were placed along the boundary between the BMO surface and the optic cup. (c) The radial slice was rotated at 15° intervals and landmarks were placed along the BMO-optic cup boundary on each B-scan until (d) the entire optic cup was demarcated. (e) The radial B-scan was hidden leaving just the landmarks, which were then (f) joined to create a 3D surface demonstrating the optic cup below BMO. (g) The landmarks were hidden, leaving just the surface, which was then (h) superimposed over a radial slice of the OCT tomogram.

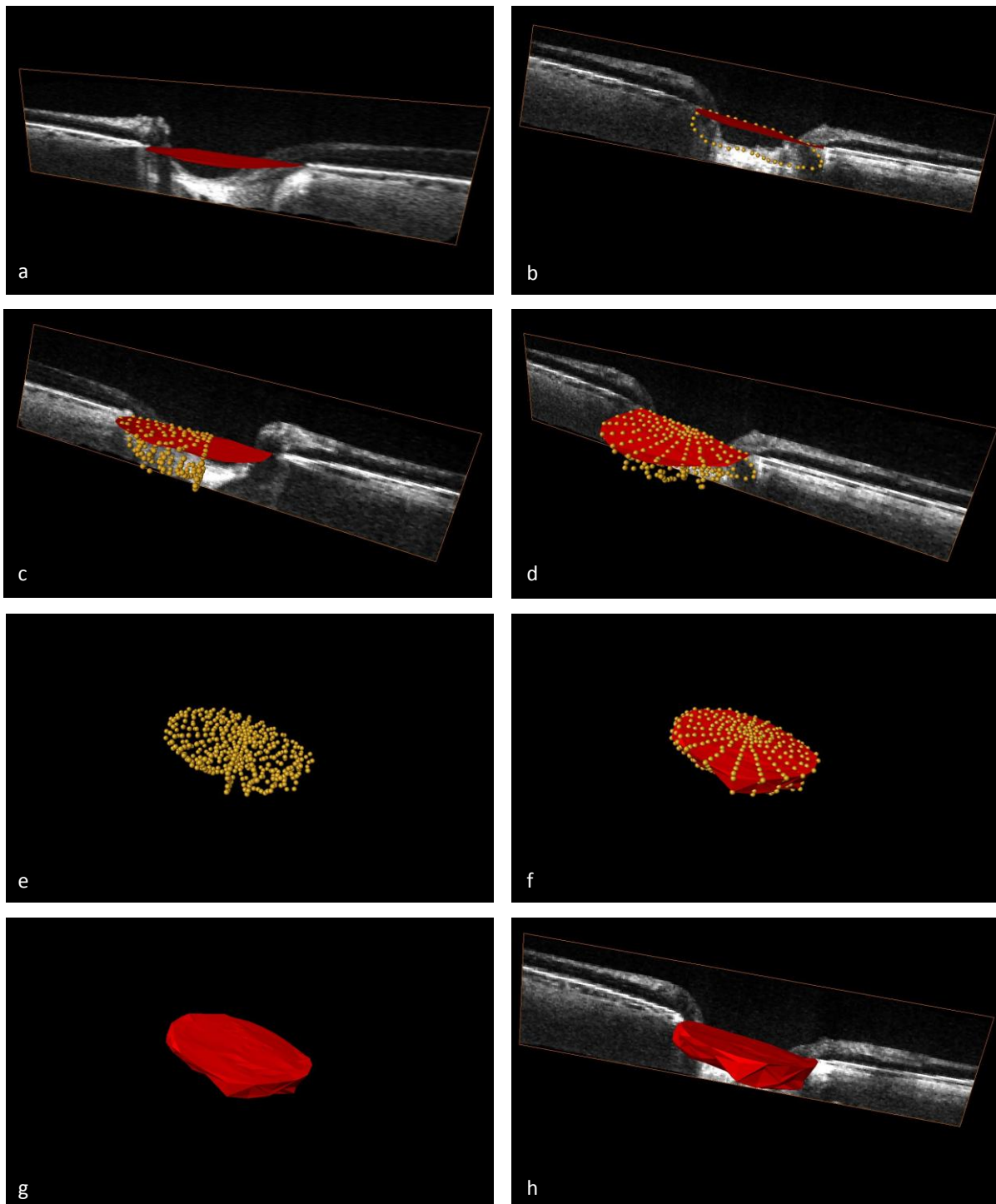


Figure 2.20: (a) An oblique radial slice of the ONH in the left eye of a myopic 65 year old male with glaucoma. The BMO surface is superimposed over the B-scan. (b) Landmarks were placed along the boundary between BMO surface and the posterior prelamina surface, i.e. the anterior LC surface. (c) The radial slice was rotated at 15° intervals and the BMO-prelaminar boundary was marked on each B-scan until (d) the entire prelaminar volume below BMO was demarcated. (e) The radial B-scan was hidden leaving just the landmarks, which were then (f) joined to create a 3D surface demonstrating the volume of the prelaminar and optic cup below BMO. (g) The landmarks were hidden, leaving just the surface, which was then (h) superimposed over a radial slice of the OCT tomogram.

2.8 Microstructural analysis of the lamina cribrosa in healthy and glaucoma eyes

The following methods were used in the study ‘Microstructural analysis of the lamina cribrosa in healthy and glaucomatous eyes’ (Chapter 7). The aim was to investigate LC beam orientation and coherence to determine whether there were regional glaucoma-related differences compared to controls.

For this study greater resolution was required in order to resolve the microstructure of the LC connective tissue thus 10° OCT scans centred on the optic nerve head were acquired. The anterior surface of the LC was located in enface OCT datasets. The second section in each dataset (slice 2) was selected so that the structures of both the central and peripheral LC were visible. Thus the anterior LC surface was determined from the centre of the LC rather than the depth at which the LC insertion points could be determined. Because of the curvature of the LC, the initial section (slice 1) contained both peripheral LC and some prelamina. As a result, datasets were cropped from 50 μm prior to the central anterior LC surface and block averaged to create 50 μm ‘thick’ optical slices, resulting in 5-6 slices per OCT dataset, referred to by their order. The slice number with corresponding depth into the LC is shown in Table 2.3.

Slice number	Depth into lamina cribrosa
S1 (contains some prelamina)	0 - 50 μm
S2	50 - 100 μm
S3	100 - 150 μm
S4	150 - 200 μm
S5	200 - 250 μm
S6	250 - 300 μm

Table 2.3: Lamina cribrosa (LC) slice number (S) and corresponding depth into LC.

OrientationJ, an ImageJ plugin (version 19.11.2012, Resakhaniha et. al, Biomedical Imaging Group, EPFL, Sweden) was then used to create colour-coded coherence and orientation maps for each averaged section of LC, allowing visualisation of areas of the ONH with higher connective tissue alignment and the dominant orientation in a given region.

The averaged datasets were analysed using 'ONHseg' macro (version 1.0, N White, VSBL, Cardiff University) in ImageJ, which facilitated the division of the ONH into 12 clock-hour type regions (Figure 2.21). The coherence and preferred orientation of connective tissue within each of these regions was determined using 'OrientationJ'. This program defined orientation as the dominant direction of the features within a region of interest, with the outcome a value between $\pm 90^\circ$. A result of 0° represented the horizontal x-axis, $+90^\circ$ was the vertical y-axis in the superior direction, while -90° depicted the inferior vertical meridian. Coherence was defined as how closely the features within an image were orientated. A coherence of 1 indicated a region where all features within an image were aligned in the same direction, and a coherence of 0 indicated an image where the features were distributed randomly.

Retinal blood vessels produce significant shadows on OCT images, and as such, data from the nasal side of the ONH was discarded immediately. Regions from the temporal ONH were then examined and those containing blood vessels or vascular shadows were also removed prior to analysis.

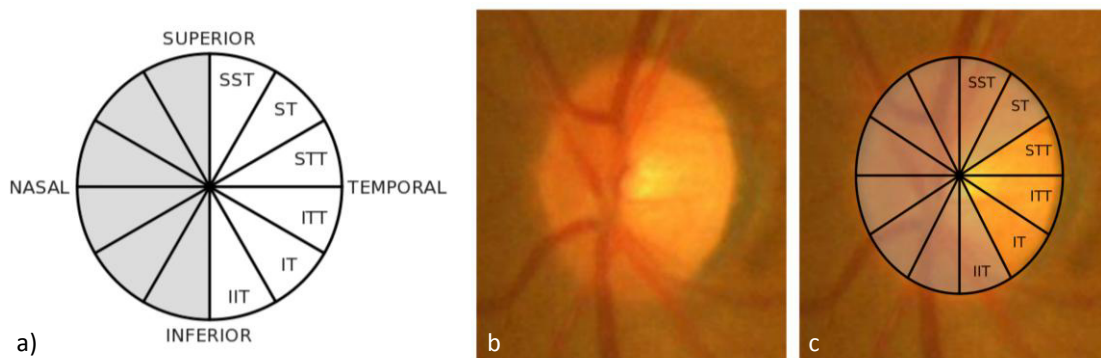


Figure 2.21: (a) Schematic diagram of division of optic nerve head (ONH) regions of a left eye, with nasal side of the ONH greyed out as the measurements were discarded due to vascular shadowing. (b) Fundus photo of optic nerve head with (c) grid overlay showing regional division. Additionally, in this example the SST, ST and IIT regions were greyed out due to blood vessels within the regions. S = superior, T = temporal, I = inferior.

2.9 Statistical analysis

The question of whether or not it is statistically appropriate to use the data of fellow eyes in ophthalmological research is an important one. A common approach to overcome the lack of independence that is inherent in fellow eye data is simply to discard it. Another commonly used approach is to average the data from fellow eyes (Cheng et al. 2000). While these methods are appropriate, a number of more advanced statistical methods exist that circumvent the issue of data autocorrelation, or independence, without having to reject fellow eye data, i.e. variance (Burton et al. 1998; Fan et al. 2011). Referring to the use of such methods (which include, e.g. general linear [mixed effects] models), Glynn and Rosner (1992) state that:

'Specific advantages [of using fellow eyes with an appropriate statistical approach] include enhanced statistical power, more interpretable regression coefficients, greater precision of estimation, and less sensitivity to missing data for some eyes', and follow to state that: 'these models should be used more frequently in ophthalmologic research'.

The journal *Ophthalmic and Physiological Optics* (OPO) refer authors of ophthalmic research articles to Murdoch et al. (1998) for advice on the matter; they state that while it is not wrong to discard data from fellow eyes is *'a waste'* and, instead, researchers should consult with a statistician to utilise techniques that account for the lack of independence in data.

A recent meta-analysis study looking at the statistical approaches used to circumvent the issue of how fellow eye data is handled showed that just 38% of studies included data from both eyes and only 7% of these appropriately account for the resulting autocorrelation (Karakosta et al. 2012). Furthermore, of the 31% or articles that chose to use just one eye, the selection method, e.g. method of randomised selection, was not outlined.

Clearly the use of fellow eye data is an important issue in ophthalmic research. In this thesis a general linear model approach was used utilising mixed effects to account for the use of both eyes in analysis.

All statistical analyses were performed in RStudio (version 0.98.1091; an open source user interface for R Statistics). Initially, histograms, QQ-plots and Shapiro-Wilk tests were used to determine the normality of data. Data were initially visualised graphically to assess correlations using the 'ggplot2' package in R Statistics. Pearson's correlation tests were applied to each dependent variable in order to determine any statistically significant associations between the two variables at a level of $p < 0.05$. Subsequently, multivariate analyses were performed using a general linear model, to test whether the variance shown by a given dependent variable (in this case, each retinal layer or ONH parameter) can be 'explained' by either multiple individual independent variables (i.e. fixed effects; such as age, axial length, etc.), and/or the combined effect of 2 fixed effects (i.e. interaction terms; such as the association axial length:mean spherical refractive error). Using such an approach allows for a more comprehensive indication of which factors are actually 'causing' potential differences in ONH thickness/depth measurements with age or glaucoma.

2.9.1 Model structure

Optimised general linear models (GLMs) were generated by stepwise deletion of the fixed effects, e.g. *stage of glaucoma*, *age*, as well as interaction terms, e.g. *axial length:mean spherical refractive error*, for each dependent variable, in order to investigate the direction and magnitude of associations with each ONH parameter. Where possible, both eyes from each subject were used in the analysis. In order to account for this, mixed-effects modelling, i.e. general linear models with a repeated-measures component (i.e. a random term) was used. Mixed-effects modelling was performed using the 'lme4' package in R Statistics (Bates et al., 2015). Due to the difficulties associated with determining degrees of freedom in mixed effects modelling, the R package 'lme4'

does not provide a p -value. In this instance a p -value is calculated using a likelihood ratio test comparing nested models, i.e. two identical models that differ only in the presence of the fixed effect for which a p -value is to be obtained. Using this method, p -values are given for each of the independent variables that were in the optimised LMM.

The effect sizes of continuous variables (e.g. *age*) within each model are presented as (effect size \pm SD, p -value) unless otherwise stated, i.e. how much the ONH parameter will change in $\mu\text{m}/\text{unit}$ change in the independent variable. For categorical fixed effects, (e.g. *stage of glaucoma*), Tukey post-hoc analysis (pairwise comparison) was performed to determine all inter-group differences. Differences within categorical variables are presented as (mean difference between groups \pm SD, p -value) unless otherwise stated. Note that the mean differences are determined from the estimated mean differences used in the LMM, which use the least-square mean to calculate an estimated value for each group.

2.9.2 Model optimisation

Each initial GLM was generated containing all of the relevant fixed effects (*stage of glaucoma*, *age*, *axial length*, *mean spherical refraction (MS)*, *mean deviation of visual field (MD)*, *anterior chamber depth (ACD)* and *central corneal thickness (CCT)*) and interaction terms (*age:MD*, *axial length:MD*, and *axial length:MS*). Step-wise deletion was then used to generate an optimised model for each ONH parameter (i.e. a model that explains the most variance in a given ONH measurement). Typically, a stepwise deletion approach to statistical model optimisation is used preferentially over a stepwise addition approach when there is not an obvious biological rationale for the order in which fixed effects are sequentially added. For this process, the Akaike Information Criterion (AIC; Akaike 1974) was determined for an initial model containing all fixed effects and interactions. The AIC is a measure of the quality of a statistical model for a given set of data, and provides a value based on the explained variance and the degrees of freedom in a given model. Fundamentally, the AIC value

allows for direct comparison of statistical models, prior to, and following deletion of a given fixed effect, such that GLMs both with and without specific factors can be compared in order to calculate which variables do not need to be included in the model to best explain the variance surrounding a specific ONH parameter.

Stepwise deletion, which uses the 'drop1' function in R (*F*-test), was used to assess the contribution of each fixed effect to a given model allowing a comparison of AIC values for hypothetical models in which each fixed effect has been removed independently. Deletion of the fixed effect that resulted in the *lowest* AIC signified the fixed effect that should be excluded from the initial model, i.e. the fixed effect that explained the least variance/degrees of freedom used, was removed. In turn, a second model, containing all the fixed effects (except for the one removed initially) was then run and the AIC determined. This process of stepwise deletion was then repeated and subsequent independent variables removed from the model until a stage whereby further removal of fixed effects did *not* improve the model, i.e. did not result in a lower AIC value.

2.9.3 Model assumptions

In the initial models a Gaussian family and an integer link function (i.e. the natural form of the data) were specified, and this met the model's assumption of a normal distribution of residual variance. However, where this assumption was not met, i.e. the residual variance was not normally distributed, a model transformation, or 'link function' was specified. Details of such transformations will be outlined in subsequent chapters, where applicable.

2.9.4 Model interpretation

The results of each optimised GLM are presented listing those fixed effects that were present in optimised models and those that explained a significant amount of variance. *P-values* describe

statistical significance while *t-values* describe the effect size of a given association, as a function of the overall variance. Statistical results are reported as mean values \pm standard deviation, *t-value*, *p-value*, unless otherwise stated. Values in the models were considered significant if $p < 0.05$. For categorical data, subsequent Tukey post-hoc analysis was carried out (e.g. between control and stages of glaucoma) and the significant *p-value* decreased to $p < 0.01$, to account for multiple comparisons.

Chapter 3:
Analysis of the inner retinal layers in
glaucomatous and healthy eyes

3 Analysis of the inner retinal layers in glaucomatous and healthy eyes

3.1 Introduction

The inner retina comprises the macula nerve fibre layer (mNFL), ganglion cell layer (GCL), and inner plexiform layer (IPL). The innermost retinal layers consist of the retinal ganglion cell (RGC) axons, cell bodies and dendrites, which are particularly prone to glaucomatous damage (Tan et al. 2009). Studies have shown the macula to be a region of interest when comparing retinal structure with visual field loss (Lederer et al. 2003; Guedes et al. 2003; Medeiros et al. 2005; Hood et al. 2014). Optical coherence tomography (OCT) has been used to measure macula thickness in healthy control eyes (Legarreta et al. 2008), as well as macula thickness and mNFL thickness in eyes with glaucoma (Greenfield et al. 2003). Indeed, a significant negative correlation has been reported to exist between the thickness of the ganglion cell complex (GCC; consisting of the mNFL, GCL and IPL combined) with increasing progression of glaucoma (Tan et al. 2008; Arintawati et al. 2013). Additionally, there has been shown to be a decrease in the thickness of the GCL-IPL combined layers in glaucoma, which is associated with visual field loss (Raza et al. 2011; Hood et al. 2013) and as such has a role in glaucoma diagnosis (Knighton et al. 2012).

Automated segmentation algorithms that have been developed for commercial OCT devices can be used to delineate the inner limiting membrane and the IPL-inner nuclear layer border, allowing for quantification of the GCC thickness (Kim et al. 2014). Non-commercial algorithms (Ishikawa et al. 2005; Savastano et al. 2014) and custom designed OCT devices have continued to improve image resolution and segmentation processes. Such advances will continue to enhance the potential for early diagnosis and subsequent monitoring of glaucoma and other ocular pathologies. Indeed, commercial OCT devices will continue to incorporate such technological developments. One such advancement is the capability to delineate the GCC in an automated manner, e.g. inbuilt in the Cirrus OCT (Carl Zeiss Meditec Inc., Germany; Tham et al. 2013). However, only very recently has it

been commercially possible to segment the individual components of the GCC, specifically separating the GCL and IPL (Spectralis software version 6.0.7, Heidelberg Engineering, Heidelberg, Germany). In spite of even these recent advances, the values and ratios of separate IPL and GCL measurements in relation to glaucomatous damage have yet to be established.

In glaucoma, detectable visual field loss using standard automated perimetry occurs following substantial loss of RGCs and their axons (Quigley et al. 1989). In order to prevent irreversible loss of vision it is critical to determine a biomarker that can assist in the identification of patients at risk of damage, *before* substantial RGC death has occurred, in order to prevent irreversible loss of vision. Thus, in order to determine if early loss of RGCs can be detected prior to vision loss, RGCs will be analysed indirectly through the quantification of mNFL, GCL and IPL thickness and volume in eyes classified into different disease stages of glaucoma in a region where the RGC cell density is greatest, i.e. within the macula.

3.2 Aim of study

- To quantify regional thickness and volume measurements of the inner retinal layers (i.e. the mNFL, GCL and IPL) in 3D OCT image datasets of maculae measured at different disease stages of glaucoma severity, in order to identify a measure of RGC integrity that can be used as a biomarker of early stage glaucomatous damage.

3.3 Experimental Design

3.3.1 Participants

Thirty-eight participants (29 with primary open angle glaucoma (POAG), 9 healthy controls) were recruited from the University Hospital of Wales, Cardiff and from within the staff, student and friends population at the School of Optometry and Vision Sciences, Cardiff University. Subjects were

recruited and imaged by BF (n=7), and KM (n = 31). Where possible, both eyes from each participant were included in the study. Demographics of the eyes included are summarised in Table 3.1.

Demographic	Control (n=16)		Preperimetric glaucoma (n=20)		Early glaucoma (n=19)		Advanced glaucoma (n=10)	
	mean	± SD	mean	± SD	mean	± SD	mean	± SD
Age (years)	65.36	± 11.33	63.25	± 9.97	69.16	± 10.44	59.30	± 10.33
Gender	4F	: 10M	13F	: 7M	12F	: 7M	5F	: 5M
MS (D)	-1.25	± 1.25	0.00	± 1.00	-1.25	± 2.00	-1.50	± 2.00
IOP (mmHg)	17.35	± 2.25	15.64	± 3.66	15.24	± 3.11	14.52	± 3.09
Axial length (mm)	24.57	± 0.69	23.53	± 1.09	24.01	± 1.15	24.64	± 0.81
MD (dB)	0.57	± 0.98	0.00	± 0.82	-3.39	± 1.55	-8.65	± 1.61

Table 3.1: Demographics for control and glaucomatous subjects. Gender: F = female, M = male. MS = mean spherical refractive error, IOP = intraocular pressure, MD = mean deviation on visual fields.

3.3.2 Clinical assessments

Participants' clinical ocular assessments included intra-ocular pressure (IOP) measurements by Goldmann contact tonometry (Haag Streight AG, Switzerland) or Non-Contact Tonometry-80 (Topcon Europe Medical B.V., Netherlands). Axial eye length, refractive error and visual field status were determined as described previously in section 2.3.1. Inclusion criteria for the study were a mean spherical refractive error within $\pm 6.00D$ and the absence of other (non-glaucomatous) ocular pathology or systemic pathology with ocular side effects. Control data were excluded if the IOP was found to be ≥ 21 mmHg or visual field loss (as defined by Hodapp et al. (1993)) was identified following visual field testing.

3.3.3 OCT data and image processing

18.7° scans centred on the macula were acquired as described in section 2.3.2. The Initial data processing was undertaken as described in section 2.4. Briefly, spectral OCT data were acquired and processed into tomographic images using custom-written MATLAB software (FDProcessing v1.0). Images were then further processed in ImageJ (v1.47n) in order to align the tomograms, remove artefacts from small eye movements, and improve image quality and contrast.

The centre of the fovea was identified in each 3D image stack. Every four b-scans were block averaged to improve definition of retinal layers. A custom-written MATLAB-based software (ManSeg_Anylayer v1.0) was used to manually demarcate the boundaries of the three innermost retinal layers, namely the macular nerve fibre layer (mNFL), ganglion cell layer (GCL) and inner plexiform layer (IPL).

3.3.4 Glaucoma classification

Participant eyes were classified into glaucoma disease stage according to the presence of glaucoma optic disc/nerve head features and degree of visual field loss (classification adapted from Hodapp et al. (1993)) as indicated in section 2.4.6. Thus eyes were categorised into preperimetric glaucoma (n=20), early glaucoma (n=19), advanced glaucoma (n=10) and non-glaucomatous control (n=16) groups. Of the 78 potential eyes for this study, 11 eyes were excluded from the study, either due to their not meeting the inclusion criteria (e.g. 'suspect glaucoma', as described in section 2.4.6, or IOP above normal limits in a healthy control; n=9) or as a result of poor image quality (n=2).

3.3.5 Generation of colour-coded thickness maps of inner retinal layers

A custom-written MATLAB program (F Rakebrant, Cardiff University) was used to create colour-coded thickness maps of the mNFL, GCL, IPL and ganglion cell complex (GCC; consisting of the mNFL, GCL and IPL). The colour maps for each dataset were visually compared to the corresponding visual field plot in order to determine whether areas of retinal thinning correlated with visual field loss patterns. Thicker regions are depicted as warmer colours (i.e. orange-red), while thinner areas are cooler colours (i.e. blue-turquoise). The colour coded thickness maps for each eye were arranged in order of increasing visual field loss, allowing for any trends in the data to become more apparent.

3.3.6 Regional analysis of retinal layer thickness and volume

In turn, the colour-coded thickness maps were regionally divided for analysis by placing a grid centred on the fovea to create a central 1.5° (fovea), and 3 concentric rings at 2.5°, 5.5° and 8.6° radial eccentricity. These rings were subdivided (4 regions in each), by superior - inferior and temporal - nasal divisions (Figure 3.1a). The mean thickness and volume for each inner retinal layer, as well as for the GCC, was calculated for each of the 13 individual regions (R1-R13). Additionally, the individual regions were grouped to form quadrants (Figure 3.1e), inner-quadrants (Figure 3.1f), hemizones (Figure 3.1g), and inner-hemizones (Figure 3.1h).

The mNFL, GCL, IPL and GCC thicknesses and volumes were quantified in each individual or grouped regions to determine what, if any changes were present between eyes as a function different stages of glaucoma. The IPL:mNFL and IPL:GCL ratios were also calculated for each region in each retinal layer. Additionally, regions of equal eccentricity from the fovea were compared (inner, Figure 3.1b, mid, Figure 3.1c; and outer, Figure 3.1d) for each stage of glaucoma to determine whether damage occurred primarily in any specific area.

3.3.7 Statistical analysis

Statistical analyses were performed using RStudio, an open source platform for R Statistics, as described in section 2.9. Briefly, the normality of data was determined using Shapiro-Wilk tests, QQ plots and histograms, and the majority of data was shown to be non-parametric. Where possible, both eyes from each participant were used for analysis. Thus, in order to compensate this, generalised linear mixed-effects models (LMM) with repeated measures component were used to assess differences between stages of glaucoma for each individual region, included in each model. Where differences were determined using the LMMs, Tukey post-hoc analysis was applied to determine within which stage of glaucoma the differences lay.

Additionally, differences between regions of equal eccentricity from the fovea were investigated for each inner retinal layer, for each stage of glaucoma, again using a repeated measures multivariate approach with a Tukey post-hoc correction.

3.4 Results

3.4.1 Colour coded thickness maps of the inner retinal layers for control and glaucoma

It was observed that there tended to be an association between increased regional thinning and visual field loss, with thinning of the inner retinal layers corresponding with visual field loss in later stages of glaucoma (Figure 3.2). Interestingly, where a significant hemianopia (or similar defect) was observed in the central visual field, a corresponding region of thinning was observed in the GCL, the IPL and the GCC, for advanced glaucoma (Figure 3.2). However, there was no apparent pattern as to whether the superior or inferior hemifield of the eye was the initial site of retinal thinning in early stages of disease. It is worthy of note that traces of retinal blood vessels were visible in the GCC and mNFL thickness maps, a factor which could potentially mask results from the nasal side of the macula (Figure 3.2)

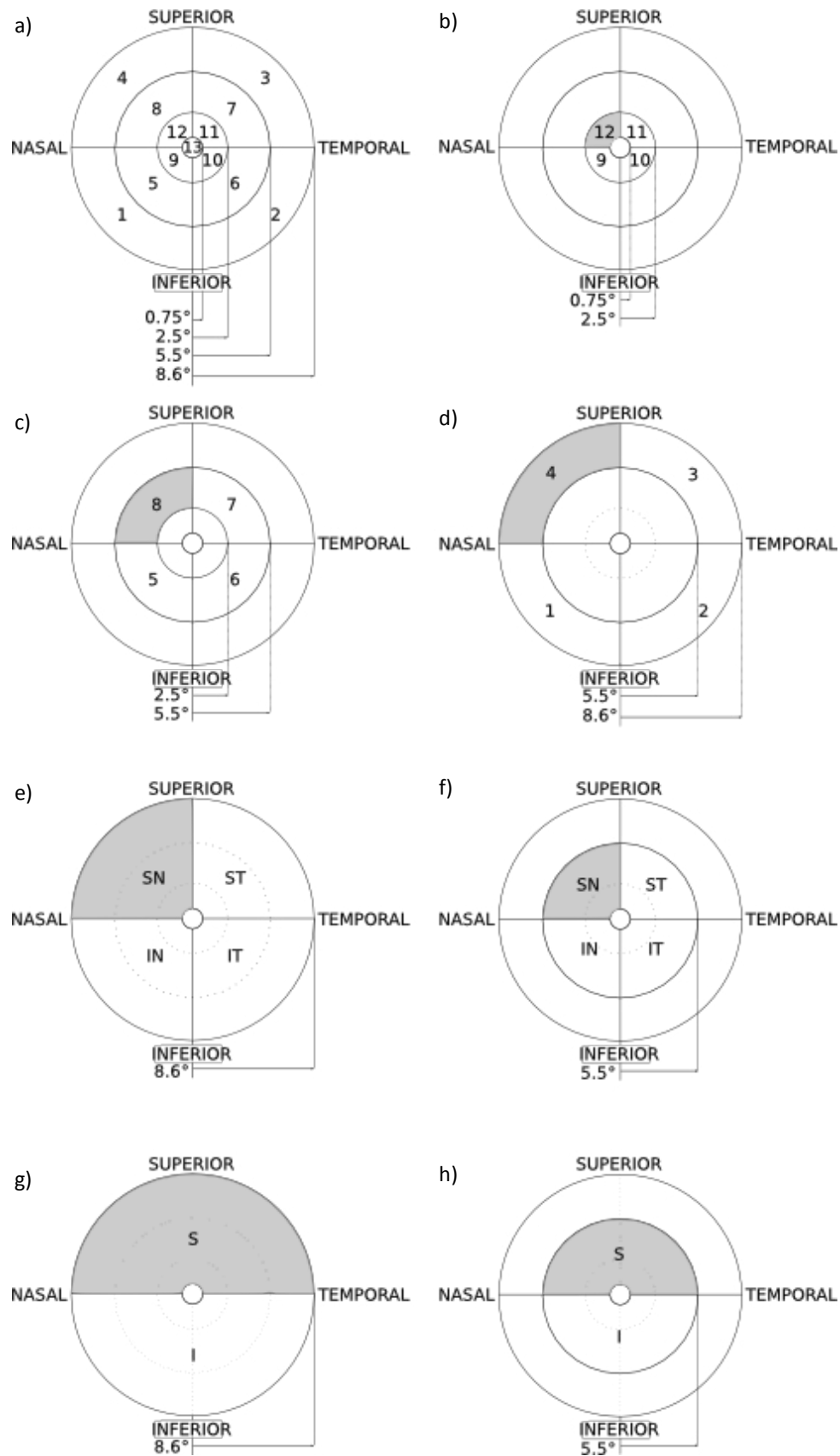


Figure 3.1: (a) Retinal thickness maps subdivisions: 13 regions centred on the fovea. Regions of equal eccentricity from the fovea were compared for (b) inner ($0.75^\circ - 2.5^\circ$); (c) mid ($3.5^\circ - 5.5^\circ$); and (d) outer ($5.5^\circ - 8.6^\circ$). Regions were grouped to form (e) quadrants (superior-nasal shaded); (f) inner-quadrants (inner superior-nasal shaded); (g) hemizones (superior shaded); and (h) inner-hemizones (inner superior shaded).

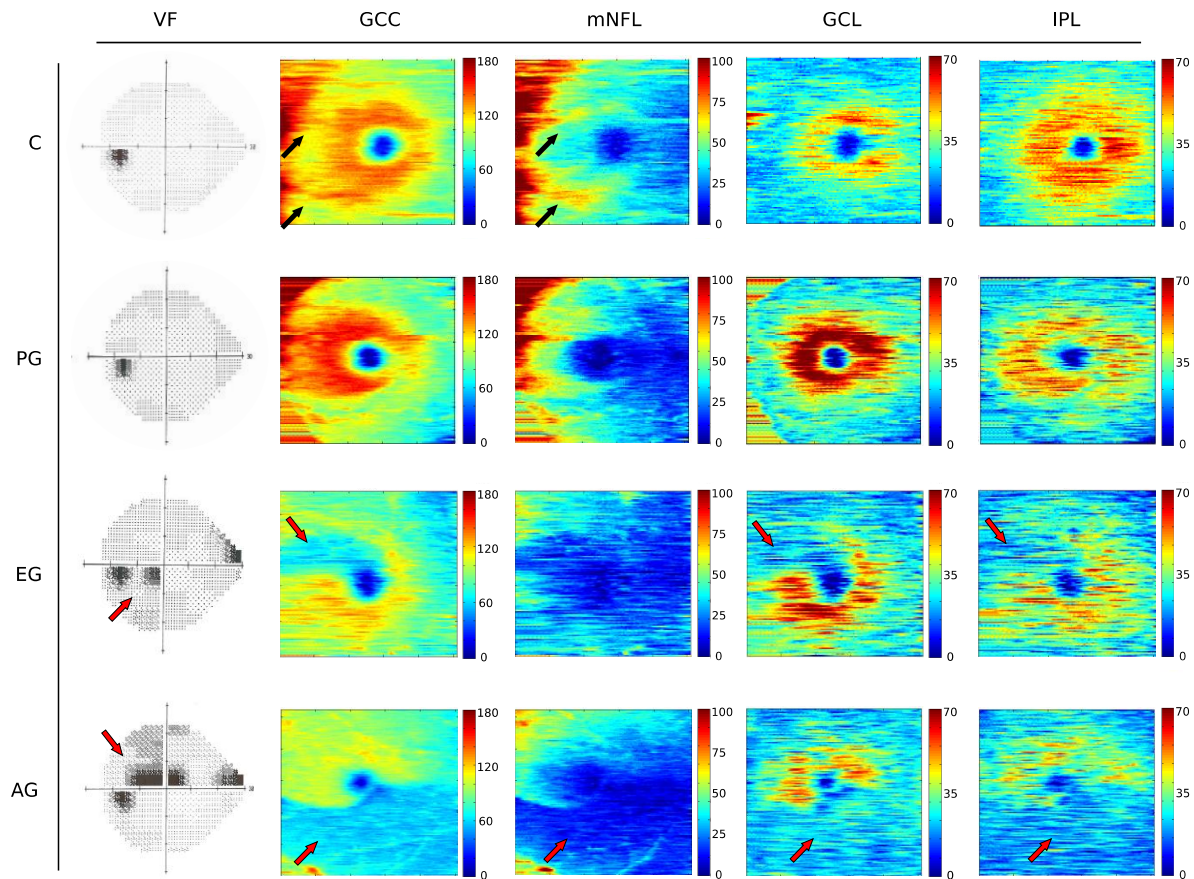


Figure 3.2: Colour-coded thickness maps of ganglion cell complex (GCC), macula nerve fibre layer (mNFL), ganglion cell layer (GCL) and inner plexiform layer (IPL), with the visual field plot (VF) for eyes at different stages of glaucoma. Focal areas of visual field loss corresponded with thinning of the GCC, GCL and IPL (EG and AG; red arrows). Artefacts from blood vessels were present in some cases in the GCC and mNFL images (C; black arrows). C = control, PG = preperimetric glaucoma, EG = early glaucoma, AG = advanced glaucoma. Colour-coded thickness maps are plotted in microns.

3.4.2 Quantitative thickness and volume measurements of inner retinal layers

The absolute values for volume of each region for the mNFL, GCL and the IPL, thickness of each region, and the IPL:mNFL and IPL:GCL ratio are presented in Appendix II.

3.4.3 Comparative analysis of macula thickness and volume of regions at equal eccentricity from the fovea in each disease stage categories

No statistically significant differences in thickness or volume were apparent in regions of equal eccentricity from the fovea, any hemizones/inner-hemizones or quadrants/inner-quadrants in either

thickness or volume for within control, preperimetric or early glaucomatous disease stage categories (see Appendix II). The same was also true for the measures of the GCC, IPL:mNFL ratio, or IPL:GCL ratio.

Maculae of patients with advanced glaucoma had reduced mNFL volume in the ST region compared to both the IN and IT outer regions ($R3 < R1$, $t=4.17$, $p=0.002$; $R3 < R2$, $t=3.13$, $p=0.021$). The IN region also had smaller mNFL volume than ST in the mid macula ($R5 < R7$, $t=3.65$, $p=0.006$) and inner macula ($R11 < R9$, $t=3.68$, $p=0.005$). Maculae with advanced glaucoma also showed a trend for thinner mNFL in the mid superior-temporal (ST) region compared to the mid inferior-nasal (IN) ($R7 < R5$, $t=3.24$, $p=0.015$). Finally, there was a trend for thicker GCL in the superior-temporal mid macula compared to that in the inferior-nasal mid macula ($R7 < R5$, $t=3.10$, $p=0.021$) and a smaller superior-nasal (SN) inner GCL volume compared to the inferior-temporal (IT) inner macula ($R12 < R10$, $t=2.80$, $p=0.043$). These differences are summarised below (Figure 3.3).

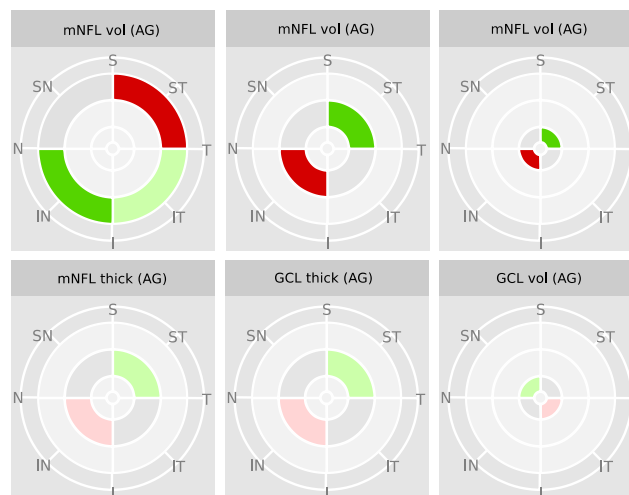


Figure 3.3: Differences in macula nerve fibre layer (mNFL) and ganglion cell layer (GCL) thickness (thick) and volume (vol) at regions of equal eccentricity from the fovea. Differences were present in eyes with advanced glaucoma (AG) only.

Maculae with advanced glaucoma Red = significantly thinner or smaller volume than green areas ($p < 0.01$). Trends are shown where pink = thinner or smaller volume than pale green ($p < 0.05$). exhibited a trend for reduced GCL thickness in the inferior zones compared to the superior

zones (hemizones: $t=-2.54$, $p=0.032$; inner-hemizones: $t=-2.70$, $p=0.023$). GCL, IPL and mNFL inferior volumes were also smaller than the superior area (hemizones: mNFL $t=-3.34$, $p=0.009$; GCL $t=-2.54$, $p=0.032$; IPL $t=-2.75$, $p=0.048$; inner-hemizones: mNFL $t=-3.81$, $p=0.003$; GCL $t=-2.67$, $p=0.024$; IPL $t=-2.36$, $p=0.040$). The differences in thickness and volume of the hemizones and inner-hemizones are shown in Figure 3.4.



Figure 3.4: Differences in moderate glaucoma maculae ganglion cell layer (GCL), inner plexiform layer (IPL) and macular nerve fibre layer (mNFL) thickness (thick) and volume (vol) at corresponding hemizones and inner-hemizones. Differences were present in eyes with advanced glaucoma (AG) only. Red = significantly thinner or smaller volume than green areas ($p<0.01$). Trends are shown where pink = thinner or smaller volume than pale green ($p<0.05$).

In eyes with advanced glaucoma the mNFL quadrants and inner-quadrants had reduced volume in the inferior-temporal area compared to both the superior-nasal and superior-temporal volumes (quadrants: $IT<SN$ $t=-3.94$, $p=0.003$; $IT<ST$ $t=-3.14$, $p=0.021$, inner-quadrants: $IT<SN$ $t=-3.08$, $p=0.022$; $IT<SN$ $t=-2.88$, $p=0.036$). The mNFL showed a trend for less volume in the inferior-temporal inner-quadrant than in both the superior-nasal and superior-temporal inner-quadrant ($IT<SN$ $t=-3.08$, $p=0.022$; $IT<SN$ $t=-2.88$, $p=0.036$), and for less volume in the inferior-nasal than the superior-nasal inner-quadrant ($t=-2.89$, $p=0.035$).

Additionally, GCL inferior-nasal innerquadrant volume was less than in the superior-temporal inner-quadrant ($t=-3.11$, $p=0.021$), although this did not quite reach statistical significance. The grouping of individual regions into quadrants or inner-quadrants is shown in Figure 3.5.

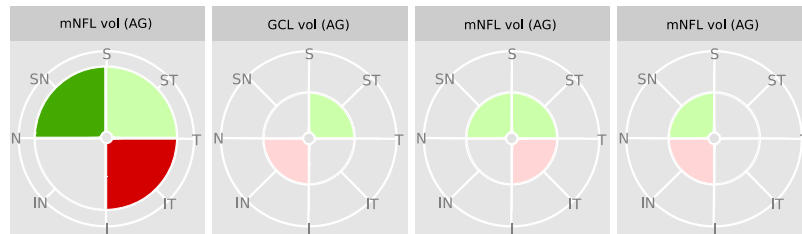


Figure 3.5: Differences in macular nerve fibre layer (mNFL) and ganglion cell layer (GCL) volume (vol) at corresponding quadrants and inner-quadrants. Differences were present in eyes with advanced glaucoma (AG) only. Red = significantly thinner or smaller volume than green areas ($p < 0.01$). Trends are shown where pink = thinner or smaller volume than pale green ($p < 0.05$).

3.4.4 Ganglion cell complex thickness and volume in control and different staged glaucoma macula

3.4.4.1 Comparative analysis of regional ganglion cell complex thickness

The ganglion cell complex (GCC) consists of the three innermost retinal layers (mNFL, GCL and IPL) combined and was found to be thinner in early glaucoma than control for each individual region ($p < 0.01$). This data is presented in Figure 3.6 as a function of position within concentric rings: inner, mid, outer or centre (fovea). The inner superior-temporal region (R11) showed a trend to be thinner in moderate glaucoma compared to control maculae ($t=2.67$, $p=0.049$).

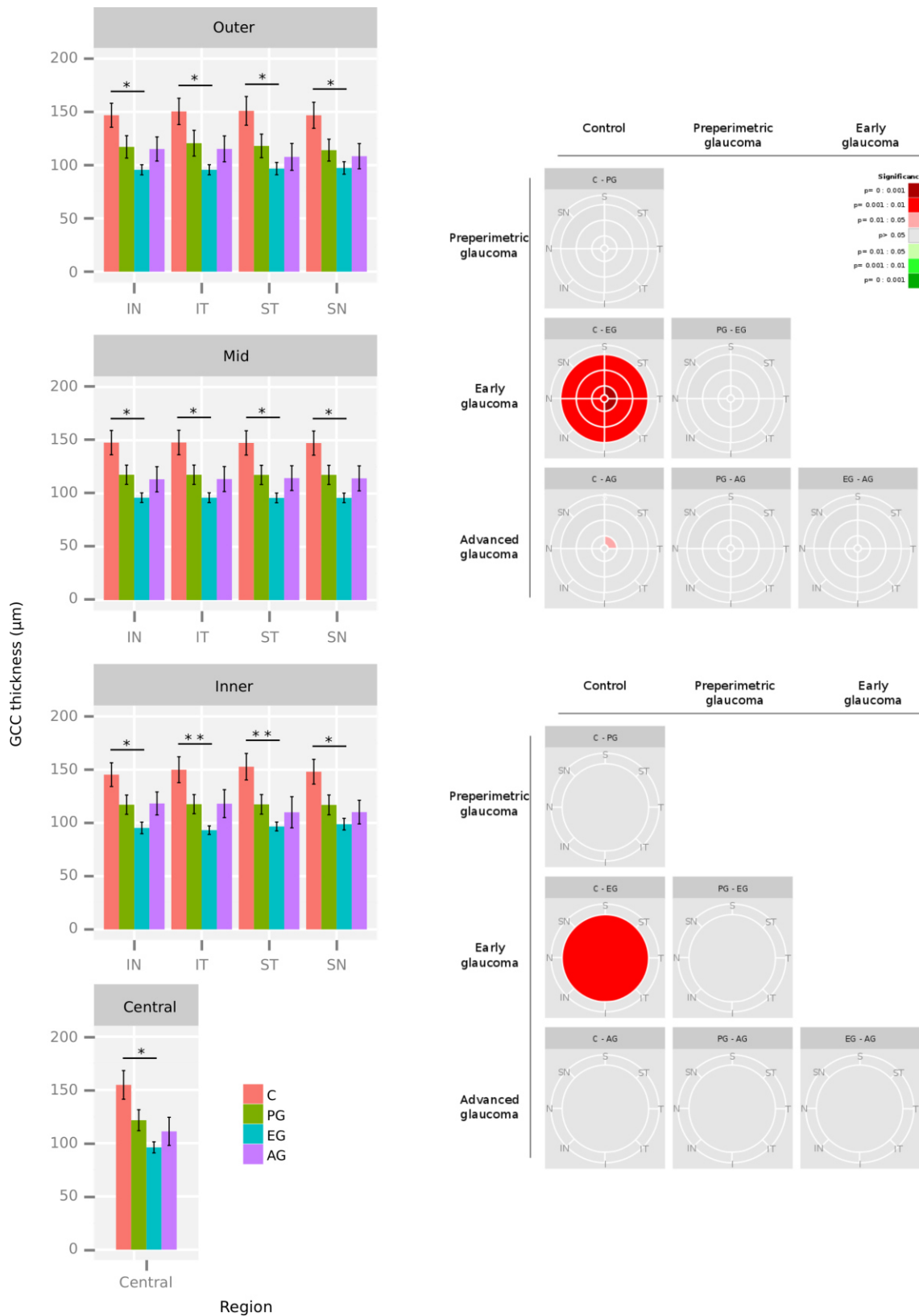


Figure 3.6: Regional ganglion cell complex (GCC) thickness for each control and each stage of glaucoma progression, and inter-stage regional and total area differences. C = control, PG = preperimetric glaucoma, EG = early glaucoma, AG = advanced glaucoma, IN = inferior-nasal, IT = inferior-temporal, ST = superior-temporal, SN = superior-nasal. * = $p < 0.01$, ** = $p < 0.001$ (linear mixed-effects models with Tukey post-hoc analysis).

The GCC was thinner in early glaucoma than in control for grouped areas (full- and inner-quadrants and hemizones $p<0.01$; Appendix III). Consistent with results above, total GCC (i.e. 13 regions combined) was significantly thinner in eyes with early glaucoma than control eyes ($t=4.12$, $p=0.001$; Figure 3.6).

3.4.4.2 Inter-stage differences in ganglion cell complex volume

The volume of the GCC showed a trend to be smaller ($p<0.05$) in early glaucoma compared to control in all mid regions (R5-8), in all inner regions except superior-nasal (R9-11), and in the central regions (R13), however this did not reach statistical significance (Figure 3.7). Additionally, the total GCC had smaller volume in eyes with early glaucoma than in control ($t=2.89$, $p=0.031$). A summary of the differences is shown below (Figure 3.7).

3.4.5 Inter stage differences in macula nerve fibre layer thickness and volume

3.4.5.1 Comparative analysis of regional macula nerve fibre layer thickness

There were no significant differences in mNFL thickness between control eyes and any of the glaucoma groups, however, there was a trend for the mNFL to be thinner in early glaucoma compared to control in outer inferior regions (R1 and R2), all mid regions (R5-8), all inner regions except the superior-nasal (R9-11), and in the central region (R13; all $p<0.05$), as shown in Figure 3.8.

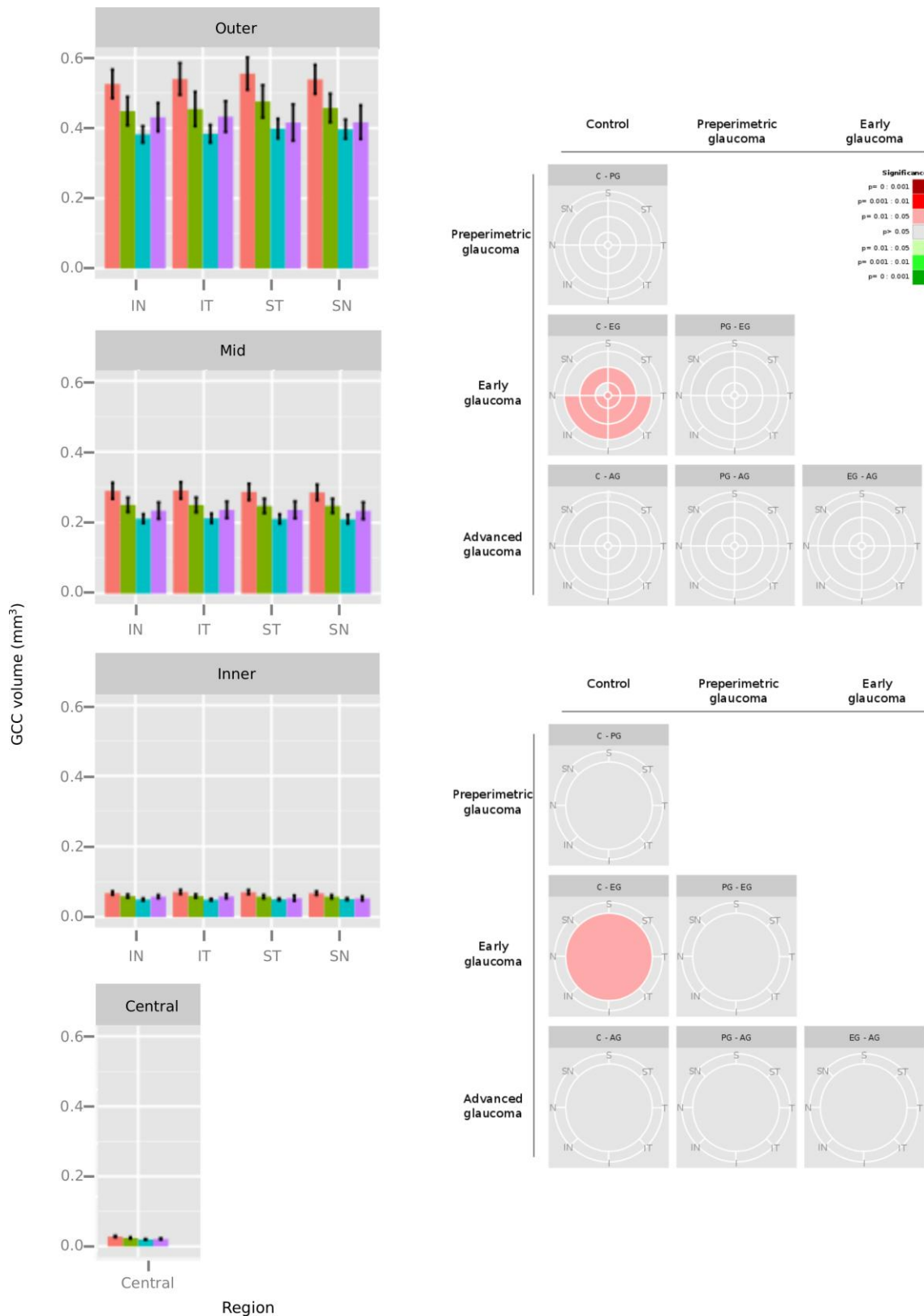


Figure 3.7: Regional ganglion cell complex (GCC) volume for each control and each stage of glaucoma progression, and inter-stage regional and total area differences. C = control, PG = preperimetric glaucoma, EG = early glaucoma, AG = advanced glaucoma, IN = inferior-nasal, IT = inferior-temporal, ST = superior-temporal, SN = superior-nasal.

The total mNFL thickness across the macula area was less in eyes with early glaucoma than in control eyes ($t=2.90$, $p=0.029$). The mNFL also showed a trend to be thinner in early glaucoma than control in the inner-quadrants and inner-hemizones, the superior hemizone, and the superior quadrants ($p<0.05$; see Appendix III).

3.4.5.2 Inter-stage differences in macula nerve fibre layer volume

There were no statistically significant differences in mNFL volume between control or any stage of glaucoma ($p>0.01$; Figure 3.9).

When the regions were grouped, there were no significant differences in the volume of the mNFL between control and any stage of glaucoma for total area ($p>0.01$), or for any full or inner-hemizones or quadrants ($p>0.01$; Appendix III).

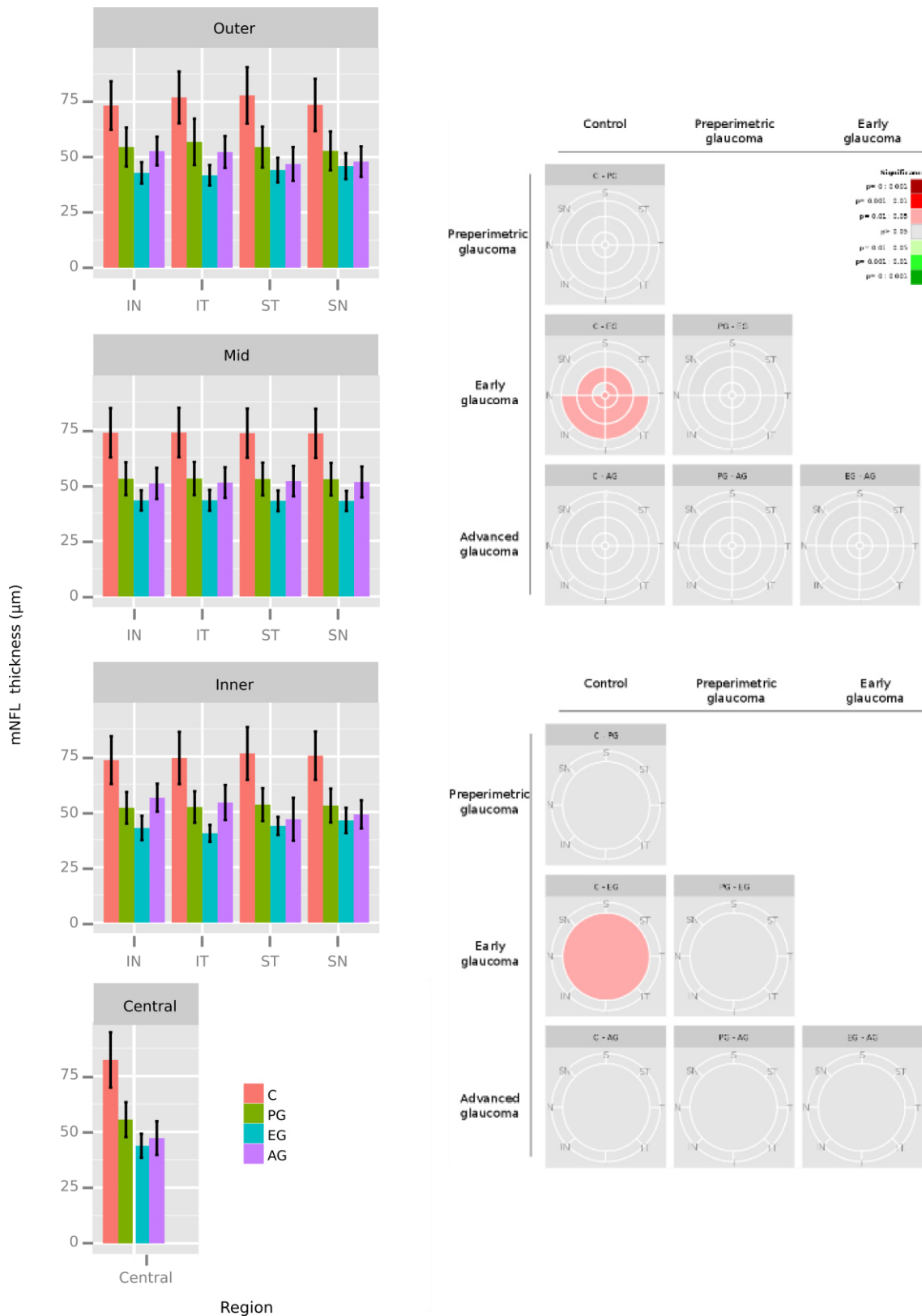


Figure 3.8: Regional macula nerve fibre layer (mNFL) thickness for each control and each stage of glaucoma progression, and inter-stage regional and total area differences. C = control, PG = preperimetric glaucoma, EG = early glaucoma, AG = advanced glaucoma, IN = inferior-nasal, IT = inferior-temporal, ST = superior-temporal, SN = superior-nasal.

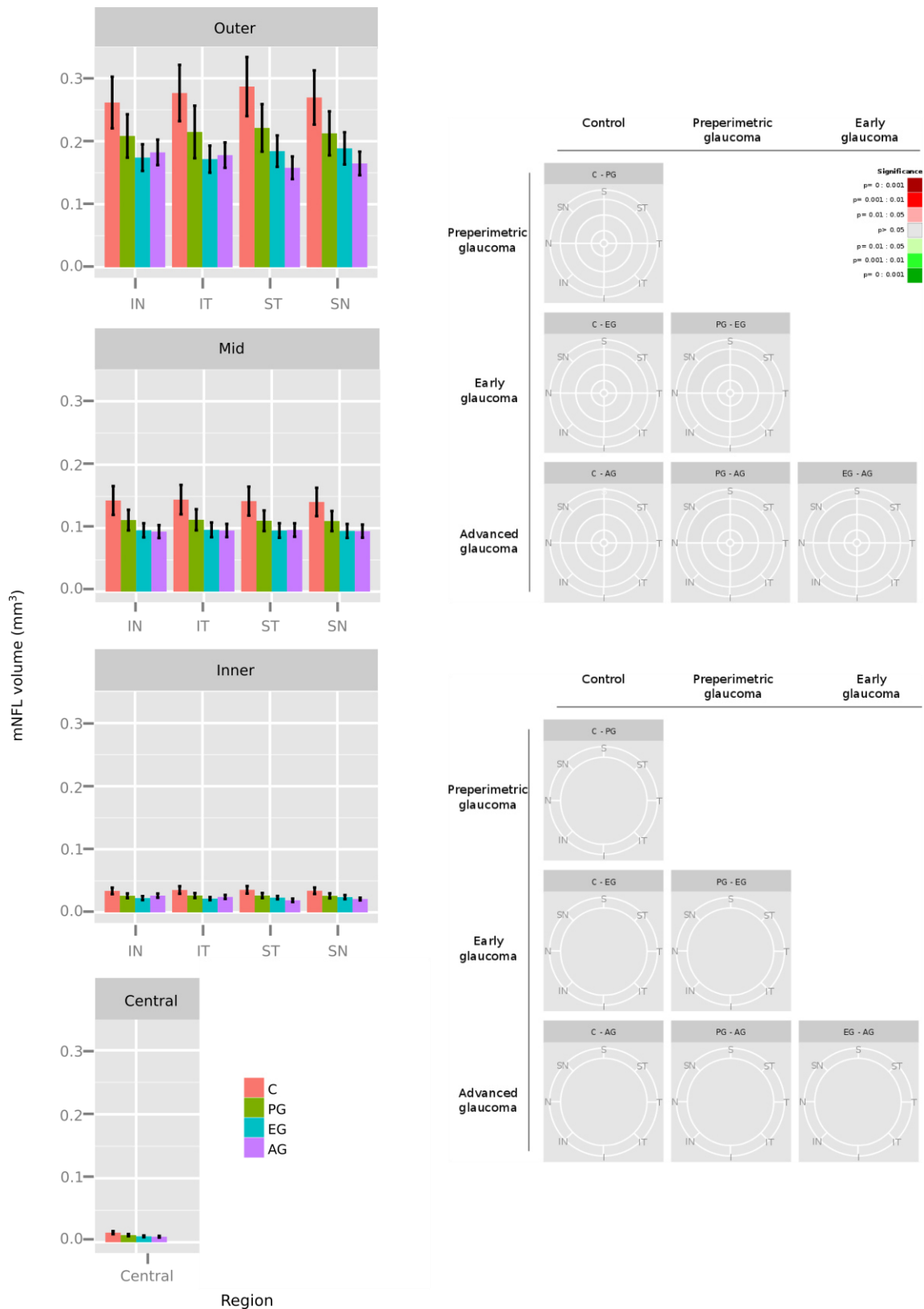


Figure 3.9: Regional macula nerve fibre layer (mNFL) volume for each control and each stage of glaucoma progression, and inter-stage regional and total area differences. C = control, PG = preperimetric glaucoma, EG = early glaucoma, AG = advanced glaucoma, IN = inferior-nasal, IT = inferior-temporal, ST = superior-temporal, SN = superior-nasal.

3.4.6 Inter stage differences in ganglion cell layer thickness and volume

3.4.6.1 Comparative analysis of regional ganglion cell layer thickness

The GCL was significantly thinner in eyes with early glaucoma than control eyes in the outer inferior-nasal (R1) and superior-nasal (R4) regions (R1 $t=3.35$, $p=0.009$; R4 $t=3.81$, $p=0.003$), the inner superior-temporal region (R11 $t=3.78$, $p=0.003$), as well as showing a trend in all other regions except the inner inferior-nasal (R9) and central (R13) regions ($p<0.05$; Figure 3.10). The GCL also showed a trend to be thinner in eyes with preperimetric glaucoma than control in the outer inferior-nasal (R1) and superior-nasal (R4) regions, as well as the inner superior-temporal (R11; $p<0.05$).

When the individual regions were grouped the GCL showed a trend to be thinner for early glaucoma than control for the total macula area ($t=3.13$, $p=0.016$), for all quadrants and inner-quadrants, and all hemizones and inner-hemizones ($p<0.05$; Appendix III). There was also a trend for eyes with preperimetric glaucoma to have thinner GCL than control eyes in the inferior hemizone ($t=2.92$, $p=0.028$); in the inferior-nasal quadrant ($t=2.78$, $p=0.040$); and in the inferior-temporal inner-quadrant ($t=2.69$, $p=0.048$). These results are summarised in Appendix III.

3.4.6.2 Inter-stage differences in ganglion cell layer volume

There were no significant differences in GCL volume between control eyes and those with any stage of glaucoma, however, there was a trend for the volume of the GCL to be reduced in eyes with early glaucoma compared to control eyes ($p<0.05$; Figure 3.11). Additionally, the volume of the GCL was significantly less for eyes with early glaucoma than control eyes for the total macula ($t=3.33$, $p=0.009$). The GCL volume was also less in both the superior and inferior hemizone in eyes with early glaucoma than control eyes ($p<0.01$), as well as in the inferior-nasal, superior-nasal and superior-temporal quadrants and the inferior-temporal inner-quadrant ($p<0.01$; see Appendix III).

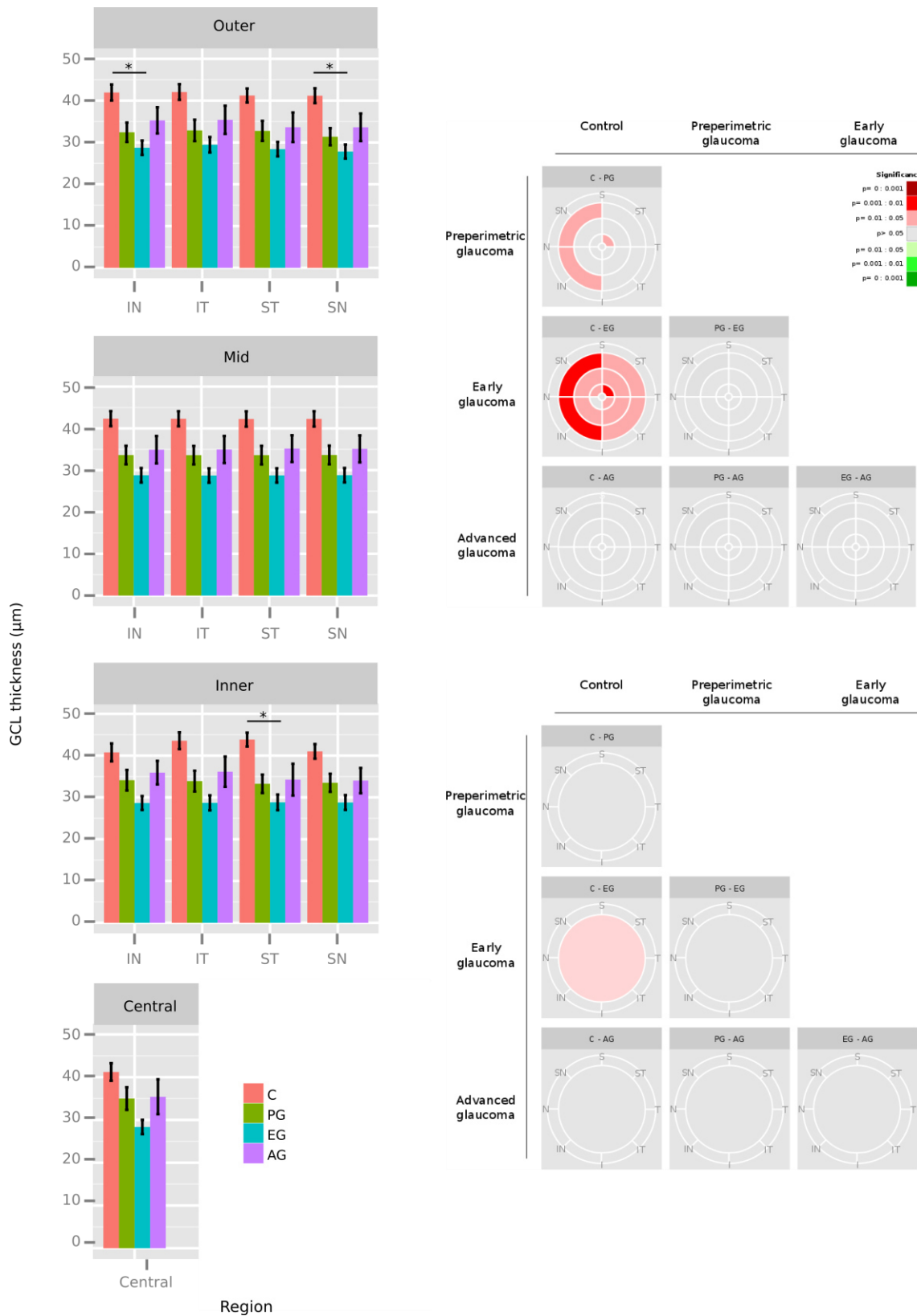


Figure 3.10: Regional ganglion cell layer (GCL) thickness for each control and each stage of glaucoma progression, and inter-stage regional and total area differences. C = control, PG = preperimetric glaucoma, EG = early glaucoma, AG = advanced glaucoma, IN = inferior-nasal, IT = inferior-temporal, ST = superior-temporal, SN = superior-nasal. * = $p < 0.01$ (linear mixed-effects models with Tukey post-hoc analysis).

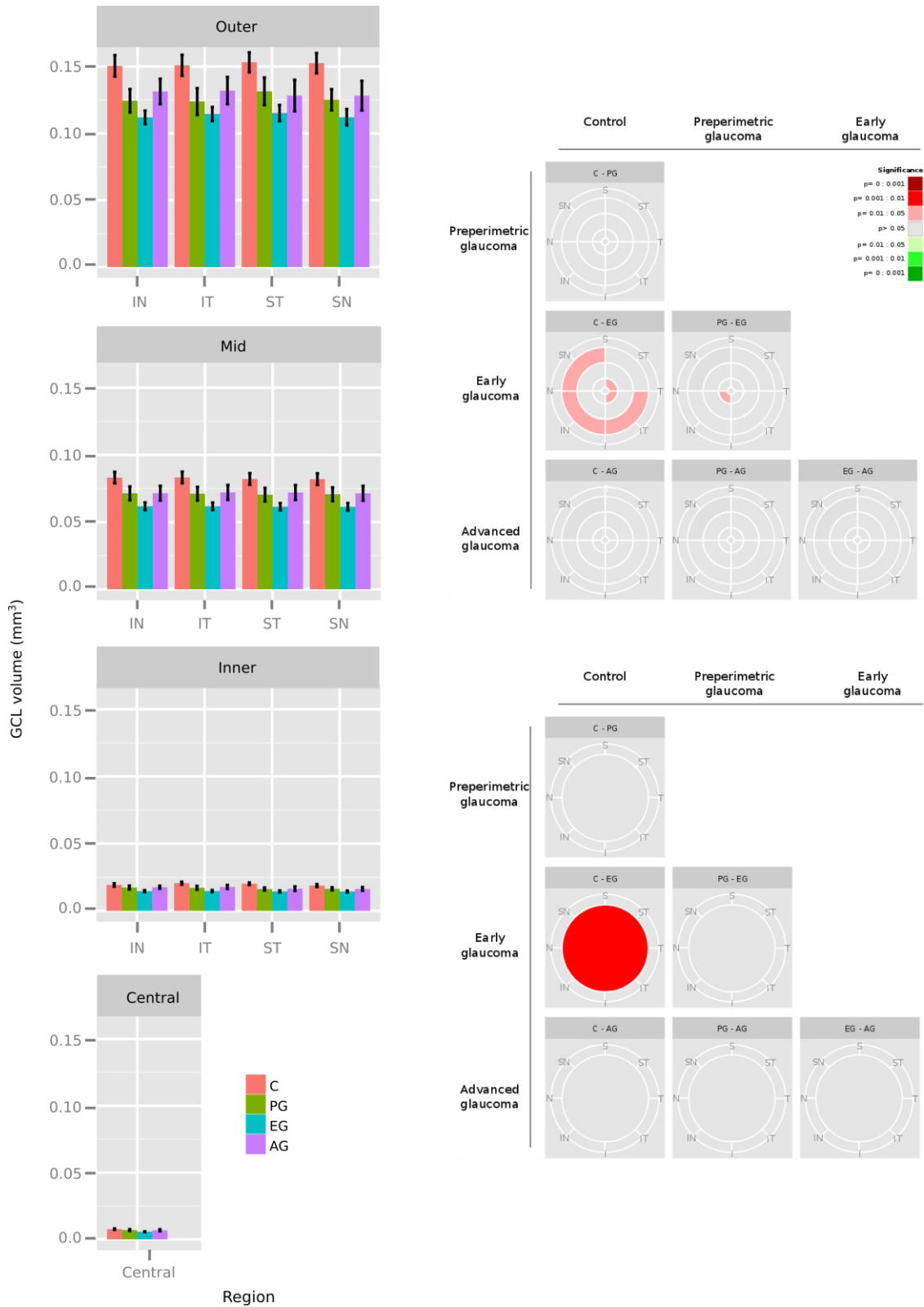


Figure 3.11: Regional ganglion cell layer (GCL) volume for each control and each stage of glaucoma progression, and inter-stage regional and total area differences. C = control, PG = preperimetric glaucoma, EG = early glaucoma, AG = advanced glaucoma, IN = inferior-nasal, IT = inferior-temporal, ST = superior-temporal, SN = superior-nasal.

3.4.7 Inner plexiform layer thickness and volume in different glaucoma disease stages

3.4.7.1 Comparative analysis of regional inner plexiform layer thickness

The IPL was significantly thinner in the early glaucoma group than the controls ($p < 0.01$) for all regions except for the outer superior and inferior temporal regions, which showed a trend ($p < 0.05$; Figure 3.12). The IPL was also significantly thinner in the early glaucoma group than preperimetric glaucoma for all the mid-macula regions ($p < 0.01$). Interestingly, eyes with moderate glaucoma showed a trend for *thicker* IPL than eyes with early glaucoma in all regions ($p < 0.05$) except the outer superior-temporal, inner superior-nasal, inner superior-temporal and central regions, where there was no significant difference ($p > 0.05$).

The IPL across the whole macula area was significantly thinner in eyes with early glaucoma than in both control ($t = 3.37$, $p = 0.008$) and preperimetric glaucoma ($t = 3.39$, $p = 0.007$), and showed a trend to be thicker in eyes with moderate glaucoma than eyes with early glaucoma ($t = 2.88$, $p = 0.028$; Figure 3.12). Additionally, the IPL was thinner early glaucoma than in control for all quadrants, and thinner in preperimetric glaucoma than control in the inferior-temporal and inferior-nasal quadrants, although this did not quite reach statistical significance ($p < 0.05$), and showed a trend to be thicker in moderate glaucoma than early in all quadrants except the inferior-temporal ($p < 0.05$). These results are summarised in Appendix III.

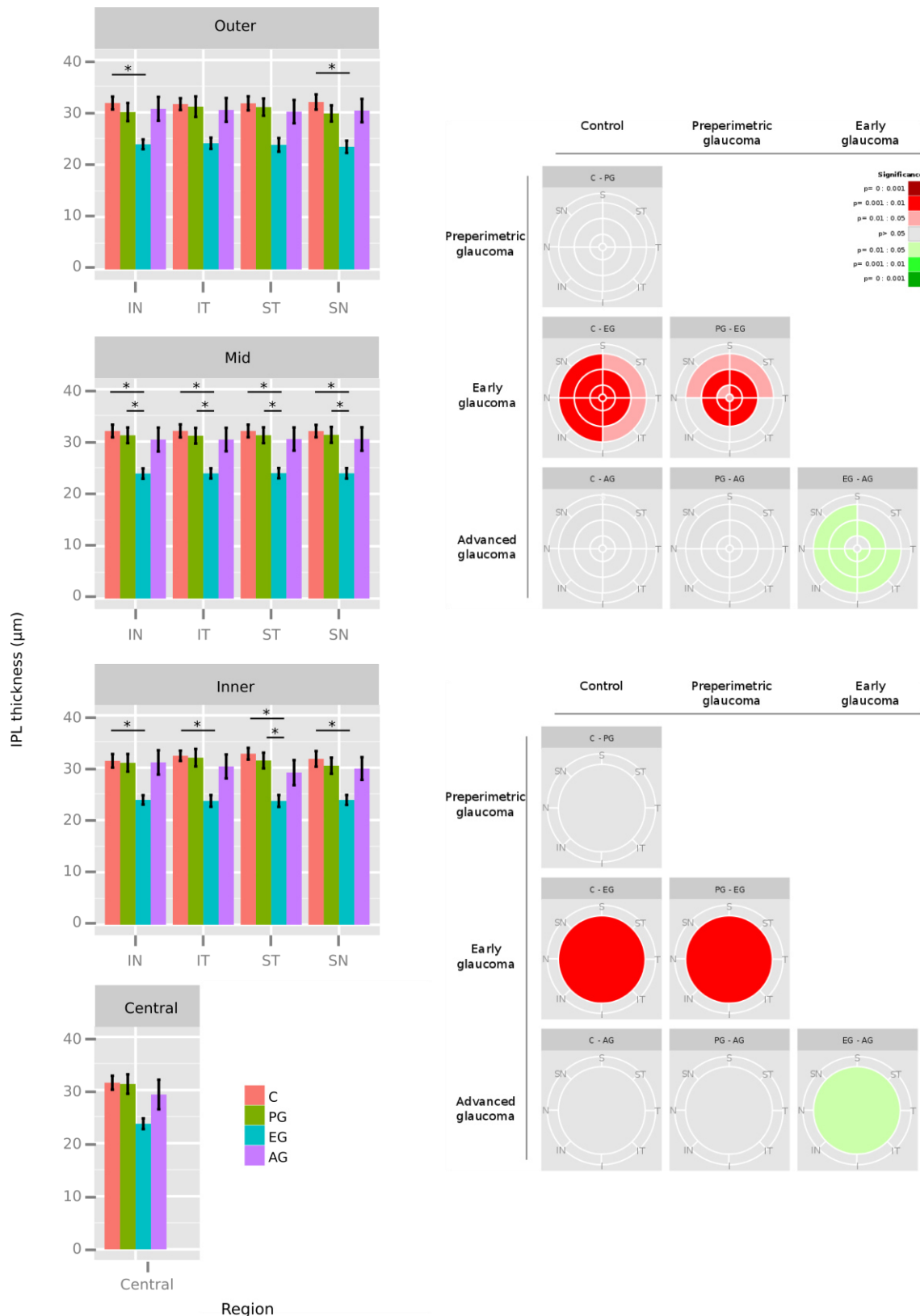


Figure 3.12: Regional inner plexiform layer (IPL) thickness for each control and each stage of glaucoma progression, and inter-stage regional and total area differences. C = control, PG = preperimetric glaucoma, EG = early glaucoma, AG = advanced glaucoma, IN = inferior-nasal, IT = inferior-temporal, ST = superior-temporal, SN = superior-nasal. * = $p < 0.01$ (linear mixed-effects models with Tukey post-hoc analysis).

3.4.7.2 Inter-stage differences in inner plexiform layer volume

There were no significant differences in IPL volume between control and the glaucoma groups ($p < 0.01$). However, there was a trend for eyes with early glaucoma to have smaller IPL volume than eyes with preperimetric glaucoma in the outer superior-nasal region (R4 $t=2.93$, $p=0.026$), in the four mid regions (R5-8, $p < 0.05$), in the inner inferior- and superior-nasal regions (R9 $t=3.10$, $p=0.016$; R12 $t=3.05$, $p=0.018$) and in the central region (R13 $t=2.67$, $p=0.048$; Figure 3.13).

When all regions were grouped there was no statistically significant difference in IPL volume between control and any stage of glaucoma (Figure 3.13). There was also no significant difference in IPL volume for either superior or inferior hemizones, and of the four quadrants, the IPL volume was less in the inferior-nasal quadrant in early glaucoma compared to preperimetric. However, all inner-quadrant and inner-hemizone regions showed a trend for less IPL volume in early glaucoma compared to preperimetric ($p < 0.05$). This is illustrated in Appendix III.

3.4.8 Differences in the ratio of inner plexiform layer to macula nerve fibre layer in control and increased stages of glaucoma

There was no significant difference identified in IPL:mNFL ratio between control or any stage of glaucoma for any of the individual regions examined (Figure 3.14). There was also no significant difference in IPL:mNFL ratio in the total area, or in any of the quadrants, inner-quadrants, hemizones, or inner-hemizones ($p > 0.01$).

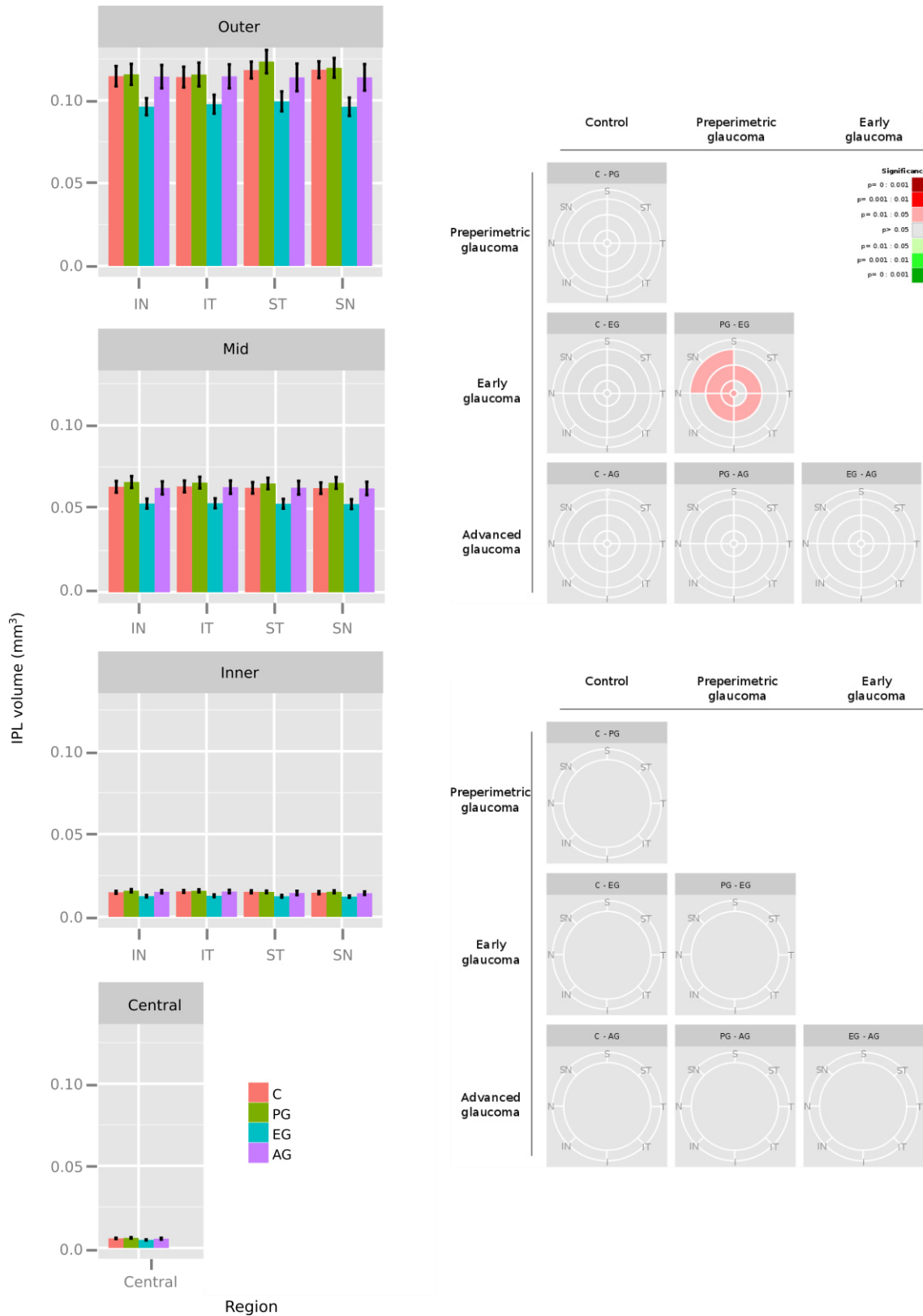


Figure 3.13: Regional inner plexiform layer (IPL) volume for each control and each stage of glaucoma progression, and inter-stage regional and total area differences. C = control, PG = preperimetric glaucoma, EG = early glaucoma, AG = advanced glaucoma, IN = inferior-nasal, IT = inferior-temporal, ST = superior-temporal, SN = superior-nasal.

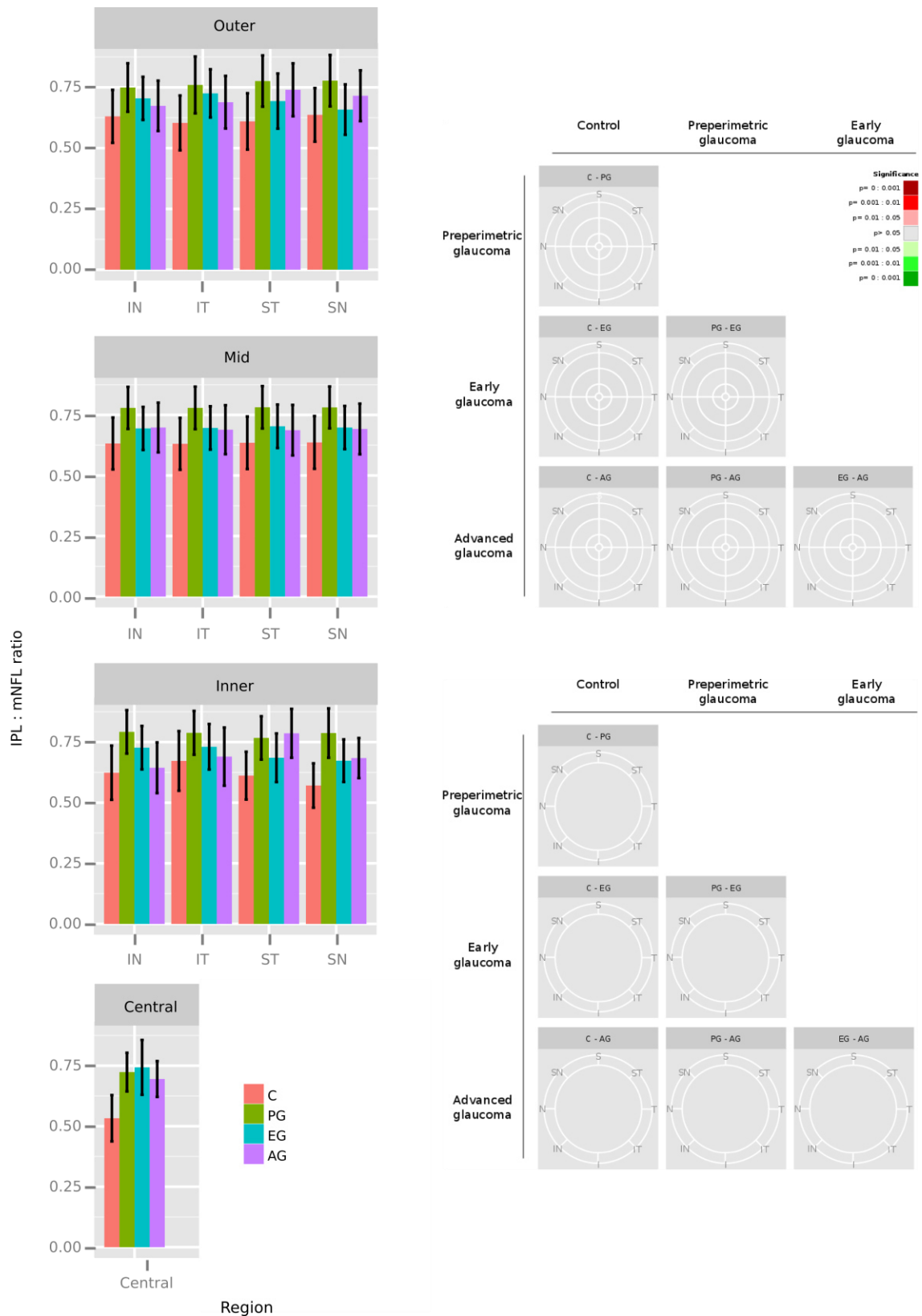


Figure 3.14: Regional inner plexiform layer : macula nerve fibre layer (IPL:mNFL) ratio for each control and each stage of glaucoma progression, and inter-stage regional and total area differences. C = control, PG = preperimetric glaucoma, EG = early glaucoma, AG = advanced glaucoma, IN = inferior-nasal, IT = inferior-temporal, ST = superior-temporal, SN = superior-nasal.

3.4.9 Differences in the ratio of inner plexiform layer to ganglion cell layer in control and increased glaucoma stages

The IPL:GCL ratio was significantly higher for eyes with preperimetric glaucoma than control eyes in the superior-nasal region ($t=3.35$, $p=0.009$), and showed a trend in all other regions ($p<0.05$) except for the central fovea (R13; Figure 3.15). The IPL:GCL ratio also showed a trend to be higher for eyes with preperimetric glaucoma than control eyes when the total macula area was considered, as well as for all quadrants, inner-quadrants, hemizones and inner-hemizones ($p<0.05$; Appendix III).

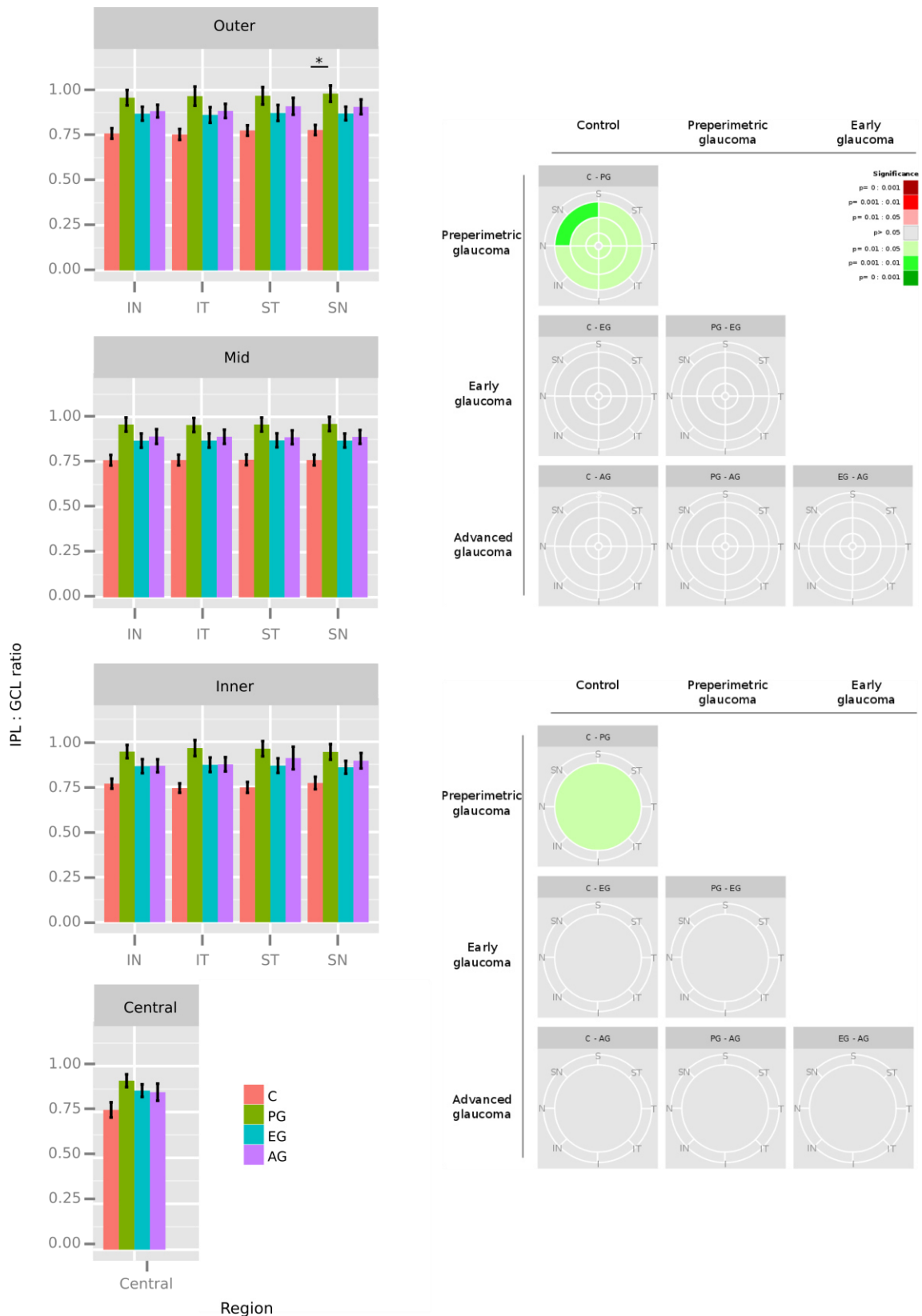


Figure 3.15: Regional inner plexiform layer : ganglion cell layer (IPL:GCL) ratio for each control and each stage of glaucoma progression, and inter-stage regional and total area differences. C = control, PG = preperimetric glaucoma, EG = early glaucoma, AG = advanced glaucoma, IN = inferior-nasal, IT = inferior-temporal, ST = superior-temporal, SN = superior-nasal.

3.4.10 Summary of results

A summary of key findings is shown below in Table 3.2.

Retinal layer	Glaucoma	Significant differences
GCC thickness	C > EG	All regions* All combined areas*
GCL thickness	C > EG	R1, R4 and R11* IN and IT quadrants, IT inner-quadrant* Inferior hemizone*
GCL volume	C > EG	Total area*
IPL thickness	C > EG PG > EG	All regions* <i>except R2, R3, R13</i> IN and SN quadrants, IN and IT inner-quadrants* Inferior inner-hemizone* Total area* R5-8 (mid-macula), R11* All inner-quadrants and inner-hemizones* Total area*
IPL:GCL ratio	C < PG	R4*

Table 3.2: Summary of significant findings. C = control, PG = preperimetric glaucoma, EG = early glaucoma. R = region. S = superior, I = inferior, IN = inferior-nasal, IT = inferior-temporal, ST = superior-temporal, SN = superior-nasal. *= $p < 0.01$.

3.5 Discussion

For the first time, differences in regional thickness and volume of separately segmented inner plexiform layer (IPL) and ganglion cell layer (GCL) of the macula in glaucoma have been assessed *in vivo*. In this study, a manual segmentation algorithm was used to demarcate the three innermost retinal layers, enabling separation of the IPL and GCL. Current-generation commercial OCT devices generally use an automated approach to segment specific retinal layers, providing full retinal thickness or peripapillary NFL measurements, while some devices (e.g. the Cirrus, Carl Zeiss Meditec Inc., Germany) utilise segmentation algorithms that identify the IPL and GCL layers as a joint complex. Only recently, however, has the capability to segment the IPL and GCL layers independently been implemented into commercial devices (Spectralis software version 6.0.7), but research on these individual parameters has not been published.

The generation of colour coded thickness maps allowed for the visualisation of regional thinning of inner retinal layers and would be beneficial for monitoring the glaucoma of a specific individual on a case-by-case basis. Indeed, many commercial OCT devices have inbuilt software to allow eye care practitioners to easily monitor changes in retinal thickness. It was interesting to note the association between visual field loss and regional thinning of the retinal layers, which has been shown previously in the mNFL and IPL-GCL complex (Hood and Raza 2011). Damage to RGCs at the macula has been shown to be arcuate in shape and associated with NFL thinning at the ONH (Hood et al. 2013); this arcuate shape was visible in the retinal layer thickness maps where visual field loss had occurred. However, for the purpose of this cross-sectional investigation, the colour coded thickness maps had limited scope. Instead, the regional thickness and volume values for each individual eye were collated and used for further analysis.

No difference in retinal thickness or volume was observed between corresponding retinal regions of equal eccentricity from the fovea for control eyes, or those with preperimetric or early glaucoma. However, eyes with advanced glaucoma showed regional differences in the thickness and volume of the mNFL. Interestingly, differences were usually found in the inferior regions in comparison to equivalent superior regions. This is particularly evident when corresponding hemizones and inner-hemizones were compared; the inferior hemizone had smaller mNFL volume than the superior hemizone.

Although assessing individual regions allowed for a more comprehensive analysis, the thickness or volume for the entire macula area was also analysed as part of this study, as well as grouping regions into hemizones, inner-hemizones, quadrants, and inner-quadrants. Measurements of the total area gave good general indications of changes, particularly if only one or two regions showed no significant differences between stages of glaucoma, but could also mask changes if only one region was affected. It was clear that the inner-hemizones and inner-quadrants were more sensitive to

differences than then full hemizones or quadrants. Investigating different combinations of grouped regions was necessary to determine which areas of interest to focus on in the future.

Indeed, the superior and inferior poles of the optic nerve head are proposed to have a higher susceptibility to damage in glaucoma (Quigley and Addicks 1981), consistent with the typical glaucomatous 'nasal step' visual field defect (Zingirian et al. 1979). A nasal step tends to appear in the superior visual field first (Sihota et al. 2007; Schiefer et al. 2010) indicating damage to the inferior retina, although the defect is also common in the inferior visual field. In this study not all the retinal layers showed equivalent regional differences to advanced glaucoma stage, suggesting that different layers have different susceptibility to damage.

In a perimetry study of visual field damage in glaucoma, Schiefer et al. (2010) found that in mild to moderate glaucoma, damage occurred preferentially in the upper rather than the lower hemifields, indicative of damage that is confined predominantly to the inferior retina. Schiefer et al. (2010) also determined that over half of the eyes they examined showed superior paracentral visual field loss within 3° eccentricity of the fovea, which corresponds with retinal damage in the inner inferior-nasal (R9) and inferior-temporal (R10) regions (within 2.5° of the fovea) in this study. Additionally, research into the GCL-IPL complex has indicated that there was more damage in the inferior retina than superior with increasing glaucoma progression (Hood et al. 2013). In the present study, differences were observed in the thickness and volume of the GCC, mNFL, GCL and IPL between early glaucoma and control groups for both of these inner inferior regions. Additional differences were observed between preperimetric glaucoma and control for the IPL.

The total GCC mean thickness for the healthy control group was found to be $142 \pm 10.42 \mu\text{m}$ and mean thickness of the IPL-GCL to be $74 \pm 2.51 \mu\text{m}$, which is slightly less than has been reported elsewhere (Tham et al. (2013) showed the average IPL-GCL thickness in healthy subjects to be 83 ± 6

μm , Francoz et al. (2014) found $82 \pm 7 \mu\text{m}$). Both of these studies were undertaken using a Zeiss Cirrus SD-OCT whereas the images in the present study were acquired using a research SD-OCT device with longer wavelength. Differences in measurements between OCT devices has previously been reported (Mylonas et al. 2009; Kiernan et al. 2010), and it may be the different device that caused the difference in macula parameters observed in the present study.

In the preperimetric glaucoma group, the average macula GCC thickness was found to be $96.6 \pm 8.81\mu\text{m}$; for early glaucoma: $95.9 \pm 8.8 \mu\text{m}$; and for advanced glaucoma the GCC increased to $114 \pm 11.2\mu\text{m}$. These data are not consistent with some published data. In the first of two studies that used the RTVue-100 (Optovue, US), an SD-OCT device, Kim et al. (2010) found GCC thickness in healthy eyes to be $95.08 \pm 7.88 \mu\text{m}$, $83.30 \pm 9.27 \mu\text{m}$ in early glaucoma and $80.13 \pm 9.60 \mu\text{m}$ in moderate glaucoma, using a similar classification model as in the present study. In the second study, Kim et al. (2013) found GCC thickness to be $95.07 \pm 7.09 \mu\text{m}$ in the healthy group and $77.02 \pm 8.90 \mu\text{m}$ in primary open angle glaucoma, where all stages of glaucoma were grouped. Kita et al. (2013) found GCC thickness $94.05 \pm 7.51\mu\text{m}$ for normal healthy eyes and $77.04 \pm 8.42 \mu\text{m}$ for the glaucoma group.

Furthermore, in the present study, the mNFL was found to have average thickness $68.5 \pm 10.0\mu\text{m}$ in the control group. Elsewhere it has been reported to be $44.8 \pm 14.8 \mu\text{m}$ (Varma et al. 2003), or up to $46.1 \pm 9.7 \mu\text{m}$ (Martinez-de-la-Casa et al. 2014). Whilst it has been established that variation exists between OCT devices (Kanamori et al. 2003; Leite et al. 2011), it is still unclear how much of the difference between these measurements is due to differences in devices and how much is due to other factors, such as scaling of the images. Indeed, in this study, OCT datasets were scaled using individual patient biometrics (Littmann 1988; Bennett et al. 1994), while it is unclear whether this was done in the studies described above.

Hood and Kardon (2007) describe a model for mNFL loss in glaucoma, whereby the mNFL thickness consists of two components, one being RGC axons and the other being everything else (including glial cells and blood vessels). They hypothesise that when the RGC axons are damaged and lost from pathology, the other component remains stable (Hood et al. 2008), and as such the mNFL thickness at a particular point stabilises at around $1/3^{\text{rd}}$ of its original thickness. This point is thought to occur when the visual field deficit at a particular point is around -10dB. The higher mNFL thickness described in the current study compared to previously published data could have been due to the segmentation protocol established at the beginning of the study; blood vessels above the mNFL were segmented around the exact surface, whereas blood vessels deeper within the retinal layers were extrapolated through. An outline of the blood vessels was visible on mNFL and GCC thickness maps (Figure 3.2) in some datasets, and this could have contributed to the greater mean thickness for mNFL and GCC described in the current study.

Differences in GCC and mNFL thickness were identified between early glaucoma and control groups that correspond with published data (Tan et al. 2008; Arintawati et al. 2013). Indeed, it has previously been suggested that both the GCC and mNFL are important in differentiating between control and all stages of glaucoma, including preperimetric. However, significant differences between control and preperimetric glaucoma were not determined here, although there was a trend for mid and inner regions to be thinner in preperimetric glaucoma than control. The latter trends would be of particular interest in subsequent longitudinal studies that make the most of the greater sensitivity afforded by within-subject regional variance.

The rationale for using the IPL:GCL thickness ratio was that, given the inter-subject variation found in cross sectional studies and subsequent insensitivity in cross sectional compared to longitudinal studies, having a measurement that was participant-specific would be particularly useful clinically. The IPL:GCL thickness ratio was used to detect differences between healthy control eyes and those

with preperimetric glaucoma, and therefore may be a key indicator of eyes at risk of glaucomatous damage. In practice, the total IPL:GCL thickness ratio for the control group (0.76) demonstrated that in healthy eyes the GCL was thicker than the IPL. In preperimetric glaucoma the GCL was 20% thinner than in the control group (IPL 3% less than in control, though this did not reach statistical significance) and both the IPL and GCL had similar thicknesses (IPL:GCL thickness ratio 0.96). In the early glaucoma group, the GCL had thinned by a further 13% (compared to preperimetric), and the IPL by 22%. The GCL was still thicker than the IPL but the difference between the two increases again (IPL:GCL thickness ratio 0.87). At this stage, both the GCL and IPL are significantly thinner than in healthy eyes. For advanced glaucoma the ratio increases slightly as both the GCL and IPL become 21% and 25% thicker respectively, compared to early glaucoma (IPL:GCL ratio 0.89, although this difference did not reach statistical significance). This is demonstrated in Figure 3.16.

The reduction in GCL thickness from control to preperimetric glaucoma is likely consistent with RGC apoptosis which is known to occur in glaucoma (Quigley et al. 1995), together with dendritic shrinkage (Morgan 2002; Shou et al. 2003). Apoptosis would include cell body shrinkage and RGC death; thus both these parameters would lead to a thinning of the GCL as RGCs and their dendrites shrink. At this stage there is no clinically detectable visual field loss as a result of the glaucomatous disease, however 25-35% RGCs loss usually occurs prior to VF loss detection (Kerrigan-Baumrind et al. 2000). The observed thinning of the IPL that occurs between preperimetric and early glaucoma is compatible with the theory of dendritic shrinkage of affected RGCs as they begin to deteriorate. This has been identified in cat, monkey and rat models of glaucoma (Weber et al. 1998; Shou et al. 2003; Liu et al. 2010). In early glaucoma, visual field loss begins functional damage as a consequence of structural damage occurs in the retina. The visual damage may result as a consequence of dendrites that protrude into the IPL of susceptible RGCs shrinking and no longer connecting to the mid-retinal cells (bipolar and amacrine cells) as they do in the normal retina, thereby inhibiting signalling throughout the RGC and, in turn, the brain.

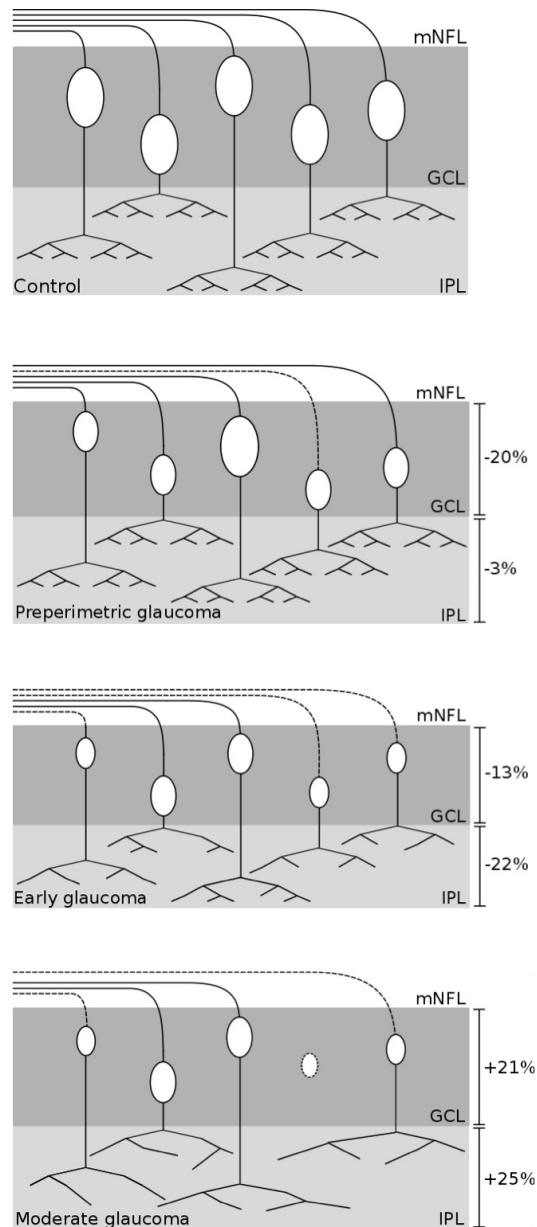


Figure 3.16: Changes in the ganglion cell layer (GCL) and inner plexiform layer (IPL) were identified between control and increasing stages of glaucoma. mNFL = macula nerve fibre layer.

From early to advanced glaucoma there was an increase in thickness for the IPL, and there was a trend for this increase in advanced glaucoma for mNFL and GCL thickness. These increases in thickness may be a consequence of an inflammatory response to RGC damage; leading to glial (Muller cells and/or astrocytes) activation and proliferation, in an attempt to rescue and provide support to the damaged retina. Additionally, RGC remodelling may occur as remaining functional RGCs extend their dendrites in an attempt to re-establish contact with other nearby cells.

3.5.1 Limitations of study

One of the limitations of this study was the number of eyes included. Obviously, if more data is acquired than firmer conclusions can be drawn. The major limitation of the technique described in this study was amount of time required for the manual segmentation of the retina; indeed, to manually segment the three retinal layers could take up to four hours for a single dataset. If the time per dataset was reduced, then potentially more datasets could be acquired and added to the study. A number of research groups are now introducing fully automated retinal segmentation software, and, as a result, in the future it may be the case that these techniques could be applied in a much more (processing) time-effective manner.

Another potential limitation was that the minimum requirements for acquired glaucomatous damage according to the Hodapp, Parrish and Anderson classification (Hodapp et al. 1993) include deviations on two consecutive visual field plots. For the purpose of this work, only one visual field test was performed per eye for each subject. However, glaucomatous participants had been recruited from within the hospital eye service, so had been exposed to visual field testing previously. Therefore the classification was based on that from Hodapp et al. (1993) and was appropriate for this work despite only using one visual field result per eye.

The grouping of individual regions to form quadrants and hemizones, as well as total area, also allows for the future comparison with data from other devices. The division of regions in the way detailed in the study uses a non-standard grid. Commercial devices use the ETDRS grid (Figure 3.17a), which has a maximum diameter of 6 mm. The grid used for this study had a maximum diameter of 17.2° (Figure 3.17b), which varies according to axial length. For example, in an eye with axial length 21 mm, the 17.2° grid would have a diameter of 4.48 mm, whereas in an eye with axial myopia, e.g. axial length 27 mm, the 17.2° grid would cover for 5.84 mm at the retina. However, although, in theory, the ETDRS grid should always give measurement of the same area, it is unclear

how commercial devices scale their images and whether they account for axial length. In this current study, by measuring the grid according to degrees and using Littmann equation to account for axial length, the scaling ensured that measurement were accurate at a given location.

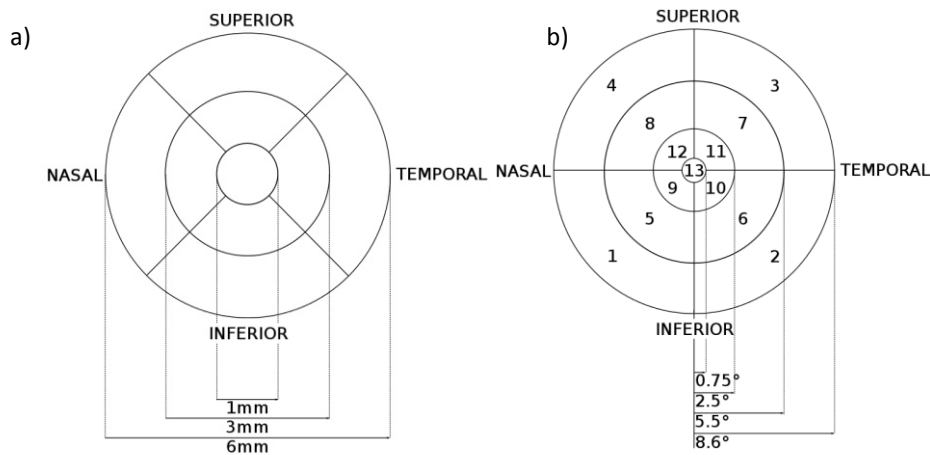


Figure 3.17: Comparison of (a) ETDRS grid and (b) the grid used to divide the macula into 13 regions in the present study.

3.5.2 Conclusion

In summary, previously unreported decreases in GCL thickness in preperimetric glaucoma and IPL thickness in early glaucoma were determined in this study, and these changes correspond with RGC apoptosis and dendritic shrinkage and remodelling in progressive stages of glaucoma. The IPL:GCL ratio has potential as a marker for differentiating between control eyes and those with preperimetric glaucoma. The latter may be clinically significant in identifying those eyes that are in the very early stages of glaucomatous disease prior to irreversible RGC death and vision loss. Some commercial devices (e.g. Spectralis) now have the ability to automatically resolve and segment each retinal layer independently, including the GCL and IPL. Therefore the use of IPL:GCL ratio could easily be used in clinical practice if a Spectralis device were available. These early changes could greatly advance analysis of glaucoma progression and aid the identification of those eyes at a very early stage of disease, so that therapeutic intervention at the earliest opportunity can prevent irreversible vision loss.

Chapter 4:
Analysis of age related changes in
in vivo human optic nerve head
microarchitecture

4 Analysis of age related changes in *in vivo* human optic nerve head microstructure

4.1 Introduction

Age is a major risk factor for glaucoma. The prevalence of primary open angle glaucoma (POAG) increases with increasing age (Leske 2007), and increasing age also increases the risk of developing POAG in patients who have ocular hypertension (Gordon et al. 2002). The optic nerve head, specifically the lamina cribrosa, is the principle site of retinal ganglion cell (RGC) axonal damage in glaucoma (Quigley et al. 1981; Minckler 1986; Burgoyne et al. 2005). Understanding changes in the optic nerve head (ONH) due to age is essential if we are to fully understand changes that occur due to glaucomatous disease.

Accordingly, in the present chapter the manner in which ageing, as well as a number of other measured ocular factors, naturally affect the structure of specific ONH parameters is investigated, including Bruch's membrane opening (BMO) diameter, nerve fibre layer (NFL) thickness, prelaminar depth and thickness, and lamina cribrosa (LC) depth and thickness. Published data suggest that the size of the optic disc is unaffected by age (Garway-Heath et al. 1997; Kee et al. 1997), which, in turn, infers that BMO diameter does not change. Previous optical coherence tomography (OCT) studies have shown that a decrease in peripapillary NFL thickness was apparent with increasing age (Hirasawa et al. 2010; Lee et al. 2012; Alasil et al. 2013), however, there has been little research into the potential changes in prelaminar depth from BMO or prelaminar thickness with age. However, an *ex vivo* study has shown that age is associated with a thickening of the LC (Kotecha et al. 2006), although this has yet to be replicated *in vivo* using OCT.

OCT has been used previously to investigate structures at the posterior pole of the eye, although due to the relatively novel nature of the technology and the speed at which it is advancing, very few

longitudinal studies have been carried out to examine the effect of ageing *in vivo*. Indeed, due to recent increases in device resolution, scan speed and modality (i.e. the advance of technology from time domain OCT to spectral domain OCT, and subsequent developments towards swept source OCT and adaptive optics), datasets from early OCT devices are no longer comparable to those generated by more modern machines. Instead, research has tended to focus on cross-sectional studies, whereby data are acquired and conclusions are drawn from comparisons between participant groups. Due to the limiting 'snapshot' nature of this type of research, it is intuitive to extract as much information, statistically, as possible from each participant episode. Thus, a multivariate analysis approach has been used in order to comprehensively characterise the eye at that particular point in time. Different factors that may contribute to each optic nerve head parameter are considered, including various ocular biometrics, while a step-wise deletion approach has been used to optimise each model in order to explain each particular measurement as fully as possible.

In the present chapter, the effect of age on the ONH in normal, healthy eyes without ocular pathology has been examined. If the effect of glaucoma on the eye is to be assessed successfully, it is logical to first examine what changes occur naturally as part of the ageing process. In turn, this information will be critical to identifying those structural parameters that specifically predict susceptibility to pathology.

4.1.1 Aims of the study

To identify if optic nerve head microstructural parameters alter with age, as age is a major risk factor for glaucoma, and if changes are present to identify whether they are region specific.

4.2 Experimental design

4.2.1 Participants

For the present study, 46 healthy participants, aged between 19-68 years (17 males and 29 females) were recruited from within staff, students and friends of Cardiff University (see Table 4.1 for comprehensive patient demographics).

Demographic	Mean \pm SD	Range
Age (years)	34.72 \pm 17.76	(19 – 68)
Gender	29F : 17M	
Mean spherical refraction (D)	-0.55 \pm 2.87	(-6.00 - +5.25)
Visual acuity (logMAR)	-0.14 \pm 0.09	(-0.20 – 0.02)
Intraocular pressure (mmHg)	13.54 \pm 2.81	(10 – 21)
Central corneal thickness (μ m)	538.57 \pm 42.77	(435 – 636)
Axial length (mm)	23.69 \pm 1.46	(20.18 - 26.68)
Anterior chamber depth (mm)	3.05 \pm 0.49	(1.88 - 4.51)
Mean deviation visual fields (dB)	-0.92 \pm 1.08	(1.29 - -3.14)

Table 4.1: Participant demographics. Data represents one eye from each participant. F = female, M = male)

4.2.2 Clinical assessments

Visual field tests (SITA 24-2 Fast Threshold, Humphrey Visual Field Analyser), refractive error, intraocular pressure, and axial length measurements were assessed as described in section 2.3.1. Inclusion criteria required for healthy controls were no history of significant ocular disease, best corrected visual acuity of 0.1 logMAR (6/7.5 Snellen), or better, in the eye being examined, IOP of \leq 21 mmHg, and no visual field defect, as defined by Hodapp et al. (1993). Subjects were also required to have a maximum refractive error of \pm 6.00 D mean sphere (less than 3.00 DC) to enable accurate focussing of the OCT device.

4.2.3 Optical coherence tomography

18.7° or 20° scans centred on the ONH of both eyes were acquired using enhanced depth imaging. Images were processed in order to remove artefacts from small eye movements and improve contrast in the images. All images were scaled and processed as previously described in section

2.4.4. One eye from each participant was chosen at random for further analysis in the study. In those instances where the chosen image was of insufficient quality (e.g. as a result of eye movements during image acquisition), the other eye dataset was selected instead.

4.2.4 2D Image analysis of optic nerve head microstructure

Datasets were sliced into 4 radial tomograms, every 45°, centred on the ONH. Bruch's membrane opening (BMO) diameter, prelamina depth and thickness, anterior and posterior LC depth and LC thickness were measured, as described in section 2.6. Additionally, the border nerve fibre layer (bNFL) and peripapillary nerve fibre layer (pNFL) were measured for each region.

4.2.5 Statistical analysis

For details of the statistical approach used in this chapter, refer to section 2.9. Briefly, both univariate (i.e. correlation tests) and multivariate (general linear models) were applied to the data in the present chapter. All statistical analyses were performed in RStudio (version 0.98.1091; an open source user interface for R Statistics). Optimised general linear models (GLMs) were generated by stepwise deletion of the fixed effects, *age*, *axial length*, *mean spherical refraction (MS)*, *mean deviation of visual field (MD)*, *anterior chamber depth (ACD)* and *central corneal thickness (CCT)*, and the interaction terms *age:MD*, *axial length:MD*, and *axial length:MS*, for each dependent variable, in order to investigate the direction and magnitude of associations with each ONH parameter. For this chapter, only one eye from each participant was used, and as such, no random term was included in the GLM.

In the majority of cases, a Gaussian family and an integer link function (i.e. the natural form of the data) were specified, and this met the model's assumption of a normal distribution of residual variance. Where this assumption was not met, i.e. the residual variance was not normally

distributed, an inverse link function was specified. In four cases (superior postlamina depth, nasal LC thickness, central LC thickness, and nasal peripapillary nerve fibre layer thickness) an inverse Gaussian family and a natural log function were specified in order to meet the assumptions of a generalised linear model, and to optimise the model for inferior-nasal anterior LC surface depth, inverse transformations were applied to the fixed effects.

Given that the focus of the present chapter is on the effect of ageing on the optic nerve head, particular focus has been placed on those models that include age as a fixed effect. Statistical results were reported as (mean \pm standard deviation, p -value) unless otherwise stated. A factor was considered to make a significant contribution to a model if $p < 0.05$. Additionally, within each section of the results a colour-coded diagram showing the p -values of *age* in each region is included, where p describes statistical significance and t describes the effect size of a given association, as a function of the overall variance.

4.3 Results

4.3.1 The effect of age and other ocular parameters on Bruch's membrane opening diameter

The mean diameter of Bruch's membrane opening (BMO) was used as a surrogate for optic disc diameter and was measured as shown in Figure 4.1.

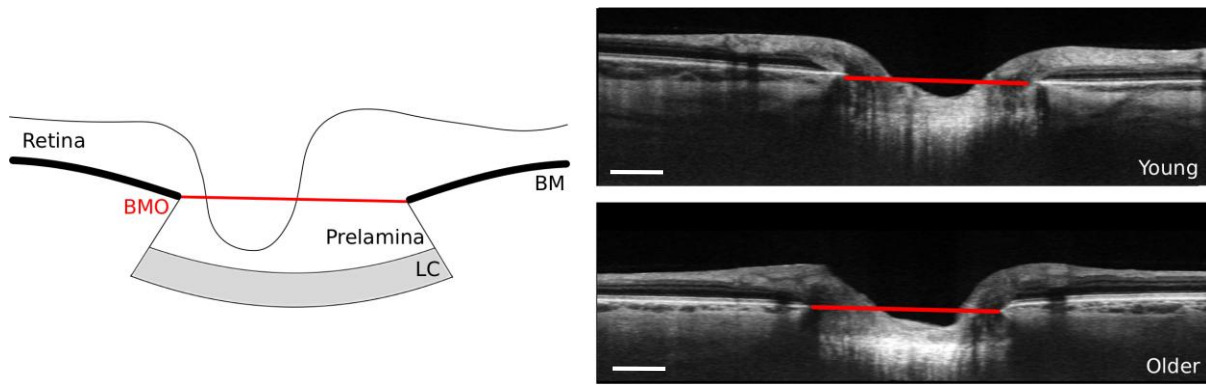


Figure 4.1: Schematic diagram of Bruch's membrane opening (BMO) diameter across the optic disc, and demonstrated on example images from old and young ONH datasets. BMO shown in red, BM = Bruch's Membrane, LC = Lamina cribrosa. Scale bar = 500 μm .

4.3.1.1 Quantification of Bruch's membrane opening diameter

The mean diameter for BMO, along with the standard deviation and range for each of the ONH regions are displayed below in Table 4.2. Following an initial univariate analysis of BMO diameter, no significant association between with age in any of the directions assessed was apparent (Pearson's correlation coefficient $p > 0.01$; Figure 4.2), suggesting that neither BMO diameter nor ONH size, altered naturally with age in the healthy eye.

Region	Mean \pm SD (μm)	Range (μm)
T-N BMO	1454.87 \pm 163.65	1144.14 - 1870.93
ST-IN BMO	1498.71 \pm 170.77	1194.85 - 1928.95
S-I BMO	1540.16 \pm 161.28	1207.89 - 1897.54
SN-IT BMO	1498.04 \pm 147.28	1143.88 - 1830.70

Table 4.2: Mean of each Bruch's membrane opening (BMO) diameter for each ONH region. (SD = standard deviation. T = temporal, ST = superior-temporal, S = superior, SN = superior-nasal, N = nasal, IN = inferior-nasal, I = inferior, IT = inferior-temporal).

Subsequently, the ratio of the horizontal (T-N) to vertical (S-I) BMO measurement was calculated to examine whether the aspect ratio, or circularity of the disc changed with age. However, again, univariate analysis revealed no significant association (Pearson's correlation coefficient, $p > 0.01$).

4.3.1.2 Multivariate analysis of Bruch's membrane opening diameter

Optimised general linear models (GLMs) generated to explain the variance in the diameter of BMO in each direction are described below in Table 4.3. Each row displays the independent variables that are included in the optimised GLM. Numbers quoted are effect size \pm standard error, i.e. how much the BMO diameter changes in μm /unit change in independent variable.

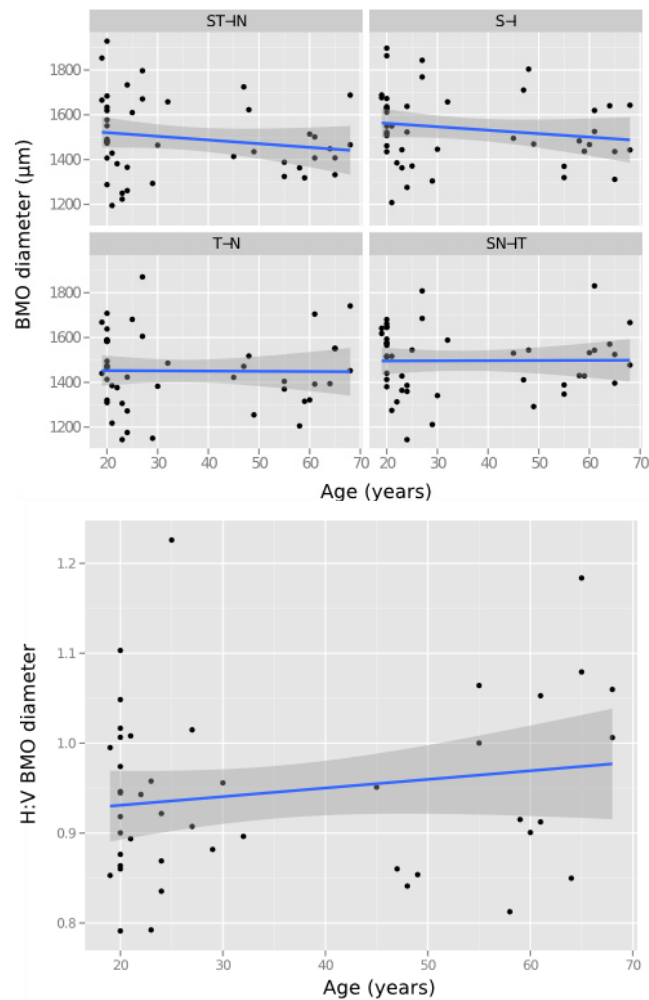


Figure 4.2: Bruch's membrane opening (BMO) diameter for each region of the optic nerve head, and horizontal:vertical BMO diameter, plotted against age. There was no significant correlation between age and increasing BMO diameter (Pearson's correlation coefficient $p > 0.01$). Grey bars = 95% confidence intervals. T = temporal, ST = superior-temporal, S = superior, SN = superior-nasal, N = nasal, IN = inferior-nasal, I = inferior, IT = inferior-temporal.

4.3.1.3 *The effect of age on Bruch's membrane opening diameter*

Age contributed significantly to explaining the variance in BMO diameter in the ST-IT ($-6.01 \pm 2.07 \mu\text{m}/\text{year}$, $p=0.006$) direction, and showed a trend in the S-I ($-5.06 \pm 2.05 \mu\text{m}/\text{year}$, $p=0.019$), i.e. BMO diameter was smaller with increasing age in these two planes (Table 4.3)

4.3.1.4 *Other factors that contribute to explain membrane opening diameter*

In addition to this effect of ageing, *axial length* was found to have a significant positive effect (of between 83 and 126 $\mu\text{m}/\text{mm}$ *axial length*) on the diameter of BMO in both the T-N ($p=0.009$) and ST-IN ($p=0.005$) planes (Table 4.3) i.e. larger eyes had larger BMO diameters. Moreover, *mean spherical refractive error* contributed significantly to BMO diameter changes in the ST-IN plane ($43.53 \pm 16.47 \mu\text{m}/\text{D}$, $p=0.012$), while *anterior chamber depth* had a significant negative effect on ST-IN BMO ($-196.28 \pm 92.61 \mu\text{m}/\text{mm ACD}$, $p=0.041$). Finally, *MD* had a significant negative contribution to the T-N BMO diameter ($-55.10 \pm 25.11 \mu\text{m}/\text{dB}$, $p=0.035$), i.e. although all eyes were healthy, eyes with greater *MD* (albeit within the normal limits specified by the participant selection criteria) had larger T-N BMO diameters.

Regional diameter	Model <i>p</i>	Model <i>R</i> ²	Age	AxL	MS	MD	ACD	CCT	Age:MD	AxL:MD	AxL:MS
T-N BMO	0.037	0.15		83.39 ± 30.23	19.68 ± 13.10	-55.10 ± 25.11	-140.36 ± 71.94				
<i>t value</i>				2.76	1.50	-2.19	-1.95				
<i>p value</i>				0.009	0.140	0.035	0.059				
ST-IN BMO	0.079	0.13	-6.01 ± 2.07	126.43 ± 42.03	43.53 ± 16.47	16.35 ± 27.67	-196.28 ± 92.61				
<i>t value</i>			-2.90	3.01	2.64	0.59	-2.12				
<i>p value</i>			0.006	0.005	0.012	0.558	0.041				
S-I BMO	0.17	0.09	-5.06 ± 2.05	88.84 ± 40.54	-206.80 ± 143.46	6.15 ± 26.75	-173.38 ± 89.72	-0.50 ± 0.69			
<i>t value</i>			-2.47	2.19	-1.44	0.23	-1.93	-0.73			
<i>p value</i>			0.019	0.035	0.160	0.819	0.062	0.472			
SN-IT BMO	0.17	0.04				-38.70 ± 23.63	-78.35 ± 51.67				
<i>t value</i>						-1.64	-1.52				
<i>p value</i>						0.109	0.137				

Table 4.3: General linear models for Bruch's membrane opening (BMO) diameter for each direction within the optic nerve head. Values are effect size ± standard error, i.e. how much BMO diameter changes in μm per one-unit change in the independent variable, as well as *t*-value and *p*-value. Red = factor is significant at *p*<0.05. T = temporal, ST = superior-temporal, S = superior, SN = superior-nasal, N = nasal, IN = inferior-nasal, I = inferior, IT = inferior-temporal, AxL = axial length, MS = mean spherical refractive error, MD = mean deviation on visual fields, ACD = anterior chamber depth, CCT = central corneal thickness.

4.3.2 The effect of age and other ocular parameters on the peripapillary and border nerve fibre layer thickness

Peripapillary nerve fibre layer (pNFL) was measured at a distance of 1.7mm from the centre of the optic disc, and border nerve fibre layer (bNFL) was measured directly above BMO (Figure 4.3).

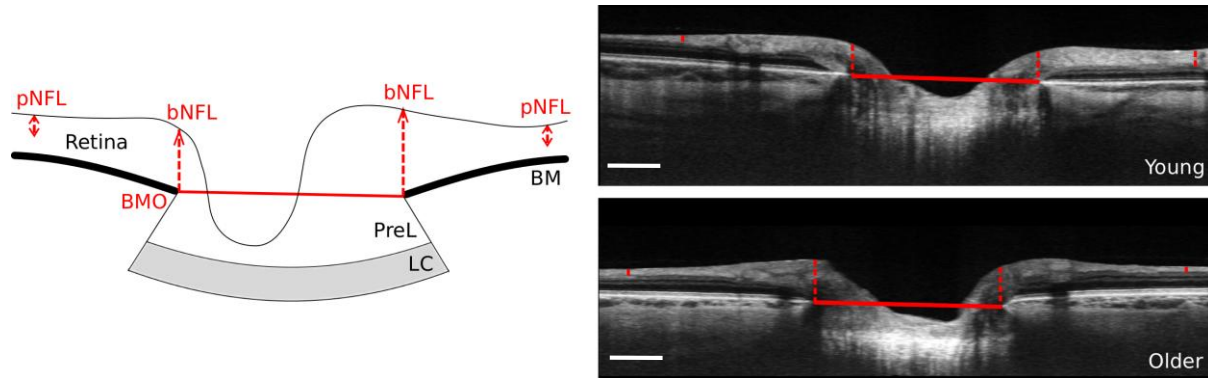


Figure 4.3: Schematic diagram of peripapillary nerve fibre layer (pNFL), measured at a distance 1.7mm from the centre of the optic disc, and border nerve fibre layer (bNFL), shown in red, and example images from old and young optic nerve heads. BM = Bruch's Membrane, PreL = prelamina, LC = Lamina cribrosa. Scale bars = 500 μm .

4.3.2.1 Quantification of nerve fibre layer parameters

The mean, standard deviation and range for each region of the nerve fibre layer parameters are shown below in Table 4.4.

Region		Mean \pm SD (μm)	Range (μm)
T	pNFL	48.07 \pm 10.92	25.99 - 74.42
ST	pNFL	100.73 \pm 29.02	60.15 - 172.33
S	pNFL	105.21 \pm 29.52	66.07 - 185.10
SN	pNFL	101.25 \pm 22.56	57.97 - 163.91
N	pNFL	50.42 \pm 15.25	24.06 - 85.10
IN	pNFL	369.36 \pm 83.35	6.67 - 541.49
I	pNFL	124.63 \pm 32.89	68.27 - 196.74
IT	pNFL	84.33 \pm 22.20	40.70 - 146.52
T	bNFL	236.93 \pm 47.06	131.35 - 360.90
ST	bNFL	315.88 \pm 49.88	210.71 - 465.76
S	bNFL	393.24 \pm 83.41	209.07 - 583.15
SN	bNFL	402.37 \pm 85.40	241.37 - 685.39
N	bNFL	341.07 \pm 77.65	200.50 - 613.44
IN	bNFL	83.10 \pm 21.00	49.10 - 139.10
I	bNFL	387.51 \pm 66.43	187.73 - 571.79
IT	bNFL	297.52 \pm 45.20	204.24 - 423.53

Table 4.4: Mean of each nerve fibre layer parameter. pNFL = peripapillary nerve fibre layer, bNFL = border nerve fibre layer, SD = standard deviation. T = temporal, ST = superior-temporal, S = superior, SN = superior-nasal, N = nasal, IN = inferior-nasal, I = inferior, IT = inferior-temporal.

4.3.2.2 Univariate analysis of nerve fibre layer parameters

Univariate analyses revealed that in the inferior, IN and IT regions pNFL thinning was associated with increasing age (I $r=-0.55$, $p=0.005$; IN $r=-0.40$, $p=0.026$; IT $r=-0.60$, $p=0.002$; Figure 4.5a). Using the same statistical method, bNFL thinning showed a significant relationship with increasing age in all regions except those on the temporal side of the ONH, i.e. IT, T and ST (S $r=-0.35$, $p=0.020$; SN $r=-0.45$, $p=0.003$; N $r=-0.39$, $p=0.008$; IN $r=-0.35$, $p=0.018$; and I $r=-0.33$, $p=0.027$; Figure 4.5).

4.3.2.3 Multivariate analysis of nerve fibre layer parameters

The optimised GLMs for the thickness of the peripapillary and border NFL for each of the ONH regions are described below in Table 4.5 and Table 4.6. Each row displays the independent variables that are included in the optimised GLM. Numbers quoted are effect size \pm standard error, i.e. how much the NFL thickness changes in μm per unit change in independent variable.

4.3.2.4 The effect of age on nerve fibre layer parameters

Age had a significant negative effect on the thickness of the pNFL in both the inferior ($-1.68 \pm 0.49 \mu\text{m}/\text{year}$, $p=0.003$) and IN ($-0.81 \pm 0.22 \mu\text{m}/\text{year}$, $p=0.001$) regions; Figure 4.4).

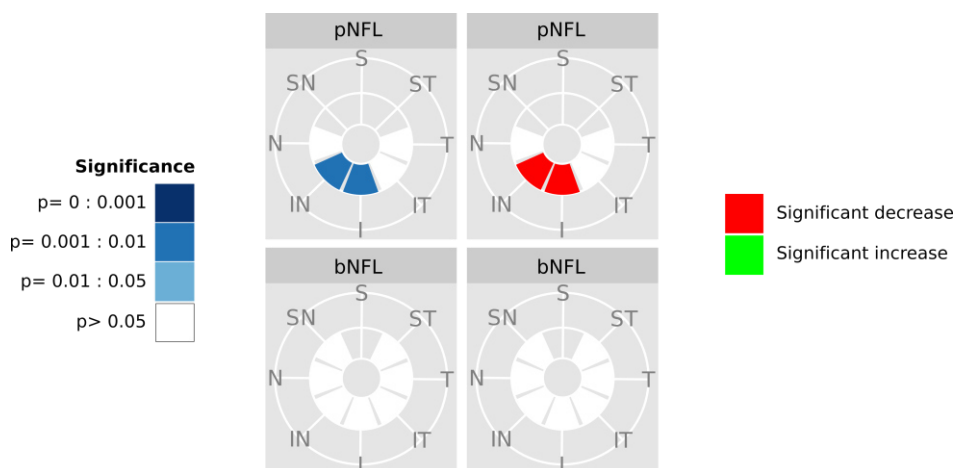


Figure 4.4: Regions of peripapillary nerve fibre layer (pNFL) and border nerve fibre layer (bNFL) that were affected by age, using general linear models. T = temporal, ST = superior-temporal, S = superior, SN = superior-nasal, N = nasal, IN = inferior-nasal, I = inferior, IT = inferior-temporal. Blue indicates significant contribution, white indicates that age was factor in the GLM but not significant. Green = increase, red = decrease.

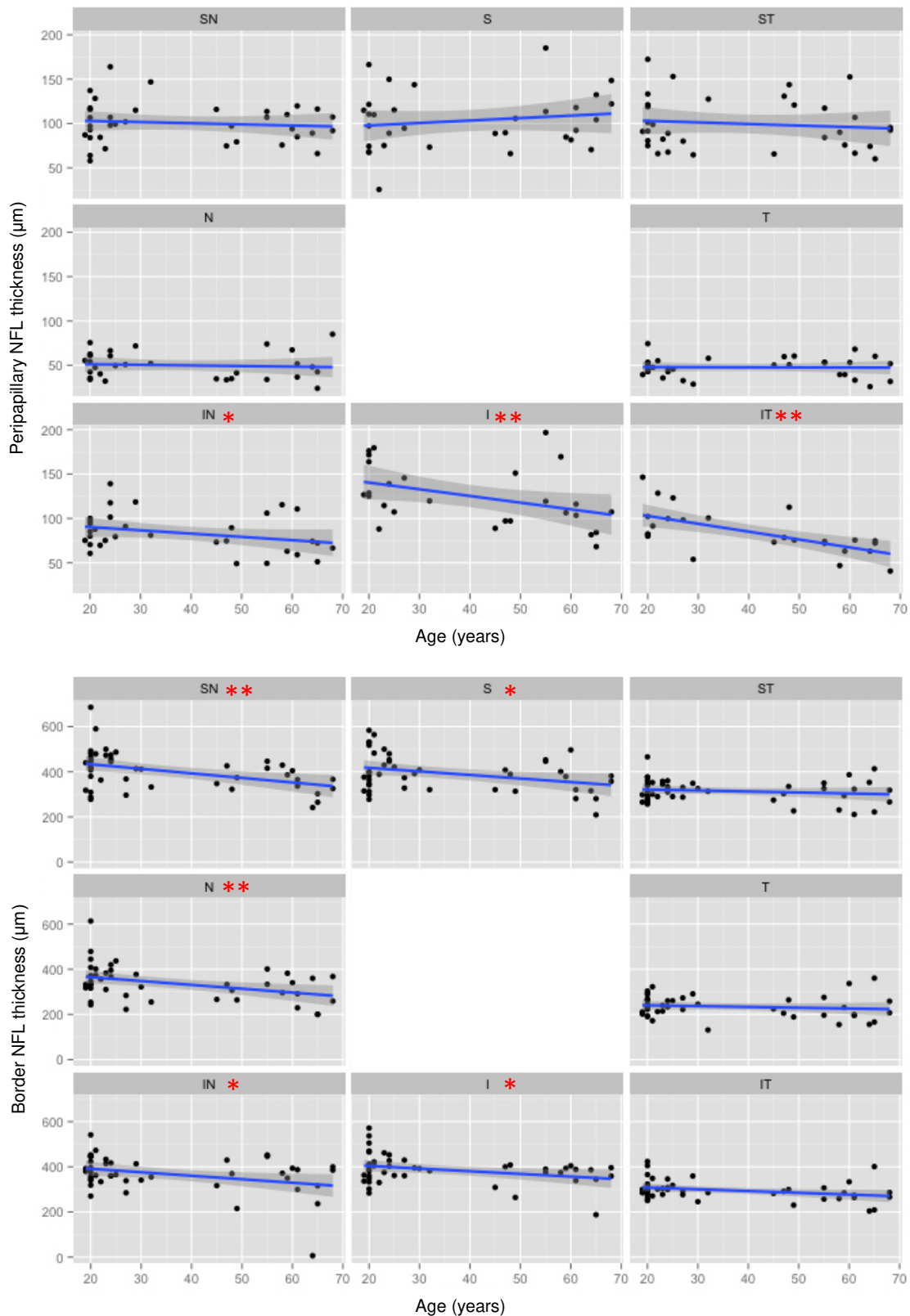


Figure 4.5: Peripapillary nerve fibre layer (pNFL) and border nerve fibre layer (bNFL) thickness as a function of age. Pearson's correlation coefficient * = $p < 0.05$, ** = $p < 0.01$. Grey bars = 95% confidence intervals, T = temporal, ST = superior-temporal, S = superior, SN = superior-nasal, N = nasal, IN = inferior-nasal, I = inferior, IT = inferior-temporal.

Regional thickness	Model <i>p</i>	Model R ²	Age	AxL	MS	MD	ACD	CCT	Age:MD	AxL:MD	AxL:MS
T pNFL	0.631	-0.06	0.21 ± 0.14	2.20 ± 3.87	-22.61 ± 17.93	-1.54 ± 2.46		-0.06 ± 0.05			0.92 ± 0.75
<i>t value</i>			1.51	0.57	-1.26	-0.63		-1.21			1.23
<i>p value</i>			0.145	0.576	0.220	0.538		0.238			0.231
ST pNFL	0.088	0.15		-8.43 ± 5.74		224.83 ± 93.93		-0.18 ± 0.12		-9.44 ± 3.87	
<i>t value</i>				-1.47		2.39		-1.57		-2.44	
<i>p value</i>				0.154		0.025		0.129		0.022	
S pNFL	0.046	0.18		10.87 ± 4.73		5.70 ± 5.42		0.25 ± 0.12			
<i>t value</i>				2.30		1.05		2.15			
<i>p value</i>				0.030		0.302		0.041			
SN pNFL	0.783	-0.03				1.14 ± 4.11					
<i>t value</i>						0.28					
<i>p value</i>						0.782					
N pNFL	0.646	-0.07	-0.16 ± 0.23	-2.99 ± 4.97	43.64 ± 26.15	0.76 ± 3.96					-1.76 ± 1.08
<i>t value</i>			-0.67	-0.60	1.67	0.19					-1.63
<i>p value</i>			0.513	0.553	0.110	0.850					0.118
IN pNFL	0.009	0.29	-0.81 ± 0.22		3.69 ± 1.61	5.10 ± 3.76					
<i>t value</i>			-3.63		2.29	1.36					
<i>p value</i>			0.001		0.031	0.187					
I pNFL	0.053	0.33	-1.68 ± 0.49	14.61 ± 13.49	-67.69 ± 63.09	-2.72 ± 6.33	-51.73 ± 21.60	0.08 ± 0.14			2.87 ± 2.60
<i>t value</i>			-3.46	1.08	-1.07	-0.43	-2.40	0.56			1.11
<i>p value</i>			0.003	0.295	0.299	0.673	0.029	0.587			0.286
IT pNFL	0.024	0.35	-0.45 ± 0.28	2.55 ± 5.30	13.93 ± 36.97			-0.11 ± 0.10			-0.63 ± 1.49
<i>t value</i>			-1.62	0.48	0.38			-1.08			-0.42
<i>p value</i>			0.123	0.374	0.711			0.294			0.679

Table 4.5: General linear models for peripapillary nerve fibre layer (pNFL) thickness, containing effect size ± standard error, i.e. how much pNFL changes in µm per one-unit change in the independent variable, as well as *t*-value and *p*-value. Red text = factor is significant at *p*<0.05. T = temporal, ST = superior-temporal, S = superior, SN = superior-nasal, N = nasal, IN = inferior-nasal, I = inferior, IT = inferior-temporal, AxL = axial length, MS = mean spherical refractive error, MD = mean deviation on visual fields, ACD = anterior chamber depth, CCT = central corneal thickness.

Regional thickness		Model p	Model R ²	Age	AxL	MS	MD	ACD	CCT	Age:MD	AxL:MD	AxL:MS
T	bNFL	0.037	0.23	1.00 ± 0.64	-11.03 ± 12.26	75.24 ± 40.11	-176.82 ± 109.08	69.04 ± 25.19	0.29 ± 0.18	0.66 ± 0.38	6.75 ± 4.63	-3.25 ± 1.66
	<i>t value</i>			1.57	-0.90	1.88	-1.62	2.74	1.58	1.71	1.46	-1.96
	<i>p value</i>			0.127	0.375	0.070	0.115	0.010	0.123	0.097	0.155	0.059
ST	bNFL	0.014	0.29	1.23 ± 0.65	-18.72 ± 12.40	67.66 ± 40.55	-211.61 ± 110.28	81.86 ± 25.46	0.25 ± 0.19	0.56 ± 0.39	8.60 ± 4.68	-3.15 ± 1.68
	<i>t value</i>			1.90	-1.51	1.67	-1.92	3.22	1.35	1.44	1.84	-1.87
	<i>p value</i>			0.066	0.141	0.105	0.064	0.003	0.186	0.160	0.075	0.070
S	bNFL	0.016	0.23		-21.10 ± 19.24	182.61 ± 66.45	-240.16 ± 185.14	55.86 ± 34.74			10.81 ± 7.80	-8.03 ± 2.73
	<i>t value</i>				-1.10	2.75	-1.30	1.61			1.39	-2.94
	<i>p value</i>				0.280	0.009	0.203	0.117			0.175	0.006
SN	bNFL	0.013	0.26	-0.79 ± 0.97	-16.96 ± 19.22	124.29 ± 68.01	3.03 ± 12.68	19.70 ± 42.53	-0.51 ± 0.33			-5.71 ± 2.83
	<i>t value</i>			-0.81	-0.88	1.83	0.24	0.46	-1.55			-2.02
	<i>p value</i>			0.422	0.383	0.076	0.813	0.646	0.130			0.051
N	bNFL	0.007	0.28	0.56 ± 0.99	-27.81 ± 17.01	-15.73 ± 6.66	-45.67 ± 24.86	71.65 ± 39.42		1.40 ± 0.58		
	<i>t value</i>			0.57	-1.64	-2.36	-1.84	1.82		2.41		
	<i>p value</i>			0.573	0.111	0.024	0.075	0.078		0.022		
IN	bNFL	0.247	0.060	-0.52 ± 1.08	-19.73 ± 21.38	89.38 ± 75.65	-1.61 ± 14.11	32.27 ± 47.31	-0.36 ± 0.36			-4.07 ± 3.14
	<i>t value</i>			-0.48	-0.92	1.18	-0.11	0.68	-0.99			-1.30
	<i>p value</i>			0.634	0.363	0.246	0.910	0.500	0.332			0.204
I	bNFL	0.027	0.15	-1.00 ± 0.68			-18.50 ± 22.71			0.81 ± 0.51		
	<i>t value</i>			-1.46		-0.82		1.61				
	<i>p value</i>			0.154		0.420		0.117				
IT	bNFL	0.016	0.23	0.46 ± 0.54	7.80 ± 7.65		-233.67 ± 99.37	42.64 ± 23.16		0.94 ± 0.34	8.30 ± 4.18	
	<i>t value</i>			0.87	1.02	-2.35	1.84	2.73	1.99			
	<i>p value</i>			0.392	0.315	0.025	0.074	0.010	0.055			

Table 4.6: General linear models for border nerve fibre layer (bNFL) thickness, containing effect size ± standard error, i.e. how much bNFL changes in µm per one-unit change in the independent variable, as well as *t*-value and *p*-values. Red text = factor is significant at $p < 0.05$. T = temporal, ST = superior-temporal, S = superior, SN = superior-nasal, N = nasal, IN = inferior-nasal, I = inferior, IT = inferior-temporal, AxL = axial length, MS = mean spherical refractive error, MD = mean deviation on visual fields, ACD = anterior chamber depth, CCT = central corneal thickness.

4.3.2.5 *The effect of other ocular parameters on the nerve fibre layer*

Conversely, *axial length* did not contribute significantly to explain the thickness of the bNFL in any of the ONH regions assessed. In the superior region, *axial length* explained a significant amount of variance in pNFL thickness ($10.87 \pm 4.73 \mu\text{m}/\text{mm}$ *axial length*, $p=0.030$), i.e. larger eyes had thicker superior pNFL.

Mean spherical refractive error showed significant positive association with pNFL thickness in the IN ($3.69 \pm 1.61 \mu\text{m}/\text{D}$, $p=0.031$; Table 4.5) and the S regions ($182.61 \pm 66.45 \mu\text{m}/\text{D}$, $p=0.009$; Table 4.6), i.e. eyes with greater amounts of hyperopia tended to have thicker bNFL in these regions. Conversely, in the nasal region, *MS* was shown to have a significant negative effect on the bNFL ($-15.73 \pm 6.66 \mu\text{m}/\text{D}$, $p=0.024$), i.e. more hyperopic eyes had thinner nasal bNFL than myopic eyes.

Although the inclusion criteria stated 'no visual field defect, as described by Hodapp et al. (1993)', *mean deviation of visual field (MD)* contributed significantly to explain the thickness of the IT bNFL ($-233.67 \pm 99.37 \mu\text{m}/\text{dB}$, $p=0.025$), i.e. the IT bNFL appeared to be thicker in eyes with greater *MD*. Also, in the ST region, *MD* had a significant positive effect on pNFL thickness ($224.83 \pm 93.93 \mu\text{m}/\text{dB}$, $p=0.025$), i.e. eyes with greater *MD* had thinner ST pNFL.

Anterior chamber depth (ACD) contributed to a change in up to $82 \mu\text{m}/\text{mm}$ in the thickness of the bNFL in both the temporal ($p=0.009$) and ST regions ($p=0.003$), i.e. eyes with deeper *ACD* had thicker temporal and ST bNFL (Table 4.6). *ACD* also contributed to explaining a significant amount of variance in the pNFL, exhibiting a negative association in the inferior region ($p=0.029$; Table 4.5).

Central corneal thickness (CCT) did not contribute significantly to explain changes in thickness of the bNFL in any region of the ONH. *CCT* did, however, have a significant positive contribution to explaining the pNFL thickness in the superior region ($0.25 \pm 0.12 \mu\text{m}/\mu\text{m}$ *CCT*, $p=0.041$; Table 4.5).

The association between *axial length:MS* had a significant negative effect on the thickness of the superior bNFL ($-8.03 \pm 2.73 \mu\text{m}$, $p=0.006$). The interaction between *axial length:MD* contributed negatively to explain the thickness of the ST pNFL ($-9.44 \pm 3.87 \mu\text{m}$, $p=0.022$). Additionally, the association between *age:MD* had a significant positive contribution to the thickness of the bNFL in the N ($1.40 \pm 0.58 \mu\text{m}$, $p=0.022$) and IT ($0.94 \pm 0.34 \mu\text{m}$, $p=0.010$) regions.

4.3.3 The effect of age and other ocular parameters on the prelamina

The depth of the prelamina surface from BMO and the prelamina thickness were measured as denoted in Figure 4.6. Prelamina depth measures that were above BMO were negative, and measurements below BMO were assigned as positive; however, for ease of understanding, in scatter plots representing prelamina depth the y-axis was reversed in order for ONHs where the prelamina surface was above BMO the data points would be towards the top of the graph and for data points where the prelamina surface was below BMO the data points were lower on the graph.

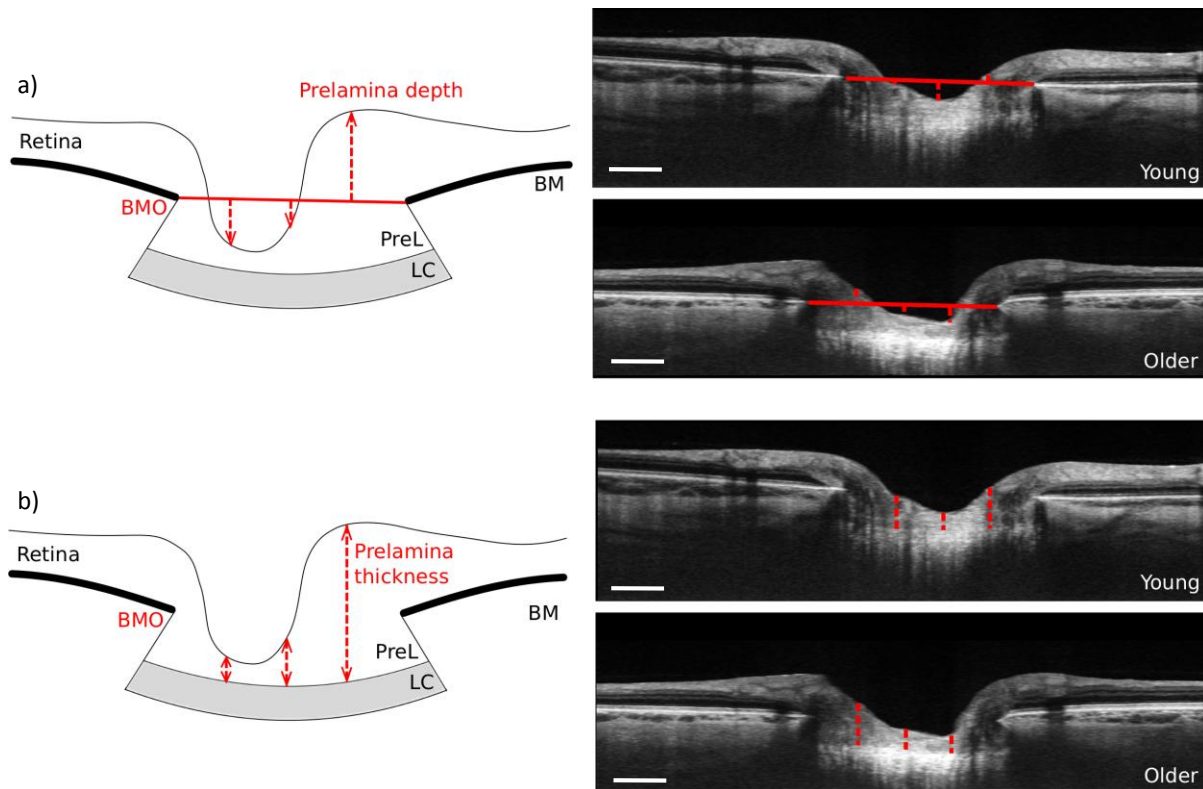


Figure 4.6: Schematic diagram of prelamina depth and prelamina thickness, shown in red, and example images from old and young optic nerve heads (BM = Bruch's Membrane, BMO = Bruch's membrane opening, PreL = prelamina, LC = Lamina cribrosa). Scale bars = 500 μm .

4.3.3.1 Quantification of prelamina parameters

The mean prelamina measurements, along with the standard deviation and range for each of the ONH regions are displayed below in Table 4.7.

Region		Mean	±	SD (µm)	Range (µm)	
T	PreL depth	42.72	±	158.13	-254.28	- 383.42
ST	PreL depth	-16.08	±	173.99	-469.55	- 321.60
S	PreL depth	-139.74	±	202.59	-617.23	- 357.61
SN	PreL depth	-237.11	±	193.63	-598.29	- 294.94
N	PreL depth	-256.51	±	197.08	-605.87	- 451.40
IN	PreL depth	-212.29	±	256.97	-545.28	- 493.60
I	PreL depth	-162.09	±	220.45	-530.13	- 457.15
IT	PreL depth	-42.37	±	154.84	-303.18	- 443.04
C	PreL depth	70.15	±	193.88	-337.41	- 468.67
T	PreL thick	293.28	±	148.21	95.86	- 658.24
ST	PreL thick	337.03	±	155.21	75.34	- 678.08
S	PreL thick	479.03	±	184.26	135.22	- 845.61
SN	PreL thick	549.30	±	159.15	191.71	- 890.20
N	PreL thick	578.40	±	138.81	118.03	- 783.16
IN	PreL thick	555.95	±	145.69	269.13	- 799.51
I	PreL thick	495.28	±	171.51	70.05	- 719.84
IT	PreL thick	199.70	±	47.29	103.51	- 338.26
C	PreL thick	269.40	±	176.13	72.39	- 736.76

Table 4.7: Mean of each regional optic nerve head parameter. PreL depth = prelamina depth, PreL thick = prelamina thickness, SD = standard deviation. T = temporal, ST = superior-temporal, S = superior, SN = superior-nasal, N = nasal, IN = inferior-nasal, I = inferior, IT = inferior-temporal, C = central.

4.3.3.2 Univariate analysis of prelamina measurements

Prelamina surface depth was found to decrease with age in the S, I and N regions of the ONH (Figure 4.7). However, univariate analysis revealed that only the negative association that existed between prelamina depth and age was only significant in the IN region of the ONH only ($r=0.32$, $p=0.040$). Although prelamina thickness appeared to thin with increasing age in the I and IN regions of the ONH (Figure 4.7), no significant correlations were defined as a function of age in any ONH regions (Pearson's correlation coefficient, $p>0.05$).

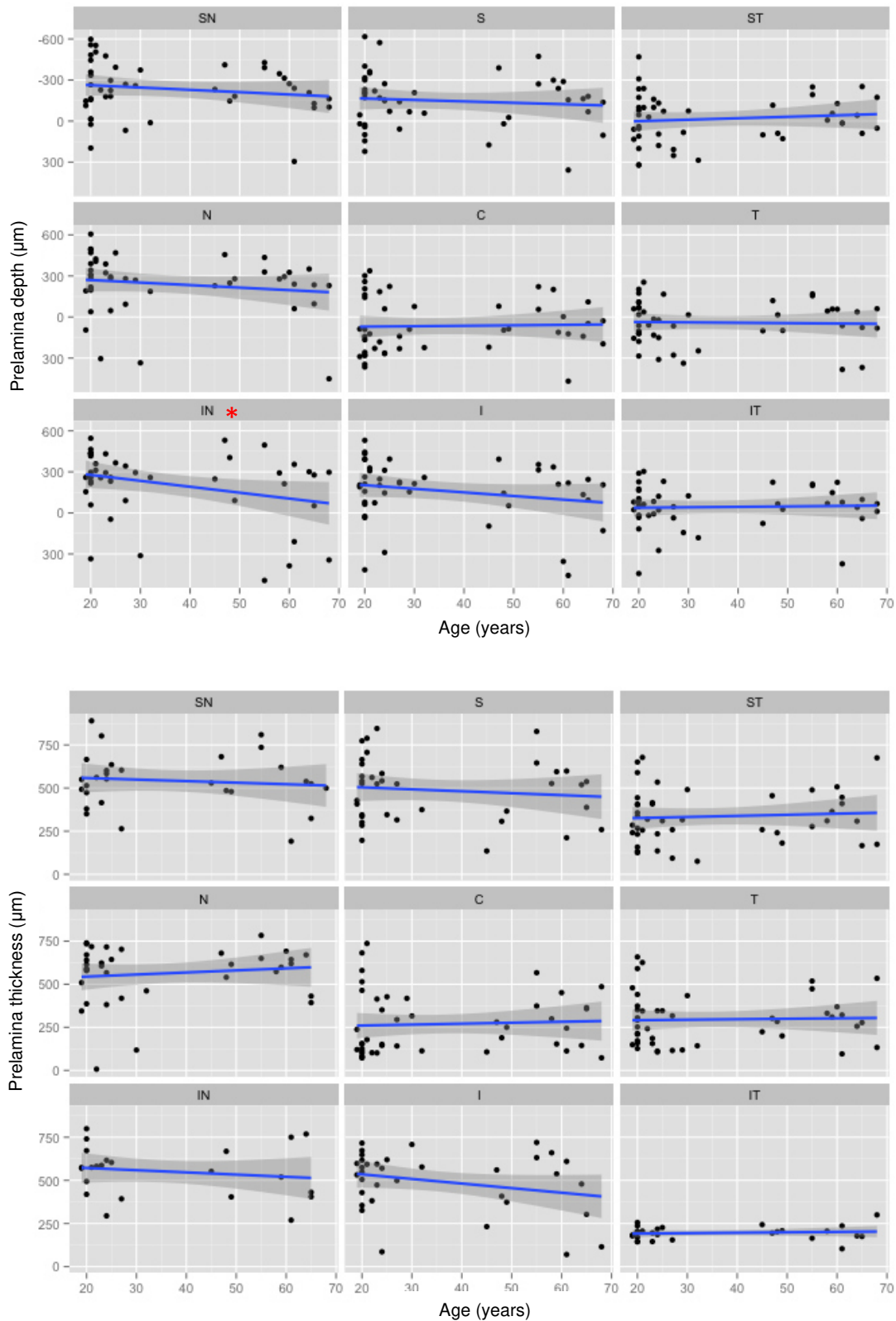


Figure 4.7: Prelamina depth and prelamina thickness plotted against age, for each region of the optic nerve head. For plotting purposes, the y-axis was reversed for prelamina depth so that negative values denoting depth above BMO are above zero and positive values are below y-axis zero. Pearson's correlation coefficient $*=p < 0.05$. Grey bars = 95% confidence intervals. T = temporal, ST = superior-temporal, S = superior, SN = superior-nasal, N = nasal, IN = inferior-nasal, I = inferior, IT = inferior-temporal, C = central.

4.3.3.3 Multivariate analysis of prelamina measurements

The optimised general linear models (GLMs) for prelamina depth (Table 4.8) and prelamina thickness (Table 4.9) for each ONH region are described below. Each row displays the independent variables that were required to describe the optimised GLM. Numbers quoted are effect size \pm standard error, i.e. how much the prelamina depth or thickness changes in μm per unit change in independent variable.

4.3.3.4 The effect of age on prelamina parameters

Although *age* was a factor in the optimised GLMs for prelamina surface depth in the T, ST, S, SN and IN regions, a significant effect was only identified in the ST region ($p=0.036$), where prelamina depth decreased by $3.77 \pm 1.73 \mu\text{m}/\text{year}$. Additionally, *age* demonstrated a significant positive effect on the prelamina thickness in the ST ($3.74 \pm 1.74 \mu\text{m}/\text{year}$, $p=0.039$) and N ($4.02 \pm 1.83 \mu\text{m}/\text{year}$, $p=0.037$) regions, implying a decrease in thickness with increasing age. These effects are summarised in Figure 4.8 below.

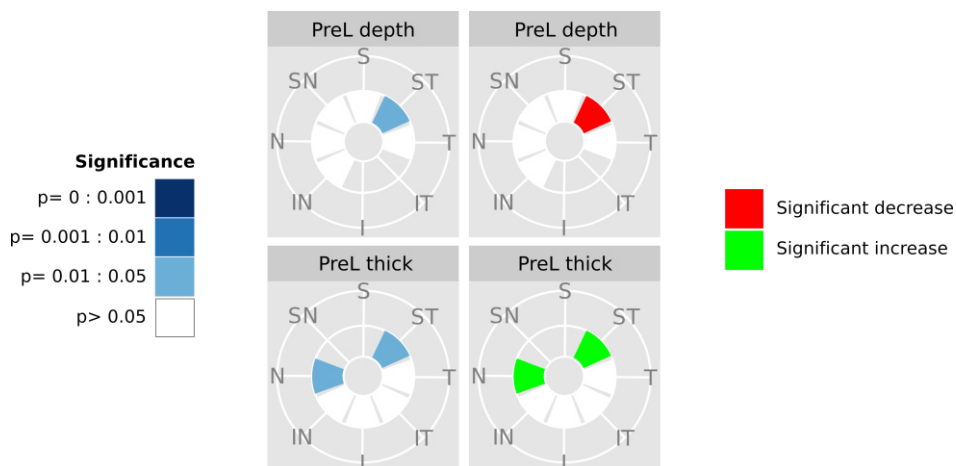


Figure 4.8: Optic nerve head regions where prelamina depth (PreL depth) or thickness (PreL thick) was affected as a function of age in general linear models (GLM). T = temporal, ST = superior-temporal, S = superior, SN = superior-nasal, N = nasal, IN = inferior-nasal, I = inferior, IT = inferior-temporal, C = central Blue indicates significant factor, white indicates that age was part of the GLM but not significant. Green = increase, red = decrease.

Regional depth		Model <i>p</i>	Model R ²	Age	AxL	MS	MD	ACD	CCT	Age:MD	AxL:MD	AxL:MS
T	PreL depth	0.252	0.03	-1.98±1.69			110.84±54.90			-1.89±1.08		
	<i>t value</i>			-1.17			2.02			-1.75		
	<i>p value</i>			0.248			0.050			0.089		
ST	PreL depth	0.077	0.13	-3.77±1.73	65.82±31.06	-173.43±146.95	8.47±27.46					9.09±6.11
	<i>t value</i>			-2.18	2.12	-1.18	0.31					1.49
	<i>p value</i>			0.036	0.041	0.246	0.760					0.145
S	PreL depth	0.421	0.01	-2.31±2.62	98.50±52.48	-196.49±184.04	25.98±34.71	-88.79±116.15				9.56±7.67
	<i>t value</i>			-0.88	1.88	-1.07	0.75	-0.76				1.25
	<i>p value</i>			0.384	0.069	0.293	0.459	0.450				0.221
SN	PreL depth	0.433	0.004	19.01±31.34	61.89±58.25	-340.98±175.89	-2.69±33.89		0.34±0.85			14.96±7.29
	<i>t value</i>			0.61	1.06	-1.94	-0.08		0.47			2.05
	<i>p value</i>			0.548	0.296	0.061	0.937		0.640			0.048
N	PreL depth	0.073	0.14	-1.27±2.36	100.61±47.48	51.49±18.92	48.92±31.14	-152.94±104.70	-1.12±0.80			
	<i>t value</i>			-0.54	2.12	2.72	1.57	-1.46	1.40			
	<i>p value</i>			0.595	0.041	0.010	0.125	0.153	0.171			
IN	PreL depth	0.087	0.12	3.51±2.59	35.47±46.47	384.50±219.84	71.32±41.08					-15.57±9.14
	<i>t value</i>			1.35	0.76	1.75	1.74					-1.70
	<i>p value</i>			0.184	0.450	0.089	0.091					0.097
I	PreL depth	0.004	0.26		62.94±30.97	49.04±16.11	89.29±27.94		-1.26±0.74			
	<i>t value</i>				2.03	3.05	3.20		-1.71			
	<i>p value</i>				0.049	0.004	0.003		0.095			
IT	PreL depth	0.088	0.07				46.30±24.06	93.48±52.62				
	<i>t value</i>						1.92	1.78				
	<i>p value</i>						0.062	0.083				
C	PreL depth	0.15	0.07		2.50±31.53	-353.28±164.22	30.70±28.56					14.45±6.79
	<i>t value</i>				0.08	-2.15	1.08					2.13
	<i>p value</i>				0.937	0.038	0.289					0.040

Table 4.8: General linear models for prelamina (PreL) depth for each optic nerve head region. Values are effect size ± standard error, i.e. how much the prelamina depth changes in μm per one-unit change in the independent variable, as well as *t*-value and *p*-value. Red text = factor is significant at *p*<0.05. T = temporal, ST = superior-temporal, S = superior, SN = superior-nasal, N = nasal, IN = inferior-nasal, I = inferior, IT = inferior-temporal, C = central, AxL = axial length, MS = mean spherical refractive error, MD = mean deviation on visual fields, ACD = anterior chamber depth, CCT = central corneal thickness.

Regional thickness	Model p	Model R^2	Age	AxL	MS	MD	ACD	CCT	Age:MD	AxL:MD	AxL:MS
T Prel thick	0.214	0.05	2.60 ± 1.55	22.48 ± 16.07		-106.72 ± 50.35			0.36 ± 1.14		
<i>t value</i>			1.68	1.40		-2.12			2.07		
<i>p value</i>			0.102	0.171		0.041			0.046		
ST Prel thick	0.105	0.11	3.74 ± 1.74	-61.41 ± 27.76	-26.13 ± 13.91	-75.03 ± 52.41			1.82 ± 1.19		
<i>t value</i>			2.15	-2.21	-1.88	-1.43			1.53		
<i>p value</i>			0.039	0.034	0.069	0.161			0.135		
S Prel thick	0.112	0.09		37.66 ± 44.76		-1026.83 ± 547.99				41.41 ± 22.62	
<i>t value</i>				0.84		-1.87				1.83	
<i>p value</i>				0.407		0.071				0.077	
SN Prel thick	0.395	0.01		-34.88 ± 28.98	181.24 ± 212.10	25.63 ± 35.11					-8.53 ± 8.69
<i>t value</i>				-1.20	0.86	0.73					-0.98
<i>p value</i>				0.241	0.402	0.473					0.336
N Prel thick	0.079	0.18	4.02 ± 1.83	-32.09 ± 26.79	-403.36 ± 158.85	-128.97 ± 62.44			2.68 ± 1.45		15.54 ± 6.60
<i>t value</i>			2.20	-1.20	-2.54	-2.07			1.86		2.36
<i>p value</i>			0.037	0.242	0.017	0.049			0.075		0.026
IN Prel thick	0.592	-0.05	-1.78 ± 1.79			-7.16 ± 31.36					
<i>t value</i>			-1.00			-0.23					
<i>p value</i>			0.331			0.822					
I Prel thick	0.015	0.25	-2.88 ± 1.65		-28.40 ± 11.93	-61.95 ± 28.51	-149.87 ± 69.23				
<i>t value</i>			-1.74		-2.38	-2.17	-2.17				
<i>p value</i>			0.092		0.024	0.038	0.039				
IT Prel thick	0.119	0.18	-0.21 ± 0.69	-11.65 ± 16.01	8.69 ± 5.24	325.97 ± 173.18			0.86 ± 0.48	-14.14 ± 7.21	
<i>t value</i>			-0.30	-0.73	1.66	1.88			1.81	-1.96	
<i>p value</i>			0.770	0.475	0.113	0.074			0.086	0.064	
C Prel thick	0.082	0.14		-12.07 ± 33.97	345.04 ± 149.25	-12.80 ± 27.52	67.82 ± 79.87	1.21 ± 0.71			-13.99 ± 6.15
<i>t value</i>				-0.36	2.31	-0.47	0.85	1.71			-2.28
<i>p value</i>				0.725	0.027	0.645	0.402	0.097			0.029

Table 4.9: General linear models for prelamina (PreL) thickness, containing effect size ± standard error, i.e. how much the prelamina thickness changes in μm per one-unit change in the independent variable, as well as *t*-value and *p*-value. Red text = factor is significant at $p < 0.05$. T = temporal, ST = superior-temporal, S = superior, SN = superior-nasal, N = nasal, IN = inferior-nasal, I = inferior, IT = inferior-temporal, C = central, AxL = axial length, MS = mean spherical refractive error, MD = mean deviation on visual fields, ACD = anterior chamber depth, CCT = central corneal thickness.

4.3.3.5 *The effect of other ocular parameters on the prelamina*

The optimised GLMs revealed that *axial length* had a significant positive effect of up to 100 $\mu\text{m}/\text{mm}$ *axial length* on the prelamina depth in the ST ($p=0.041$), N ($p=0.041$) and I ($p=0.049$) regions (Table 4.8). In the ST region, prelamina thinning was significantly associated with larger *axial length* ($-61.41 \pm 27.76 \mu\text{m}/\text{mm}$ *axial length*, $p=0.034$; Table 4.9).

Mean spherical refractive error (MS) had a significant positive effect on the prelamina depth by around 50 $\mu\text{m}/\text{D}$ in the N ($p=0.010$) and I ($p=0.004$) regions and a significant negative association in the central region ($-353.28 \pm 164.22 \mu\text{m}/\text{D}$, $p=0.038$). In the same way, there was a significant association between prelamina thinning and *MS* in the N ($p=0.017$) and I regions ($p=0.024$). In the central region the prelamina was $345.04 \pm 149.25 \mu\text{m}$ thicker with each additional D of spherical refractive error ($p=0.027$).

Mean deviation on visual field (MD) was significantly associated with a decrease in prelamina depth ($89.29 \pm 27.94 \mu\text{m}/\text{dB}$, $p=0.003$). Additionally, greater *MD* was associated with thicker prelamina in the T ($p=0.041$), N ($p=0.049$) and I regions ($p=0.038$). However, visual field deficit was controlled as one of the exclusion criteria so there was a small difference within MD overall.

Anterior chamber depth (ACD) had a significant effect on thinning of the I prelamina only ($-149.87 \pm 69.23 \mu\text{m}/\text{mm}$ *ACD*, $p=0.039$), and *central corneal thickness (CCT)* was not a significant factor in the GLMs to describe any of the prelamina parameters (Table 4.8).

Age and *MD* demonstrated a significant positive correlation (Pearson's correlation coefficient, $r=0.33$, $p=0.033$; Figure 4.9). The association between them, the interaction term *age:MD*, was a significant factor in the general linear model for T prelamina thickness ($0.36 \pm 1.14 \mu\text{m}$, $p=0.046$).

MS and *axial length* had a significant negative association (Pearson's correlation coefficient, $r=-0.77$, $p<0.001$), meaning larger eyes were associated with more negative, or more myopic, mean spherical refractive error (Figure 4.9). The interaction between *axial length:MS* had a significant positive effect on SN ($14.96 \pm 7.29 \mu\text{m}$, $p=0.048$) and central prelamina depth ($14.45 \pm 6.80 \mu\text{m}$, $p=0.040$; Table 4.8) and N prelamina thickness ($15.54 \pm 6.60 \mu\text{m}$, $p=0.026$; Table 4.9); as well as a significant negative effect on central prelamina thickness ($-13.99 \pm 6.15 \mu\text{m}$, $p=0.029$).

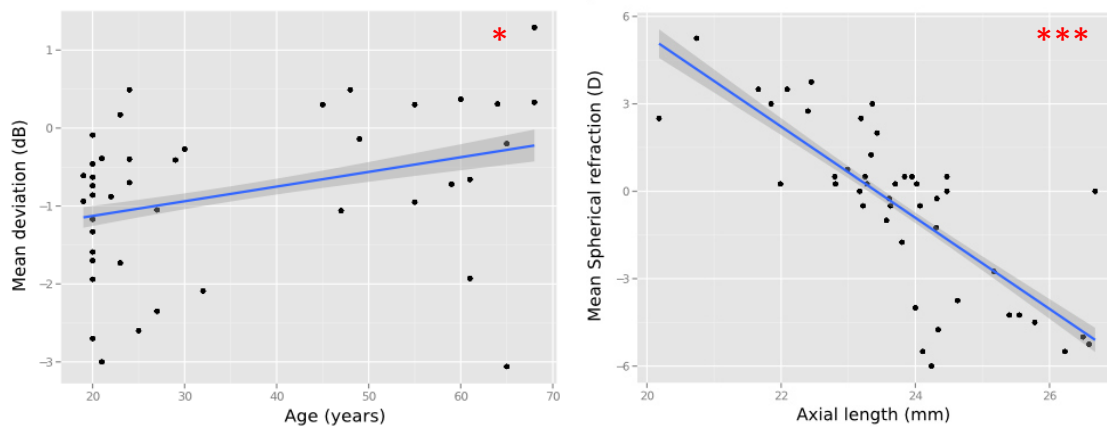
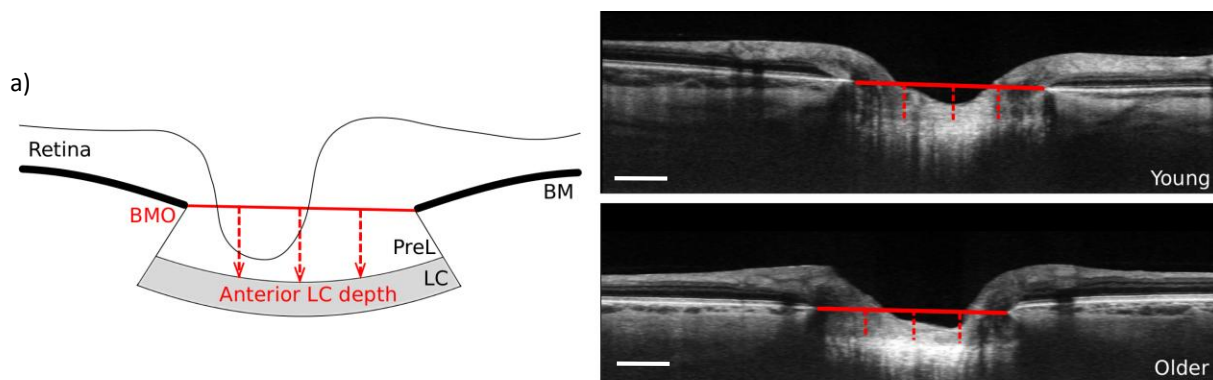


Figure 4.9: Mean deviation (MD) in visual field, plotted against age, and mean spherical refraction plotted against axial length. Pearson's correlation coefficient, * = $p<0.05$, *** = $p<0.001$. Grey bars = 95% confidence intervals.

4.3.4 The effect of age and other ocular parameters on the lamina cribrosa

The depth of the anterior and posterior LC surface from the BMO plane was measured in each region of the ONH, and the LC thickness calculated, as shown below in Figure 4.10.



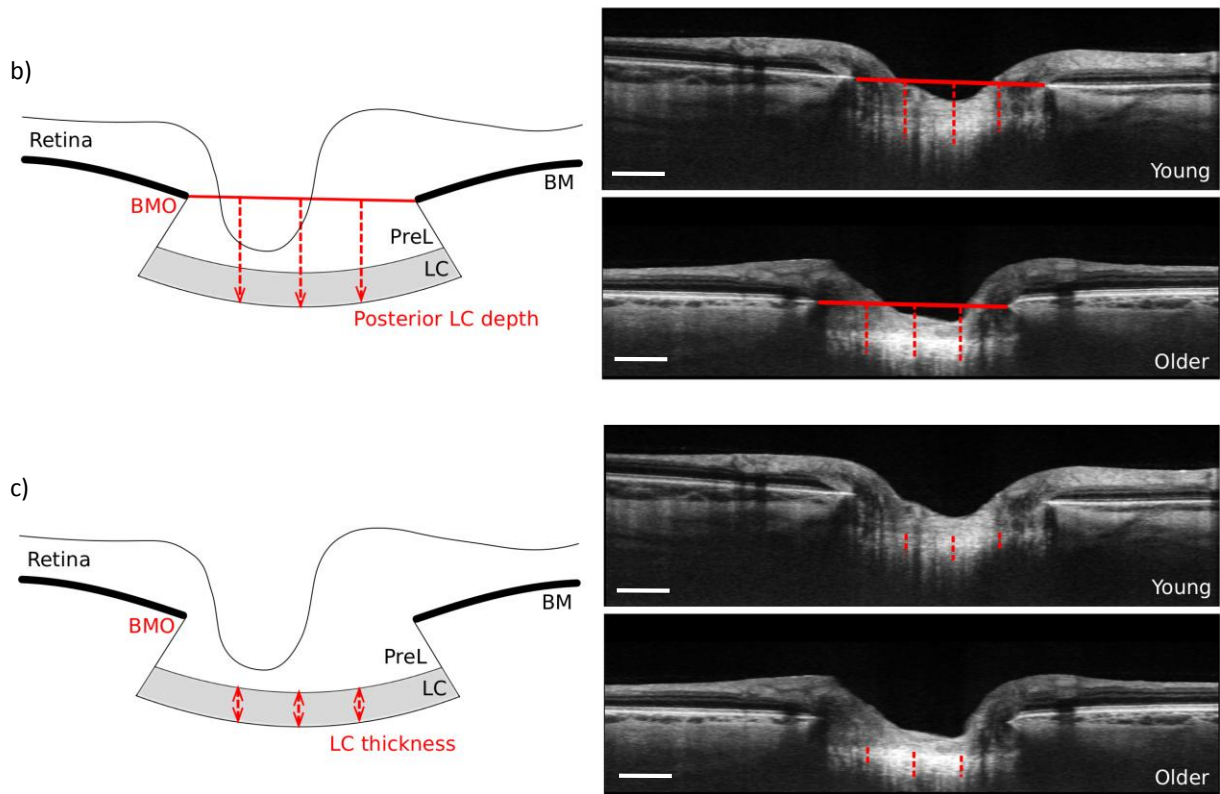


Figure 4.10: Schematic diagram of measurements of (a) anterior lamina cribrosa (LC) depth, (b) posterior LC depth, and (c) LC thickness shown in red, and example images from old and young optic nerve heads. BM = Bruch's membrane, BMO = Bruch's membrane opening, PreL = prelamina. Scale bars = 500 μm .

4.3.4.1 Quantification of lamina cribrosa parameters

The mean, standard deviation and range of the LC parameters in each region are shown in Table 4.10.

Region		Mean (μm)	\pm SD (μm)	Range (μm)
T	Ant LC	328.42	\pm 81.28	178.80 - 479.27
ST	Ant LC	337.38	\pm 88.23	27.67 - 502.21
S	Ant LC	372.06	\pm 62.60	264.11 - 569.60
SN	Ant LC	341.58	\pm 61.03	226.13 - 497.84
N	Ant LC	326.10	\pm 77.13	174.83 - 558.54
IN	Ant LC	321.18	\pm 72.01	153.60 - 479.27
I	Ant LC	334.74	\pm 79.50	168.15 - 527.20
IT	Ant LC	335.16	\pm 84.81	190.57 - 528.23
C	Ant LC	352.15	\pm 80.62	203.63 - 581.58
T	Post LC	521.26	\pm 83.39	372.54 - 715.22
ST	Post LC	541.80	\pm 68.56	433.10 - 703.84
S	Post LC	571.60	\pm 71.43	451.80 - 764.99
SN	Post LC	500.62	\pm 62.28	401.07 - 594.00
N	Post LC	515.05	\pm 88.00	341.33 - 631.31
IN	Post LC	511.74	\pm 93.00	281.60 - 635.96
I	Post LC	521.27	\pm 82.24	362.46 - 763.15
IT	Post LC	519.32	\pm 80.99	349.87 - 718.68
C	Post LC	562.68	\pm 76.46	413.87 - 762.23
T	LC thick	205.25	\pm 40.32	127.40 - 298.93
ST	LC thick	209.94	\pm 44.49	127.68 - 310.92
S	LC thick	195.50	\pm 38.03	138.60 - 282.02
SN	LC thick	178.37	\pm 25.74	126.23 - 233.94
N	LC thick	188.66	\pm 48.30	127.40 - 296.04
IN	LC thick	194.02	\pm 41.43	128.00 - 274.30
I	LC thick	194.57	\pm 39.77	103.51 - 299.70
IT	LC thick	197.99	\pm 32.32	144.88 - 259.25
C	LC thick	215.96	\pm 34.34	166.70 - 279.74

Table 4.10: Mean of each regional optic nerve head parameter. Ant LC = anterior lamina cribrosa (LC) depth, Post LC = posterior LC depth, LC thick = LC thickness, SD = standard deviation. T = temporal, ST = superior-temporal, S = superior, SN = superior-nasal, N = nasal, IN = inferior-nasal, I = inferior, IT = inferior-temporal, C = central

4.3.4.2 Univariate analysis of lamina cribrosa parameters

There was no significant association between the depth of the anterior or posterior LC surface and increasing age in any ONH region using Pearson's correlation coefficient (Pearson's correlation coefficient, $p > 0.05$, Figure 4.11 respectively). Using univariate analysis, there were also no significant associations between regional LC thickness and increasing age (Pearson's correlation coefficient, $p > 0.05$; Figure 4.12).

For ease of understanding, in scatter plots representing anterior and posterior LC depth the y-axis was reversed in order for data points where the LC surface depth was greater, or deeper from BMO, the data points were lower on the graph.

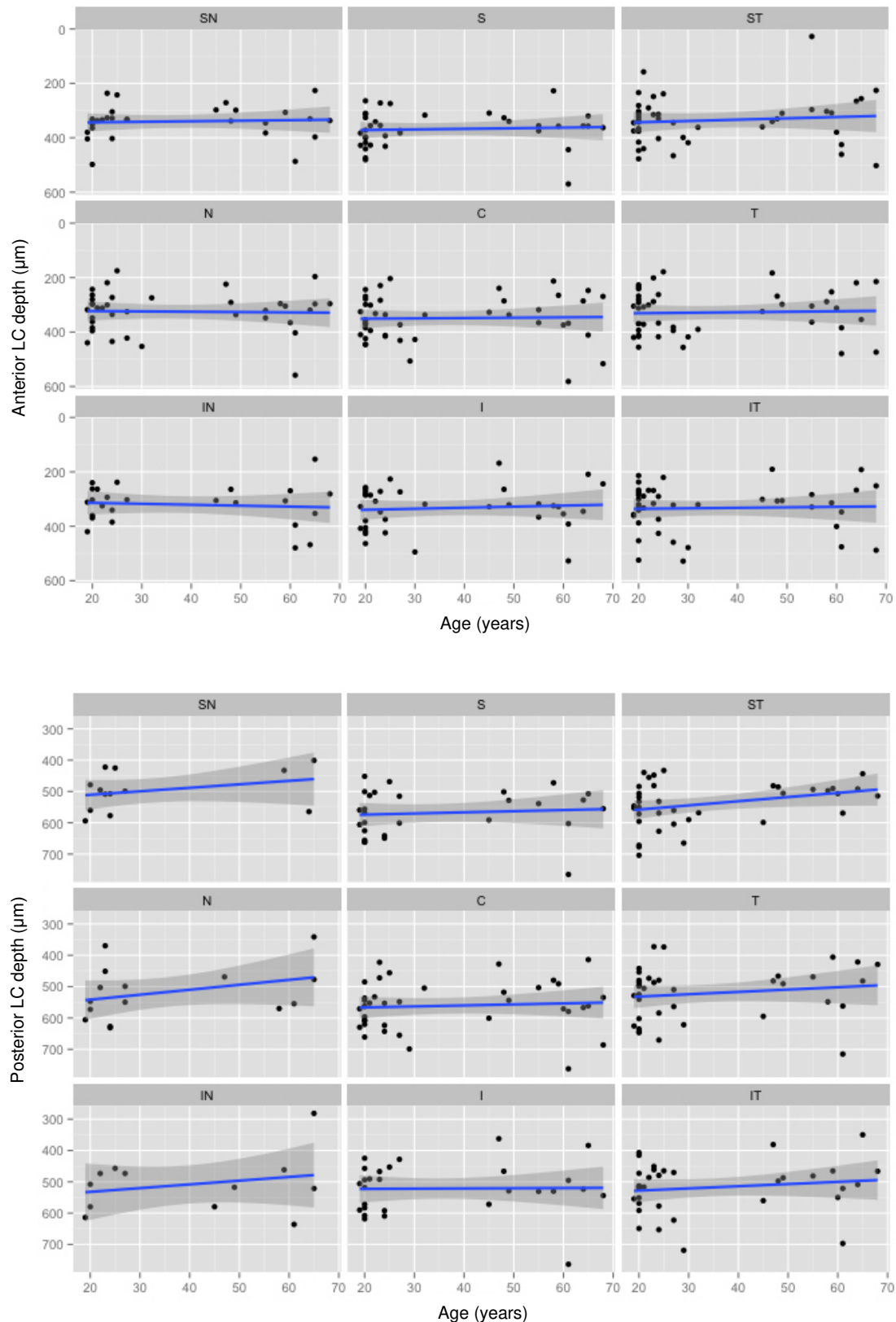


Figure 4.11: Anterior and posterior lamina cribrosa (LC) depth as a function of age for each region of the optic nerve head. There were no significant associations between LC depth and increasing age (Pearson's correlation coefficient $p > 0.05$). For plotting purposes, the y-axis was reversed so that values denoting greater anterior LC depth are lower on the graph. Grey bars = 95% confidence intervals. T = temporal, ST = superior-temporal, S = superior, SN = superior-nasal, N = nasal, IN = inferior-nasal, I = inferior, IT = inferior-temporal, C = central.

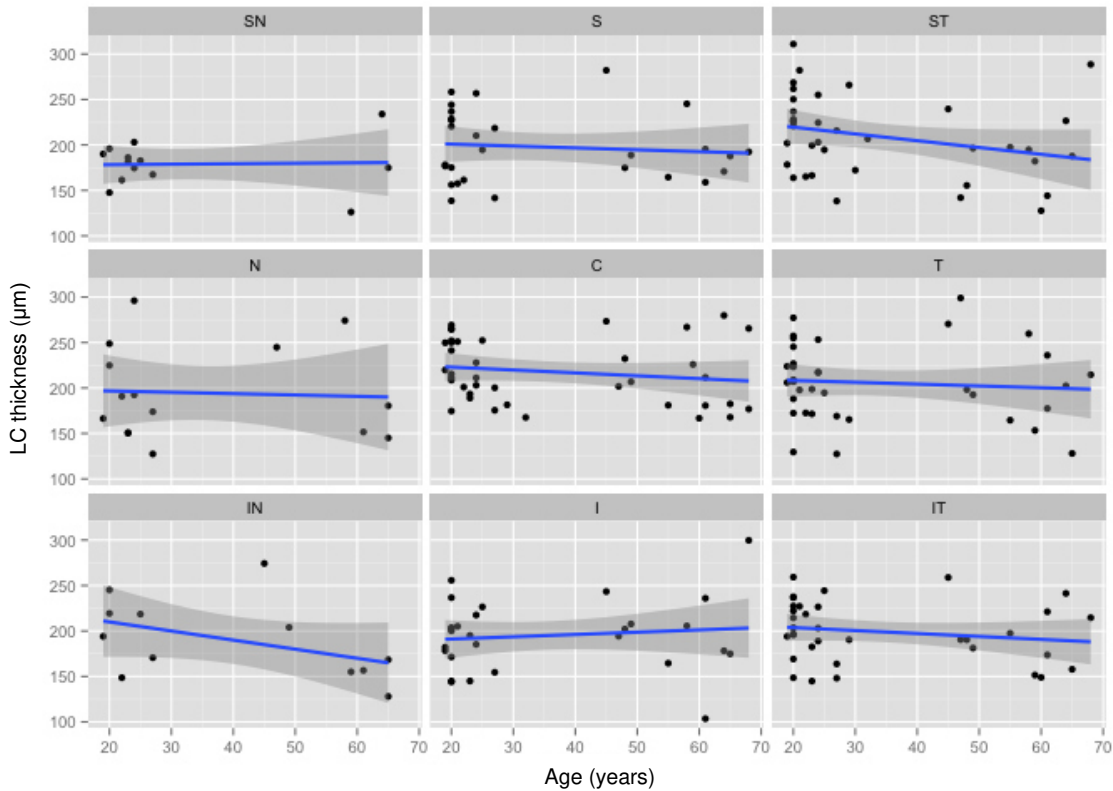


Figure 4.12: Lamina cribrosa (LC) thickness as a function of age for each region of the optic nerve head. There were no significant associations between LC thickness and increasing age (Pearson's correlation coefficient $p > 0.05$). Grey bars = 95% confidence intervals. T = temporal, ST = superior-temporal, S = superior, SN = superior-nasal, N = nasal, IN = inferior-nasal, I = inferior, IT = inferior-temporal, C = central.

4.3.4.3 Multivariate analysis of lamina cribrosa parameters

The optimised general linear models (GLMs) for the depth of the anterior and posterior LC surface from BMO (Table 4.11 and Table 4.12 respectively), and LC thickness (Table 4.13) for each ONH region are described below. Each row displays the independent variables that are included in the optimised GLM. Numbers quoted are effect size \pm standard error, i.e. how much the LC depth or thickness changes in μm per unit change in independent variable.

Regional depth	Model <i>p</i>	Model R ²	Age	AxL	MS	MD	ACD	CCT	Age:MD	AxL:MD	AxL:MS
T Ant LC	0.341	0.02	-0.87 ± 0.87	28.71 ± 15.20	16.09 ± 7.76	12.15 ± 13.38					
<i>t value</i>			-1.00	1.89	2.07	0.91					
<i>p value</i>			0.323	0.067	0.046	0.370					
ST Ant LC	0.258	0.03	-0.89 ± 0.87		10.05 ± 5.26	8.92 ± 14.					
<i>t value</i>			-1.02		1.91	0.62					
<i>p value</i>			0.313		0.064	0.537					
S Ant LC	0.510	-0.02			4.06 ± 4.20	8.37 ± 10.65					
<i>t value</i>					0.97	0.79					
<i>p value</i>					0.341	0.438					
SN Ant LC	0.308	0.17		-9.29 ± 8.53		13.79 ± 12.82					
<i>t value</i>				-1.09		1.08					
<i>p value</i>				0.286		0.292					
N Ant LC	0.067	0.11				20.46 ± 13.53	-43.71 ± 29.12				
<i>t value</i>						1.51	-1.50				
<i>p value</i>						0.141	0.143				
IN Ant LC	0.079	0.14				12.72 ± 13.86	-60.23 ± 31.22				
<i>t value</i>						0.92	-1.93				
<i>p value</i>						0.369	0.067				
I Ant LC	0.060	0.08				26.04 ± 13.34					
<i>t value</i>						1.95					
<i>p value</i>						0.060					
IT Ant LC	0.005	0.24	-1.01 ± 0.70		11.98 ± 4.21	31.41 ± 11.46					
<i>t value</i>			-1.44		2.84	2.74					
<i>p value</i>			0.160		0.007	0.009					
C Ant LC	0.087	0.07				15.04 ± 12.25		0.51 ± 0.31			
<i>t value</i>						1.23		1.66			
<i>p value</i>						0.227		0.105			

Table 4.11: General linear models for anterior lamina cribrosa depth (Ant LC) containing effect size ± standard error, i.e. how much the anterior LC depth changes in μm per one-unit change in the independent variable, as well as t-value and p-value. Red text = factor is significant at $p < 0.05$. T = temporal, ST = superior-temporal, S = superior, SN = superior-nasal, N = nasal, IN = inferior-nasal, I = inferior, IT = inferior-temporal, C = central, AxL = axial length, MS = mean spherical refractive error, MD = mean deviation on visual fields, ACD = anterior chamber depth, CCT = central corneal thickness.

Regional depth	Model <i>p</i>	Model R ²	Age	AxL	MS	MD	ACD	CCT	Age:MD	AxL:MD	AxL:MS
T Post LC	0.046	0.22	-3.04 ± 1.05	64.97 ± 23.13	17.34 ± 7.73	-521.15 ± 255.67			-1.82 ± 0.78	25.23 ± 10.84	
<i>t value</i>			-2.90	2.81	2.24	-2.04			-2.33	2.33	
<i>p value</i>			0.007	0.009	0.033	0.051			0.028	0.028	
ST Post LC	0.002	0.37	-3.06 ± 0.74	37.03 ± 14.38	-103.00 ± 50.43		-54.12 ± 33.31				5.18 ± 2.11
<i>t value</i>			-4.12	2.58	-2.04		-1.63				2.46
<i>p value</i>			<0.001	0.012	0.050		0.115				0.020
S Post LC	0.242	0.04			7.40 ± 5.53	13.41 ± 13.81					
<i>t value</i>					1.34	0.97					
<i>p value</i>					0.194	0.342					
SN Post LC	0.350	0.20	-1.85 ± 1.78	30.42 ± 18.01	24.00 ± 12.10	5.85 ± 41.85		-0.49 ± 0.50	1.00 ± 0.92		
<i>t value</i>			-1.04	1.69	1.98	0.14		-0.97	1.08		
<i>p value</i>			0.348	0.152	0.104	0.894		0.378	0.328		
N Post LC	0.074	0.64	-6.58 ± 2.34	82.33 ± 22.31	14.16 ± 10.99	103.50 ± 51.12	-199.91 ± 57.37	0.50 ± 0.53	-1.77 ± 1.26		
<i>t value</i>			-2.81	3.69	1.29	2.03	-3.48	0.94	-1.40		
<i>p value</i>			0.038	0.014	0.254	0.099	0.018	0.390	0.221		
IN Post LC	n/a	n/a									
<i>t value</i>											
<i>p value</i>											
I Post LC	0.030	0.15				35.05 ± 15.22					
<i>t value</i>						2.30					
<i>p value</i>						0.030					
IT Post LC	0.014	0.22	-1.49 ± 0.76		9.29 ± 4.63	35.85 ± 13.25					
<i>t value</i>			-1.96		2.01	2.71					
<i>p value</i>			0.060		0.054	0.011					
C Post LC	0.023	0.22	-2.26 ± 0.88	40.45 ± 18.08	19.18 ± 7.14	33.66 ± 12.25	-66.79 ± 41.19				
<i>t value</i>			-2.56	2.24	2.69	2.75	-1.62				
<i>p value</i>			0.016	0.033	0.012	0.010	0.115				

Table 4.12: General linear models for posterior lamina cribrosa depth (Post LC) containing effect size ± standard error, i.e. how much the posterior LC depth changes in µm per one-unit change in the independent variable, as well as t-value and p-value. Red text = factor is significant at $p < 0.05$. T = temporal, ST = superior-temporal, S = superior, SN = superior-nasal, N = nasal, IN = inferior-nasal, I = inferior, IT = inferior-temporal, C = central, AxL = axial length, MS = mean spherical refractive error, MD = mean deviation on visual fields, ACD = anterior chamber depth, CCT = central corneal thickness. n/a = not sufficient data available to construct a GLM,

Regional thickness		Model p	Model R^2	Age	AxL	MS	MD	ACD	CCT	Age:MD	AxL:MD	AxL:MS
T	LC thick	0.116	0.16	-1.12 ± 0.54	11.66 ± 10.30	-59.99 ± 37.42	9.17 ± 7.35	-41.33 ± 24.23	-0.32 ± 0.19			2.67 ± 1.56
	<i>t value</i>			-2.09	1.13	-1.60	1.25	-1.71	-1.69			1.72
	<i>p value</i>			0.047	0.268	0.121	0.223	0.100	0.102			0.097
ST	LC thick	0.150	0.10	-1.26 ± 0.51	26.57 ± 12.40	8.72 ± 4.44	-161.95 ± 130.80				7.09 ± 5.39	
	<i>t value</i>			-2.46	2.14	1.97	-1.24				1.31	
	<i>p value</i>			0.020	0.040	0.059	0.225				0.199	
S	LC thick	0.208	0.10	-1.62 ± 0.69	38.36 ± 16.93	-131.41 ± 65.11		-47.14 ± 30.59				5.88 ± 2.74
	<i>t value</i>			-2.35	2.27	-2.02	-1.54				2.14	
	<i>p value</i>			0.029	0.034	0.057	0.138				0.044	
SN	LC thick	0.290	0.22		7.86 ± 5.46	65.87 ± 38.59	17.04 ± 8.42		0.26 ± 0.20			-2.61 ± 1.58
	<i>t value</i>				1.44	1.71	2.02			1.28		-1.65
	<i>p value</i>				0.200	0.139	0.089			0.248		0.151
N	LC thick	0.053	0.85	3.03 ± 0.98	145.46 ± 28.92	-561.35 ± 113.33	-2387.22 ± 543.95	163.38 ± 4.63	-1.85 ± 0.34	0.78 ± 0.63	98.09 ± 22.44	24.51 ± 4.77
	<i>t value</i>			3.09	5.03	-4.95	-4.39	3.66	-5.50	1.23	4.37	5.14
	<i>p value</i>			0.054	0.015	0.016	0.022	0.035	0.012	0.307	0.022	0.014
IN	LC thick	n/a	n/a									
	<i>t value</i>											
	<i>p value</i>											
I	LC thick	0.015	0.41	0.30 ± 0.51	-1.23 ± 11.91	10.23 ± 3.87	205.93 ± 129.83		-0.36 ± 0.19	0.96 ± 0.34	-9.45 ± 5.37	
	<i>t value</i>			0.60	-0.10	2.65	1.59	-1.93	2.81	-1.76		
	<i>p value</i>			0.559	0.919	0.016	0.130	0.070	0.012	0.096		
IT	LC thick	0.074	0.18	-1.27 ± 0.43	14.18 ± 9.69	5.01 ± 3.21	182.08 ± 117.42	-54.93 ± 21.56			-7.11 ± 4.84	
	<i>t value</i>			-2.96	1.46	1.56	1.55	-2.55	-1.47			
	<i>p value</i>			0.006	0.155	0.131	0.133	0.017	0.154			
C	LC thick	0.195	0.08	-0.54 ± 0.39	7.14 ± 6.28		6.77 ± 5.89	-27.07 ± 19.48	-0.26 ± 0.15			
	<i>t value</i>			-1.40	1.14		1.13	-1.39	-1.77			
	<i>p value</i>			0.171	0.265		0.267	0.175	0.087			

Table 4.13: General linear models for lamina cribrosa thickness (LC thick), containing effect size \pm standard error, i.e. how much LC thickness changes in μm per one-unit change in the independent variable, as well as t-value and p-value. Red text = factor is significant at $p < 0.05$. T = temporal, ST = superior-temporal, S = superior, SN = superior-nasal, N = nasal, IN = inferior-nasal, I = inferior, IT = inferior-temporal, C = central, AxL = axial length, MS = mean spherical refractive error, MD = mean deviation on visual fields, ACD = anterior chamber depth, CCT = central corneal thickness. n/a = not sufficient data available to construct a GLM,

4.3.4.4 The effect of age on lamina cribrosa parameters

Age had no significant effect on the depth of the anterior LC surface from BMO in any of the ONH regions examined. However, the posterior LC surface depth was shown to be significantly less with increasing age by up to $-6.58 \mu\text{m}/\text{year}$ in the T ($p=0.007$), ST ($p<0.001$), N ($p=0.038$) and central ($p=0.016$) regions (Table 4.12; Figure 4.13).

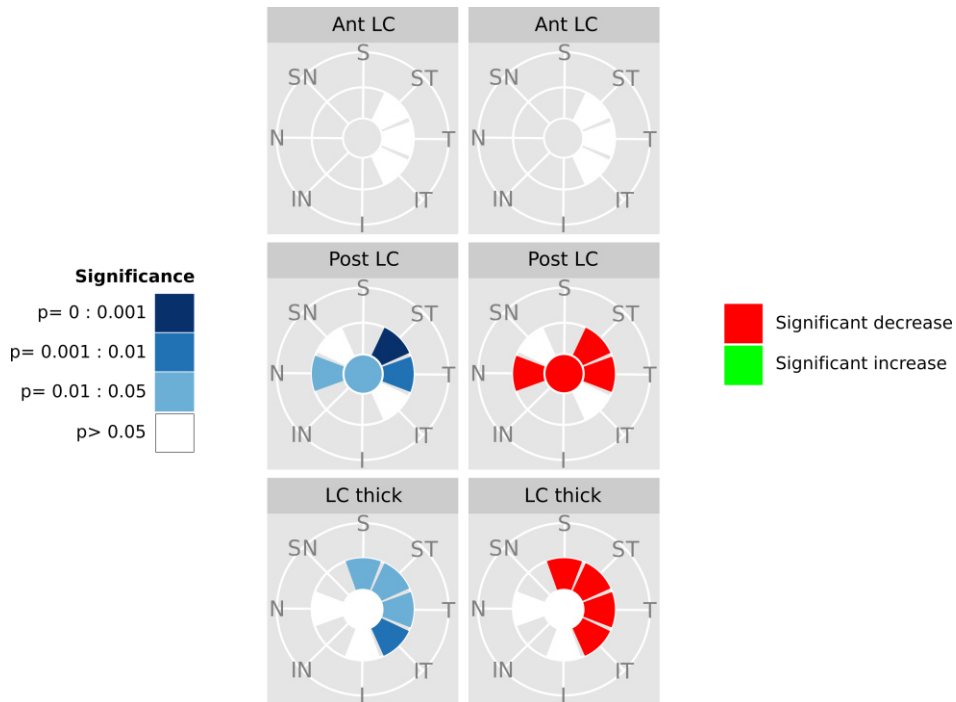


Figure 4.13: Regions of the anterior lamina cribrosa depth (Ant LC), posterior lamina cribrosa depth (Post LC), and lamina cribrosa thickness (LC thick) that were affected as a function of age, using general linear models (GLM). T = temporal, ST = superior-temporal, S = superior, SN = superior-nasal, N = nasal, IN = inferior-nasal, I = inferior, IT = inferior-temporal. Blue indicates a significant contribution, white indicates that age was part of the GLM but not significant. Green = increase, red -decrease.

The LC thickness decreased with increasing age by around $-1.12 \mu\text{m}/\text{year}$ in the IT ($p=0.006$), T ($p=0.047$), ST ($p=0.020$) and S ($p=0.029$) regions. Although the physical change in LC thickness with increasing age was greatest in the S region, it was most significant in the IT region.

4.3.4.5 *The effect of other ocular parameters on the lamina cribrosa*

The anterior LC depth showed no significant differences with greater *axial length* in any region of the ONH (Table 4.11). The posterior LC depth was significantly more shallow in smaller eyes and deeper in larger eyes in the T ($p=0.009$), ST ($p=0.012$), N ($p=0.014$) and central ($p=0.033$) regions (Table 4.12). Additionally the LC was significantly thicker in the ST, S and N regions in eyes with longer *axial length* (ST $p=0.040$, S $p=0.034$ and N $p=0.015$, Table 4.13).

The anterior LC depth was significantly increased in hyperopic eyes compared to eyes with greater amounts of myopia in the T ($16.09 \pm 7.76 \mu\text{m/D}$, $p=0.046$) and IT regions ($11.98 \pm 4.21 \mu\text{m/D}$, $p=0.007$; Table 4.11). The posterior LC surface depth was also significantly greater in the T ($17.34 \pm 7.73 \mu\text{m/D}$, $p=0.033$) and central regions ($19.18 \pm 7.14 \mu\text{m/D}$, $p=0.012$) in eyes with greater amounts of hyperopia. In the ST region the posterior LC depth was significant less in hyperopic eyes ($p=0.050$; Table 4.12). Additionally, in the nasal region *MS* contributed negatively to LC thickness ($p=0.016$), i.e. hyperopic eyes had thinner nasal LC, and in the inferior region *MS* had a significant positive contribution ($p=0.016$; Table 4.13), i.e. hyperopic eyes had thicker inferior LC.

Mean visual field deviation (*MD*) had a significant contribution towards the IT anterior LC depth, i.e. for every 1 dB less in *MD* the anterior LC surface was $31.41 \pm 11.46 \mu\text{m}$ further from BMO ($p=0.010$). Similarly, the posterior LC depth was also significantly greater with greater *MD* in the IT region ($p=0.011$), I region ($p=0.030$) and central region ($p=0.010$; Table 4.12). *MD* also had a significant contribution to the nasal LC thickness ($p=0.022$; Table 4.13).

Posterior LC depth was significantly affected by *ACD* in the nasal region ($-199.91 \pm 57.37 \mu\text{m/mm ACD}$, $p=0.018$), i.e. eyes with deeper anterior chambers had shallower nasal posterior LC surface, closer to BMO. The IT LC was thinner in eyes with greater *ACD* ($-54.93 \pm 21.56 \mu\text{m/mm ACD}$,

$p=0.017$), whereas the nasal LC was shown to be $163.38 \pm 4.63 \mu\text{m}$ thicker with each mm *ACD* ($p=0.035$).

Central corneal thickness (CCT) did not contribute significantly to explain anterior or posterior LC depth in any region of the ONH ($p>0.05$). *CCT* did, however, have a significant negative contribution to the thickness of the nasal LC ($-1.85 \pm 0.34 \mu\text{m}/\mu\text{m CCT}$, $p=0.012$), i.e. eyes with thicker central corneas had thinner nasal LC.

The anterior LC depth was not affected by the interactions between *age:MD*, *axial length:MD*, or *axial length:MS* ($p>0.05$; Table 4.11). The association between *age:MD* had a significant negative effect on the posterior LC depth in the temporal region ($p=0.028$; Table 4.12) and a significant positive effect on LC thickness in the inferior region ($p=0.012$; Table 4.13). The interaction between *axial length:MD* showed a positive contribution to both temporal posterior LC depth ($p=0.028$) and nasal LC thickness ($p=0.022$). Additionally, the association between *axial length:MS* had a significant positive effect on ST posterior LC depth ($p=0.020$), as well as superior ($p=0.044$) and nasal LC thickness ($p=0.014$).

4.3.5 Summary of results

The key findings from this study were:

- ST-IN and S-I BMO diameter decreased with increasing age
- IN and inferior regions of the pNFL thinned with increasing age
- ST prelamina depth decreased with increasing age
- ST and nasal regions of the prelamina increased in thickness with increasing age
- ST prelamina depth increased with increasing age
- ST and nasal regions of the prelamina increased in thickness with increasing age

- T, ST, nasal and central region of the posterior LC depth decreased with increasing age
- There were no significant changes in bNFL or anterior LC depth with increasing age.

Regions where significant associations ($p < 0.05$) were identified, together with direction of change, are shown below in Figure 4.14.

4.4 Discussion

In the present chapter, the effect of age on a number of optic nerve head parameters was investigated in 2D images extracted from 3D OCT datasets of normal, healthy adults. As detailed above in Figure 4.14, significant region-specific differences in prelamina depth and thickness, lamina cribrosa (LC) depth and thickness, and peripapillary and border nerve fibre layer (NFL) were identified as a function of age. Measurements of Bruch's membrane opening (BMO) diameter were used as a surrogate for optic disc diameter as it is generally accepted to be an accurate reference for assessment of changes to the most anterior part of the optic canal. Furthermore, the BMO diameter can also be used as a reference plane from which prelamina depth, anterior LC and posterior LC depth measurements are made.

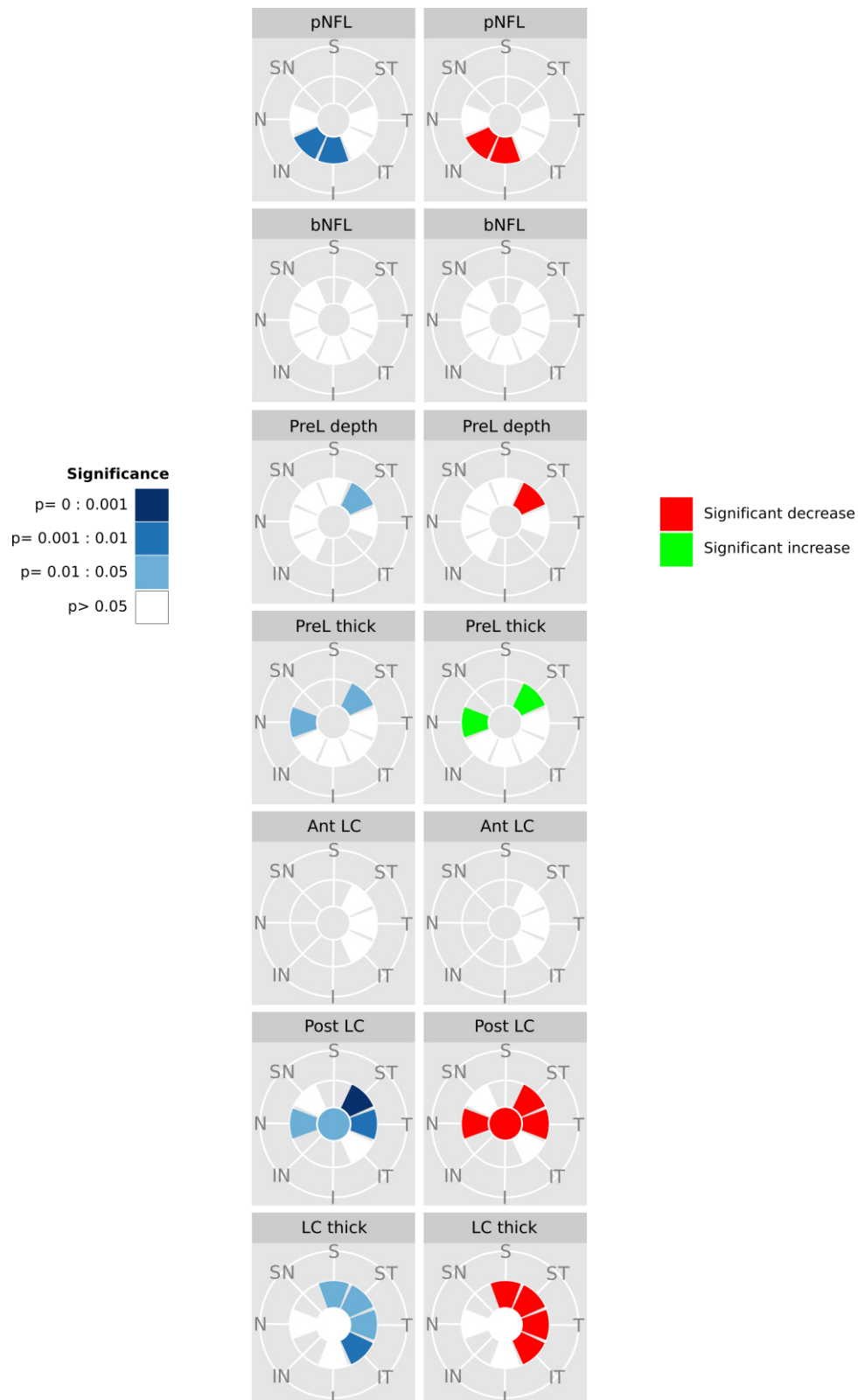


Figure 4.14: Regions of the optic nerve head that were affected as a function of age, using general linear models (GLM). pNFL = peripapillary nerve fibre layer, bNFL = border nerve fibre layer, PreL depth = prelamina depth, PreL thick = prelamina thickness, Ant LC = anterior lamina cribrosa (LC) depth, Post LC = posterior LC depth, LC thick = LC thickness, T = temporal, ST = superior-temporal, S = superior, SN = superior-nasal, N = nasal, IN = inferior-nasal, I = inferior, IT = inferior-temporal. Blue indicates a significant contribution to the GLM, white indicates that age was part of the GLM but not significant. Green t-values = positive effect, red t-values = negative effect.

4.4.1 The effect of age on Bruch's membrane opening diameter

Prior to the wide-spread use of OCT, the BMO diameter could not easily be visualised *in vivo* and, instead, studies of optic disc size utilised fundus photography (Bengtsson 1980), stereo-photography (Cavallotti et al. 2002), scanning laser ophthalmoscopy (Garway-Heath et al. 1997) or direct ophthalmoscopy (Carpel and Engstrom 1981). Of these studies, Garway-Heath et al. (1997) found optic disc diameter to be unaffected by age, and Britton et al. (1987) and Kee et al. (1997) found no change in disc area with increasing age. Moya et al. (1999) went on to suggest that any disc area loss detected was not sufficient to confuse with glaucoma, implying that age does not need to be accounted for when assessing a glaucomatous optic nerve. Contrary to this, Bengtsson (1980) determined that the optic disc diameter did increase with age, and the neuroretinal rim width decreased, leading to an increase in the diameter of the optic cup. Interestingly, in an *ex vivo* study, Cavallotti et al. (2002) discovered the intra-cranial portion of the human optic nerve became thicker with increasing age, which they attribute to an increase of the optic nerve:meningeal membrane ratio.

Given the contradiction in the above conclusions and the relative inaccuracy of the techniques with they were reached, a critical first step in this project was to identify those changes that occur naturally with age in order to provide a comprehensive frame of reference for subsequent investigations involving participants with ocular pathology (i.e. Chapter 5).

The major findings of the present dataset are that BMO diameter decreased significantly with age in the superior – inferior and superior-temporal – inferior-nasal directions. As yet, no other groups have reported a decrease in BMO diameter with increasing age in any plane. A summary of significant factors in the GLMs to describe BMO diameter is shown below (Table 4.14).

Region	Age	AxL	MS	MD	ACD	CCT	Age: MD	AxL: MD	AxL: MS
T-N BMO		✓	✓	✓	✓				
ST-IN BMO	✓	✓	✓	✓	✓				
S-I BMO	✓	✓	✓	✓	✓	✓			✓
SN-IT BMO					✓				

Table 4.14: Independent variables included in the optimised general linear model to explain variance in Bruch's membrane opening diameter. A tick indicates the factor is included in the optimised GLM, red = significant negative association ($p < 0.05$), green = significant positive association ($p < 0.05$). BMO = Bruch's membrane opening. T = temporal, ST = superior-temporal, S = superior, SN = superior-nasal, N = nasal, IN = inferior-nasal, I = inferior, IT = inferior-temporal; AxL = axial length, MS = mean spherical refractive error, MD = mean visual field deviation, ACD = anterior chamber depth, CCT = central corneal thickness.

4.4.2 The effect of age on the nerve fibre layer thickness

In concordance with previous studies (Parikh et al. 2007; Wong et al. 2010; Hirasawa et al. 2010; Lee et al. 2012; Alasil et al. 2013), the present study found that peripapillary nerve fibre layer (pNFL) thickness decreased significantly with age in the inferior and IN regions. This NFL thinning is generally accepted to be due to a decrease in the number of retinal ganglion cell (RGC) axons with age (as has been shown in a number of *ex vivo* studies; Dolman et al. 1980; Johnson et al. 1987; Mikelberg et al. 1989; Jonas et al. 1990; Moya et al. 1999; Balazsi et al. 1984). Unexpectedly, this was not reflected in the border nerve fibre layer (bNFL) measurements, which are taken from BMO to the top of the nerve fibre layer/prelamina. This discrepancy could be due to variability in the location of BMO with respect to the peripapillary sclera between subjects, as described by Johnstone et al. (2014), as well as the reported posterior shift of BMO with age.

While age was not a significant determinant for any of the regions within the NFL, it, along with MS, MD, anterior chamber depth, and central corneal thickness all contributed to optimised GLMs for all regions except superior-temporal and temporal border, while axial length also contributed to explaining the variance in bNFL thickness for each regional GLM (except for in the inferior region). Thus, when taking into account structural changes that result from pathology these variables should be accounted for. A summary of significant factors in the GLMs to describe nerve fibre layer changes is shown below (Table 4.15).

Region		Age	AxL	MS	MD	ACD	CCT	Age: MD	AxL: MD	AxL: MS
T	pNFL	✓	✓	✓	✓		✓			✓
ST	pNFL		✓		✓		✓		✓	
S	pNFL		✓		✓		✓			
SN	pNFL				✓					
N	pNFL	✓	✓	✓	✓					✓
IN	pNFL	✓		✓	✓					
I	pNFL	✓	✓	✓	✓	✓	✓			✓
IT	pNFL	✓	✓	✓			✓			✓
T	bNFL	✓	✓	✓	✓	✓	✓	✓	✓	✓
ST	bNFL		✓	✓	✓	✓	✓	✓	✓	✓
S	bNFL		✓	✓	✓	✓			✓	✓
SN	bNFL	✓	✓	✓	✓	✓	✓			✓
N	bNFL	✓	✓	✓	✓	✓		✓		
IN	bNFL	✓	✓	✓	✓	✓	✓			✓
I	bNFL	✓			✓			✓		
IT	bNFL	✓	✓		✓	✓		✓	✓	

Table 4.15: Independent variables included in the optimised general linear model to explain variance in nerve fibre layer parameters. A tick indicates the factor is included in the optimised GLM, red = significant negative association ($p < 0.05$), green = significant positive association ($p < 0.05$). pNFL = peripapillary nerve fibre layer, bNFL = border nerve fibre layer. T = temporal, ST = superior-temporal, S = superior, SN = superior-nasal, N = nasal, IN = inferior-nasal, I = inferior, IT = inferior-temporal, AxL = axial length, MS = mean spherical refractive error, MD = mean visual field deviation, ACD = anterior chamber depth, CCT = central corneal thickness.

4.4.3 The effect of age and ocular parameters on the prelamina

Prelamina thickness was found to increase with age in the superior-temporal and nasal regions ($p > 0.05$) while inferior prelaminar thickness was found to decrease with age. Additionally, although it did not reach significance, age was a factor in the optimised GLMs to describe the variance in prelaminar thickness in both the inferior and IT regions.

Previous studies have shown that with age, optic cup diameter increased and neuroretinal rim width decreased, resulting in an increased cup:disc (CD) ratio (Garway-Heath et al. 1997; Sung et al. 2009). Conversely, Healey et al. (1997) showed that while such an association existed there was no association with age. In another study, Klein et al. (2006) found that, using a multivariate analytical approach that accounted for both refraction and IOP, there was no significant change in optic disc cupping with age, but that ageing increased the optic disc's susceptibility to cupping at a given IOP. An increase in optic cup diameter combined with a decrease in neuroretinal rim width and a

subsequent increase in the CD ratio (Moya et al. 1999), could be explained by a decrease in the number of RGC axons that is associated with ageing (Dolman et al. 1980; Jonas et al. 1990). Hypothetically these age-related changes could lead to a thinner prelamina and increasing prelamina depth from BMO.

A multivariate approach took into consideration a number of other relevant factors in order to build optimised statistical models to describe changes in prelamina depth within each region. The GLMs determined age to be a factor in six of the nine regions described, excluding inferior, inferior-temporal, and central prelamina depth. Moreover, age contributed significantly towards explaining a decrease in superior-temporal prelamina depth. Interestingly, axial length, mean spherical refractive error, and MD were also positive contributors towards explaining the variance in prelamina depth, significantly so in the inferior, nasal and superior-temporal regions. Indeed, MD was a factor in the optimised models for prelamina depth in all nine regions (but significant only in the inferior region), and both mean spherical refraction and axial length were factors in seven of the nine regions. When assessing prelamina depth, axial length and mean spherical refraction had a larger effect size than age or MD. Consequently, these two variables should be considered when investigating prelamina depth in the ageing eye and also for assessing glaucomatous progression.

It is worth noting that, in order to acquire measurements for prelamina thickness, both the prelamina surface and the anterior LC surface need to be visible in the OCT dataset. However, in some cases, blood vessels can cause shadows in the OCT datasets that obscure view of the anterior and posterior LC surface (Girard et al. 2011), particularly on the nasal side. In the present study, the prelamina surface was visible in both nasal and temporal ONH for all 46 datasets; however, the anterior LC surface was visible in only 37 nasal compared to 45 temporal ONH datasets, and the posterior LC surface visible in 16 nasal compared to 37 temporal ONH datasets. As a result, fewer

viable measurements for the nasal side of the ONH compared to temporal may have distorted the resulting in the relatively large effect sizes and large ranges reported in prelamina thickness.

Where the association in the GLM was significant, axial length, mean spherical refraction and visual field status had a negative effect on prelamina thickness. Of these, the biggest effect size was seen in the contribution of mean spherical refraction (MS) to the nasal and central prelamina thickness, although the standard deviation was large. This may be due to restricting the MS for inclusion in this study to ± 6.00 D in order to allow accurate focussing of the OCT device during image acquisition. MD also appeared to have a large effect on temporal and nasal prelamina thickness (T -106.72 ± 50.35 $\mu\text{m}/\text{dB}$; N -128.97 ± 62.44 $\mu\text{m}/\text{dB}$), and a trend was observed in the inferior-temporal region. Again, this may be due to the restriction of MD to 'no visual field defect, as defined by Hodapp et al. (1993).' Since the range of MD was narrow, it is likely that small differences in prelamina thickness would have an association with MD. However, both MS and MD showed large effect on the nasal prelamina thickness.

In comparison to univariate statistical analysis, for each of the optimised GLMs a combination of factors was associated with regional prelamina depth and thickness, implying that a number of independent variables contribute to prelamina measurements, and these need to be considered when investigating the ageing prelamina, predominantly axial length, MS and MD.

A summary of significant factors in the GLMs to describe changes in the prelamina changes is shown below (Table 4.16).

Region		Age	AxL	MS	MD	ACD	CCT	Age: MD	AxL: MD	AxL: MS
T	PreL depth	✓			✓			✓		
ST	PreL depth	✓	✓	✓	✓					✓
S	PreL depth	✓	✓	✓	✓	✓				✓
SN	PreL depth	✓	✓	✓	✓		✓			✓
N	PreL depth	✓	✓	✓	✓	✓	✓			
IN	PreL depth	✓	✓	✓	✓					✓
I	PreL depth		✓	✓	✓		✓			
IT	PreL depth				✓	✓				
C	PreL depth		✓	✓	✓					✓
T	PreL thick	✓	✓		✓			✓		
ST	PreL thick	✓	✓	✓	✓			✓		
S	PreL thick		✓		✓				✓	
SN	PreL thick		✓		✓					✓
N	PreL thick	✓	✓	✓	✓			✓		✓
IN	PreL thick	✓			✓					
I	PreL thick	✓		✓	✓	✓				
IT	PreL thick	✓	✓	✓	✓			✓	✓	
C	PreL thick		✓	✓	✓	✓	✓			✓

Table 4.16: Independent variables included in the optimised general linear model to explain variance in prelamina parameters. A tick indicates the factor is included in the optimised GLM, red = significant negative association ($p < 0.05$), green = significant positive association ($p < 0.05$). PreL depth = prelamina depth, PreL thick = prelamina thickness. T = temporal, ST = superior-temporal, S = superior, SN = superior-nasal, N = nasal, IN = inferior-nasal, I = inferior, IT = inferior-temporal, C = central. AxL = axial length, MS = mean spherical refractive error, MD = mean visual field deviation, ACD = anterior chamber depth, CCT = central corneal thickness.

4.4.4 The effect of age on the lamina cribrosa

Although age was a factor in the GLMs describing variance in the T, ST and IT anterior LC depth, statistical significance was not reached. In the T and IT region anterior LC depth regions, a higher levels of hyperopia was significantly associated with more anteriorly placed LC surface, i.e. decreased anterior LC depth. Additionally, MD, present as a factor in all regional GLMs for anterior LC depth, was significant only for the IT region.

In the T, ST, N and central regions the posterior LC depth decreased with increasing age, but increased with increasing axial length, i.e. a larger eye had a deeper posterior LC surface. MD was also a factor in determining posterior LC depth (exceptions were for ST and IN regions) and was significant in I, IT and central regions.

Previously, a study by Kotecha et al. (2006) showed the mean LC thickness in *ex vivo* human eyes significantly increased with age. Indeed, Kotecha et al. and others (Hernandez et al. 1987; Hernandez et al. 1989; Morrison et al. 1989; Albon et al. 1995) have suggested this may be a consequence of collagen accumulating in the LC throughout life. However, it is worth noting that most studies have not evaluated regional variations in LC thickness with age, such that any localised differences may be overlooked. Building upon this lack of understanding, the present study found that a decrease in LC thickness was associated with ageing in the temporal, superior-temporal, superior and inferior-temporal regions. Of particular note, the superior and temporal LC regions decreased in thickness with increasing age. In these two regions the anterior LC surface appeared to be stable with increasing age, whereas the posterior LC surface became closer to BMO. However, as with prelamina thickness, the LC thickness measurement is subject to the visibility of two surfaces, in this case the anterior and posterior LC; and often the nasal LC regions were affected by vascular shadowing.

No significant association with LC thickness and central corneal thickness was observed in any of the regions examined in this study, except the nasal region. This finding is consistent with other studies investigating the association between central corneal thickness and LC thickness as a marker of susceptibility for glaucoma (Jonas and Holbach 2005; Ren et al. 2010). The current analysis also showed that longer axial length had a significant positive effect on superior-temporal, superior and nasal LC thickness, i.e. in these regions eyes that were larger had a thicker LC. These conclusions appear contradictory to data published by Ren et al. (2009) which showed that the LC was thinner in larger eyes with high axial myopia (>27.5 mm), however, the inclusion criteria of this study limited the degree of myopia to -6.00 D and the axial length to 26.7 mm. For each region of the above regions, LC thickness was also affected by age, axial length, MS, and MD, with additional influence from anterior chamber depth and central corneal thickness in some, but not all, regions. In conclusion, a considerable number of factors need to be taken into account when trying to characterise ageing ONH parameters.

In comparison to the multivariate GLM results outlined above, univariate statistical analysis revealed no significant association between age and any regional LC parameters (anterior and posterior LC depth, and LC thickness), further highlighting the importance of a more comprehensive statistical approaches when assessing the ONH. A summary of significant factors in the GLMs to describe LC parameters is shown below (Table 4.17).

Region		Age	AxL	MS	MD	ACD	CCT	Age: MD	AxL: MD	AxL: MS
T	Ant LC	✓	✓	✓	✓					
ST	Ant LC	✓		✓	✓					
S	Ant LC			✓	✓					
SN	Ant LC		✓		✓					
N	Ant LC				✓	✓				
IN	Ant LC				✓	✓				
I	Ant LC				✓					
IT	Ant LC	✓		✓	✓					
C	Ant LC				✓		✓			
T	Post LC	✓	✓	✓	✓			✓	✓	
ST	Post LC	✓	✓	✓		✓				✓
S	Post LC			✓	✓					
SN	Post LC	✓	✓	✓	✓		✓	✓		
N	Post LC	✓	✓	✓	✓	✓	✓	✓		
IN	Post LC									
I	Post LC				✓					
IT	Post LC	✓		✓	✓					
C	Post LC	✓	✓	✓	✓	✓				
T	LC thick	✓	✓	✓	✓	✓	✓			✓
ST	LC thick	✓	✓	✓	✓				✓	
S	LC thick	✓	✓	✓		✓				✓
SN	LC thick		✓	✓	✓		✓			✓
N	LC thick	✓	✓	✓	✓	✓	✓	✓	✓	✓
IN	LC thick									
I	LC thick	✓	✓	✓	✓		✓	✓	✓	
IT	LC thick	✓	✓	✓	✓	✓	✓		✓	
C	LC thick	✓	✓		✓	✓	✓			

Table 4.17: Independent variables included in the optimised general linear model to explain variance in regional lamina cribrosa parameters. A tick indicates the factor is included in the optimised GLM, red = significant negative association ($p < 0.05$), green = significant positive association ($p < 0.05$). Ant LC = anterior LC depth. Post LC = posterior LC depth. LC thick = LC thickness. T = temporal, ST = superior-temporal, S = superior, SN = superior-nasal, N = nasal, IN = inferior-nasal, I = inferior, IT = inferior-temporal, C = central. AxL = axial length, MS = mean spherical refractive error, MD = mean visual field deviation, ACD = anterior chamber depth, CCT = central corneal thickness.

4.4.5 Axial length

Interestingly, although axial length was a factor in many of the optimised GLMs, when each of the ONH parameters was paired with age in univariate analysis, there were very few measurements that were directly associated with axial length. This suggests that, as with age, axial length is a contributing factor to ONH changes, but is not solely responsible for the changes that occur.

4.4.6 Limitations of the study

As previously mentioned, in order to acquire the prelamina and LC thickness measurements, two surfaces were required to be visible in the dataset. Blood vessels cause shadows in the OCT datasets that can obscure the view of the anterior and posterior LC surface (Girard et al. 2011), particularly on the nasal side of the optic disc, resulting in fewer useable measurements. In this study, the prelamina surface was visible in both nasal and temporal ONH for all 46 datasets; however, the anterior LC surface was visible in 37 nasal compared to 45 temporal ONH, and the posterior LC surface visible in 16 nasal compared to 37 temporal ONH. There are less viable measurements for the nasal side of the ONH compared to temporal, and this may cause the large effect sizes and ranges displayed in prelamina and LC thickness. Potentially, increasing the amount of datasets used in this experiment may lead to clearer, more definitive conclusions.

Additionally, one of the major difficulties with this particular study was the age range of the participants. Of the 46 eyes used in analysis, 27 were younger than 30 years, with most of the remaining participants clustered between 45-65. This is partially due to the population from which control participants were recruited (staff, students and friends at Cardiff University, UK), however, this study would benefit from additional subjects, particularly aged 30-40 years, the age at which glaucoma becomes a risk factor, and aged >65 years.

4.4.7 Conclusion

Significant changes in prelamina and LC thickness and depth were identified, particularly in the superior-temporal and temporal regions. However, other ocular factors have been identified that have a significant role in changes in ONH parameters, and as such, any conclusions drawn about the aging optic nerve i.e. those that investigate changes that occur with glaucoma (i.e. Chapter 5) need to take these other variables into full consideration in order to comprehensively evaluate changes that occur. Crucially, this identification of those regions that are susceptible to change during the process of normal ageing is a critical step towards isolating those changes that potentially indicate a predisposition to pathological change which, in turn, may permit earlier diagnosis and treatment.

Chapter 5:
2D optic nerve head parameters as a
function of glaucoma

5 2D optic nerve head parameters as a function of glaucoma

5.1 Introduction

The optic nerve head (ONH) is the primary site of retinal ganglion cell (RGC) axonal damage in glaucoma (Anderson and Hendrickson 1974; Minckler et al. 1976; Gaasterland et al. 1978; Quigley et al. 1981). Changes at the ONH occur as a result of the glaucomatous disease process, including thinning of the lamina cribrosa (LC) due to compression of the cribriform sheets (Quigley et al. 1983), excavation of the optic cup and deformation of the lamina cribrosa (Bellezza et al. 2001; Sigal et al. 2011; Wu et al. 2015). These changes are thought to compromise support for RGC axons as they pass through the ONH.

More recently, optical coherence tomography (OCT) has allowed *in-vivo* assessment of the structures of the ONH for comparison of eyes with and without glaucoma. Studies include characterisation of the shape of the anterior surface of the LC (Kiumehr et al. 2012; Park et al. 2012) and delineation of the posterior LC surface, using enhanced depth imaging, allowing for LC thickness measurements (Lee et al. 2011; Lee et al. 2012). Other OCT studies have shown that both the LC and prelamina thicken following IOP-reduction surgery in glaucomatous eyes, (Lee, Kim and Weinreb 2012).

Glaucoma is primarily a disease of ageing (Gordon et al. 2002; Leske et al. 2003); therefore, having already evaluated changes in optic nerve head and other parameters that occur at the optic nerve head as a result of the normal aging process, this chapter will explore changes that occur at the ONH as a result of the glaucomatous process, whilst accounting for the same factors that contributed to differences between older eyes and younger eyes. The hypothesis is that the prelamina and LC thin as a function of disease stage advancement in glaucoma, and that a number of factors (e.g. age, axial length and refractive error) are likely to influence/contribute to the observed ONH changes.

5.1.1 Aims of chapter

To identify those microstructural changes that occur in the optic nerve head at different glaucoma disease stages, i.e. preperimetric, early and advanced glaucoma, and subsequently determine those factors that best explain the observed changes.

5.2 Experimental design

5.2.1 Subjects

52 participants (19 control and 33 glaucoma) were recruited from the glaucoma clinic at UHW and from within the staff, students and friends of Cardiff University (control subjects). The inclusion criteria required for participants were: mean spherical refractive error within ± 6.00 D and no other (non-glaucomatous) ocular pathology. For the control group, additional inclusion criteria were: no visual field defect, as defined by Hodapp et al. (1993), best corrected visual acuity 0.10 logMAR, and IOP ≤ 21 mmHg (Table 5.1).

	Control (n=34)	Preperimetric glaucoma (n=8)	Early glaucoma (n=26)	Advanced glaucoma (n=12)
	mean \pm SD	mean \pm SD	mean \pm SD	mean \pm SD
Age (years)	55.97 \pm 9.69	68.25 \pm 10.74	69.69 \pm 9.14	73.58 \pm 10.32
Gender	15F : 19M	4F : 4M	14F : 12M	4F : 8M
MS (D)	0.00 \pm 2.00	-1.00 \pm 3.75	0.75 \pm 2.75	0.75 \pm 1.50
VA (logMAR)	-0.10 \pm 0.06	0.02 \pm 0.12	0.06 \pm 0.16	0.16 \pm 0.22
IOP (mmHg)	12.79 \pm 2.54	11.63 \pm 1.11	12.98 \pm 2.07	11.00 \pm 1.99
CCT (μ m)	561.21 \pm 46.21	531.25 \pm 33.43	553.58 \pm 50.53	526.92 \pm 34.60
Axial length (mm)	23.88 \pm 1.06	23.81 \pm 2.19	23.53 \pm 1.50	23.85 \pm 1.44
ACD (mm)	2.83 \pm 0.58	3.10 \pm 0.61	3.06 \pm 0.89	2.96 \pm 0.66
MD (dB)	-0.65 \pm 1.93	-0.76 \pm 1.50	-3.06 \pm 1.81	-11.77 \pm 6.01

Table 5.1: Participant demographics for those eyes included in the study. MS = mean spherical refractive error, VA = visual acuity, IOP = intraocular pressure, CCT = central corneal thickness, ACD = anterior chamber depth, MD = mean deviation visual fields, F = female, M = male, SD = standard deviation.

Datasets from 13 of the potential 104 eyes were excluded as 'glaucoma suspects'. The designation criteria for glaucoma suspects were i) the eye did not have a positive or negative glaucoma diagnosis and was being monitored under the hospital eye service, or ii) the healthy fellow eye of a pair,

where one had a positive glaucoma diagnosis, was excluded in case of pre-clinical changes. Image datasets of a further 9 eyes were excluded from analysis due to poor OCT image quality, and two eyes from one participant were excluded due to detection of a macula haemorrhage during data acquisition.

5.2.2 Clinical assessments

Visual acuity, intraocular pressure (IOP), refractive error, axial length, anterior chamber depth and central corneal thickness measurements were determined for each eye, as previously described in section 2.3.1, and visual field tests were performed (SITA 24-2 Fast Threshold, Humphrey Visual Field Analyser).

5.2.3 2D Image analysis of optic nerve head microstructure

20° scans centred on the ONH of both participant eyes (unless exclusion criteria applied) were acquired using enhanced depth imaging, and the image datasets were processed and scaled as described in section 2.4. Three-dimensional datasets were sliced every 45° into 4 radial tomograms centred on the ONH, as described in section 2.6. Bruch's membrane opening (BMO) diameter was determined in the temporal (T) – nasal (N), superior-temporal (ST) – inferior-nasal (IN), superior (S) – inferior (I), and superior-nasal (SN) – inferior-temporal (IT) directions as a measure of ONH diameter in each plane. The mid point and two quartiles within each BMO diameter were calculated to determine the location for central and peripheral ONH measurements, from which calliper lines were drawn to the surfaces of the prelamina, anterior LC and posterior LC. This enabled measurement of prelamina, anterior LC and posterior LC surface depth relative to BMO reference plane. The prelamina surface depth measurement was subtracted from that of the anterior LC to calculate prelamina thickness. The anterior LC depth measurement was subtracted from posterior LC depth to calculate LC thickness.

NFL thickness was measured at two locations: immediately above BMO at the ONH border (i.e. border NFL or bNFL,) and at a distance 1.7mm from the centre of the ONH (i.e. peripapillary NFL, or pNFL). All measurements were performed as described in section 2.6.

5.2.4 Statistical analysis

All statistical analysis was performed in RStudio version 0.98.1091, as described in section 2.9. Statistical modelling was performed using the CRAN package ‘lme4’ (Bates and Maechler, 2010; <http://cran.r-project.org/packages/lme4>), and post-hoc analysis performed using ‘lsmeans’ (Lenth 2015; <http://cran.r-project.org/packages/lsmeans>). All graphs were generated using the ‘ggplot2’ package (Wickham and Chang, 2012; <http://cran.r-project.org/packages/ggplot2>).

ONH parameters were plotted as a function of visual field loss or disease stage, in order to visualise the data. Normality of data were established using histograms, QQ-plots and Shapiro Wilk tests. All parameter data, except prelamina thickness and BMO diameter, followed a normal distribution, and either Spearman’s or Pearson’s correlation was applied as appropriate.

Linear mixed-effects models (LMM) were generated for each ONH parameter using a stepwise deletion of the fixed effects, *stage of glaucoma*, *age*, *axial length*, *mean spherical refractive error (MS)*, *mean deviation of visual field (MD)*, *anterior chamber depth (ACD)* and *central corneal thickness (CCT)*, and the interaction terms *age:MD*, *axial length:MD*, and *axial length:MS*, in order to investigate the direction and magnitude of associations with each ONH parameter. A linear mixed-effects model assumes a normal distribution of the residual variance. In cases where this assumption was not met i.e. residuals were not normally distributed, a link function (transformation) was applied, creating a generalised linear mixed-effects model (GLMM).

The effects of variables within each model are presented as (effect size \pm SD, p -value) unless otherwise stated, i.e. how much the ONH parameter will change in μm for every one-unit change in the independent variable. A factor in the model was considered significant if $p < 0.05$. Due to the categorical nature of *stage of glaucoma*, LMMs supplied effect size, standard error, and t value for each stage of glaucoma in comparison to control only, so Tukey post-hoc analysis (pairwise comparison) was performed to determine all inter-group differences. P -values were adjusted as part of this analysis, and were considered significant if $p < 0.01$, and a trend if $p < 0.05$. P -values are given to three decimal places.

5.3 Results

5.3.1 BMO diameter as a of glaucoma disease stage

The diameter of BMO was used as surrogate optic nerve head diameter. The diagram and images in Figure 5.1 are representative of BMO diameter measured in control (C), preperimetric glaucoma (PG), early glaucoma (EG) and advanced glaucoma (AG) ONHs.

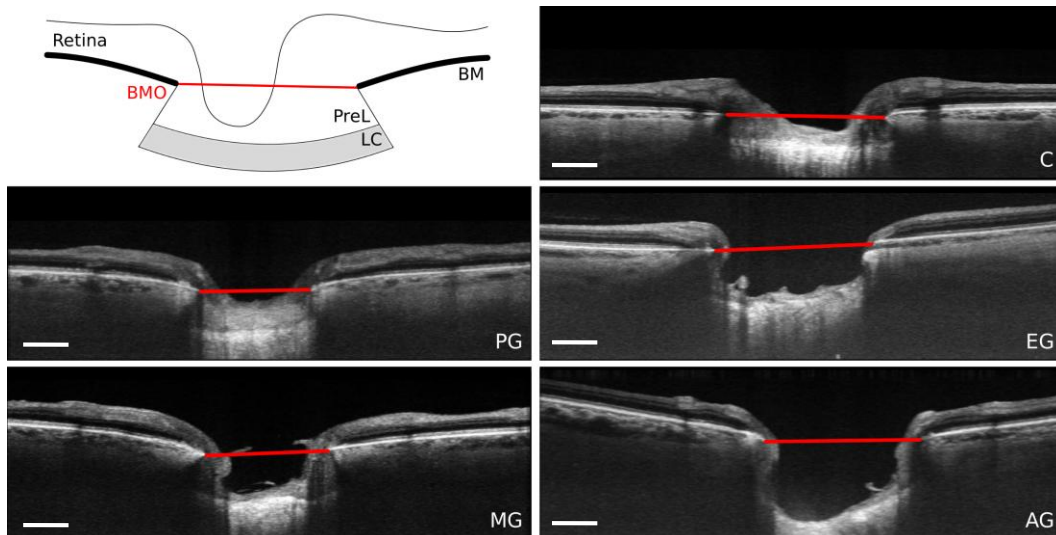


Figure 5.1: Diagram of the Bruch's membrane opening (BMO) diameter across the optic disc on a schematic and OCT images from each stage of glaucoma (G), in the superior-inferior plane. BMO shown in red, BM = Bruch's Membrane, PreL = prelamina, LC = Lamina cribrosa, C = control. PG = preperimetric G, EG = early G, MG = moderate glaucoma, AG = advanced G. Scale bars = 500 μm .

5.3.1.1 Changes in Bruch's membrane opening diameter as a function of visual field progression

No significant correlations were identified between visual field loss and BMO diameter in any of the 4 orientations (S-I, SN-IT, T-N, ST-IN) through the ON examined ($p > 0.05$ Spearman's rho; Figure 5.2). Moreover, the ratio of horizontal (T-N) to vertical (S-I) BMO diameter did not correlate with visual field loss ($p < 0.05$ Pearson's correlation; Figure 5.2).

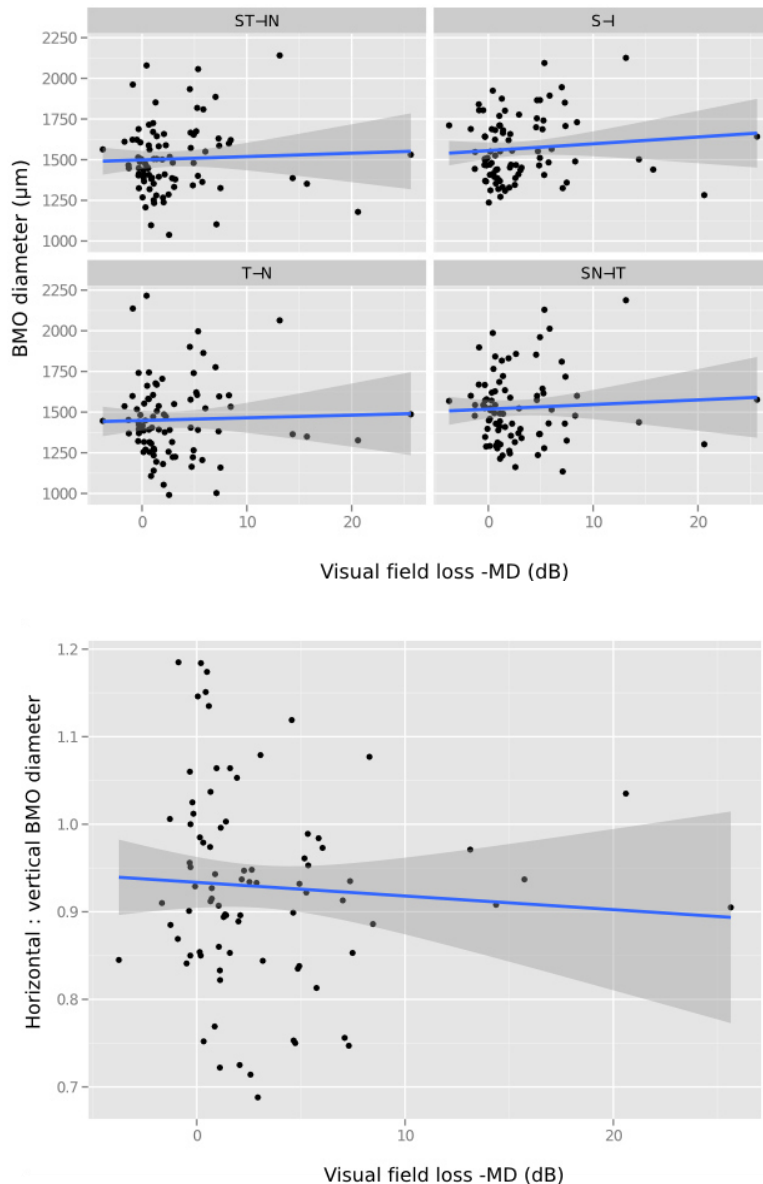


Figure 5.2: Bruch's membrane opening (BMO) diameter and Horizontal:vertical ratio of BMO diameter as a function of visual field loss. No significant association was found between BMO diameter (T-N/ST-IN/S-I/SN-IT) or its horizontal:vertical ratio and increasing visual field loss ($p > 0.05$ Spearman's rho). x-axis shows increasing visual field loss from left to right. T = temporal, ST = superior-temporal, S = superior, SN = superior-nasal, N = nasal, IN = inferior-nasal, I = inferior, IT = inferior-temporal, grey bars = 95% confidence intervals.

5.3.1.2 Quantitative analysis of Bruch's membrane opening diameter for different glaucoma disease stage

Mean and standard deviation for regional BMO diameter values for each stage of glaucoma are shown below in Table 5.2.

Regional BMO diameter	Control mean \pm SD (μm)	Preperimetric Glaucoma mean \pm SD (μm)	Early Glaucoma mean \pm SD (μm)	Advanced Glaucoma mean \pm SD (μm)
T-N	1439.75 \pm 130.81	1606.97 \pm 354.43	1415.00 \pm 269.03	1481.94 \pm 265.76
ST-IN	1476.88 \pm 127.61	1598.30 \pm 268.96	1509.02 \pm 252.24	1521.51 \pm 276.17
S-I	1544.49 \pm 150.04	1611.45 \pm 215.48	1578.63 \pm 217.03	1592.71 \pm 243.09
SN-IT	1521.18 \pm 141.73	1600.10 \pm 223.04	1501.26 \pm 268.15	1553.16 \pm 271.17

Table 5.2: Mean of each regional Bruch's membrane opening (BMO) diameter for each stage of glaucoma. SD = standard deviation. T = temporal, ST = superior-temporal, S = superior, SN = superior-nasal, N = nasal, IN = inferior-nasal, I = inferior, IT = inferior-temporal.

5.3.1.3 Multivariate analysis of Bruch's membrane opening diameter for different glaucoma disease stage

Multivariate analysis of Bruch's membrane opening diameter in glaucomatous eyes was performed using optimised linear mixed-effects models (LMMs) for the BMO diameter in each orientation (Table 5.3). Glaucoma disease stage significantly affected the S-I BMO diameter ($p=0.003$), but had no effect on other BMO orientations, while other factors that contributed to BMO diameter in glaucomatous eyes included *mean spherical refractive error* (negative effect on the S-I BMO: $-32.76 \pm 11.23\mu\text{m}/\text{D}$, $p=0.003$), i.e. eyes with greater amounts of hyperopia had smaller vertical BMO, or smaller vertical optic disc diameter. Additionally, *anterior chamber depth (ACD)* had a negative effect on BMO diameter in S-I and SN-IT planes ($p<0.05$), meaning that eyes with deeper ACD had smaller BMO diameter in those directions.

The interaction between *axial length:MD* had a negative effect on SN-IT BMO diameter ($p=0.021$), and the *age:MD* association negatively effected BMO diameter in the T-N ($p=0.012$) direction.

Additionally, *axial length* and *MS* had a significant association (Figure 5.3) and the interaction *axial length:MS* had a negative effect on T-N BMO diameter ($p=0.030$).

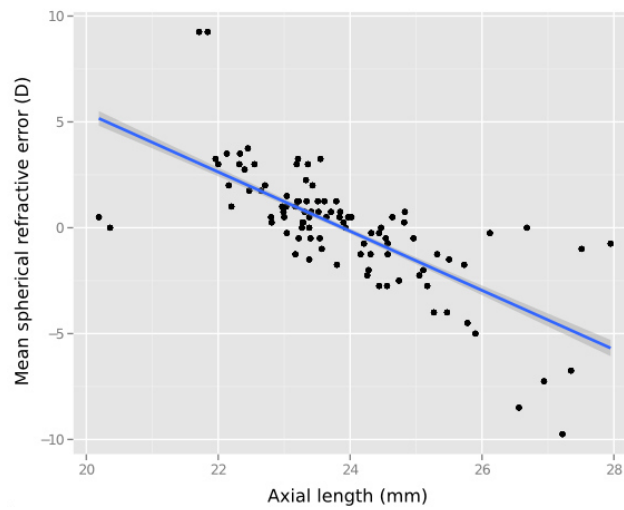


Figure 5.3: The association between mean spherical refractive error and axial length. Grey bars = 95% confidence interval

An optimised LMM generated to describe the variance in the horizontal:vertical ratio of BMO diameter contained the independent variable *central corneal thickness*, and the interactions between *age:MD*, *axial length:MD*, and *axial length:MS*. Of these, only *age:MD* (i.e. the association between age and vision loss, a combination of two prominent features associated with the progression of glaucoma), was a contributing factor in the determination of horizontal:vertical BMO diameter ($p=0.025$).

Region		Dx	Age	AxL	MS	MD	ACD	CCT	Age:MD	AxL:MD	AxL:MS
T-N	BMO		-2.15 ± 2.18	37.35 ± 25.86	205.26±115.91	78.20 ± 33.68	-68.64 ± 36.09		-1.27 ± 0.49		-9.84 ± 4.74
	<i>t value</i>		-0.99	1.44	1.77	2.32	-1.90		-2.58		-2.07
	<i>p value</i>		-	-	-	-	0.054		0.012		0.030
ST-IN	BMO			36.42 ± 31.56	242.79± 144.16		-84.85 ± 45.71				-10.73 ± 5.87
	<i>t value</i>			1.15	1.68		-1.86				-1.83
	<i>p value</i>			-	-		0.056				0.059
S-I	BMO		-3.72 ± 2.64		-32.76 ± 11.23		-125.76 ± 41.18				
	<i>t value</i>		-1.41		-2.92		-3.05				
	<i>p value</i>	0.003	0.137		0.003		0.002				
SN-IT	BMO		-5.39 ± 2.74	65.98 ± 26.52		373.70± 151.10	-113.97 ± 44.67		-1.24 ± 0.69	-13.17 ± 5.71	
	<i>t value</i>		-1.96	2.49		2.47	-2.55		-1.79	-2.31	
	<i>p value</i>		-	-		-	0.009		0.091	0.021	
H-V	BMO		-0.001 ± 0.001	0.030 ± 0.015	0.08 ± 0.06	-0.001 ± 0.042		0.0004±0.0003	-0.0007±0.0003	0.002 ± 0.001	-0.004 ± 0.002
	<i>t value</i>		-0.97	2.08	1.32	-0.03		1.39	-2.24	1.54	-1.44
	<i>p value</i>		-	-	-	-		0.132	0.025	0.133	0.121

Table 5.3: Linear mixed-effects model for Bruch's membrane opening (BMO) diameter for each direction within the optic nerve head. Values are effect size ± standard error, i.e. how much BMO diameter changes in μm per one-unit change in the independent variable, as well as *t*-value and *p*-value. Red text indicates factor is significant at $p < 0.05$. T = temporal, ST = superior-temporal, S = superior, SN = superior-nasal, N = nasal, IN = inferior-nasal, I = inferior, IT = inferior-temporal, H-V = ratio horizontal:vertical, AxL = axial length, MS = mean spherical refractive error, MD = mean deviation on visual fields, ACD = anterior chamber depth, CCT = central corneal thickness.

5.3.1.4 The effect of glaucoma on Bruch's membrane opening diameter

Regional BMO diameter for each stage of glaucoma is shown below in Figure 5.4. Post-hoc analysis of optimised LMM data revealed that the S-I BMO diameter was significantly larger in eyes with preperimetric glaucoma (PG; $1611 \pm 215 \mu\text{m}$) when compared to advanced glaucoma (AG; $1593 \pm 243 \mu\text{m}$; $p=0.005$). The *stage of glaucoma* was not a factor in the models to describe BMO diameter in other planes. Neither was it a factor in the optimised LMM to describe variance in horizontal:vertical BMO diameter (i.e. circularity of the disc; Table 5.3).

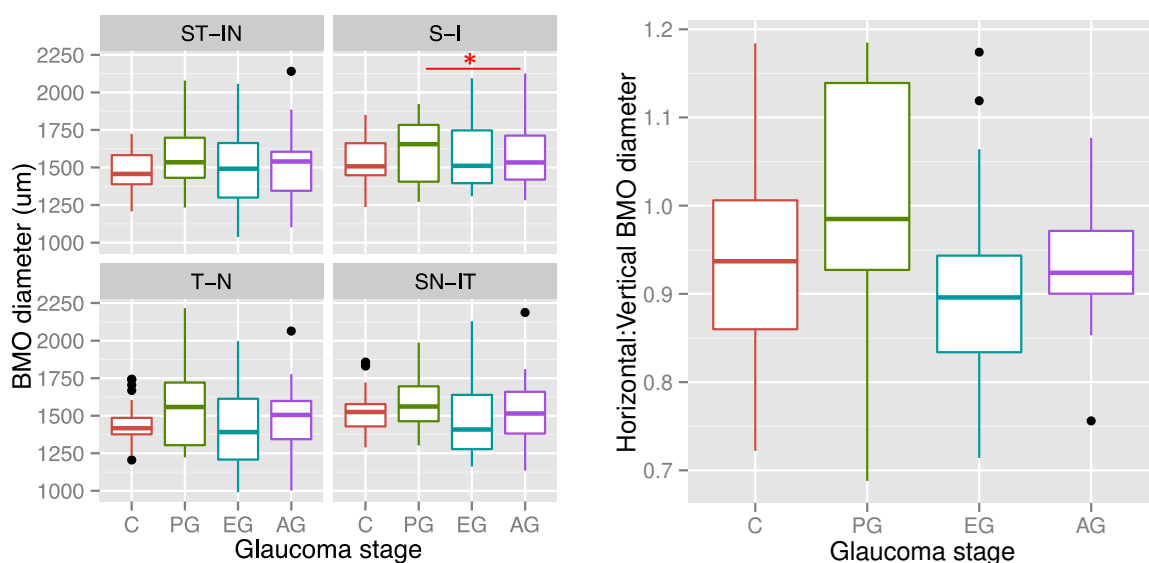


Figure 5.4: a) Regional Bruch's membrane opening (BMO) diameter and b) Horizontal:vertical BMO diameter ratio for each stage of glaucoma (G). C = control, PG = preperimetric G, EG = early G, AG = advanced G. T = temporal, S = superior, N = nasal, I = inferior. Boxplots denote median and 1st to 3rd quartiles, whiskers extend to the highest or lowest data value that is within a 1.5 x interquartile range. Black spots denote outliers. Red stars indicates *stage of glaucoma* made a significant contribution to variance in BMO diameter, * = $p<0.01$.

5.3.2 Changes in peripapillary and border nerve fibre layer thickness as a function of glaucoma

Peripapillary nerve fibre layer (pNFL) was measured at a distance of 1.7mm from the optic disc centre, and border nerve fibre layer (bNFL) was measured directly above BMO, as shown in Figure 5.5, for different glaucoma stages.

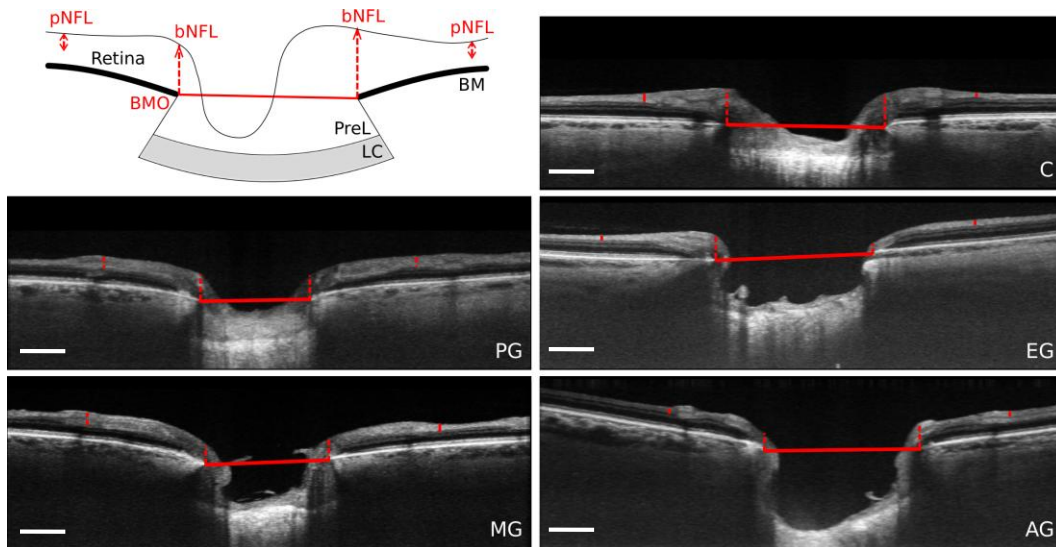


Figure 5.5: Diagram of measurements of peripapillary nerve fibre layer (pNFL), measured at a distance 1.7mm from the centre of the optic disc, and border NFL (bNFL), measured above Bruch's membrane opening (BMO), on a schematic and OCT images from each stage of glaucoma. Measurements are shown in red, measured on a superior-inferior slice. BM = Bruch's Membrane, PreL = prelamina, LC = Lamina cribrosa, C = control. PG = preperimetric glaucoma, EG = early glaucoma, MG = moderate glaucoma, AG = advanced glaucoma. Scale bars = 500 μm .

5.3.2.1 Changes in nerve fibre layer thickness as a function of visual field loss

Thinning of the peripapillary nerve fibre layer (pNFL) in all regions (except for the superior-nasal and inferior and bNFL in all regions) was significantly associated with increasing visual field loss (Figure 5.6).

5.3.2.2 Quantitative analysis of nerve fibre layer parameters for stages of glaucoma

The mean and standard deviation for regional pNFL and bNFL values for each stage of glaucoma is shown below in Table 5.4.

Region	Control mean \pm SD (μm)	Preperimetric Glaucoma mean \pm SD (μm)	Early Glaucoma mean \pm SD (μm)	Advanced Glaucoma mean \pm SD (μm)
T pNFL	49.52 \pm 14.30	61.73 \pm 25.46	42.23 \pm 14.07	38.53 \pm 11.92
ST pNFL	91.33 \pm 27.80	101.80 \pm 32.12	73.01 \pm 24.11	57.93 \pm 33.25
S pNFL	106.31 \pm 36.62	88.45 \pm 49.58	74.60 \pm 29.56	83.13 \pm 25.59
SN pNFL	90.68 \pm 28.27	135.01 \pm 61.74	78.64 \pm 30.78	85.54 \pm 40.60
N pNFL	50.29 \pm 16.15	48.08 \pm 11.28	48.76 \pm 20.78	35.74 \pm 22.51
IN pNFL	84.45 \pm 31.76	95.77 \pm 22.73	71.47 \pm 28.91	63.71 \pm 18.91
I pNFL	101.69 \pm 34.51	109.03 \pm 36.04	91.50 \pm 25.58	79.40 \pm 36.85
IT pNFL	84.82 \pm 23.22	103.64 \pm 37.65	63.56 \pm 32.82	46.05 \pm 20.08
T bNFL	248.44 \pm 81.39	250.72 \pm 84.17	194.12 \pm 46.43	174.28 \pm 37.08
ST bNFL	314.66 \pm 72.67	318.24 \pm 95.59	229.23 \pm 53.21	189.61 \pm 77.45
S bNFL	362.25 \pm 59.26	377.48 \pm 156.73	298.91 \pm 70.51	201.19 \pm 88.06
SN bNFL	335.42 \pm 63.92	368.98 \pm 110.33	264.39 \pm 99.38	213.98 \pm 95.54
N bNFL	284.61 \pm 68.17	280.35 \pm 91.93	233.97 \pm 78.70	182.19 \pm 103.25
IN bNFL	333.72 \pm 81.76	332.35 \pm 103.84	275.45 \pm 94.27	231.43 \pm 89.89
I bNFL	360.43 \pm 51.50	339.07 \pm 127.15	254.25 \pm 97.56	198.10 \pm 81.24
IT bNFL	299.14 \pm 56.70	254.83 \pm 68.01	219.66 \pm 58.05	163.62 \pm 59.34

Table 5.4: Mean of each regional nerve fibre layer (NFL) parameter for each stage of glaucoma. pNFL = peripapillary NFL, bNFL = border NFL, SD = standard deviation. T = temporal, ST = superior-temporal, S = superior, SN = superior-nasal, N = nasal, IN = inferior-nasal, I = inferior, IT = inferior-temporal, C = central.

5.3.2.3 Multivariate analysis of nerve fibre layer parameters in glaucomatous eyes

Using optimised LMMs to explain the variance in the regions within the peripapillary and border nerve fibre layer thicknesses (Table 5.5 and Table 5.6) it was revealed that *glaucomatous stage* significantly affected pNFL thickness in the T ($p=0.033$), S and SN ($p<0.001$) regions of the optic nerve head (see Table 5.5); and the T ($p=0.010$), ST, S ($p=0.015$), SN, I, IT (all others $p<0.001$) bNFL thickness (Table 5.6).

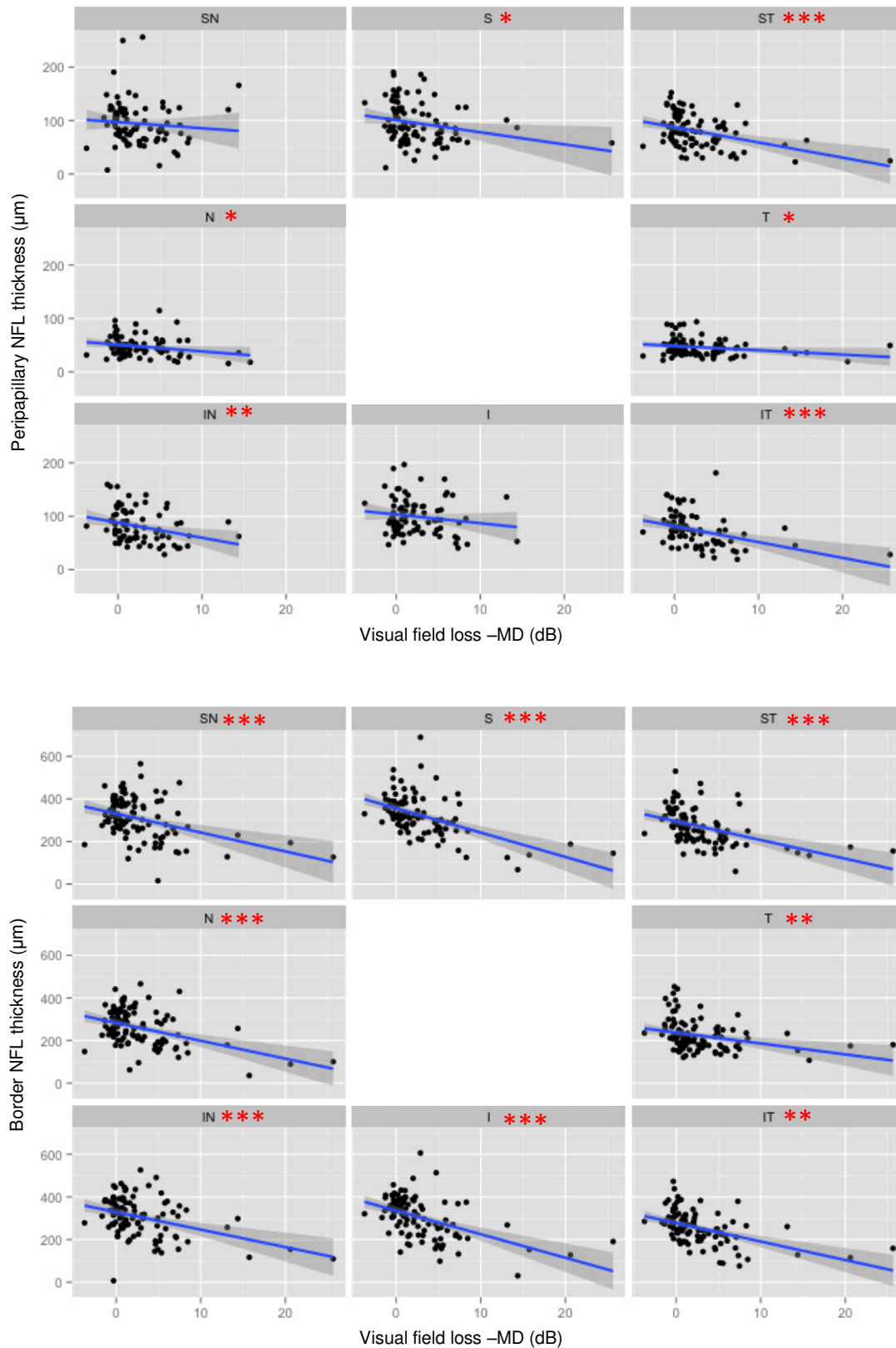


Figure 5.6: Peripapillary nerve fibre layer (pNFL) and border nerve fibre layer (bNFL) thickness as a function of visual field loss for each region. The x-axis is reversed so that greater visual field loss is further along the x-axis. T = temporal, ST = superior-temporal, S = superior, SN = superior-nasal, N = nasal, IN = inferior-nasal, I = inferior, IT = inferior-temporal, grey bars = 95% confidence intervals. * = $p < 0.05$, ** = $p < 0.01$, *** = $p < 0.001$, Pearson's correlation.

Other factors that contributed in the LMM generated to explain nerve fibre layer parameters in glaucomatous eyes were *age*, *AxL*, *MS*, *MD*, *ACD* (Table 5.5 and Table 5.6). Specifically, *Age* had a significant negative effect on pNFL thickness in the IT ($-0.80 \pm 0.27 \mu\text{m}/\text{year}$, $p=0.003$) and ST ($-0.71 \pm 0.26 \mu\text{m}/\text{year}$, $p=0.008$) regions, and a positive effect on superior pNFL thickness ($1.31 \pm 0.34 \mu\text{m}/\text{year}$, $p<0.001$). *Axial length* negatively affected bNFL thickness in all regions except for nasal. *Mean spherical refractive error* had a significant negative effect on S and IT pNFL thickness ($-4.49 \pm 1.56 \mu\text{m}/\text{D}$, $p=0.004$; $-3.09 \pm 1.49 \mu\text{m}/\text{D}$, $p=0.035$), as well as a significant negative effect of around $-12 \mu\text{m}/\text{D}$ on bNFL thickness in the T ($p<0.001$), ST ($p=0.015$) and IT regions ($p=0.002$; Table 5.6). Finally, *MD* had a significant positive effect on the N and IN regions of the bNFL thickness ($p<0.001$), and IN pNFL ($p=0.040$; Table 5.6).

Additionally, *anterior chamber depth (ACD)* also had a positive effect, on SN bNFL thickness ($29.56 \pm 14.53 \mu\text{m}/\text{mm ACD}$, $p=0.037$). *Central corneal thickness (CCT)* had a positive effect on the bNFL thickness by $0.49 \mu\text{m}/\mu\text{m CCT}$ in the ST ($p=0.026$) and SN ($p=0.012$) regions.

5.3.2.4 The effect of stage of glaucoma on peripapillary and border nerve fibre layer thickness

As described in Table 5.5, *glaucoma stage* significant affected T, S and SN pNFL thickness (Figure 5.7) and all regions of the bNFL, except N and IN ($p>0.05$; Figure 5.7; Table 5.6). Post-hoc analysis revealed the presence of significant inter-disease stage differences in bNFL and pNFL, which have been summarised in Figure 5.8).

Region	Dx	Age	AxL	MS	MD	ACD	CCT	Age:MD	AxL:MD	AxL:MS
T	pNFL		2.44 ± 1.35							
	<i>t value</i>		1.80							
	<i>p value</i>	0.033	0.069							
ST	pNFL	-0.71 ± 0.26								
	<i>t value</i>	-2.79								
	<i>p value</i>	0.008								
S	pNFL	1.31 ± 0.34		-4.49 ± 1.56						
	<i>t value</i>	3.84		-2.88						
	<i>p value</i>	<0.001	<0.001	0.004						
SN	pNFL	0.09 ± 0.48			3.24 ± 7.18			-0.15 ± 0.11		
	<i>t value</i>	0.19			0.45			-1.39		
	<i>p value</i>	<0.001	-		-			0.058		
N	pNFL		-1.47 ± 3.16	34.07 ± 16.15	1.15 ± 0.64					-1.34 ± 0.63
	<i>t value</i>		-0.46	2.11	1.80					-2.12
	<i>p value</i>		-	-	0.064					0.029
IN	pNFL			-2.18 ± 1.48	2.32 ± 1.10					
	<i>t value</i>			-1.48	2.10					
	<i>p value</i>			0.130	0.040					
I	pNFL		-15.67 ± 6.32	-4.47 ± 2.63	62.80 ± 33.05				-2.56 ± 1.40	
	<i>t value</i>		-2.48	-1.70	1.87				-1.83	
	<i>p value</i>		-	0.078	-				0.059	
IT	pNFL	-0.80 ± 0.27		-3.09 ± 1.49	1.28 ± 0.77					
	<i>t value</i>	-2.99		-2.07	1.66					
	<i>p value</i>	0.003		0.035	0.088					

Table 5.5: Linear mixed-effects models for peripapillary nerve fibre layer (pNFL) thickness, containing effect size ± standard error, i.e. how much pNFL changes in µm per one-unit change in the independent variable, as well as t-value and p-value. Red text indicates factor is significant at $p < 0.05$. T = temporal, ST = superior-temporal, S = superior, SN = superior-nasal, N = nasal, IN = inferior-nasal, I = inferior, IT = inferior-temporal, AxL = axial length, MS = mean spherical refractive error, MD = mean deviation on visual fields, ACD = anterior chamber depth, CCT = central corneal thickness.

Region	Dx	Age	AxL	MS	MD	ACD	CCT	Age:MD	AxL:MD	AxL:MS
T bNFL			-23.64 ± 7.64	-13.87 ± 4.16			0.26 ± 0.17			
t value			-3.09	-3.33			1.54			
p value	0.010		0.002	<0.001			0.106			
ST bNFL			-28.37 ± 8.89	-10.68 ± 4.59		19.86 ± 12.44	0.41 ± 0.19			
t value			-3.19	-2.34		1.60	2.11			
p value	<0.001		0.001	0.015		0.107	0.026			
S bNFL		0.27 ± 1.06	-34.55 ± 9.95	-7.14 ± 5.15	-17.11 ± 14.54	20.12 ± 14.19		0.30 ± 0.21		
t value		0.25	-3.47	-1.39	-1.18	1.42		1.42		
p value	0.015	-	<0.001	0.132	-	0.149		0.135		
SN bNFL			-21.87 ± 7.21			29.56 ± 14.53	0.49 ± 0.21			
t value			-3.03			2.03	2.27			
p value	<0.001		0.002			0.037	0.012			
N bNFL			-12.09 ± 6.34		7.91 ± 1.76					
t value			-1.90		4.51					
p value			0.055		<0.001					
IN bNFL			-19.03 ± 7.63		7.44 ± 1.96	22.14 ± 15.35				
t value			-2.49		3.80	1.44				
p value			0.013		<0.001	0.146				
I bNFL			-23.68 ± 7.10		3.42 ± 2.40					
t value			-3.34		1.43					
p value	<0.001		<0.001		0.140					
IT bNFL			-22.21 ± 7.65	-11.67 ± 3.96	2.99 ± 2.11		0.21 ± 0.16			
t value			-2.96	-2.95	1.42		1.36			
p value	<0.001		0.003	0.002	0.139		0.153			

Table 5.6: Linear mixed-effects models for border nerve fibre layer (bNFL) thickness, containing effect size ± standard error, i.e. how much bNFL changes in µm per one-unit change in the independent variable, as well as t-value and p-values. Red text indicates factor is significant at $p < 0.05$. T = temporal, ST = superior-temporal, S = superior, SN = superior-nasal, N = nasal, IN = inferior-nasal, I = inferior, IT = inferior-temporal, AxL = axial length, MS = mean spherical refractive error, MD = mean deviation on visual fields, ACD = anterior chamber depth, CCT = central corneal thickness

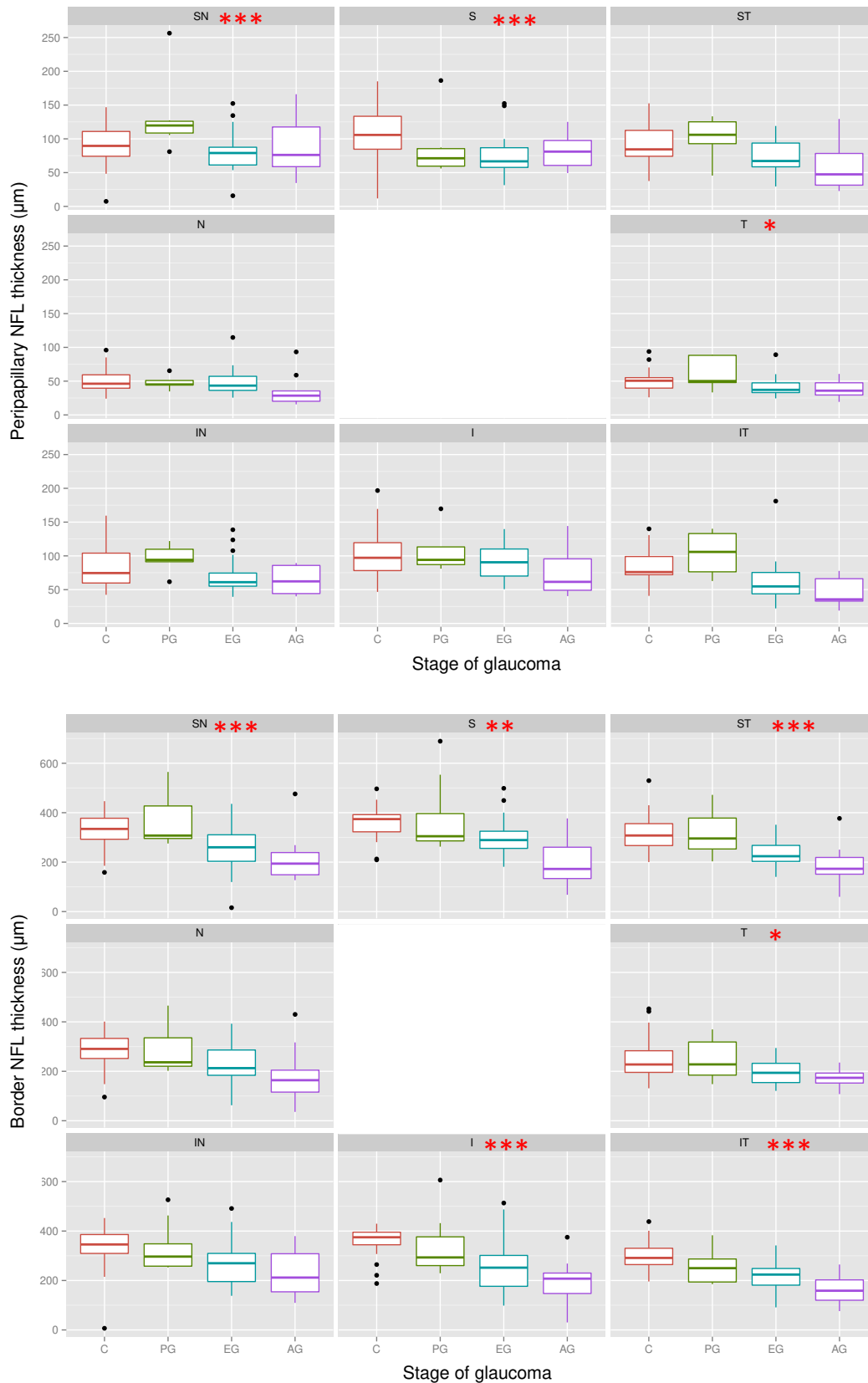


Figure 5.7: a) Peripapillary nerve fibre layer and b) Border NFL thickness for each glaucoma (G) stage. C = control, PG = preperimetric G, EG = early G, MG = moderate G, AG = advanced G. T = temporal, S = superior, N = nasal, I = inferior. Boxplots denote median and 1st to 3rd quartiles; whiskers extend to the highest or lowest data value that is within a 1.5 x interquartile range. Black spots denote outliers. Red stars: significance as a function of glaucoma stage * = $p < 0.05$, ** = $p < 0.01$, *** = $p < 0.001$.

No statistically significant differences were found in temporal pNFL thickness between any of the glaucoma groups and the control group. In the S region, control eyes had a significantly thicker pNFL ($106.31 \pm 36.62 \mu\text{m}$) than eyes with early glaucoma ($74.60 \pm 29.56 \mu\text{m}$) and advanced glaucoma ($83.13 \pm 25.59 \mu\text{m}$; $C>EG$ $p<0.001$; $C>AG$ $p=0.004$).

In the SN region the pNFL was thinner in early ($78.64 \pm 30.78 \mu\text{m}$) and advanced glaucoma ($85.54 \pm 40.60 \mu\text{m}$) than in preperimetric glaucoma ($135.01 \pm 61.74 \mu\text{m}$; $p<0.001$) but was significantly thicker in preperimetric glaucoma than in control ($PG>C$ $p=0.007$). In contrast, the temporal bNFL showed no significant differences between groups ($p>0.01$). In the ST region, bNFL was thinner in both early ($229.23 \pm 53.21 \mu\text{m}$) and advanced glaucoma ($189.61 \pm 77.45 \mu\text{m}$) than in control eyes ($314.66 \pm 72.67 \mu\text{m}$; $p<0.001$). The differences identified by post-hoc testing are summarised in Figure 5.8.

For the superior region of the ONH, post-hoc pairwise comparisons revealed no significant differences in bNFL thickness between control and any glaucoma groups ($p>0.01$). Both early glaucoma ($264.39 \pm 99.38 \mu\text{m}$) and advanced glaucoma ($213.98 \pm 95.54 \mu\text{m}$) showed SN bNFL thinning compared to the control ($335.42 \pm 63.92\mu\text{m}$) and preperimetric glaucoma groups ($368.98 \pm 110.33 \mu\text{m}$; $C>EG$ $p=0.007$; $C>AG$ $p=0.003$; $PG>EG$ $p=0.004$; $PG>AG$ $p=0.001$).

The bNFL in the inferior region was significantly thinner for eyes with early glaucoma ($254.25 \pm 97.56 \mu\text{m}$) compared to control ($360.43 \pm 51.50 \mu\text{m}$) and preperimetric glaucoma ($339.07 \pm 127.15 \mu\text{m}$; $C>EG$ $p<0.001$; $PG>EG$ $p=0.006$). Finally, in the IT region the bNFL was significantly thinner in early glaucoma ($219.66 \pm 58.05 \mu\text{m}$) than in control ($299.14 \pm 56.70 \mu\text{m}$; $C>EG$ $p<0.001$).

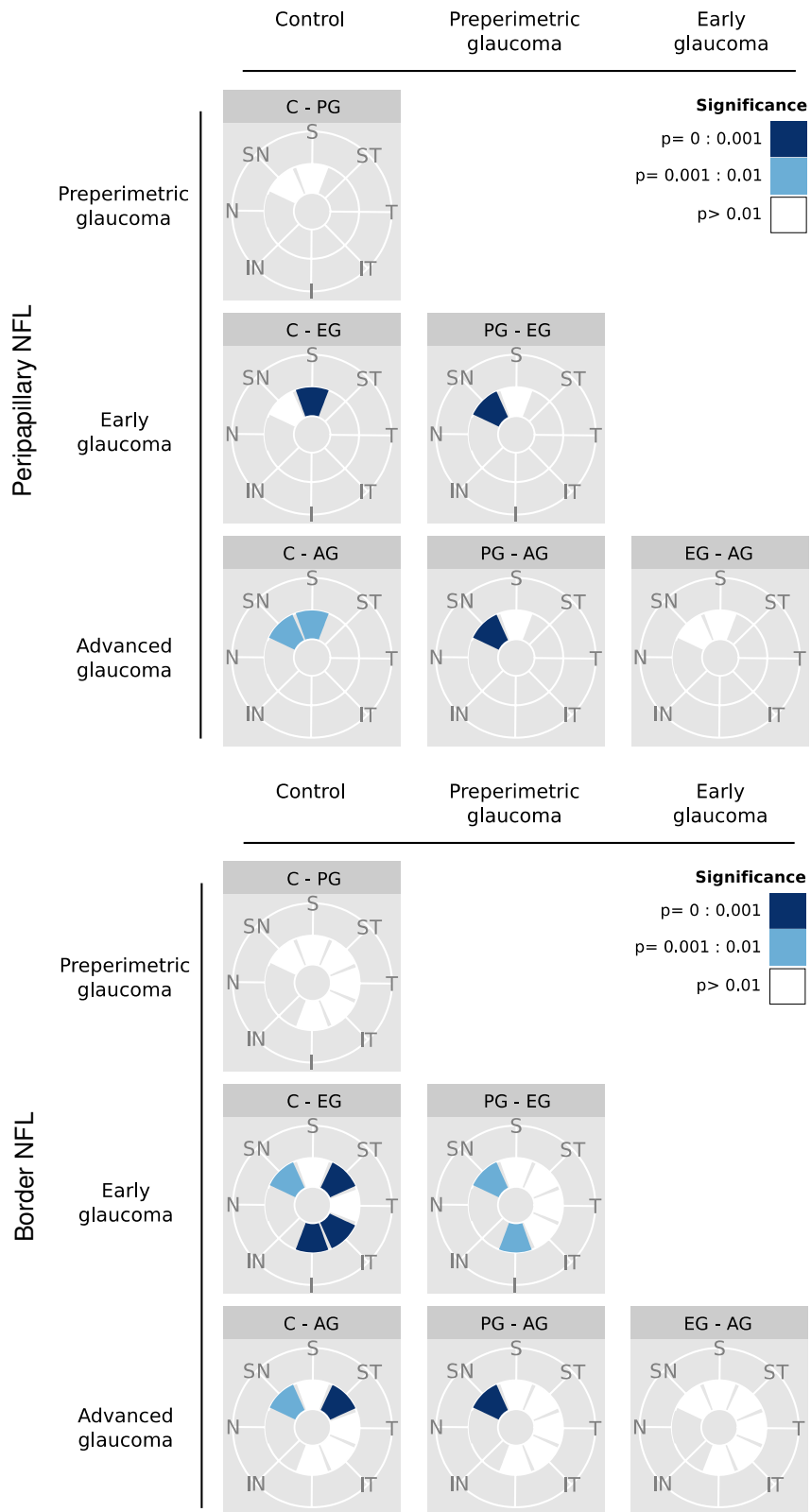


Figure 5.8: Regional changes in peripapillary nerve fibre layer (pNFL) and border nerve fibre layer (bNFL) as a function of glaucoma (G) stage detected using linear mixed-effects models and subsequent posthoc analysis (Tukey). C = control, PG = preperimetric G, EG = early G, AG = advanced G. T = temporal, ST = superior-temporal, S = superior, SN = superior-nasal, N = nasal, IN = inferior-nasal, I = inferior, IT = inferior-temporal. Blue indicates significant differences, white indicates that glaucomatous progression was a factor in the model but there were no significant differences, grey indicates regions where stage of glaucoma was not a factor in the model.

5.3.3 The effect of glaucoma and other ocular parameters on the prelamina

The prelamina surface depth from BMO and the prelamina thickness were measured as shown below in Figure 5.9.

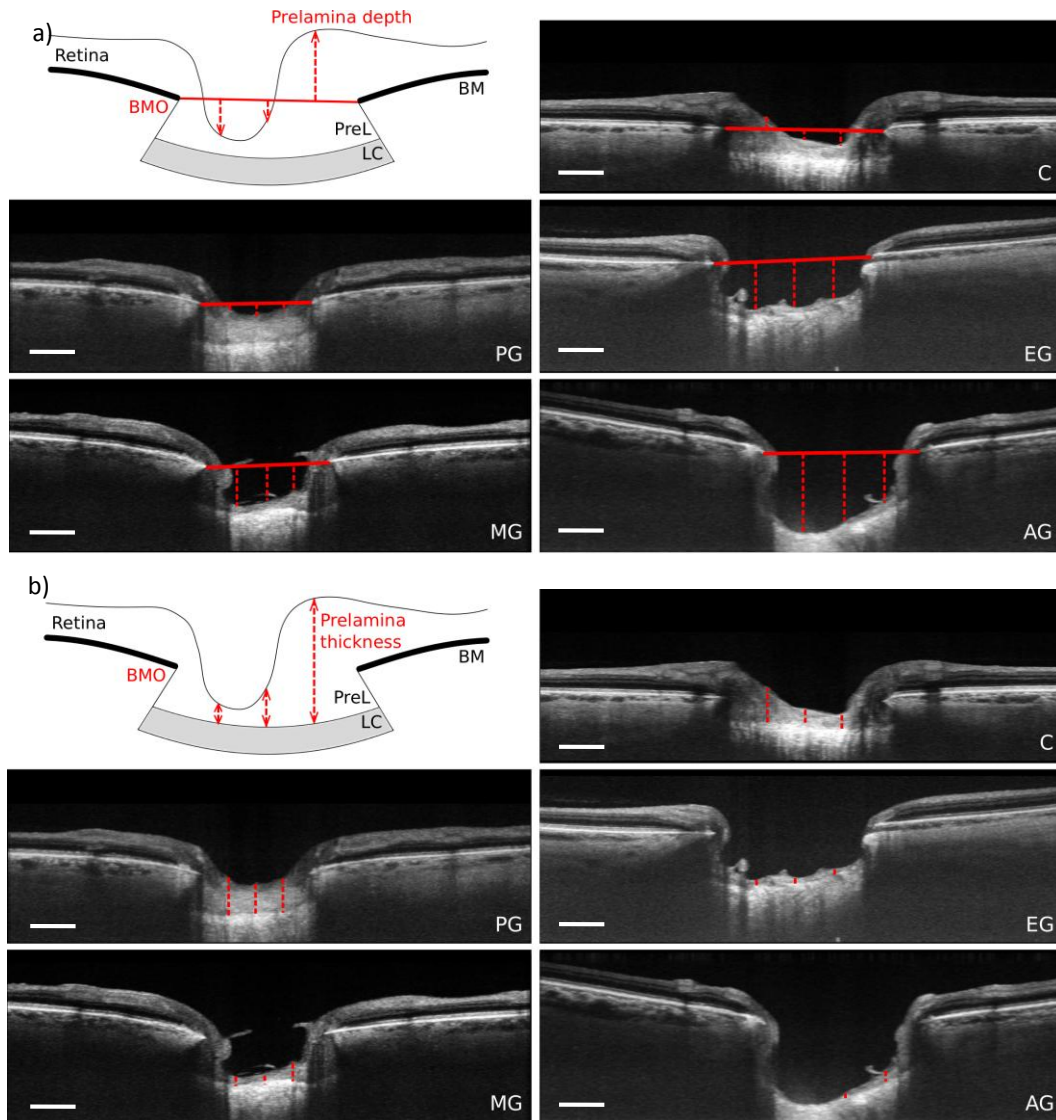


Figure 5.9: Diagram of measurements of (a) prelamina depth and (b) thickness on a schematic and OCT images from each stage of glaucoma, on a superior-inferior slice. Measurements are shown in red. BM = Bruch's Membrane, PreL = prelamina, LC = Lamina cribrosa, C = control. PG = preperimetric glaucoma, EG = early glaucoma, MG = moderate glaucoma, AG = advanced glaucoma. Scale bars = 500 μm .

5.3.3.1 Changes in prelamina parameters as a function of visual field progression

Prelamina depth increased (i.e. further posterior to BMO) as a function of deteriorating visual field in all regions ($p < 0.01$ Pearson's correlation, Figure 5.10a), while thinning of the prelamina was

associated with increasing visual field loss in all regions ($p < 0.05$ Spearman's rho), except for the nasal prelamina (Figure 5.10b).

5.3.3.2 Quantitative analysis of prelamina parameters as a function of glaucoma stage

The mean and standard deviation for regional prelamina values for each stage of glaucoma are shown below in Table 5.7.

Regional prelamna	Control mean \pm SD (μm)	Preperimetric Glaucoma mean \pm SD (μm)	Early Glaucoma mean \pm SD (μm)	Advanced Glaucoma mean \pm SD (μm)
T PreL depth	-60.71 \pm 192.26	124.63 \pm 192.52	133.93 \pm 177.04	253.03 \pm 175.39
ST PreL depth	-96.42 \pm 196.21	183.90 \pm 214.06	181.32 \pm 219.46	347.18 \pm 182.74
S PreL depth	-123.95 \pm 205.49	124.81 \pm 280.88	218.89 \pm 230.45	394.60 \pm 182.45
SN PreL depth	-157.40 \pm 182.77	24.34 \pm 293.35	115.01 \pm 254.76	244.00 \pm 241.79
N PreL depth	-168.01 \pm 225.36	-3.82 \pm 225.36	-25.43 \pm 264.96	170.36 \pm 259.63
IN PreL depth	-130.22 \pm 271.03	-1.47 \pm 256.75	82.26 \pm 287.44	175.57 \pm 255.85
I PreL depth	-125.69 \pm 194.60	63.85 \pm 276.41	133.62 \pm 224.13	321.54 \pm 120.11
IT PreL depth	-89.07 \pm 158.36	104.85 \pm 184.96	135.87 \pm 181.33	273.71 \pm 153.27
C PreL depth	65.48 \pm 173.52	226.52 \pm 106.95	244.95 \pm 191.66	345.09 \pm 126.80
T PreL thick	369.31 \pm 171.98	210.49 \pm 157.48	205.81 \pm 131.37	129.01 \pm 81.29
ST PreL thick	407.66 \pm 197.72	186.06 \pm 178.11	196.40 \pm 138.21	102.66 \pm 72.87
S PreL thick	447.28 \pm 186.30	201.65 \pm 120.48	170.75 \pm 116.25	112.46 \pm 131.04
SN PreL thick	479.31 \pm 183.63	349.01 \pm 248.84	259.31 \pm 182.39	193.03 \pm 122.38
N PreL thick	437.58 \pm 214.97	423.13 \pm 289.41	343.14 \pm 218.69	340.06 \pm 205.41
IN PreL thick	473.19 \pm 211.53	284.55 \pm 106.06	298.63 \pm 197.71	257.04 \pm 209.18
I PreL thick	440.59 \pm 174.69	290.31 \pm 212.30	245.77 \pm 144.80	140.04 \pm 73.43
IT PreL thick	408.96 \pm 152.51	240.51 \pm 140.23	222.12 \pm 131.00	144.21 \pm 74.19
C PreL thick	263.69 \pm 161.63	127.84 \pm 53.38	124.08 \pm 71.34	133.90 \pm 65.33

Table 5.7: Mean of each regional prelamina parameter for each stage of glaucoma. PreL depth = prelamina depth, PreL thick = prelamina thickness, SD = standard deviation. T = temporal, ST = superior-temporal, S = superior, SN = superior-nasal, N = nasal, IN = inferior-nasal, I = inferior, IT = inferior-temporal, C = central.

5.3.3.3 Multivariate analysis of prelamina parameters in glaucomatous eyes

Optimised linear mixed-effects models (LMMs) for prelamina depth and prelamina thickness for each ONH region are presented in Table 5.8 and Table 5.9 respectively. Prelamina depth was affected as a function of glaucoma stage in all regions except N and IN ($p < 0.001$). Stage of glaucoma also had a significant effect on prelamina thickness in all regions ($p < 0.001$) except N.

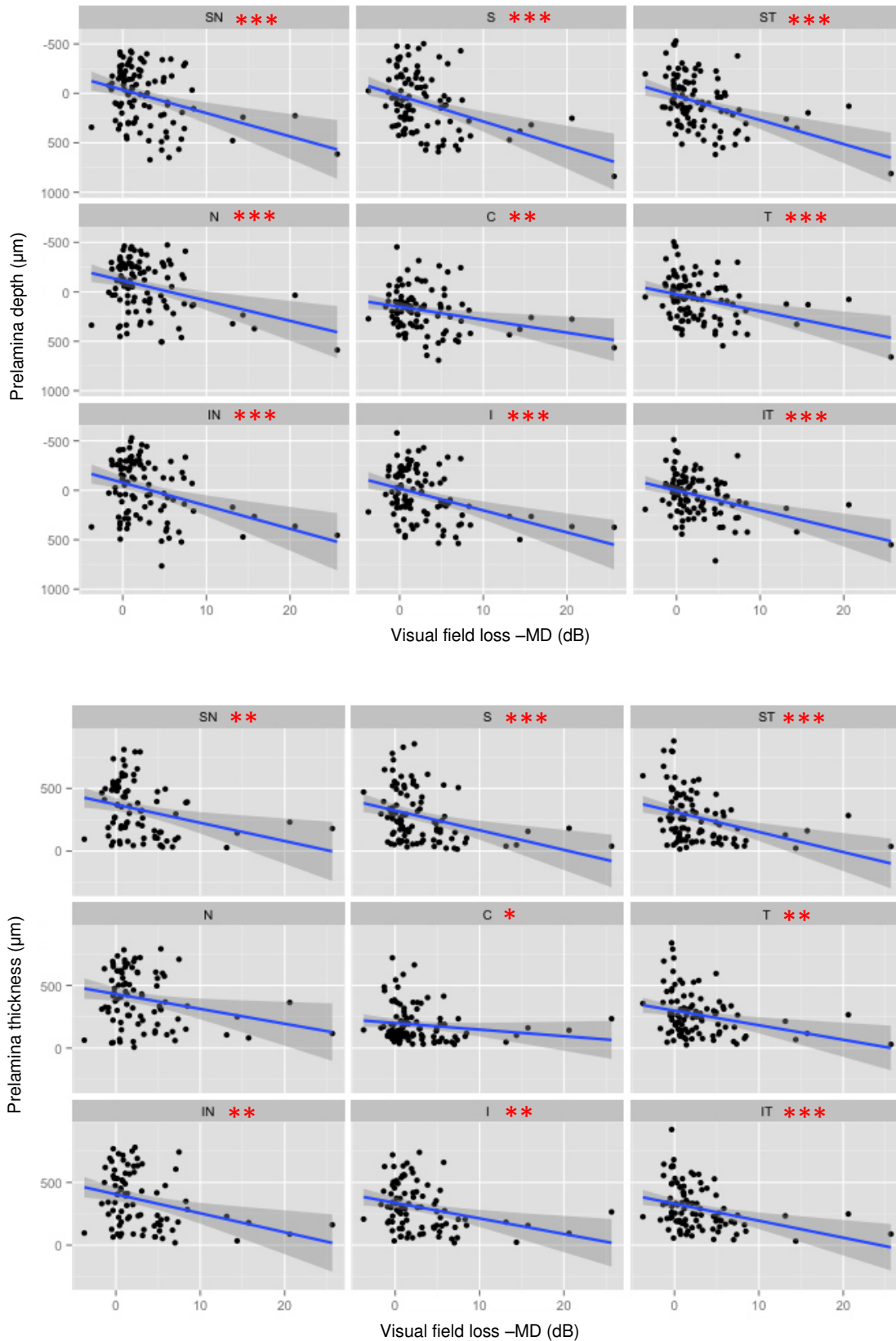


Figure 5.10: a) Prelamina (PreL) depth and b) PreL thickness as a function of visual field loss for each region. x-axis is reversed so greater visual field loss is further along the x-axis. T = temporal, ST = superior-temporal, S = superior, SN = superior-nasal, N = nasal, IN = inferior-nasal, I = inferior, IT = inferior-temporal, C = central. Grey bars = 95% confidence intervals. * = $p < 0.05$, ** = $p < 0.01$, *** = $p < 0.001$, Pearson's correlation.

Region	Dx	Age	AxL	MS	MD	ACD	CCT	Age:MD	AxL:MD	AxL:MS
T	PreL depth		45.07 ± 22.08	223.20±105.82			-1.42 ± 0.49			-7.70 ± 4.29
	<i>t value</i>		2.04	2.11			-2.90			-1.79
	<i>p value</i>	0.002	-	-			0.002			0.058
ST	PreL depth		104.38 ± 26.15	46.41 ± 12.34	-91.26 ± 53.77	-77.58 ± 33.47	-1.89 ± 0.51		3.57 ± 2.31	
	<i>t value</i>		3.99	3.76	-1.70	-2.32	-3.75		-1.55	
	<i>p value</i>	<0.001	-	<0.001	-	0.015	<0.001		0.100	
S	PreL depth		96.78 ± 26.63	32.58 ± 13.00	-55.32 ± 36.68	-63.08 ± 34.44	-1.72 ± 0.53		2.30 ± 1.56	
	<i>t value</i>		3.63	2.51	-1.51	-1.83	-3.24		1.47	
	<i>p value</i>	<0.001	-	0.010	-	0.082	0.002		0.119	
SN	PreL depth	-0.31 ± 2.93	48.95 ± 19.75		64.60 ± 44.34	-58.56 ± 39.34	-1.96 ± 0.59	-1.04 ± 0.65		
	<i>t value</i>	-0.11	2.48		1.46	-1.49	-3.34	-1.61		
	<i>p value</i>	0.002	0.009		-	0.101	<0.001	0.093		
N	PreL depth	2.67 ± 1.91	36.96 ± 17.91		-13.04 ± 5.49		-2.29 ± 0.56			
	<i>t value</i>	1.39	2.06		-2.37		-4.05			
	<i>p value</i>	0.145	0.034		0.018		<0.001			
IN	PreL depth	5.04 ± 2.40	47.05 ± 31.76	242.47±151.45	-10.80 ± 6.40		-1.51 ± 0.71			-9.17 ± 6.08
	<i>t value</i>	2.11	1.48	1.60	-1.69		-2.13			-1.51
	<i>p value</i>	0.003	-	-	0.075		0.026			0.112
I	PreL depth	-1.51 ± 2.65	83.14 ± 24.58	38.45 ± 12.87	-56.99 ± 40.53	-70.00 ± 34.74	-1.56 ± 0.53	-0.85 ± 0.60		
	<i>t value</i>	-0.57	3.38	2.99	-1.41	-2.02	-2.92	-1.41		
	<i>p value</i>	<0.001	<0.001	0.002	-	0.029	0.002	0.118		
IT	PreL depth		61.86 ± 22.23	34.78 ± 11.18		-64.88 ± 29.96	-1.20 ± 0.45			
	<i>t value</i>		2.78	3.11		-2.17	-2.64			
	<i>p value</i>	<0.001	0.004	0.001		0.024	0.006			
C	PreL depth	-3.51 ± 1.94	31.49 ± 21.16	159.15± 95.75	8.58 ± 4.82		-1.54 ± 0.45			5.51 ± 3.91
	<i>t value</i>	-1.81	1.49	1.66	1.78		-3.41			-1.41
	<i>p value</i>	<0.001	0.054	-	-	0.065	<0.001			0.123

Table 5.8: Linear mixed-effects model (LMM) for prelamina depth (PreL depth) for each optic nerve head region. Values are effect size ± standard error, i.e. how much the prelamina depth changes in μm per one-unit change in the independent variable, as well as t-value and p-value. Red text indicates factor is significant at $p < 0.05$. T = temporal, ST = superior-temporal, S = superior, SN = superior-nasal, N = nasal, IN = inferior-nasal, I = inferior, IT = inferior-temporal, C = central; AxL = axial length, MS = mean spherical refractive error, MD = mean deviation on visual fields, ACD = anterior chamber depth, CCT = central corneal thickness.

Region	Dx	Age	AxL	MS	MD	ACD	CCT	Age:MD	AxL:MD	AxL:MS
T	PreL thick		-55.23 ± 17.18	-140.73 ± 81.75		37.98 ± 25.08	1.21 ± 0.37			4.47 ± 3.32
	<i>t value</i>		-3.22	-1.72		1.51	3.31			1.35
	<i>p value</i>	<0.001	-	-		0.101	<0.001			0.147
ST	PreL thick		-70.11 ± 20.11	-30.58 ± 10.36		38.97 ± 28.20	1.28 ± 0.43			
	<i>t value</i>		-3.49	-2.95		1.38	3.00			
	<i>p value</i>	<0.001	<0.001	0.002		0.137	0.002			
S	PreL thick						1.14 ± 0.44			
	<i>t value</i>						2.58			
	<i>p value</i>	<0.001					0.010			
SN	PreL thick	-0.93 ± 2.22	-44.81 ± 13.33		-77.59 ± 41.71		1.41 ± 0.44	1.14 ± 0.59		
	<i>t value</i>	-0.42	-3.36		-1.86		3.24	1.92		
	<i>p value</i>	0.006	<0.001		-		0.001	0.044		
N	PreL thick		54.43 ± 27.96	27.54 ± 16.22	8.60 ± 5.01					
	<i>t value</i>		1.95	1.70	1.72					
	<i>p value</i>		0.047	0.082	0.092					
IN	PreL thick	4.26 ± 2.87	-25.89 ± 15.97		-121.73 ± 48.84			1.95 ± 0.70		
	<i>t value</i>	0.49	-1.62		-2.49			1.79		
	<i>p value</i>	0.010	0.088		-			0.004		
I	PreL thick		-53.01 ± 19.21	-19.63 ± 10.17			1.21 ± 0.45			
	<i>t value</i>		-2.76	-1.93			2.69			
	<i>p value</i>	<0.001	0.005	0.042			0.006			
IT	PreL thick		-72.03 ± 16.55	-32.21 ± 8.38		50.27 ± 22.46	0.78 ± 0.34			
	<i>t value</i>		-4.35	-3.84		2.24	2.28			
	<i>p value</i>	<0.001	<0.001	<0.001		0.019	0.017			
C	PreL thick				-7.95 ± 3.54		0.98 ± 0.31			
	<i>t value</i>				-2.24		3.18			
	<i>p value</i>	<0.001			0.022		0.002			

Table 5.9: Linear mixed-effects model (LMM) for prelamina thickness (PreL thick), containing effect size ± standard error, i.e. how much the prelamina thickness changes in μm per one-unit change in the independent variable, as well as t-value and p-value. Red text indicates factor is significant at $p < 0.05$. T = temporal, ST = superior-temporal, S = superior, SN = superior-nasal, N = nasal, IN = inferior-nasal, I = inferior, IT = inferior-temporal, C = central, AxL = axial length, MS = mean spherical refractive error, MD = mean deviation on visual fields, ACD = anterior chamber depth, CCT = central corneal thickness.

In the inferior-nasal region *age* had a significant positive effect ($5.04 \pm 2.40 \mu\text{m}/\text{year}$, $p=0.003$) on prelamina depth, i.e. older eyes had a prelamina surface that was deeper from BMO in the IN region. *Axial length* also made a significant positive contribution to prelamina depth in the SN ($p=0.009$), N ($p=0.034$), I ($p<0.001$), and IT ($p=0.004$) regions (Table 5.8). Additionally, *axial length* had a significant negative effect (of up to $-72.03 \pm 16.55 \mu\text{m}/\text{mm}$) on prelamina thickness in the ST, SN, IT (all $p<0.001$) and I regions ($p=0.005$), i.e. eyes with longer *axial length* had thinner prelamina in those regions (Table 5.9).

Mean spherical refractive error had a significant positive effect of between 32 and 46 $\mu\text{m}/\text{D}$ on the depth of the prelamina in the ST ($p<0.001$), S ($p=0.010$), I ($p=0.002$), and IT ($p=0.001$) regions (Table 5.8). In addition, *mean spherical refractive error* also had a significant negative effect of around -30 $\mu\text{m}/\text{D}$ on the ST, I and IT prelamina thickness ($p<0.05$), i.e. when all the other ocular factors were accounted for, hyperopic eyes had deeper prelamina surface and thinner prelamina in those regions.

In the ST, I and IT regions, *anterior chamber depth (ACD)* made a significant negative contribution to prelamina depth of up to -78 $\mu\text{m}/\text{mm ACD}$ (ST $p=0.015$; I $p=0.029$; IT $p=0.024$; Table 5.8), suggesting that eyes with deeper anterior chambers had a prelamina surface that was closer to BMO. Conversely, *ACD* had a significant positive effect on the IT prelamina thickness ($50.27 \pm 22.46 \mu\text{m}/\text{mm ACD}$, $p=0.019$), i.e. eyes with deeper anterior chambers had thicker prelamina in this region.

Central corneal thickness made a significant negative contribution to prelamina depth of between -1.20 and -2.29 $\mu\text{m}/\mu\text{m CCT}$ in all regions ($p<0.01$) of the ONH. This indicates that eyes with thicker corneas had a prelamina surface that was more shallow, or closer to BMO, and eyes with thinner corneas had prelamina surface that was more posterior to BMO. *CCT* also had a significant positive effect of up to 1.41 $\mu\text{m}/\mu\text{m CCT}$ on the thickness of the prelamina in all regions ($p<0.01$) except N and IN (Table 5.9), indicating that eyes with thicker corneas had thicker prelamina in these regions.

Finally, the association between *age:MD* had a positive contribution to explaining the thickness of the SN and IN prelamina ($p < 0.05$).

5.3.3.4 The effect of stage of glaucoma on prelamina depth

Stage of glaucoma was a significant factor in determination of all regions of prelamina depth except for the IN region ($p < 0.01$; Figure 5.11).

Temporal: Post-hoc pairwise comparisons revealed that prelamina depth in the T region in eyes with early glaucoma ($133.93 \pm 177.04 \mu\text{m}$) and advanced glaucoma ($253.03 \pm 175.39 \mu\text{m}$) was significantly greater than control eyes ($-60.71 \pm 192.26 \mu\text{m}$; $C < EG$ $p = 0.010$; $C < AG$ $p = 0.005$). The control group also had significantly thicker T prelamina ($369.31 \pm 171.98 \mu\text{m}$) than eyes with early or advanced glaucoma ($C > EG$ $p = 0.001$; $C > AG$ $p = 0.002$), and the same pattern was revealed in the inferior ($C > EG$, $C > AG$; $p < 0.001$) and central ($C > EG$, $C > AG$; $p < 0.001$) regions. In addition, the control group had thinner prelamina than all stages of glaucoma in the IT ($p < 0.001$), S ($p < 0.01$) and ST regions ($p < 0.001$).

Superior: Control eyes ($-123.95 \pm 205.49 \mu\text{m}$) had a superior prelamina depth that was significantly shallower when compared to all glaucoma groups, with the depth increasing with disease severity ($C < PG$ $p = 0.009$; $C < EG$ $p < 0.001$; $C < AG$ $p = 0.001$; Table 5.8). The ST region the prelamina depth was greater in both preperimetric ($183.90 \pm 214.06 \mu\text{m}$) and early glaucoma ($181.32 \pm 219.46 \mu\text{m}$) groups than in the control group ($-96.42 \pm 196.21 \mu\text{m}$; $C < PG$ $p = 0.001$; $C < EG$ $p < 0.001$).

In the SN region, the prelamina depth was less for control eyes ($-157.40 \pm 182.77 \mu\text{m}$) than for eyes with early glaucoma ($115.01 \pm 254.76 \mu\text{m}$; $C < EG$ $p < 0.005$).

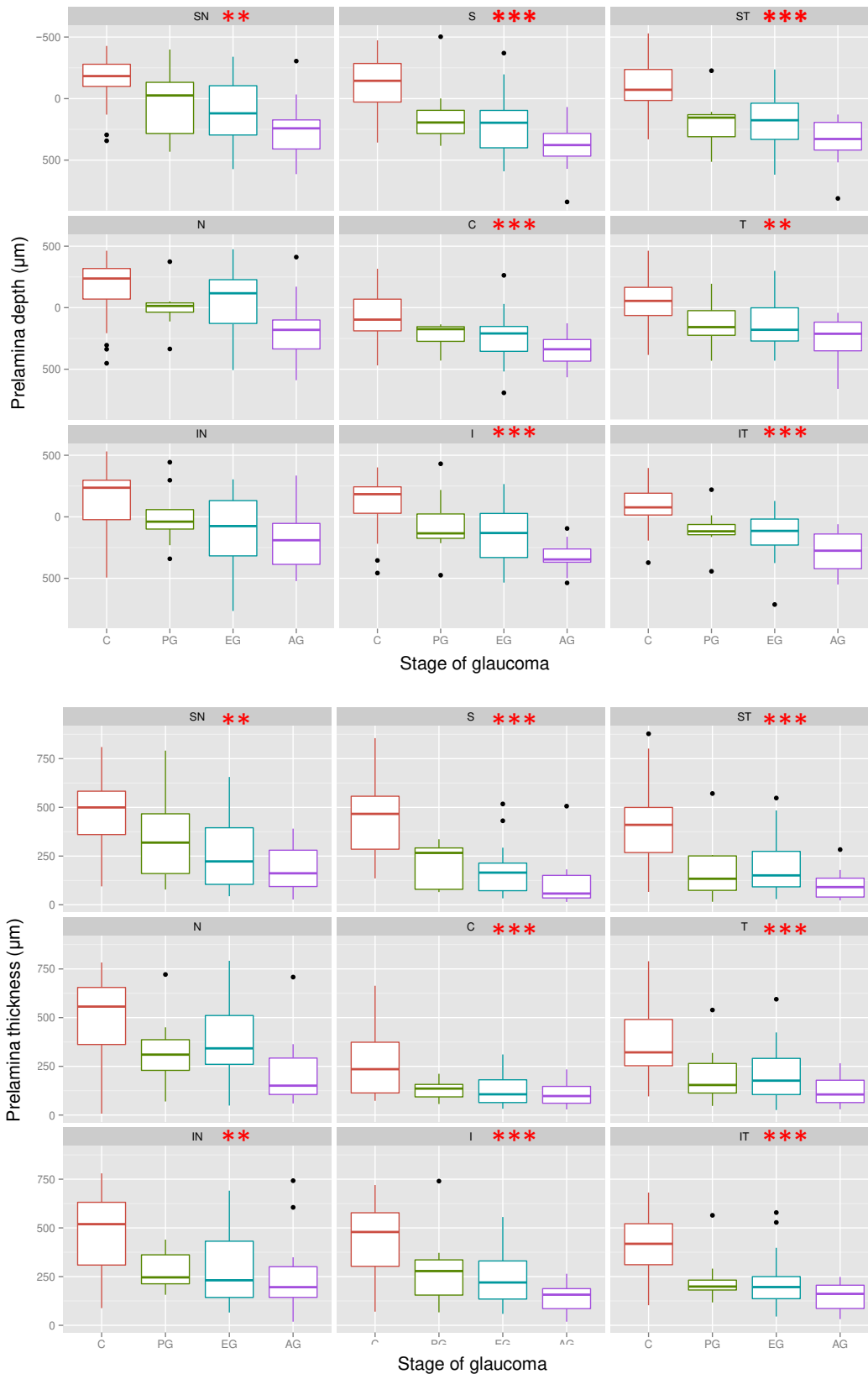


Figure 5.11: Mean prelaminar depth and thickness for each glaucoma (G) stage. C = control, PG = preperimetric G, EG = early G, AG = advanced G. T = temporal, ST = superior-temporal, S = superior, SN = superior-nasal, N = nasal, IN = inferior-nasal, I = inferior, IT = inferior-temporal. Boxplots denote median and 1st to 3rd quartiles, whiskers extend to the highest or lowest data value that is within a 1.5 x interquartile range. Black spots denote outliers. Red stars: significance as a function of glaucoma stage * = p<0.05, ** = p<0.01, *** = p<0.001.

There were no significant differences between control eyes or any of the glaucoma groups for nasal prelamina depth or thickness ($p>0.01$; Table 5.8). There were also no differences in IN prelamina depth or thickness with increasing glaucoma stages. The control group also had inferior prelamina depth that was significantly less, or closer to BMO, than eyes with early glaucoma ($p<0.001$). Additionally, in the IT region control eyes had prelamina depth that was significantly less than in all stages of glaucoma ($C<PG$ $p=0.003$; $C<EG$ $p<0.001$; $C<AG$ $p<0.001$).

Control eyes had central prelamina depth ($65.48 \pm 173.52 \mu\text{m}$) that was significantly shallower than early and advanced glaucoma ($C<EG$ $p<0.001$; $C<AG$ $p=0.001$). A summary of differences in prelamina depth and thickness between control and different stages of glaucoma are summarised Figure 5.12.

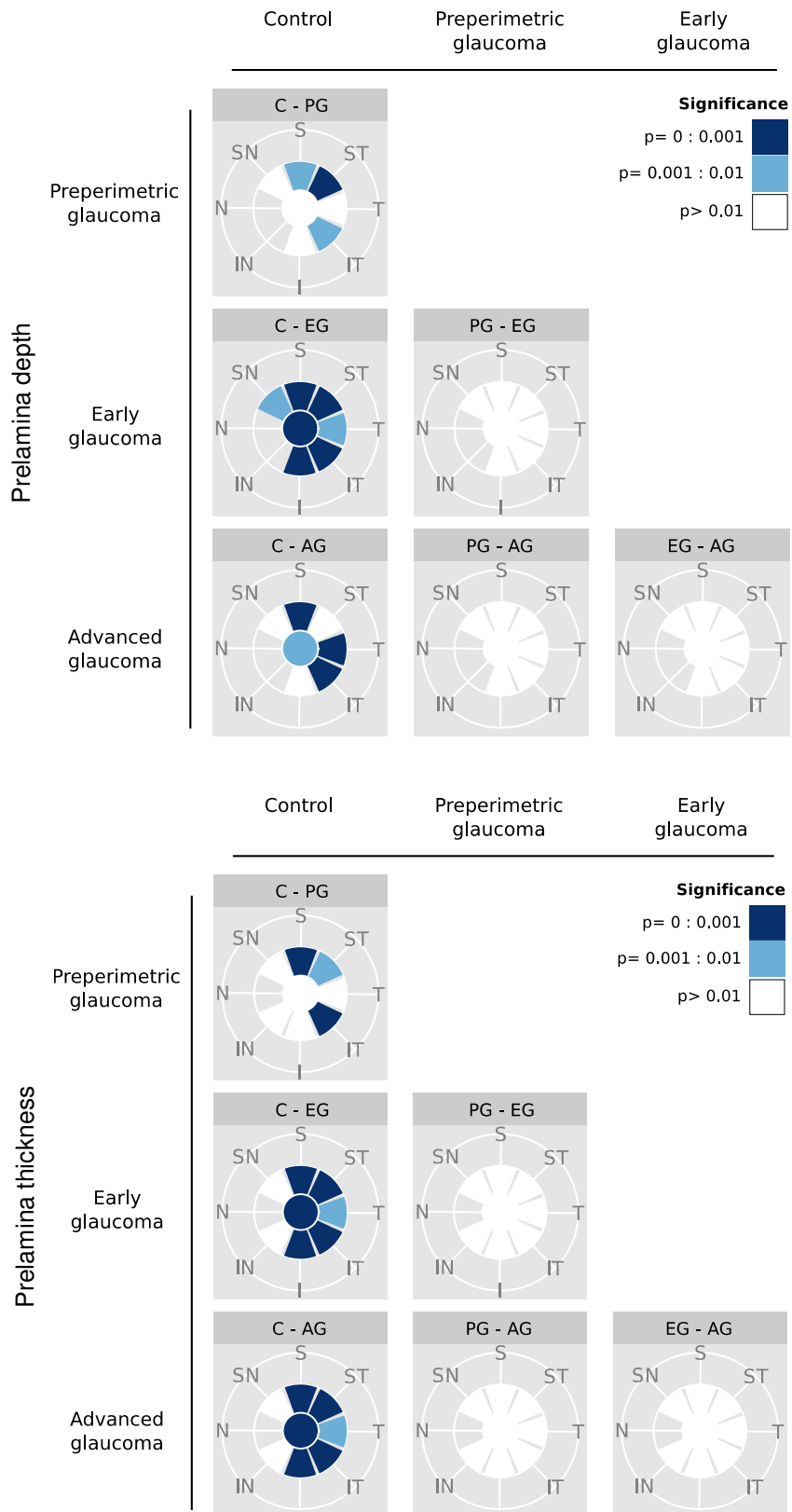


Figure 5.12: Regions of the optic nerve head where prelaminar depth was affected by stage of glaucoma, using linear mixed-effects models and subsequent pairwise comparisons. C = control, PG = preperimetric glaucoma, EG = early glaucoma, AG = advanced glaucoma. T = temporal, ST = superior-temporal, S = superior, SN = superior-nasal, N = nasal, IN = inferior-nasal, I = inferior, IT = inferior-temporal. Blue indicates significant differences, white indicates that glaucomatous progression was a factor in the model but there were no significant differences, grey indicates regions where stage of glaucoma was not a factor in the model

5.3.4 The effect of glaucoma and other ocular parameters on the lamina cribrosa

The depth of the anterior and posterior LC surface was measured in each region of the ONH, and the LC thickness calculated, as shown below in Figure 5.13 and Figure 5.14.

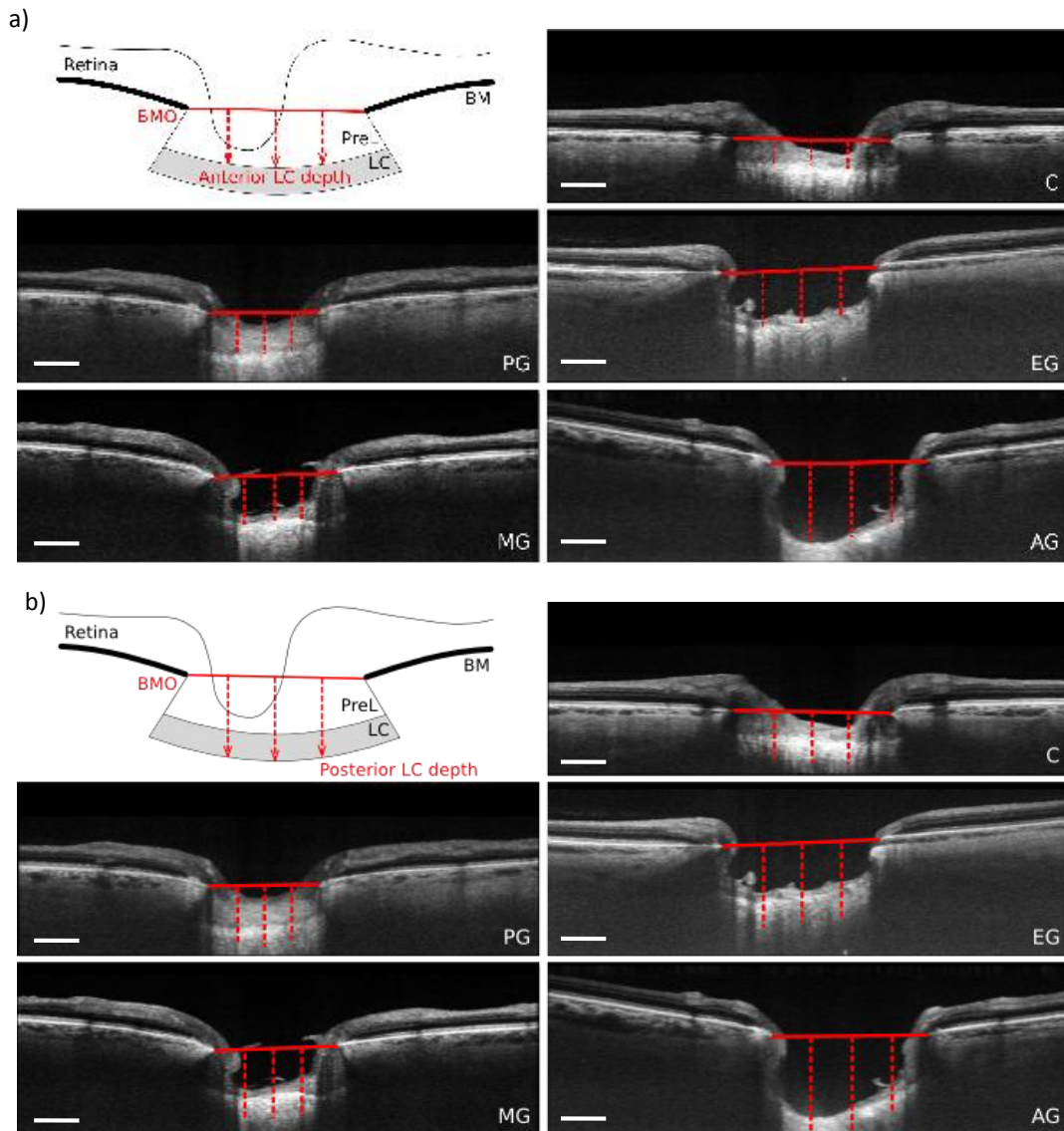


Figure 5.13: Diagram of measurements of (a) anterior and (b) posterior lamina cribrosa (LC) depth on a schematic and OCT images from each stage of glaucoma, on a superior-inferior slice. Measurements are shown in red. BM = Bruch's Membrane, PreL = prelamina, C = control. PG = preperimetric glaucoma, EG = early glaucoma, MG = moderate glaucoma, AG = advanced glaucoma.

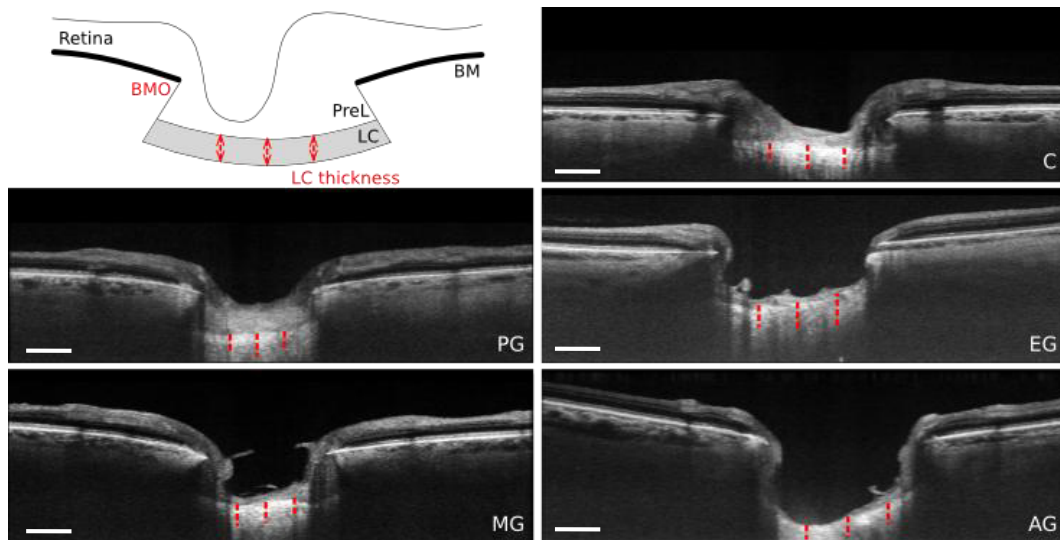


Figure 5.14: Diagram of measurements of lamina cribrosa (LC) thickness on a schematic and OCT images from each stage of glaucoma, on a superior-inferior slice. Measurements are shown in red. BM = Bruch's Membrane, PreL = prelamina, C = control. PG = preperimetric glaucoma, EG = early glaucoma, MG = moderate glaucoma, AG = advanced glaucoma.

5.3.4.1 Changes in lamina cribrosa parameters as a function of visual field progression

A significant increase in anterior lamina cribrosa (LC) depth was associated with increasing visual field loss in all regions of the ONH ($p < 0.01$ Pearson's correlation) meaning that the anterior surface of the LC was more posteriorly positioned from BMO, i.e. deeper within the optic nerve head, in eyes with greater visual field deficit. The results from the univariate analysis are displayed in Figure 5.15.

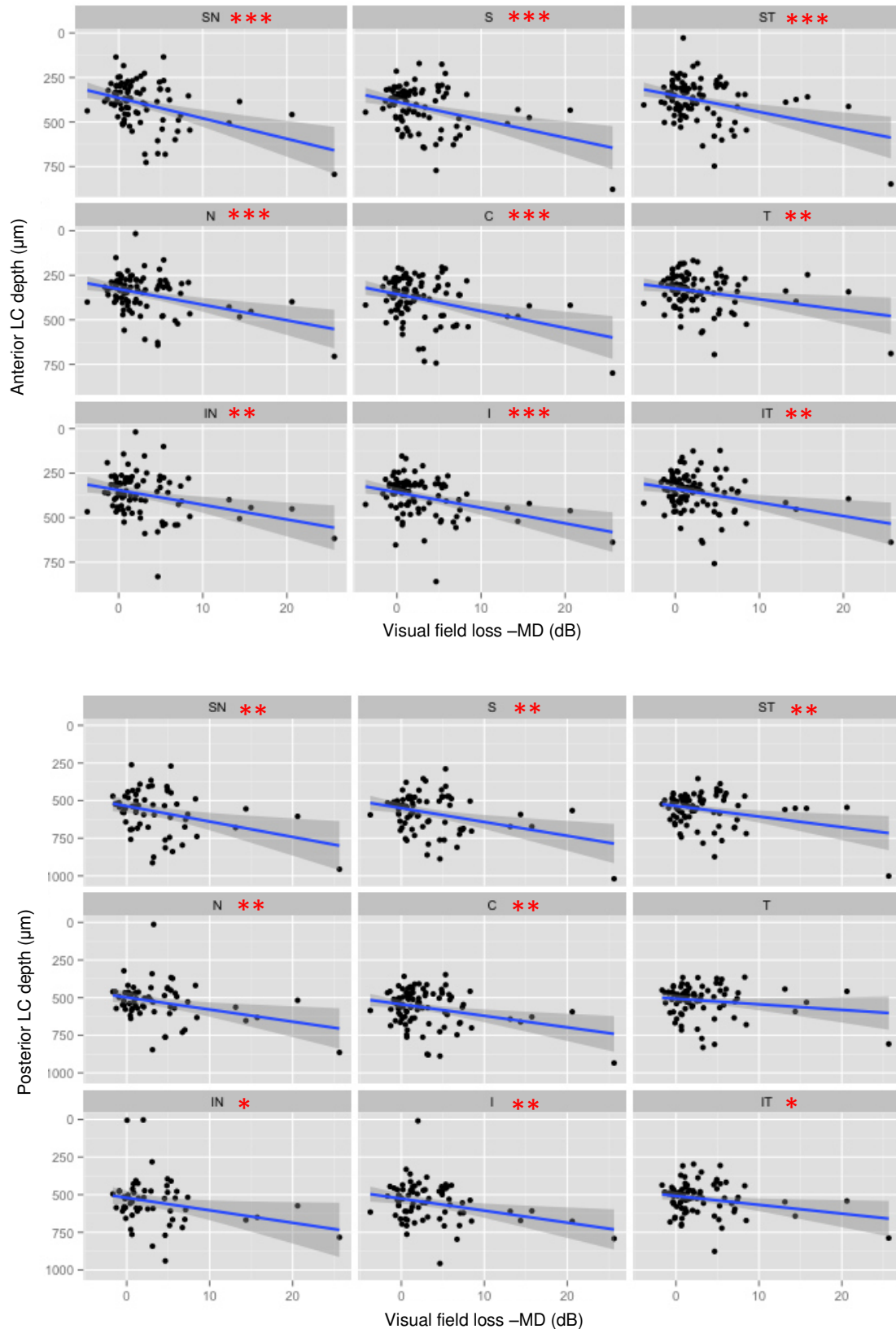


Figure 5.15: Anterior and posterior lamina cribrosa (LC) depth as a function of visual field loss for each region. x-axis is reversed so greater visual field loss is further along the x-axis. T = temporal, ST = superior-temporal, S = superior, SN = superior-nasal, N = nasal, IN = inferior-nasal, I = inferior, IT = inferior-temporal, C = central. Grey bars = 95% confidence intervals. * = $p < 0.05$, ** = $p < 0.01$, *** = $p < 0.001$, Pearson's correlation.

Thinning of the LC was significantly associated with increasing visual field loss in the temporal, inferior-temporal and central regions, using univariate analysis ($p < 0.05$ Pearson's correlation; Figure 5.16).

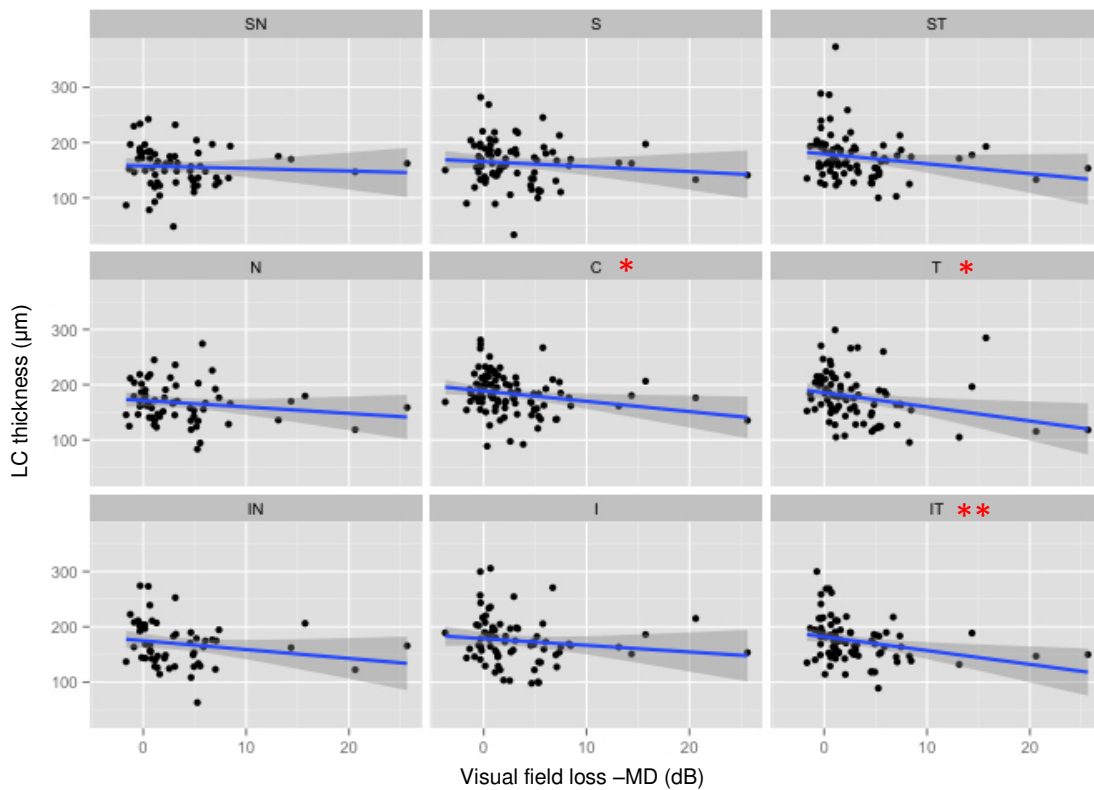


Figure 5.16: Lamina cribrosa (LC) thickness as a function of visual field loss for each region. x-axis is reversed so greater visual field loss is further along the x-axis. T = temporal, ST = superior-temporal, S = superior, SN = superior-nasal, N = nasal, IN = inferior-nasal, I = inferior, IT = inferior-temporal, grey bars = 95% confidence intervals. * = $p < 0.05$, ** = $p < 0.01$, *** = $p < 0.001$, Pearson's correlation. (b) Regional Pearson's correlation (r) for associations between LC and visual field loss.

5.3.4.2 Quantitative analysis of lamina cribrosa for stages of glaucomatous progression

The mean and standard deviation for regional LC values for each stage of glaucoma is shown below in Table 5.10.

Region	Control mean \pm SD (μm)	Preperimetric Glaucoma mean \pm SD (μm)	Early Glaucoma mean \pm SD (μm)	Advance Glaucoma mean \pm SD (μm)
T Ant LC	312.17 \pm 75.70	335.12 \pm 101.72	351.57 \pm 103.82	382.04 \pm 122.54
ST Ant LC	329.77 \pm 95.24	369.96 \pm 86.88	393.36 \pm 112.56	449.84 \pm 146.15
S Ant LC	497.58 \pm 69.56	507.19 \pm 80.47	510.26 \pm 102.16	507.06 \pm 138.34
SN Ant LC	337.96 \pm 66.74	418.15 \pm 68.87	404.08 \pm 125.32	491.89 \pm 119.96
N Ant LC	321.75 \pm 69.30	334.02 \pm 53.09	359.87 \pm 133.63	429.23 \pm 114.38
IN Ant LC	341.61 \pm 76.37	346.22 \pm 125.69	370.97 \pm 161.71	432.61 \pm 95.40
I Ant LC	335.95 \pm 88.36	354.16 \pm 115.04	411.10 \pm 121.65	461.58 \pm 91.24
IT Ant LC	331.85 \pm 77.14	345.36 \pm 104.36	358.00 \pm 117.38	417.92 \pm 107.36
C Ant LC	337.53 \pm 80.80	354.36 \pm 98.57	388.57 \pm 132.12	458.99 \pm 132.92
T Post LC	497.58 \pm 69.56	507.19 \pm 80.47	510.26 \pm 102.16	537.98 \pm 117.42
ST Post LC	517.68 \pm 65.01	544.29 \pm 87.34	556.79 \pm 113.60	614.13 \pm 141.15
S Post LC	538.14 \pm 77.33	530.94 \pm 93.66	578.00 \pm 141.17	667.56 \pm 130.64
SN Post LC	498.19 \pm 56.87	554.14 \pm 126.79	555.34 \pm 147.41	643.82 \pm 126.35
N Post LC	505.20 \pm 63.17	499.55 \pm 64.42	537.28 \pm 104.80	601.71 \pm 120.40
IN Post LC	515.64 \pm 77.69	559.59 \pm 110.42	565.77 \pm 142.80	616.72 \pm 90.03
I Post LC	519.03 \pm 89.33	530.11 \pm 115.28	567.68 \pm 123.37	625.80 \pm 80.53
IT Post LC	515.61 \pm 83.00	499.29 \pm 96.58	524.13 \pm 114.63	574.43 \pm 99.98
C Post LC	536.90 \pm 80.09	544.51 \pm 99.52	557.39 \pm 128.27	630.17 \pm 116.32
T LC thick	196.84 \pm 40.86	172.07 \pm 41.09	161.15 \pm 36.12	155.95 \pm 49.36
ST LC thick	189.95 \pm 56.64	174.34 \pm 43.89	163.42 \pm 35.36	164.29 \pm 29.70
S LC thick	182.06 \pm 34.03	127.84 \pm 62.24	150.46 \pm 39.39	160.49 \pm 27.66
SN LC thick	174.83 \pm 32.07	131.70 \pm 54.33	147.21 \pm 35.55	151.92 \pm 21.46
N LC thick	172.87 \pm 47.69	189.05 \pm 20.61	166.47 \pm 32.43	146.70 \pm 8.25
IN LC thick	176.01 \pm 37.56	179.45 \pm 39.61	155.39 \pm 46.57	165.41 \pm 28.13
I LC thick	197.44 \pm 54.67	175.95 \pm 35.16	156.58 \pm 37.37	164.22 \pm 20.70
IT LC thick	192.73 \pm 33.66	153.94 \pm 15.93	168.70 \pm 41.00	156.51 \pm 20.44
C LC thick	203.13 \pm 39.42	190.14 \pm 33.72	168.82 \pm 30.36	171.18 \pm 23.92

Table 5.10: Mean of each lamina cribrosa (LC) parameter for each stage of glaucoma. Ant LC = anterior LC depth, Post LC = posterior LC depth, LC thick = LC thickness, SD = standard deviation. T = temporal, ST = superior-temporal, S = superior, SN = superior-nasal, N = nasal, IN = inferior-nasal, I = inferior, IT = inferior-temporal, C = central.

5.3.4.3 Multivariate analysis of lamina cribrosa parameters in glaucomatous eyes

The optimised LMMs for the anterior LC depth (Table 5.11), posterior LC depth (Table 5.12) and LC thickness (Table 5.13) for each ONH region are described below.

Stage of glaucoma made a significant contribution to explaining the variance in anterior LC depth in the I ($p=0.036$) and central ($p=0.039$) regions, while also having a significant effect on the posterior LC depth in the SN ($p=0.004$), IN ($p=0.021$) and IT ($p=0.025$) regions. Similarly, LC thickness was significantly affected by *stage of glaucoma* in the T ($p=0.007$), IN ($p=0.017$) and central ($p=0.001$) regions.

Region	Dx	Age	AxL	MS	MD	ACD	CCT	Age:MD	AxL:MD	AxL:MS
T Ant LC			10.65 ± 13.54	10.75 ± 6.60	-36.28 ± 20.27		-0.56 ± 0.27		1.57 ± 0.85	
<i>t value</i>			0.79	1.63	-1.79		-2.07		1.84	
<i>p value</i>			-	0.095	-		0.037		0.060	
ST Ant LC			7.07 ± 15.48	117.99 ± 62.93	-38.50 ± 24.16		-0.69 ± 0.31		1.53 ± 1.02	-4.39 ± 2.57
<i>t value</i>			0.50	1.88	-1.59		-2.22		1.50	-1.71
<i>p value</i>			-	-	-		0.022		0.123	0.076
S Ant LC			0.27 ± 17.34	125.66 ± 67.45	-3.42 ± 1.93		-0.91 ± 0.34			-4.75 ± 2.74
<i>t value</i>			0.02	1.86	-1.78		-2.68			-1.73
<i>p value</i>			-	-	0.065		0.006			0.071
SN Ant LC			2.01 ± 14.00	150.85 ± 59.62	-4.37 ± 1.84		-0.79 ± 0.29			-5.80 ± 2.43
<i>t value</i>			0.14	2.53	-2.38		-2.74			-2.39
<i>p value</i>			-	-	0.015		0.005			0.014
N Ant LC			19.47 ± 13.14	12.96 ± 7.14	-4.83 ± 2.23	-24.60 ± 18.01	-0.55 ± 0.29			
<i>t value</i>			1.48	1.82	-2.17	-1.37	-1.89			
<i>p value</i>			0.123	0.059	0.029	0.156	0.050			
IN Ant LC			31.83 ± 16.92	19.62 ± 9.02		-34.65 ± 22.32	-0.54 ± 0.36			
<i>t value</i>			1.88	2.18		-1.55	-1.51			
<i>p value</i>			0.053	0.028		0.106	0.115			
I Ant LC										
<i>t value</i>										
<i>p value</i>	0.036									
IT Ant LC			-25.60 ± 12.92	90.30 ± 54.64			-0.43 ± 0.27			-3.64 ± 2.25
<i>t value</i>			-1.98	1.65			-1.62			-1.62
<i>p value</i>			-	-			0.097			0.096
C Ant LC						-25.80 ± 18.06	-0.67 ± 0.30			
<i>t value</i>						-1.43	-2.23			
<i>p value</i>	0.039					0.142	0.024			

Table 5.11: Linear mixed-effects models for anterior LC (Ant LC) depth containing effect size ± standard error, i.e. how much Ant LC changes in μm per one-unit change in the independent variable, as well as t-value and p-values. Red text indicates factor is significant at $p < 0.05$. T = temporal, ST = superior-temporal, S = superior, SN = superior-nasal, N = nasal, IN = inferior-nasal, I = inferior, IT = inferior-temporal, Dx = stage of glaucoma, AxL = axial length, MS = mean spherical refractive error, MD = mean deviation on visual fields, ACD = anterior chamber depth, CCT = central corneal thickness.

Region	Dx	Age	AxL	MS	MD	ACD	CCT	Age:MD	AxL:MD	AxL:MS
T Post LC				8.01 ± 4.46			-0.65 ± 0.25			
<i>t value</i>				1.80			-2.62			
<i>p value</i>				0.069			0.009			
ST Post LC		-1.99 ± 1.20	38.30 ± 14.05	17.27 ± 6.85	-70.11 ± 20.12	-24.33 ± 17.50	-0.79 ± 0.28		2.91 ± 0.86	
<i>t value</i>		-1.65	2.73	2.52	-3.49	-1.39	-2.78		3.39	
<i>p value</i>	0.106	0.077	-	0.008	-	0.132	0.003		<0.001	
S Post LC			40.26 ± 20.62	17.02 ± 8.66	-39.51 ± 25.00	-58.79 ± 24.54	-0.98 ± 0.37		1.53 ± 1.05	
<i>t value</i>			1.95	1.96	-1.58	-2.40	-2.64		1.44	
<i>p value</i>			-	0.041	-	0.013	0.007		0.138	
SN Post LC		-3.71 ± 1.66	23.99 ± 19.98	210.81±104.47			-1.17 ± 0.41			-7.78 ± 4.06
<i>t value</i>		-2.24	1.20	2.02			-2.86			-1.92
<i>p value</i>	0.004	0.018	-	-			0.003			0.038
N Post LC					-5.46 ± 2.11		-0.66 ± 0.29			
<i>t value</i>					-2.58		-2.25			
<i>p value</i>					0.011		0.024			
IN Post LC						-37.01 ± 21.33	-1.25 ± 0.42			
<i>t value</i>						-1.74	-2.96			
<i>p value</i>	0.021					0.087	0.003			
I Post LC			2.74 ± 15.15	141.63 ± 66.58			-0.73 ± 0.36			-5.22 ± 2.70
<i>t value</i>			0.18	2.13			-2.06			-1.93
<i>p value</i>			-	-			0.034			0.051
IT Post LC		-2.71 ± 1.24		12.81 ± 4.76			-0.64 ± 0.27			
<i>t value</i>		-2.19		2.69			-2.42			
<i>p value</i>	0.025	0.025		0.006			0.015			
C Post LC			8.17 ± 14.20	128.55 ± 61.12			-0.78 ± 0.31			-4.73 ± 2.50
<i>t value</i>			0.58	2.10			-2.52			-1.89
<i>p value</i>			-	-			0.011			0.051

Table 5.12: Linear mixed-effects models for posterior LC (Post LC) depth containing effect size ± standard error, i.e. how much Post LC changes in μm per one-unit change in the independent variable, as well as *t*-value and *p*-values. Red text indicates factor is significant at $p < 0.05$. T = temporal, ST = superior-temporal, S = superior, SN = superior-nasal, N = nasal, IN = inferior-nasal, I = inferior, IT = inferior-temporal, Dx = stage of glaucoma, AxL = axial length, MS = mean spherical refractive error, MD = mean deviation on visual fields, ACD = anterior chamber depth, CCT = central corneal thickness.

C		Dx	Age	AxL	MS	MD	ACD	CCT	Age:MD	AxL:MD	AxL:MS
T	LC thick			-0.60 ± 3.85		44.18 ± 12.82	-15.33 ± 6.79	-0.19 ± 0.11		-1.90 ± 0.55	
	<i>t value</i>			-0.16		3.45	-2.26	-1.80		-3.44	
	<i>p value</i>	0.007		-		-	0.018	0.057		<0.001	
ST	LC thick		-0.94 ± 0.38	11.28 ± 4.76	-30.09 ± 23.77						1.35 ± 0.95
	<i>t value</i>		-2.45	2.37	-1.27						1.42
	<i>p value</i>		0.013	-	-						0.139
S	LC thick		-1.13 ± 0.34	25.71 ± 7.21	-41.44 ± 21.23	-17.08 ± 12.69	-18.83 ± 8.63			0.74 ± 0.54	2.01 ± 0.87
	<i>t value</i>		-3.29	3.56	-1.94	-1.35	-1.95			1.37	2.32
	<i>p value</i>		<0.001	-	-	-	0.041			0.147	0.016
SN	LC thick		-0.89 ± 0.34	17.14 ± 5.49	5.34 ± 2.80						
	<i>t value</i>		-2.62	3.12	1.90						
	<i>p value</i>		0.008	0.002	0.054						
N	LC thick					1.90 ± 1.06					
	<i>t value</i>					1.79					
	<i>p value</i>					0.073					
IN	LC thick		-0.80 ± 0.55	25.90 ± 7.51	-88.39 ± 36.88	-27.26 ± 9.15	-19.31 ± 9.86			1.23 ± 0.39	3.68 ± 1.44
	<i>t value</i>		-1.47	3.45	-2.40	-2.98	-1.96			3.16	2.56
	<i>p value</i>	0.017	0.103	-	-	-	0.031			0.003	0.005
I	LC thick		-1.58 ± 0.48					-0.23 ± 0.13			
	<i>t value</i>		-3.26					-1.70			
	<i>p value</i>		0.001					0.088			
IT	LC thick		-1.33 ± 0.39	10.82 ± 4.20	6.84 ± 2.14	19.16 ± 8.30			-0.25 ± 0.12		
	<i>t value</i>		-3.43	2.58	3.19	2.31			-2.16		
	<i>p value</i>		-	0.009	0.001	-			0.030		
C	LC thick										
	<i>t value</i>										
	<i>p value</i>	0.001									

Table 5.13: Linear mixed-effects models for lamina cribrosa thickness (LC thick) containing effect size ± standard error, i.e. how much LC thickness changes in μm per one-unit change in the independent variable, as well as t-value and p-values. Red text indicates factor is significant at $p < 0.05$. T = temporal, ST = superior-temporal, S = superior, SN = superior-nasal, N = nasal, IN = inferior-nasal, I = inferior, IT = inferior-temporal, Dx = stage of glaucoma, AxL = axial length, MS = mean spherical refractive error, MD = mean deviation on visual fields, ACD = anterior chamber depth, CCT = central corneal thickness.

Age made a significant negative contribution to posterior LC depth of $-3.71 \pm 1.66 \mu\text{m}/\text{year}$ in the SN region ($p=0.018$) and $-2.71 \pm 1.24 \mu\text{m}/\text{year}$ in the IT region ($p=0.025$), i.e. older eyes had a posterior LC surface that was closer to BMO in these regions. *Age* also had a significant negative effect on LC thickness of up to $-1.58 \mu\text{m}/\text{year}$, i.e. older eyes had thinner LC, in the ST, S, SN and I regions ($p<0.01$).

Mean spherical refractive error (MS) had a significant positive effect on the depth of the anterior LC in the IN region ($19.62 \pm 9.02 \mu\text{m}/\text{D}$, $p=0.028$), and a significant positive effect on posterior LC depth of up to $17.27 \mu\text{m}/\text{D}$ in the ST ($p=0.008$), S ($p=0.041$) and IT ($p=0.006$) regions (Table 5.12), suggesting that in the above regions the anterior or posterior LC were deeper in hyperopic eyes and, thus, closer to BMO in more myopic eyes. Additionally, in the IT region the LC was thicker with increasing *MS* ($6.84 \pm 2.14 \mu\text{m}/\text{D}$, $p=0.001$), i.e. eyes with greater amounts of hyperopia had greater inferior temporal LC thickness while more myopic eyes had thinner inferior temporal LCs.

MD had a significant negative effect of around $4 \mu\text{m}/\text{dB}$ in the SN ($p=0.015$) and N ($p=0.029$) anterior LC depth, as well as on the N posterior LC depth ($p=0.011$; Table 5.12), i.e. eyes with greater visual field defect had anterior and posterior LC surface that was deeper, or further from BMO, in those regions.

Anterior chamber depth (ACD) made a significant negative contribution of $-58.79 \pm 24.54 \mu\text{m}/\text{mm ACD}$ to S posterior LC depth ($p=0.013$). LC thickness was also significantly negatively affected by *ACD* in the T ($-15.33 \pm 6.79 \mu\text{m}/\text{mm ACD}$, $p=0.018$), S ($-18.83 \pm 8.63 \mu\text{m}/\text{mm ACD}$, $p=0.041$) and IN ($-19.31 \pm 9.86 \mu\text{m}/\text{mm ACD}$, $p=0.031$) ONH, meaning that eyes with deeper anterior chamber had thinner LCs in those regions.

Central corneal thickness (CCT) made a significant negative contribution explain variance in anterior LC depth of between -0.55 and $-0.91 \mu\text{m}/\mu\text{m CCT}$ in all regions ($p < 0.05$) except IN, I and IT (see Table 5.11). Similarly, *CCT* had a significant negative effect on all regions for posterior LC depth ($p < 0.05$; Table 5.12), suggesting that eyes with thinner central corneas had deeper anterior and posterior LC surfaces in all regions except for the inferior and inferior-nasal anterior LC. Interestingly, *CCT* did not have any significant effect on LC thickness.

Axial length had a significant positive effect on the thickness of the LC in the SN ($p = 0.002$) and IT ($p = 0.009$) regions. The interaction between *axial length:MD* contributed positively to explain ST posterior LC depth ($p < 0.001$). There was a significant positive effect from the association *axial length:MD* on the thickness of the IN LC ($p = 0.003$). Additionally, there was a significant negative effect in the T LC thickness ($p = 0.001$). The association between *axial length:MS* contributed negatively to the anterior LC depth ($p = 0.014$) and posterior LC depth ($p = 0.038$) in the SN. Additionally, the interaction between *axial length:mean spherical refractive error* contributed to thicker LC in the S ($p = 0.016$) and IN ($p = 0.005$) regions.

5.3.4.4 The effect of stage of glaucoma on the lamina cribrosa

Stage of glaucoma had a significant effect on the depth of the anterior LC depth in the I and central regions, and on the posterior LC depth in the SN, IN and IT regions ($p < 0.05$; Figure 5.17). However, subsequent post hoc analysis revealed no significant differences between groups when $p < 0.01$, although there was a trend for the anterior LC depth to be greater in early glaucoma than control eyes ($p = 0.044$).

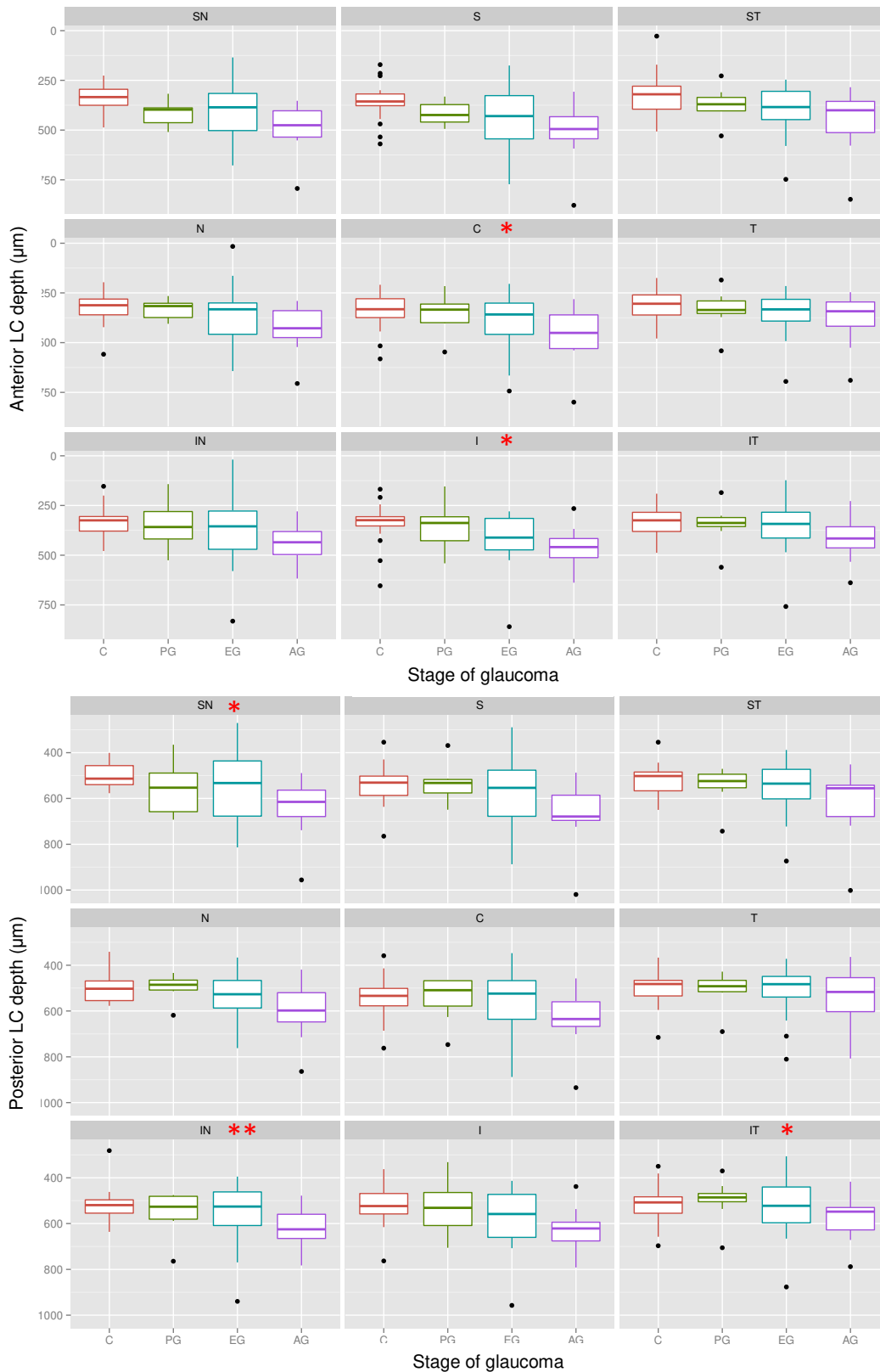


Figure 5.17: Regional anterior and posterior lamina cribrosa (LC) depth for each glaucoma (G) stage. C = control, PG = preperimetric G, EG = early G, AG = advanced G. T = temporal, ST = superior-temporal, S = superior, SN = superior-nasal, N = nasal, IN = inferior-nasal, I = inferior, IT = inferior-temporal. Boxplots denote median and 1st to 3rd quartiles, whiskers extend to the highest or lowest data value that is within a 1.5 x interquartile range. Black spots denote outliers. Red stars: significance as a function of glaucoma stage * = p<0.05, ** = p<0.01, *** = p<0.001

5.3.4.5 The effect of stage of glaucoma on lamina cribrosa thickness

The thickness of the LC was significantly affected by *stage of glaucoma* in the T, IN and central regions. When grouped according to glaucomatous progression, these data suggest an overall LC thinning with disease progression (Figure 5.19).

Subsequent *post hoc* analysis revealed that the LC was thinner for eyes with early glaucoma than control eyes in the central region ($C > EG$ $p=0.002$). Additionally, there was a trend for the LC to be thinner in eyes with early glaucoma than control eyes in the T region ($C > EG$, $p=0.016$). A summary of these regional differences in LC thickness is shown in (Figure 5.19).

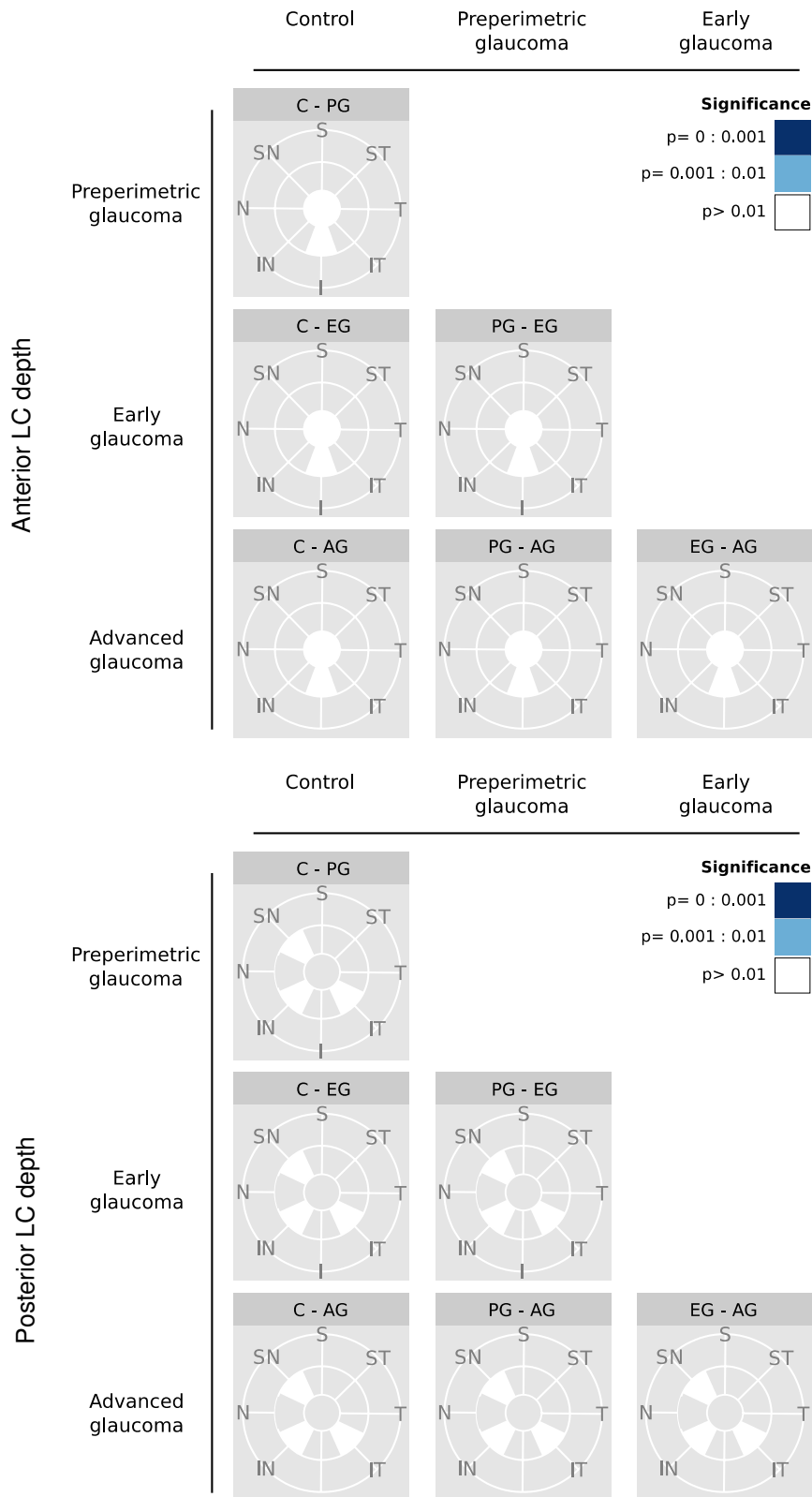


Figure 5.18: Regions of the optic nerve head where posterior lamina cribrosa depth was affected by stage of glaucoma, using linear mixed-effects models and subsequent pairwise comparisons. C = control, PG = preperimetric glaucoma, EG = early glaucoma, AG = advanced glaucoma. T = temporal, ST = superior-temporal, S = superior, SN = superior-nasal, N = nasal, IN = inferior-nasal, I = inferior, IT = inferior-temporal. Blue indicates significant differences, white indicates that glaucomatous progression was a factor in the model but there were no significant differences, grey indicates regions where stage of glaucoma was not a factor in the model.

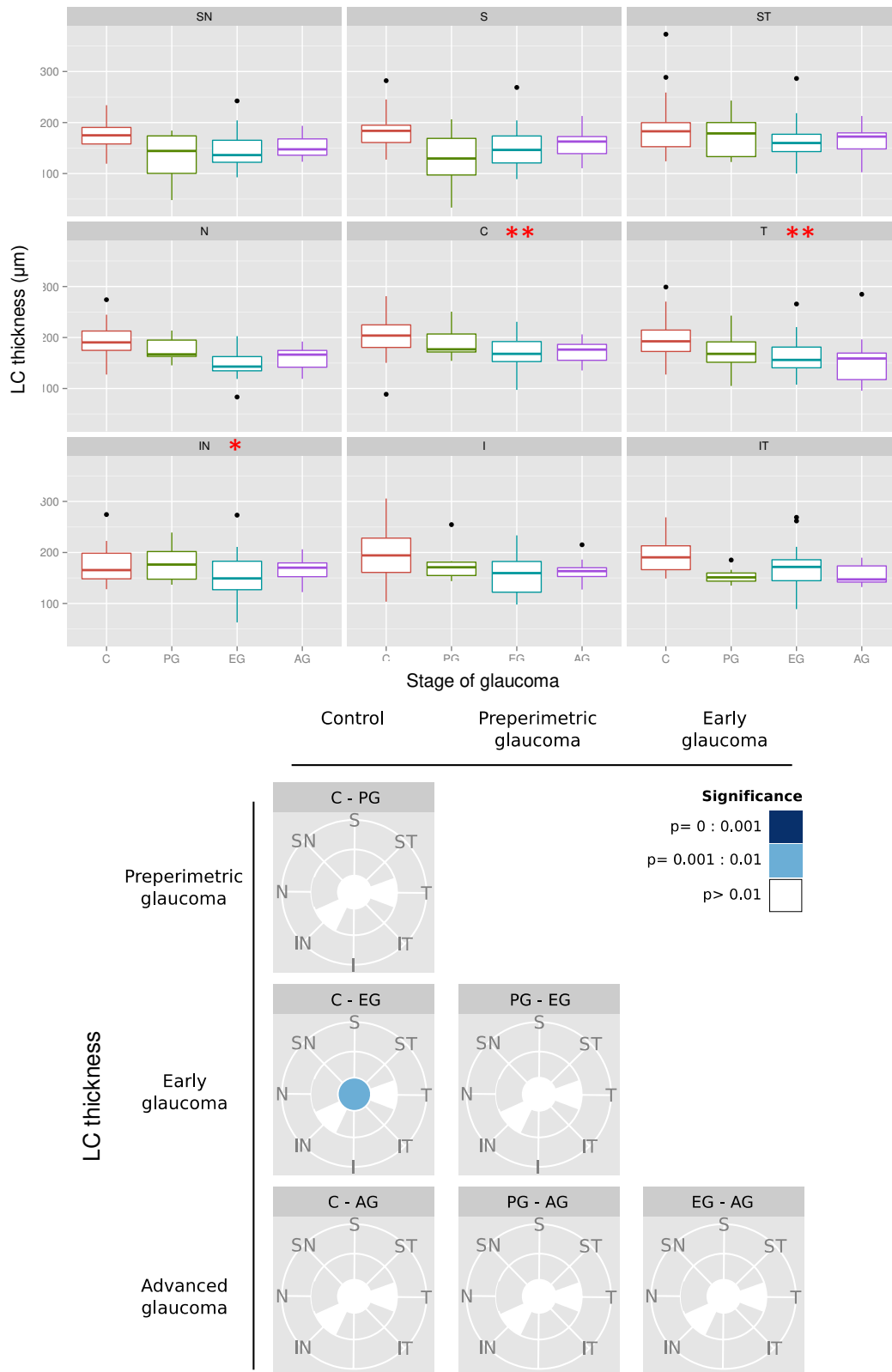


Figure 5.19: Lamina cribrosa (LC) thickness for each region of the ONH for glaucoma (G) stage, and regions of the LC that were affected by glaucoma using linear mixed effects models (LMM). C = control, PG = preperimetric G, EG = early G, AG = advanced G. T = temporal, S = superior, N = nasal, I = inferior. Boxplots denote median and 1st to 3rd quartiles, whiskers extend to the highest or lowest data value that is within a 1.5 x interquartile range. Black spots denote outliers. Red stars: significance as a function of glaucoma stage * = p<0.05, ** = p<0.01, *** = p<0.001.

5.3.5 Summary of results

The key findings from this study are as follows:

- The superior-inferior Bruch's membrane opening diameter was significantly greater in the preperimetric glaucoma group when compared with the advanced glaucoma group.
- Significant pNFL thickness differences were determined between control and preperimetric glaucoma eyes compared to those with early and advanced glaucoma, in the superior and superior-nasal regions.
- bNFL was thinner in early and advanced glaucoma groups than control and preperimetric in the inferior, inferior-temporal, temporal, superior-temporal and superior-nasal regions.
- Prelamina depth was greater in preperimetric, early and advanced glaucoma than in control eyes.
- Prelamina was thinner in all stages of glaucoma than in control eyes.
- Central LC was thinner in EG than control eyes

A summary of significant differences in ONH parameters as a function of glaucoma stage is shown in Figure 5.20.

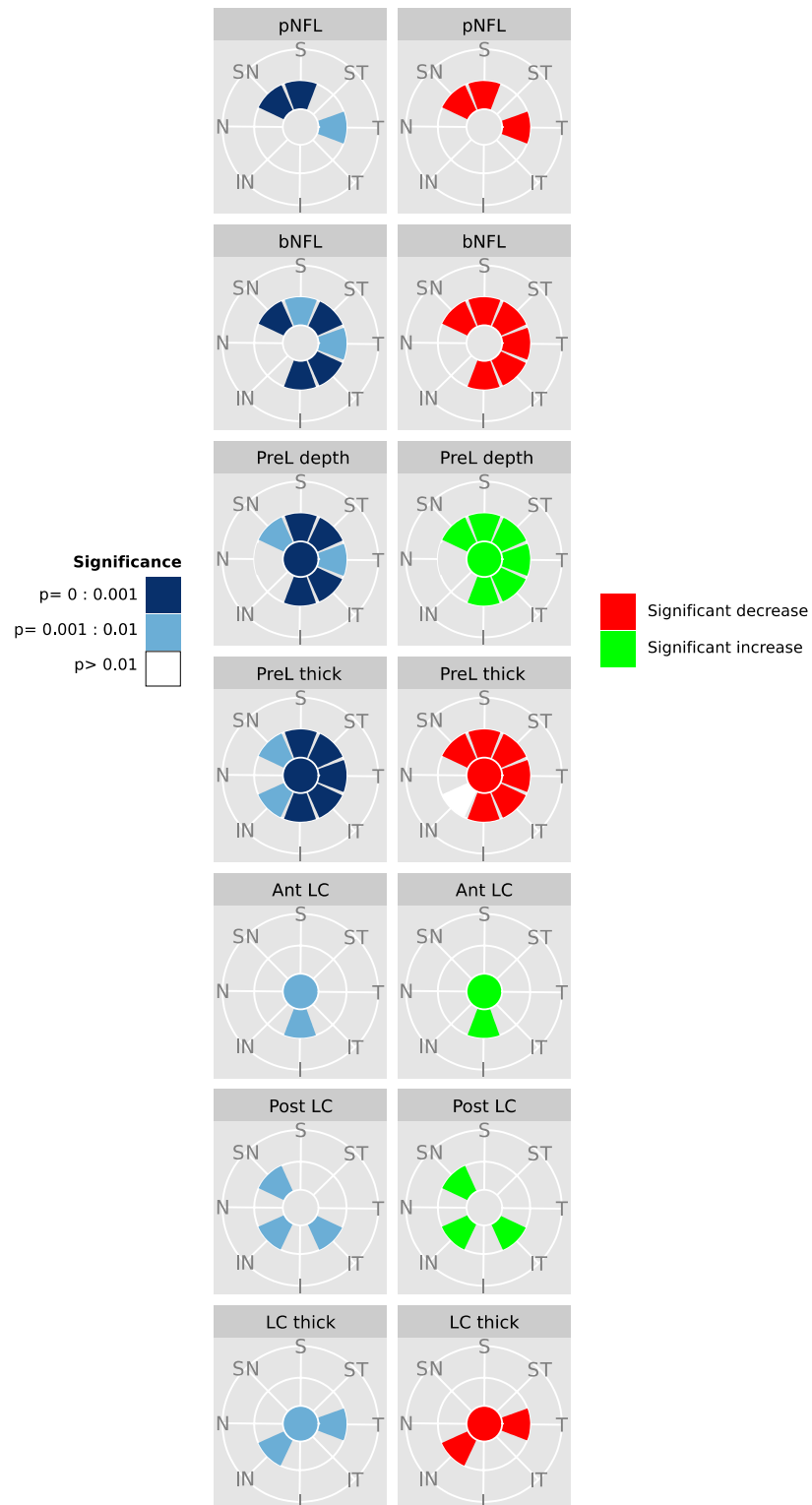


Figure 5.20: Regions of the optic nerve head that were affected by *stage of glaucoma*, using linear mixed-effects models (LMM). pNFL = peripapillary nerve fibre layer, bNFL = border nerve fibre layer, PreL depth = prelamina depth, PreL thick = prelamina thickness, Ant LC = anterior lamina cribrosa (LC) depth, Post LC = posterior LC depth, LC thick = LC thickness, T = temporal, ST = superior-temporal, S = superior, SN = superior-nasal, N = nasal, IN = inferior-nasal, I = inferior, IT = inferior-temporal. Blue indicates a significant contribution to the GLM, white indicates that *stage of glaucoma* was part of the GLM but not significant, grey indicates that *stage of glaucoma* was not a factor in the optimised LMM.

5.4 Discussion

The aims of this chapter were to identify changes in the optic nerve head microstructure with glaucoma, to identify factors that contribute to these changes, and to examine the role of aging in the glaucoma-related changes that occur. In order to do this, the effect of glaucoma and ocular parameters was assessed on 2D images from 3D volumetric OCT datasets. Significant changes were discovered in the prelamina and lamina cribrosa (LC) with visual field loss as well as with progressive stages of glaucoma. Those differences that were discovered due to glaucoma will now be considered in the context of those changes that occur independently as a result of normal ageing, as described in Chapter 4.

5.4.1 The effect of glaucoma and other ocular parameters on Bruch's membrane opening diameter

Bruch's membrane opening (BMO) diameter was used as a surrogate for optic disc diameter. Although having a large optic disc is, in itself, not an established risk factor for glaucoma, previous studies have found that eyes with a larger optic disc have a greater susceptibility to glaucomatous damage at what is considered a 'normal' IOP (Burk et al. 1992) and thus, are more vulnerable to damage with increases in IOP (Tomita et al. 1994). Conversely, other studies disagree and have revealed no significant association between optic disc size and glaucoma (Jonas, Gusek and Naumann 1988; Jonas et al. 1991). As such, further work into this area is required.

In the present study there were no significant associations between the diameter of BMO and increasing visual field loss in any direction, when directly compared with univariate analysis. Interestingly, using multivariate statistical modelling, the superior – inferior BMO diameter (or vertical BMO diameter) was shown to be larger in eyes with preperimetric glaucoma than in eyes with early or moderate glaucoma, although there was no difference between control eyes and any of the glaucoma groups.

For each of the BMO planes assessed there were several other ocular factors required in the optimized model to explain changes in BMO diameter, and, as such, it would appear that the use of additional ocular parameters to investigate changes in BMO diameter provides a more thorough evaluation. Age was a contributing factor in the model for S-I BMO diameter but did not offer a significant contribution to explain the variance. Comparatively, in a healthy control population (Ch3), age was a significant factor in the models to explain ST-IN and S-I BMO diameter. A summary of the significant factors in the LMMs to describe BMO diameter is shown below (Table 5.14).

Regional BMO diameter	Dx	Age	AxL	MS	MD	ACD	CCT	Age: MD	AxL: MD	AxL: MS
T-N		✓	✓	✓	✓	✓		✓		✓
ST-IN			✓	✓		✓				✓
S-I	✓	✓		✓		✓				
SN-IT		✓	✓		✓	✓		✓	✓	
H:V		✓	✓	✓	✓		✓	✓	✓	✓

Table 5.14: Independent variables included in the linear mixed-effects model to explain variance in regional Bruch's membrane opening (BMO) parameters. A tick indicates the factor is included in the optimised LMM, red = significant negative association ($p < 0.05$), green = significant positive association ($p < 0.05$). T = temporal, ST = superior-temporal, S = superior, SN = superior-nasal, N = nasal, IN = inferior-nasal, I = inferior, IT = inferior-temporal. AxL = axial length, MS = mean spherical refractive error, MD = mean visual field deviation, ACD = anterior chamber depth, CCT = central corneal thickness.

In the present study glaucoma had no effect on the horizontal:vertical BMO diameter, i.e. disc circularity, which is in agreement with research from Jonas and Papastathopoulos (1996) who found that a comparable measure, i.e. optic disc shape was not important in the diagnosis of glaucoma, although in highly myopic eyes the optic disc was found to be more oval than in glaucoma or control groups.

5.4.2 The effect of glaucoma and other ocular parameters on the peripapillary and border nerve fibre layer

Peripapillary nerve fibre layer (pNFL) thickness has been shown to have high sensitivity for detecting visual field defects (Wollstein et al. 2004) and distinguishing healthy control eyes from those with glaucoma (Jeoung and Park 2010; Li et al. 2010), even in eyes with early glaucoma or mild visual

field defects (Mwanza et al. 2011). Peripapillary NFL thickness is reported to be an accurate predictor for glaucoma using both TD-OCT (Leung et al. 2008) and SD-OCT (Park et al. 2009; Jeoung and Park 2010; Bussel et al. 2014), and it has been suggested that pNFL thickness is, in fact, a better indicator for than ONH parameters for detecting glaucoma particularly in preperimetric (Lisboa et al. 2013) or early stages of the disease (Sung et al. 2012). However, in a different study Jeoung and Park (2010) compared an SD-OCT and TD-OCT device and determined that neither were adequate to detect changes in pNFL thickness between control eyes and those with preperimetric glaucoma.

In 2012, Sung et al. separated a cohort of glaucomatous ONH into small and large based on optic disc area and found thinner pNFL, smaller rim area, and less cup volume in the smaller eyes. Thickness of the pNFL was determined to be a better predictor for determining the presence of glaucoma than measuring ONH parameters in eyes with small ONH, and it was suggested that this was because pNFL is measured at a fixed diameter from the centre of the disc and pNFL thickness decreases with increased distance from the disc margin.

In the present study there was a significant association between peripapillary NFL thinning and increasing visual field loss in all regions of the ONH except inferior and superior-nasal, when compared directly using a univariate approach. However, when a multivariate statistical approach was utilised, the superior-nasal pNFL thickness *was* affected by glaucoma, as were the temporal and superior regions. Post-hoc analysis revealed differences between control eyes and glaucoma in the superior and superior-nasal regions, and between preperimetric glaucoma and early glaucoma in the superior-nasal region, although there were no significant differences between early and advanced glaucoma. A summary of the significant factors in the LMMs to describe pNFL and bNFL is shown below (Table 5.15).

Region		Dx	Age	AxL	MS	MD	ACD	CCT	Age: MD	AxL: MD	AxL: MS
T	pNFL	✓		✓							
ST	pNFL		✓								
S	pNFL	✓	✓		✓						
SN	pNFL	✓	✓			✓			✓		
N	pNFL			✓	✓	✓					✓
IN	pNFL				✓	✓					
I	pNFL			✓	✓	✓				✓	
IT	pNFL		✓		✓	✓					
T	bNFL	✓		✓	✓			✓			
ST	bNFL	✓		✓	✓	✓		✓			
S	bNFL	✓	✓	✓	✓		✓		✓		
SN	bNFL	✓		✓			✓	✓			
N	bNFL			✓		✓					
IN	bNFL			✓		✓	✓				
I	bNFL	✓		✓		✓					
IT	bNFL	✓	✓	✓	✓	✓		✓			

Table 5.15: Independent variables included in the linear mixed-effects model to explain variance in regional peripapillary nerve fibre layer (pNFL) and border nerve fibre layer (bNFL) parameters. A tick indicates the factor is included in the optimised LMM, red = significant negative association ($p < 0.05$), green = significant positive association ($p < 0.05$). T = temporal, ST = superior-temporal, S = superior, SN = superior-nasal, N = nasal, IN = inferior-nasal, I = inferior, IT = inferior-temporal. AxL = axial length, MS = mean spherical refractive error, MD = mean visual field deviation, ACD = anterior chamber depth, CCT = central corneal thickness.

Border NFL was significantly associated with increasing visual field loss in all regions, and there were significant changes with glaucoma in all regions except nasal and inferior-nasal. The post-hoc analysis revealed significant changes in all regions between control and early glaucoma, and between control and advanced glaucoma. There were no differences in bNFL thickness between control and preperimetric glaucoma. There were, however, changes between preperimetric glaucoma and early and advanced glaucoma, showing that control and preperimetric glaucoma had similar bNFL thickness, whereas the bNFL became thinner with increasing levels of glaucoma. Eyes with preperimetric glaucoma, by definition, have glaucomatous disc changes in the absence of visual field loss. It is likely, therefore, that the RGC axon loss for this early stage of glaucoma has not reached a point where it is clinically detectable and that changes, such as an increase in LC depth, have occurred prior to RGC damage.

There are currently no available studies describing bNFL measurements. The closest equivalent measurement is the BMO minimum rim width (MRW), which is used to measure the neuroretinal

rim from the edge of Bruch's membrane to the closest point of the inner limiting membrane (Figure 5.21) and has been demonstrated to have better diagnostic capabilities than pNFL thickness measurements (Chauhan et al. 2013). Although MRW was not measured in this current study, the ONH structure it is measuring (i.e. RGC axons and supporting connective tissue) is the same as bNFL. While, logically, these measurements should reveal comparable characteristics, it has yet to be confirmed how well correlated they are.

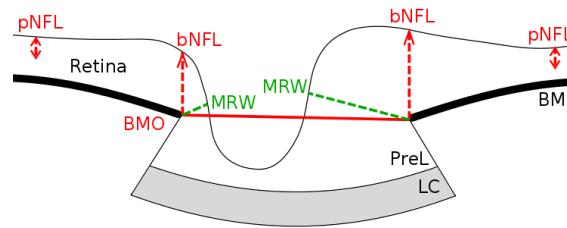


Figure 5.21: Comparison of minimum rim width (MRW, shown in green) and peripapillary nerve fibre layer (pNFL) and border nerve fibre layer (bNFL) measurements demonstrated in red dashed lines, both in relation to Bruch's membrane opening (BMO; red solid line). BM = Bruch's Membrane, PreL = prelamina, LC = Lamina cribrosa.

Bearing in mind this limitation, it is interesting to note that in this study the bNFL thickness measurement appeared to be a *better* predictor than pNFL for early and advanced glaucoma, i.e. more regions of the ONH showed significant differences and those differences showed higher significance. However, pNFL was able to detect differences between control eyes and those with preperimetric glaucoma that the bNFL did not. This may be because above BMO, where bNFL is measured, RGC axons are stacked above one another and so are more concentrated, so any loss of axons due to glaucomatous damage was less apparent. In the peripapillary region axons are more spread out so the early changes associated with preperimetric glaucoma may be more easily detectable at this point.

Age had a significant contribution to describe both pNFL and bNFL thickness in a population of control eyes. However, in glaucomatous eyes, age was only significant in describing the superior, superior-temporal and inferior-temporal pNFL thickness. Interestingly, axial length was a significant

factor in the model to describe bNFL in all regions except for nasal, i.e. eyes with greater axial length had thinner bNFL. This could be due to the fact that larger eyes have larger optic discs (Oliveira et al. 2007) so the RGC axons could be more spread across the ONH to reveal a thinner bNFL, and potentially a thinner prelamina.

5.4.3 The effect of glaucoma and other ocular parameters on the prelamina

The prelamina region of the optic nerve head contains RGC axons as they gather from across the retina and bundle together to exit the eye as the optic nerve. Glaucoma is associated with excavation of the optic cup due to deformation of the lamina cribrosa (Bellezza et al. 2003) and RGC drop out (Quigley 1999), so it is to be expected that the prelamina depth increases with glaucoma and the prelamina thickness decreases. Indeed, prelamina thickening has been reported following IOP-lowering surgery (Reis et al. 2012; Barrancos et al. 2014), possibly due to an increase in blood volume or a shift in axoplasmic fluid from the prelamina tissue once the IOP-related pressure on the prelamina is relieved. Additionally, Agoumi et al. (2011) reported compression of the prelamina immediately following acute IOP elevations in human eyes. However, in a longitudinal study over 5 years, 9% of the glaucomatous eyes in the study demonstrated prelamina thinning and 2.2% demonstrated prelamina thickening (Wu et al. 2015). In the same study roughly one quarter of the glaucomatous eyes showed a change in prelamina depth; of these, two thirds showed a greater prelamina depth over the 5 years and one third showed a decrease in prelamina depth.

The prelamina is easily measureable using commercial OCT devices, therefore it is advantageous to determine prelamina parameters that can assist in the detection of early glaucoma as well as enhance understanding of the glaucomatous disease process.

In the current study an increase in the depth of the prelamina surface was significantly associated with increasing visual field loss in all regions examined using direct correlation, suggesting that as

RGC axons are lost during glaucomatous damage, the prelamina surface becomes backwardly displaced deeper into the ONH, corresponding to increased cupping of the optic nerve head (Vrabec 1976; Yang et al. 2011; Kokotas et al. 2012). Using linear mixed-effects modelling to account for other ocular parameters, it was shown in the current study that the prelamina depth was significantly affected by stage of glaucoma disease in all regions except nasal and inferior-nasal. Differences were predominantly between control eyes and eyes with all stages of glaucoma, and of particular note the prelamina depth in preperimetric glaucoma was greater in the superior, superior-temporal, and inferior-temporal regions. Similarly, in early glaucoma the prelamina depth was greater than control eyes for all regions except nasal and inferior-nasal. The ability to distinguish between healthy control eyes and those with the earliest signs of disease is of particular benefit for the initial diagnosis of glaucoma, and as such, prelamina depth is potentially a useful biomarker for the diagnosis and monitoring of glaucoma in its earliest stages.

Age did not play a major role in describing the prelamina depth or thickness in either the glaucomatous or the healthy control group. Previous research has investigated RGC dropout with increasing age (Dolman et al. 1980; Jonas et al. 1990) and RGC axon loss of up to 0.6%/year with increasing age has been reported (Harwerth et al. 2008). Potentially this could lead to a decrease in prelamina depth and thickness, however, once the effect of glaucoma had been accounted for, age was not a significant factor to explain prelamina depth in the present study.

Prelamina thinning was also shown in the current study to be associated with increasing visual field loss in all regions except nasal using direct correlations, and was significantly affected by stage of glaucomatous in all regions except nasal and superior-nasal using a multivariate approach. A summary of the significant factors in the LMMs to describe prelamina depth and thickness is shown below (Table 5.16). Post-hoc pairwise comparisons revealed that the differences were predominantly between control and all stages of glaucoma, suggesting that prelamina thinning

occurs early in the disease. Notably there were significant differences in prelamina thickness between early glaucoma and control in all regions except nasal, superior-nasal and inferior-nasal, and between control and preperimetric glaucoma in the superior, superior-temporal, and inferior-temporal regions. This current study suggests that prelamina measurements from the temporal side of the optic disc are another potential biomarker for the detection of the earliest stages of glaucoma.

Region		Dx	Age	AxL	MS	MD	ACD	CCT	Age: MD	AxL: MD	AxL: MS
T	PreL depth	✓	✓	✓	✓	✓		✓			✓
ST	PreL depth	✓	✓	✓	✓	✓	✓	✓		✓	
S	PreL depth	✓	✓	✓	✓	✓	✓	✓		✓	
SN	PreL depth	✓	✓	✓	✓	✓	✓	✓	✓		
N	PreL depth	✓	✓	✓		✓		✓			
IN	PreL depth		✓	✓	✓	✓		✓			✓
I	PreL depth	✓	✓	✓	✓	✓	✓	✓	✓		
IT	PreL depth	✓		✓	✓		✓	✓			
C	PreL depth	✓	✓	✓	✓	✓		✓			✓
T	PreL thick	✓	✓	✓	✓	✓	✓	✓	✓		✓
ST	PreL thick	✓	✓	✓	✓		✓	✓	✓		
S	PreL thick	✓		✓		✓		✓		✓	
SN	PreL thick	✓	✓	✓		✓		✓	✓		✓
N	PreL thick		✓	✓	✓	✓			✓		✓
IN	PreL thick	✓	✓	✓		✓			✓		
I	PreL thick	✓	✓	✓	✓	✓	✓	✓			
IT	PreL thick	✓	✓	✓	✓	✓	✓	✓	✓	✓	
C	PreL thick	✓		✓	✓	✓	✓	✓			✓

Table 5.16: Independent variables included in the linear mixed-effects model to explain variance in regional prelamina (PreL) depth and thickness parameters. A tick indicates the factor is included in the optimised GLM, red = significant negative association ($p < 0.05$), green = significant positive association ($p < 0.05$). T = temporal, ST = superior-temporal, S = superior, SN = superior-nasal, N = nasal, IN = inferior-nasal, I = inferior, IT = inferior-temporal, C = central. AxL = axial length, MS = mean spherical refractive error, MD = mean visual field deviation, ACD = anterior chamber depth, CCT = central corneal thickness.

Axial length and mean spherical refractive error contributed to both prelamina depth and thickness.

It is known that larger eyes with greater amounts of myopia are more at risk of glaucoma (Mitchell et al. 1999); it would make sense that both axial length and refractive error are part of the models to explain the prelamina parameters. The models suggest that larger eyes have greater prelamina depth and thinner prelamina, which may be due to the RGC axons being more spread out across the optic disc. However, a more myopic refractive error appears to have a shallower prelamina depth

and thicker prelamina than more hyperopic eyes. Although this does not appear logical initially, this result may be due to the construct of the model; axial length and refractive error are closely linked, so once the axial length aspect of the variance has been described the mean spherical refractive error (MS) component of the model has the remaining refractive error to account for. Additionally, the participants for the study were recruited from an aging population, and as such had normal aging-related ocular conditions. Participants were excluded if they had a non-glaucomatous ocular pathology, however, due to the age-associated nature of glaucoma eyes with IOLs and early lens opacities were accepted into the study, provided the lens opacities did not obscure the OCT image of the ONH. As a result of this, 12 eyes had IOL implants and 21 eyes had early lens opacities, which could have altered the refractive state of the eye and as such the axial length may no longer have correlated with the expected MS.

It is interesting to note the association between central corneal thickness and prelamina depth and thickness in this study, especially compared to the results in the previous chapter whereby central corneal thickness did not significantly contribute to prelamina measurements in a healthy aging cohort (Chapter 4). Eyes with thinner corneas had deeper prelamina surface and thinner prelamina than eyes with thick corneas. There are established links between corneal thickness and glaucoma due to the influence of corneal thickness on IOP measurements (Ehlers et al. 1975), and central corneal thickness has been identified as a predictor for POAG (Gordon et al. 2002). However, there is currently no published studies linking prelamina measurements to corneal thickness in glaucomatous eyes, and this is the first study to discuss such a relationship.

If both prelamina thickness and bNFL thickness are considered together then effectively prelamina is observed across edges of BMO, at the centre of the disc, and at the midpoints between these points (Figure 5.22).

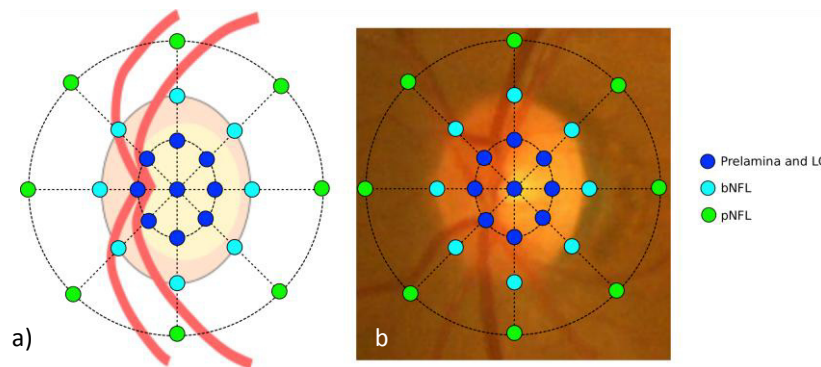


Figure 5.22: (a) Schematic diagram and (b) fundus photograph of a left optic nerve, with a grid superimposed demonstrating the location of prelamina and lamina cribrosa measurements (blue), border nerve fibre layer (bNFL, cyan) and peripapillary nerve fibre layer (pNFL, green).

Interestingly both the nasal and inferior-nasal regions have not shown any changes as a result of glaucoma, but where both the bNFL and prelamina show significant differences between early glaucoma and control, only prelamina thickness shows differences between preperimetric glaucoma and control.

5.4.4 The effect of glaucoma and other ocular parameters on the lamina cribrosa

The lamina cribrosa is acknowledged to be the principle site of RGC axonal insult in glaucoma (Quigley and Green 1979; Quigley et al. 1981; Bellezza et al. 2001). The aim of investigating differences in LC depth and thickness between stages of glaucoma was to attempt to determine what changes occur at different time points in the disease and to determine what other ocular factors contributed to changes in the LC.

Previous research has found that the superior and inferior poles of the lamina cribrosa contained less connective tissue than temporal and nasal, and proposed that superior and inferior regions were more susceptible to glaucomatous damage (Quigley and Addicks 1981; Radius and Gonzales 1981). An increase in LC depth has been described previously in experimental glaucoma in non-human primate models; Bellezza et al. (2003) determined an increase in the depth (or posterior

displacement) of the LC, and an enlarged scleral canal, in eyes with early glaucoma. Additionally, Yang et al. (2011) found that the insertion point of the anterior LC migrated posteriorly from BMO in early glaucoma. They concluded that this posterior migration was due to loss of anterior connective tissue beams in the LC, due to either primary damage from the increase in IOP or due to damage during disrupted remodelling. Yang et al. (2011) also suggested that the migration of the LC insertion regions may contribute to reducing the resistance of the scleral canal to expansion, which would in turn contribute to the typical glaucomatous excavation of the ONH (Quigley et al. 1981; Burgoyne et al. 2005). In a longitudinal study following participants diagnosed with POAG, around 25% of the eyes showed a change in anterior LC depth after five years, with half showing an increase in depth and half showed a decrease in depth (Wu et al. 2015).

In the present study, both the anterior LC depth and posterior LC depth increased with increasing visual field loss using univariate analysis. Using a multivariate approach the inferior region the anterior LC was significantly deeper in control eyes than those with early glaucoma. There were no significant differences in posterior LC depth between different stages of glaucoma.

These differences in LC depth with glaucoma are likely due to the nature of IOP-induced mechanical changes in the LC. ONH biomechanics is used as a way of describing the LC, peripapillary sclera and scleral canal as a biological system that is susceptible to changes in IOP (Burgoyne et al. 2005; Downs et al. 2008; Sigal and Ethier 2009). In a study using finite element modelling, Sigal et al. (2011) altered scleral thickness, scleral canal size and eccentricity, and LC position and thickness based on biological measures from non-human primates. Using a range of parameters they found that the depth of the LC was associated with expansion of the scleral canal. Put simply, if the peripapillary sclera was compliant, then an increase in IOP would lead to posterior displacement of the sclera and expansion of the scleral canal, and the LC would be pulled taut, decreasing the LC depth. If the peripapillary sclera was stiff, an increase in IOP would not displace the sclera, the sclera canal would

not increase and the LC would displace under the increase in pressure. This is summarised in Figure 5.23.

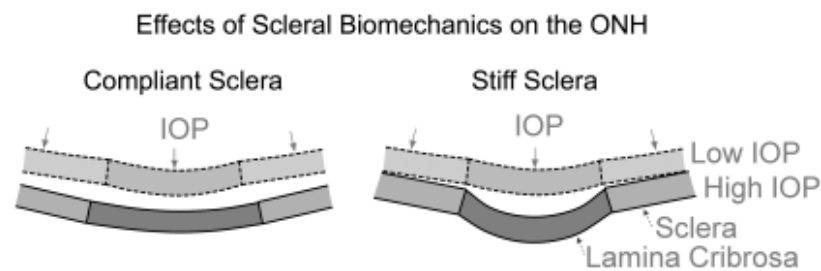


Figure 5.23: Schematic diagram of how deformation of the sclera and lamina cribrosa (LC), may be related. For a compliant sclera, and increase in IOP induces scleral deformation which increases the size of the scleral canal and pulls the LC taut, resulting in a decrease in LC depth. For a stiff sclera, an increase in IOP does little to deform the sclera so there is little scleral canal expansion, and the LC is pushed outwards under the pressure. Taken from Sigal and Ethier (2009).

However, Sigal et al. (2011) also found that under some conditions the LC depth and scleral expansion were not related or showed an inverse relationship. Some models had particularly deep LC or large scleral canal, which they suggested predisposed the ONH to being more sensitive to changes in IOP, and therefore more susceptible to glaucomatous damage.

LC thinning was associated with increasing visual field loss in the central, temporal and inferior-temporal regions, using univariate analysis. Linear mixed-effects modelling revealed that there were significant changes in the LC due to glaucoma in the temporal, inferior-nasal and central regions, and post-hoc analysis showed that these differences were significant in the central region between control and early glaucoma. This is consistent with *ex-vivo* studies where compression of the cribriform sheets within the LC was found to be one of the earliest abnormalities detected in eyes with glaucoma (Quigley et al. 1983). The same work also determined backwards bowing of the whole LC at later stages of glaucoma, with the effect being more pronounced at the superior and inferior poles. This is thought to be due to the relatively reduced amount of connective tissue at the superior and inferior poles of the LC compared to the temporal and nasal (Quigley and Addicks 1981).

Central LC thickness in this study was found to be $203.13 \pm 39.42\mu\text{m}$ in control eyes and dropping to $171.18 \pm 23.92 \mu\text{m}$ in advanced glaucoma. Other OCT studies have found similar results; Lee et al. (2011) found LC thickness to be $254.80 \pm 69.31\mu\text{m}$ in control and $215.67 \pm 58.26\mu\text{m}$ in grouped stages of glaucoma, and Inoue et al. (2009) found near-central LC thickness to be $244.44 \pm 47.2\mu\text{m}$ in eyes with ocular hypertension and no vision loss. However, in that study the LC was $130.1 \pm 32.7\mu\text{m}$ in advanced glaucoma. This difference may be due to the region in which the 'central' LC was measured. In the present study the centre of the ONH was determined as the centre of BMO, whereas Inoue et al. (2009) identified a different near-central where the anterior and posterior LC surfaces were both visible on an OCT b-scan for each ONH. The same study found that of the 52 eyes imaged, 3 were excluded due to vascular shadowing and 19 were excluded due to poor visibility of the LC surface. This lack of visibility is not unusual in OCT devices; in another study, 31 of 61 healthy control eyes were excluded due to poor visibility of the anterior LC surface (Park et al. 2012). In comparison, for the present study 7 of the 91 available eyes were removed prior to analysis due to poor image quality following acquisition. In cases where some ONH structures were visible and others were not, those that were visible were measured and those that were not were left blank; as a result of this, 2 measurements were not included for central prelamina thickness and 7 were excluded for central LC thickness. Vascular shadows had a significant effect on the visibility of the LC on the nasal side of the ONH; 14 measurements were left out for nasal prelamina thickness compared to 5 for temporal prelamina thickness, and 39 nasal LC thickness measurements were not possible, compared to 19 temporal LC thickness. Note that the values reported here are for thickness measurements, and as such rely on both the anterior and posterior face of the structure being visible.

Recent studies have shown that eyes with POAG that have undergone IOP-reducing surgery eventually obtain a decreased LC depth, i.e. the LC is more anterior within the ONH (Lee, Kim and Weinreb 2012; Reis et al. 2012; Yoshikawa et al. 2014), as well as thickening of the prelamina (Reis

et al. 2012, Barrancos et al. 2014) and the LC (Lee, Kim and Weinreb 2012). This reversal in LC is likely due to the reduction of IOP-related pressure that was causing compression of the prelamina and LC plates within the ONH (Quigley et al. 1983).

Age did not have a major role in determining the regional changes in anterior LC depth for either the glaucoma or the healthy control group. However, increasing age was associated with decreasing T, ST, N and central posterior LC depth in the healthy aging cohort (Chapter 4), whereas in the glaucomatous cohort in the present study aging had significant effect on the posterior LC depth in the SN and IT regions.

Similarly, age was revealed to contribute significantly to LC thickness in the superior-temporal, superior, inferior-temporal and inferior regions for eyes in the glaucomatous cohort. In the healthy aging data (Chapter 4) there were no significant changes in LC thickness with increasing age, however, age was a significant factor in describing the LC thickness in the superior-temporal, superior and inferior-temporal regions. Age affected the thickness of the LC in both cohorts, whereas glaucoma affected the temporal, central, superior-nasal and inferior-nasal regions. It is not clear what causes this regional selectivity; however, this suggests that changes at the nasal side of the LC are more indicative of glaucomatous damage than changes at the temporal side of the LC.

Interestingly, as with the prelamina measurements, deeper anterior and posterior LC surfaces showed a significant association with thinner central cornea in many of the regions assessed. Previous work has shown no association between LC *thickness* and corneal thickness in healthy eyes (Jonas and Holbach 2005; Ren et al. 2010; Lee et al. 2012), and this was also show here; however, to date, there have been no investigations into LC or prelamina *depth* and corneal thickness. Perhaps this association between thinner corneas and deeper prelamina surface (suggesting deeper cupping of the optic nerve), anterior and posterior LC surface (suggesting more posteriorly placed LC) in eyes

with glaucoma reflects the differences in connective tissue structure between glaucomatous eyes and healthy. As mentioned earlier, having a thinner cornea has been shown to be a risk factor for POAG (Gordon et al. 2002), although the reason for this is still unclear. Perhaps the thinner connective tissue structure at the cornea reflects a difference in the connective tissue arrangement within LC structure, allowing it to be more easily displaced backwards with IOP. This may be due to the disruption and overall decrease in collagen density as well as the unchanged density of elastin in the lamina cribrosa in eyes with glaucoma (Hernandez et al. 1990; Quigley et al. 1991). The increase in ratio of elastin to collagen may cause the LC to become more susceptible to damage with changes in IOP. In another *ex-vivo* study, elastin fibres in the LC of glaucomatous eyes were found to be 'wavy' instead of straight in glaucomatous eyes (Hernandez et al. 1986; Morrison et al. 1988; Quigley et al. 1991); this may also contribute to the additional displacement of the LC in glaucomatous eyes, or, the additionally waviness may be due to an inability of the LC to return to its original position post-stretching from IOP. A summary of the significant factors in the LMMs to describe prelamina depth and thickness is shown below (Table 5.17).

Region		Dx	Age	AxL	MS	MD	ACD	CCT	Age: MD	AxL: MD	AxL: MS
T	Ant LC		✓	✓	✓	✓		✓		✓	
ST	Ant LC		✓	✓	✓	✓		✓		✓	✓
S	Ant LC			✓	✓	✓		✓			✓
SN	Ant LC			✓	✓	✓		✓			✓
N	Ant LC			✓	✓	✓	✓	✓			
IN	Ant LC			✓	✓	✓	✓	✓			
I	Ant LC	✓									
IT	Ant LC		✓	✓	□	✓		✓			✓
C	Ant LC	✓				✓	✓	✓			
T	Post LC		✓	✓	✓	✓		✓	✓	✓	
ST	Post LC	✓	✓	✓	✓	✓	✓	✓		✓	✓
S	Post LC			✓	✓	✓	✓	✓		✓	
SN	Post LC	✓	✓	✓	✓	✓	✓	✓	✓		✓
N	Post LC		✓	✓	✓	✓	✓	✓	✓		
IN	Post LC	✓					✓	✓			
I	Post LC			✓	✓	✓		✓			✓
IT	Post LC	✓	✓		✓	✓		✓			
C	Post LC		✓	✓	✓	✓	✓	✓			✓
T	LC thick	✓	✓	✓	✓	✓	✓	✓		✓	✓
ST	LC thick		✓	✓	✓	✓				✓	✓
S	LC thick		✓	✓	✓	✓	✓			✓	✓
SN	LC thick		✓	✓	✓			✓			✓
N	LC thick			✓	✓	✓	✓	✓		✓	✓
IN	LC thick	✓	✓	✓	✓	✓	✓			✓	✓
I	LC thick		✓	✓	✓	✓		✓	✓		
IT	LC thick		✓	✓	✓	✓	✓	✓	✓		
C	LC thick	✓	✓	✓		✓	✓	✓			

Table 5.17: Independent variables included in the linear mixed-effects model to explain variance in regional lamina cribrosa (LC) parameters. A tick indicates the factor is included in the optimised GLM, red = significant negative association ($p < 0.05$), green = significant positive association ($p < 0.05$). Ant LC = anterior LC depth. Post LC = posterior LC depth. LC thick = LC thickness. T = temporal, ST = superior-temporal, S = superior, SN = superior-nasal, N = nasal, IN = inferior-nasal, I = inferior, IT = inferior-temporal, C = central. AxL = axial length, MS = mean spherical refractive error, MD = mean visual field deviation, ACD = anterior chamber depth, CCT = central corneal thickness.

5.4.5 Limitations of study

As with Chapter 4, one of the limitations of this study was the reliance on both prelamina depth and anterior LC depth to calculate prelamina thickness, and anterior and posterior LC measurements to calculate LC thickness. Eyes with more advanced glaucoma tended to have less prelamina tissue obstructing the view of the LC compared to healthy control eyes, so LC thickness measurements were less visible on control eyes than those with glaucoma, particularly for the posterior LC surface. However, as described in the methods, where a prelamina or LC boundary was not visible then the measurement was left blank, and the data not used to calculate that particular parameter. In the

same way, blood vessels obscured the nasal side of the optic disc in both healthy and glaucomatous eyes so measurements from there were also limited.

There was uneven number of eyes in the control and glaucomatous progression groups. This is partly due to the recruitment emphasis being on earlier stages of disease, and partly because, observationally, subjects with greater disease progression tended to find it more difficult to fixate on the target for OCT imaging. Additionally, older participants often appeared to find it more difficult to hold stable fixation, meaning some eyes had to be discarded due to poor image quality.

Another potential limitation was that IOP was not included as a factor in the LMMs. This was because participants with glaucoma were already undergoing treatment. As it was not a longitudinal study the effect of changes in IOP for an individual participant could not be assessed, and this study did not control for modality of treatment, or regularity and compliance with treatment. Therefore it was decided IOP could be a confounding factor in this study, as glaucomatous participants who were undergoing treatment may have IOPs that were lower than the untreated healthy controls.

Additionally, the regional nerve fibre layer, prelamina and LC measurements were all derived from 20° OCT scans. 10° OCT scans were also acquired for the majority of participants and these may have allowed for improved measurement accuracy due to the increased image resolution. However, small eye movements appeared enhanced on the 10° OCT scans, and as such, reliable, stable images were not always possible. Similarly, radial b-scans were taken at 45° intervals around the ONH; in the future it would be interesting to establish whether greater number of radial scans and larger scan magnification would allow more information to be extracted from the images.

5.4.6 Conclusion

There were regional decreases in nerve fibre layer, prelamina and LC thickness and regional increases in prelamina and LC depth between control eyes and those with glaucoma. Of particular interest are differences between preperimetric and early glaucoma and control. Differences between control eyes and the earliest stages of disease have the potential to be used as biomarkers for the diagnosis of glaucoma, and as such, can assist the decision to treat prior to irreversible vision loss. Differences in ONH measurements were affected by other ocular parameters, such as central corneal thickness, age and refractive error. Therefore, in order to understand and accurately predict the progression of glaucoma the contribution of these other factors needs to be considered.

Chapter 6:
3D volumetric measurements of the optic
nerve head in glaucomatous and healthy
subjects

6 3D volumetric measurements of the optic nerve head in glaucomatous and healthy subjects

6.1 Introduction

Glaucoma is known to cause excavation of the optic cup, as the LC bows backwards and prelamina tissue is lost. The optic nerve is a 3D structure, and as such, this study is novel as the first to quantify ONH structural changes in 3D. This study is aimed at assessing previously characterised glaucomatous changes, as mentioned above, using OCT, in order to develop parameters that can be used as tools to identify early changes in glaucomatous ONH, prior to vision loss, and also monitor an individual ONH's progression.

Controversy exists as to where the neuroretinal rim starts, and where the most accurate place to measure the optic cup is. For this study, BMO was used as a reference and the cup volume was measured below BMO only. Until now, Bruch's membrane opening (BMO) has been considered as a 2D reference plane from which to measure prelamina and lamina cribrosa (LC) depth and thickness. However, the eye is a 3D biological structure; with the optic nerve exiting the eye at an angle Bruch's membrane is not necessarily perpendicular to the optic nerve. As such, BMO should be considered as a 3D reference plane rather than 2D. The BMO area will provide an index by which to determine at what stage, if at all, expansion of the optic canal occurs in glaucoma. One theory of damage, presented as a result of computational modelling, is that scleral expansion creates tensional forces i.e. exerts stress on the edges of LC, the LC thins and damage results (Sigal et al. 2005). Several investigators are now researching therapies to stiffen the peripapillary sclera, to prevent LC stress. However, this is risky, and before therapies are developed, it is essential that we determine if scleral expansion occurs in glaucoma, and if it does at what stage of development.

LC thinning is associated with glaucoma (Quigley et al. 1983; Park et al. 2012). However, there are reports of LC thickening during early glaucoma and/or when remodelling in monkey models of experimental hypertensions (Yang et al. 2011). Although in this project, the ONH is not assessed longitudinally, LC volume will be determined to determine if similar changes in volume occur are identified in different stages of glaucoma disease.

6.1.1 Aims of study

To quantify and identify changes in volume of the optic cup, prelamina and lamina cribrosa and in the area of Bruch's membrane opening (BMO), in different stages of glaucoma.

6.2 Experimental design

6.2.1 Participants

63 eyes of thirty-seven participants (18 glaucoma and 19 control) were recruited from the glaucoma clinic at UHW or within staff, students and friends of Cardiff University respectively, and grouped according to stage of glaucoma. The demographics for each group are shown below in Table 6.1.

	Control (n=35) mean ± SD	Preperimetric glaucoma (n=3) mean ± SD	Early glaucoma (n=16) mean ± SD	Advanced glaucoma (n=9) mean ± SD
Age (years)	57.14 ± 10.70	76.00 ± 8.64	70.00 ± 8.77	77.22 ± 7.30
Gender	15F :20M	2F :1M	7F :9M	3F :6M
MS (D)	0 ± 2.00	-0.25 ± 1.25	0.25 ± 2.50	1.00 ± 1.75
VA (logMAR)	-0.10 ± 0.06	0.06 ± 0.12	0.06 ± 0.18	0.20 ± 0.22
IOP (mmHg)	12.83 ± 2.51	12.00 ± 0	13.03 ± 1.70	10.39 ± 1.45
CCT (µm)	561.91 ± 45.73	541.67 ± 24.57	552.88 ± 42.29	518.33 ± 32.38
Axial length (mm)	23.84 ± 0.58	23.26 ± 0.85	23.88 ± 1.20	23.83 ± 1.61
ACD (mm)	2.81 ± 0.33	3.29 ± 0.70	3.23 ± 1.22	3.07 ± 0.72
MD (dB)	-0.31 ± 1.27	-1.55 ± 1.00	-3.68 ± 1.71	-13.13 ± 6.37

Table 6.1: Demographics for the eyes included in the present study. MS = mean spherical refractive error, VA = visual acuity, IOP = intraocular pressure, CCT = central corneal thickness, ACD = anterior chamber depth, MD = mean deviation visual fields, F = female, M = male, SD = standard deviation.

6.2.2 Clinical assessments

Visual acuity, intraocular pressure and refractive error were determined for each eye to ensure compliance with the inclusion criteria, as described in section 2.2. Axial length, anterior chamber depth and central corneal thickness were measured, and visual field tests were performed (SITA 24-2 Fast Threshold, Humphrey Visual Field Analyser).

6.2.3 Optical coherence tomography

20° scans centred on the ONH were acquired and the image datasets were processed and scaled as described in section 2.4.4.

6.2.4 3D image analysis of optic nerve head structure

Volumetric datasets were imported into Amira (version 5.4.0, Visage Imaging, Pro Meditus, Australia), an image visualisation and analysis software. Demarcation of Bruch's membrane opening, optic cup volume, prelamina volume below BMO, and LC volume were determined as described in section 2.7. Briefly, landmarks were placed at Bruch's membrane opening at 15° intervals around the centre of the ONH, and the surface area of BMO calculated. The BMO surface was then used as a reference for placing landmarks at the vitreous-prelamina boundary and calculating the volume of the optic cup below BMO. Landmarks were then placed at the prelamina-anterior LC boundary and the volume of the prelamina below BMO was calculated. Additional landmarks were then placed at the anterior and posterior LC surfaces, where visible, in order to calculate the volume of the lamina cribrosa. A demonstration of this process for the optic cup is shown below (Figure 6.1).

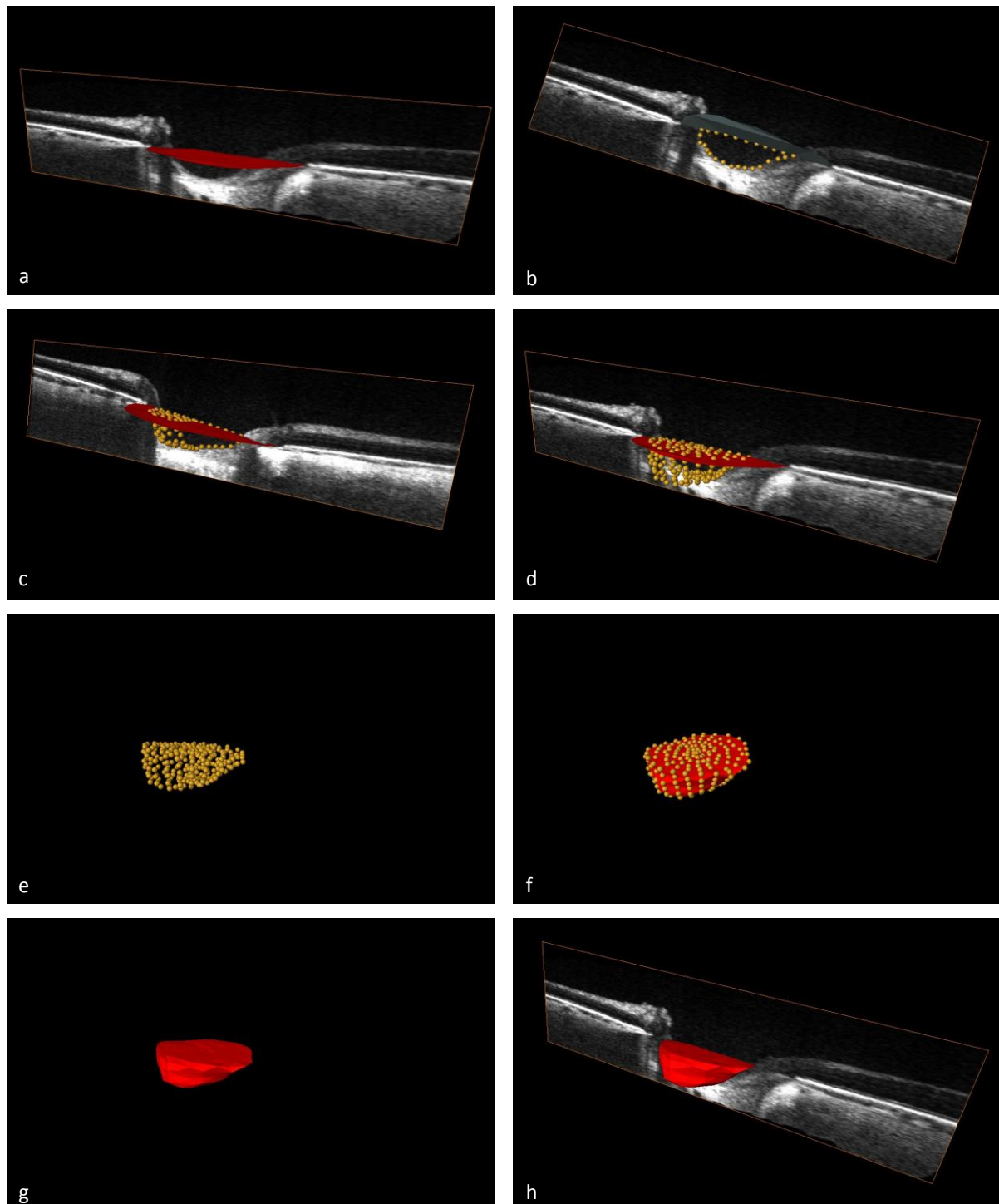


Figure 6.1: (a) An oblique radial slice of the ONH in the left eye of a myopic 65 year old male with glaucoma. The BMO surface is superimposed over the B-scan. (b) Landmarks were placed along the boundary between the BMO surface and the optic cup. (c) The radial slice was rotated at 15° intervals and landmarks were placed along the BMO-optic cup boundary on each B-scan until (d) the entire optic cup was demarcated. (e) The radial B-scan was hidden leaving just the landmarks, which were then (f) joined to create a 3D surface demonstrating the optic cup below BMO. (g) The landmarks were hidden, leaving just the surface, which was then (h) superimposed over a radial slice of the OCT tomogram. Figure repeated from Figure 2.19.

6.2.5 Statistical analysis

All statistical analysis was performed in R Studio (version 0.98.1091). The data was first visualised graphically, and normality of data was checked using histograms, QQ plots and Shapiro Wilke tests; then linear mixed-effects models (LMM) were created for BMO area, cup volume, prelamina volume and LC volume, including the fixed effects *age*, *axial length*, *mean spherical refraction*, *MD*, *central corneal thickness*, *anterior chamber depth*, the interaction terms *age:MD*, *axial length:MD*, and *axial length:MS*, and the random effect *participant* to account for both eyes from the same participants being included in the analysis, and a stepwise deletion technique was utilised to determine the optimised LMM, as described in section 2.9. Tukey post-hoc analysis was used to determine where difference between glaucoma groups lay, and significance was set at $p < 0.01$.

6.3 Results

The BMO area and cup, prelamina and LC volume are shown below in Table 6.2

	Control		Preperimetric glaucoma		Early glaucoma		Advanced glaucoma	
	mean	± SD	mean	± SD	mean	± SD	mean	± SD
BMO area (mm ²)	1.78	± 0.25	1.72	± 0.27	1.96	± 0.54	2.08	± 0.67
Cup volume (mm ³)	0.03	± 0.04	0.09	± 0.05	0.22	± 0.21	0.40	± 0.24
Prelamina volume (mm ³)	0.56	± 0.12	0.44	± 0.08	0.49	± 0.12	0.46	± 0.09
LC volume (mm ³)	0.45	± 0.10	0.28	± 0.11	0.39	± 0.13	0.45	± 0.18

Table 6.2: Quantification of optic nerve head parameters in 3D. BMO = Bruch's membrane opening, LC = lamina cribrosa.

6.3.1 Changes in Bruch's membrane opening area as a function of glaucoma disease stage

Stage of glaucoma made no significant contribution to explaining variance in BMO, and pairwise comparison revealed no significant difference in BMO area between control and any of the glaucoma stage groups ($p > 0.01$; Figure 6.2). However, *central corneal thickness* (-0.003 ± 0.001 mm²/μm CCT, $t = -2.05$, $p = 0.037$), *anterior chamber depth* (-0.18 ± 0.08 mm², $t = -2.14$, $p = 0.031$) and *mean spherical refraction* (-0.06 ± 0.03 mm², $t = -2.16$, $p = 0.027$) all showed a negative trend to explain

variance in BMO area which did not quite reach significance, i.e. eyes with thicker central corneas, deeper anterior chambers or more hyperopic refractions tended to have smaller BMO area.

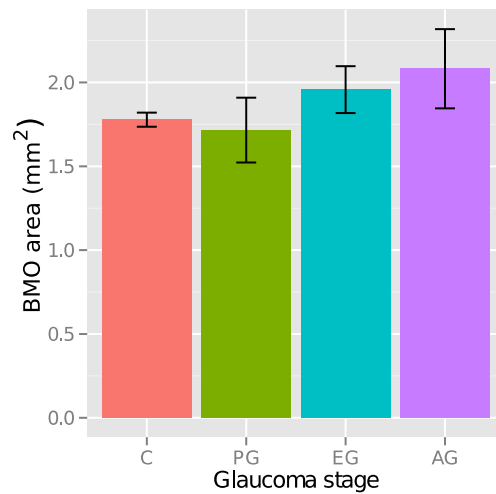


Figure 6.2: Bruch's membrane opening (BMO) area for each stage of glaucoma. There were no significant differences between control and any of the glaucoma groups. C = control, PG = preperimetric glaucoma, EG = early glaucoma, AG = advanced glaucoma. Error bars = 95% confidence intervals.

6.3.2 Changes in the volume of the optic cup as a function of glaucoma disease stage

Stage of glaucoma contributed significantly to explain variance in cup volume ($p < 0.001$). Subsequent pair-wise comparisons revealed that control eyes had cup volume that was smaller than eyes with both preperimetric and advanced glaucoma (results are presented as mean difference \pm SD; C<PG 0.22 ± 0.06 , $t = -3.52$, $p = 0.004$; C<AG 0.33 ± 0.05 , $t = -6.59$, $p < 0.0001$), and there was a trend for control eyes to have smaller cup volume than eyes with early glaucoma (C<EG 0.13 ± 0.05 , $t = -2.74$, $p = 0.044$). The volume of the cup for eyes with early glaucoma was also smaller than the cup in eyes with advanced glaucoma (EG<AG 0.19 ± 0.03 , $t = -5.64$, $p < 0.0001$; Figure 6.3). Additionally, both *central corneal thickness* (-0.001 ± 0.0004 mm³/μm CCT, $t = -2.33$, $p = 0.033$) and *anterior chamber depth* (-0.06 ± 0.03 mm³/mm, $t = -2.66$, $p = 0.014$) showed a trend for a negative contribution to cup volume, i.e. eyes with thicker corneas or deeper anterior chamber had smaller optic cups.

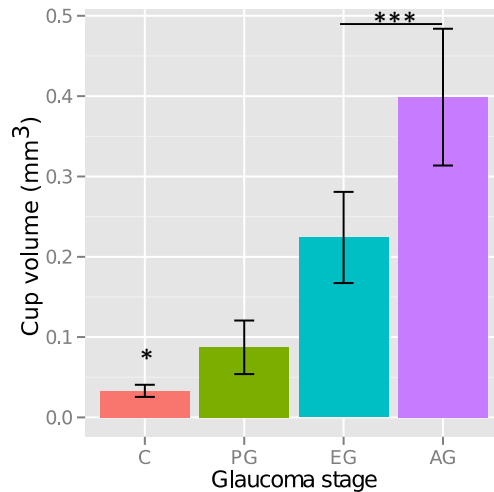


Figure 6.3: Cup volume for each stage of glaucoma. Control eyes had smaller cup than all stage of glaucoma. C = control, PG = preperimetric glaucoma, EG = early glaucoma, AG = advanced glaucoma. Error bars = 95% confidence intervals. * = $p < 0.05$, *** = $p < 0.001$.

6.3.3 Changes in the volume of the prelamina below Bruch's membrane as a function of glaucoma disease stage

Stage of glaucoma did not contribute significantly to explain variance in prelamina volume, and there was no difference between glaucoma stage groups ($p > 0.01$; Figure 6.4). However, *age* had a significant negative effect (-0.005 ± 0.001 mm³/year, $t = -3.38$, $p = 0.001$), i.e. older eyes had smaller prelamina volume than younger eyes.

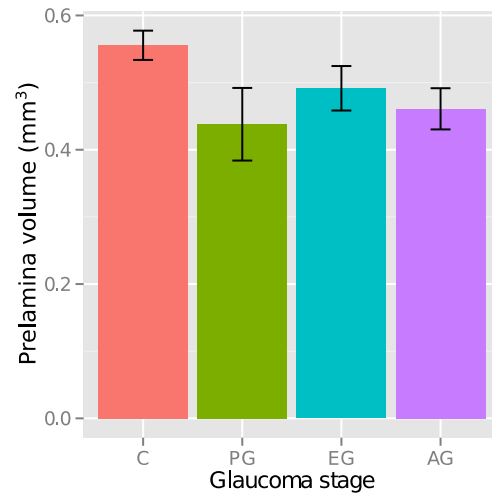


Figure 6.4: Prelamina volume for each stage of glaucoma. There were no significant differences between control or any stage of glaucoma. C = control, PG = preperimetric glaucoma, EG = early glaucoma, AG = advanced glaucoma. Error bars = 95% confidence intervals.

6.3.4 Changes in the volume of the lamina cribrosa as a function of glaucoma disease stage

Stage of glaucoma made no significant contribution to explaining variance in LC volume (Figure 6.5), and none of the other variables included in the initial analysis contributed to LC volume either ($p > 0.01$).

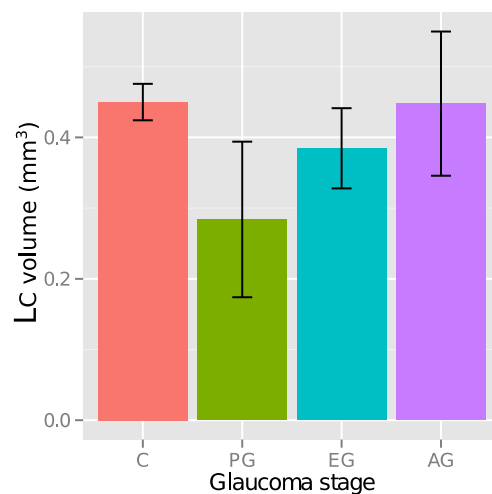


Figure 6.5: Lamina cribrosa (LC) volume for each stage of glaucoma. There were no significant differences between control or any stage of glaucoma. C = control, PG = preperimetric glaucoma, EG = early glaucoma, AG = advanced glaucoma. Error bars = 95% confidence intervals.

6.3.5 Summary of key findings

The volume of the optic cup was smaller in control eyes than eyes with all stages of glaucoma, and smaller in eyes with early glaucoma than advanced glaucoma. There were no statistically significant differences in BMO area, prelamina volume or LC volume between control and any stage of glaucoma.

6.4 Discussion

The aim of this study was to quantify and identify changes in volumes of the optic cup, prelamina and lamina cribrosa (LC) and BMO area in different stages of glaucoma. Previous research has determined that eyes with larger optic discs have higher susceptibility to glaucoma at IOP within statistically normal limits and are more vulnerable to damage with increased IOP (Burk et al. 1992; Tomita et al. 1994), no significant association has been determined between disc size and glaucoma (Jonas, Gusek and Naumann 1988; Jonas et al. 1991). In the present study, no significant difference in the area of Bruch's membrane opening was found with increasing stage of glaucoma.

Inverse associations between central corneal thickness (CCT) and optic disc size have been determined in eyes with primary open angle glaucoma (POAG; Pakravan et al. 2007; Bandyopadhyay et al. 2011). However, other work has found no association between the two (Terai et al. 2011). In the present study, CCT was found to have a significant negative effect on BMO area.

Cupping of the optic nerve is a well established biomarker for glaucoma (Quigley and Green 1979; Quigley et al. 1981; Gardiner et al. 2011; Yang et al. 2011), and the present study is no different. The cup in control eyes was found to be smaller than all stages of glaucoma, and in early glaucoma, cup volume was found to be smaller than in advanced glaucoma.

The volume of the prelamina was also measured. One would think the volume of the prelamina would decrease with disease progression, as retinal ganglion cell (RGC) loss and LC displacement progressed. However, one of the physiological responses to glaucoma is expansion of the scleral canal, as shown by Bellezza et al. (2001) and Bellezza et al. (2003) in experimental glaucoma in monkey, however, to date has not been shown in humans. If this area of expansion is included in the prelamina volume measurements then the volume may not decrease with increasing stage of glaucoma. In the current study there was no significant difference in prelamina volume with increasing stage of glaucoma. However, an increase in age was associated with a decrease in prelamina volume. It is known that there is an association between RGC axonal drop out and age (Balazsi et al. 1984), and it may be this that contributed to the association.

Although none of the differences between stages of glaucoma were statistically significant, the changes in the LC are still interesting, and if additional datasets were added to the cohort in the future the differences may reach significance. The LC appeared to thin in preperimetric glaucoma compared to control, and then became thicker in early and advanced glaucoma. This corresponds to LC remodelling in early glaucoma, as shown in monkey models (Yang et al. 2011). In the current study all eyes that had disease that had progressed further than 'early glaucoma' were classified as 'advanced'; if more data were acquired focussing on more advanced stages of glaucoma then perhaps the LC thinning that is reported in later stages of glaucoma might be apparent.

6.4.1 Limitations of study

Imaging the full volume of the LC required good visibility from all angles. Where landmarks could not be placed in one direction, the Pointwrap tool could still form a representation shape of the volume; however, if a larger proportion of the LC was not visible then the measurements were not possible. This had severe limitations on eyes with poor visibility of the LC surfaces, i.e. small, crowded ONHs, those with lots of vasculature, and eyes with a lot of prelamina tissue in front of the LC. As a result of

this, only 27 LC volume measurements were possible from the 64 eyes used in the study. In comparison, 5 prelamina volume measurements were not possible due to poor visibility of the anterior LC surface. Additionally, in order to quantify the total LC volume measurements were attempted from the region of LC insertion, which in some cases was shadowed by Bruch's membrane, potentially due to expansion of the scleral canal. Finally, LC measurements required visibility of both the anterior and posterior surface. Unfortunately this was not always possible, due to both vascular shadowing and OCT signal attenuation. The use of inverted image acquisition allowed for better LC imaging than conventional OCT use (Park et al. 2012), however, the use of image processing software to remove vascular shadowing from the images would greatly increase the number of datasets from which LC volumetric data could be extracted.

Additionally, the number of datasets included in this study was not equal in each control and glaucoma group. The addition of more datasets to the cohort could increase statistical power and potentially convert inter-group trends into solid conclusions.

6.4.2 Conclusion

Cupping of the optic nerve was smaller in control eyes than all stages of glaucoma, and smaller in early glaucoma than both moderate and advanced glaucoma. The technique used to derive volumes from OCT datasets can be used to assess the volume of the cup and prelamina in the optic nerve head. The volume of the lamina cribrosa could be determined for some datasets but not all, and further work into extracting image data from behind vascular shadows on images acquired from the research OCT device would be of particular benefit.

Chapter 7:

Microstructural analysis of the lamina cribrosa in healthy and glaucomatous eyes

7 Microstructural analysis of the lamina cribrosa in healthy and glaucomatous eyes

7.1 Introduction

The lamina cribrosa (LC) consists of up to 10 cribriform plates, formed from connective tissue beams that extend across the optic canal at the level of the sclera (Hogan et al. 1971). These beams form a sieve-like structure which supports retinal ganglion cell (RGC) axons as they leave the orbit. Importantly, this arrangement of the LC is necessary to support a region of particular mechanical vulnerability, i.e. where the optic nerve leaves the eye, and when adversely affected by factors such as increased IOP, i.e. in glaucoma, it can become a focal point for damage to RGC axons that, in turn results in vision loss (Vrabec 1976; Quigley et al. 1981; Quigley and Addicks 1981).

A substantial body of research has attempted to ascertain why the optic nerve heads of certain individuals are more susceptible to damage from glaucoma than others. Until now, *in vivo* investigations into the LC have focussed particularly on features such as LC depth and thickness (Chapters 4 and 5, Lee et al. 2011), focal defects (Kiumehr et al. 2012), LC insertion points (Park et al. 2012; Rho et al. 2012) and the characterisation of pores in the LC (Ivers et al. 2011; Wang et al. 2013).

In *ex vivo* studies the connective tissue and extracellular components of the optic nerve head (OHN) have been examined (Hernandez et al. 1990; Albon et al. 1995; Albon, Karwatowski, et al. 2000), and research has recently been published investigating the regional arrangement of the LC connective tissue in *ex vivo* eyes using small angle light scattering (Jones et al. 2015). This recent study identified regions within the inferior-temporal quadrant of the LC in which connective tissue fibres appeared to be more highly aligned, i.e. higher coherence. Such regions of high alignment were more prominent in eyes with glaucoma compared to control eyes. Critically, If these regions could be

identified and monitored *in vivo*, i.e. using OCT, it would allow further understanding of whether the areas of alignment contribute to the susceptibility of the eye to glaucoma, or whether they are enhanced as a result of glaucomatous disease. Additionally, knowledge of the regional and depth-related LC beam structure in control eyes and those with glaucoma may allow a better understanding of how the LC reacts under the stress and strain produced in glaucoma. In addition, detection of early signs of pathology through anomalies in beam orientation and coherence would be particularly beneficial, allowing for earlier, and thus more effective pharmacological or surgical intervention.

7.1.1 Aims of study

The primary aim of this study was to investigate if regional and depth-related differences in LC beam orientation and coherence occurred between healthy and glaucomatous eyes.

Specific aims were to determine:

- if there was a regional difference in LC beam orientation or coherence for control or for any individual glaucoma stage.
- whether LC beam orientation or coherence altered with increasing depth through the LC for control or any stage of glaucoma.
- the difference in regional LC beam or orientation between stages of glaucoma compared to healthy controls.

7.2 Experimental design

7.2.1 Participant demographics

Forty-seven eyes of thirty participants (18 glaucoma and 12 control), recruited from the glaucoma clinic at UHW and from within staff, students and friends of Cardiff University respectively, met the previously described inclusion criteria (section 2.2). Where possible both eyes from each participant

were used for analysis. Of the 60 possible eyes, three were excluded as either ocular hypertension (one) or glaucoma suspects (two), where one eye had a definite positive glaucoma diagnosis and the opposite was under investigation. Ten eyes were excluded due to poor OCT dataset quality, predominantly due to eye movements during image acquisition. The remaining 47 eyes that were included in the study were divided according to stage of glaucoma, as described in Table 7.1.

	Control (n=20)	Preperimetric glaucoma (n=5)	Early glaucoma (n=16)	Advanced glaucoma (n=6)
	mean \pm SD	mean \pm SD	mean \pm SD	mean \pm SD
Age (years)	56.25 \pm 8.91	65.20 \pm 5.27	68.81 \pm 10.22	69.45 \pm 12.85
Gender	9F : 11M	2F : 3M	10F : 6M	1F : 5M
MS (D)	-0.25 \pm 2.25	-1.75 \pm 4.50	1.25 \pm 2.50	1.75 \pm 1.25
VA (logMAR)	-0.12 \pm 0.06	0.02 \pm 0.09	0.08 \pm 0.18	0.16 \pm 0.21
IOP (mmHg)	13.15 \pm 2.95	11.20 \pm 1.17	13.09 \pm 1.69	12.28 \pm 1.25
CCT (μ m)	560.85 \pm 48.12	520.00 \pm 32.23	559.25 \pm 54.49	540.71 \pm 37.15
Axial length (mm)	23.88 \pm 1.01	24.12 \pm 2.59	23.12 \pm 1.20	23.37 \pm 1.02
ACD (mm)	2.81 \pm 0.33	3.11 \pm 0.35	3.23 \pm 0.93	2.72 \pm 0.23
MD (dB)	-0.21 \pm 1.85	-0.83 \pm 1.22	-3.75 \pm 1.72	-12.25 \pm 6.49

Table 7.1: Demographics for the eyes included in the present study. Abbreviations: MS, mean spherical refractive error; VA, visual acuity; IOP, intraocular pressure; CCT, central corneal thickness; ACD, anterior chamber depth; MD, mean deviation visual fields; F, female; M, male; SD, standard deviation.

7.2.2 Clinical assessments

Visual acuity, intraocular pressure and refractive error were determined for each eye to ensure compliance with the inclusion criteria, as described in section 2.2. Axial length was measured as a required factor for image scaling, and visual field tests were performed (SITA 24-2 Fast Threshold, Humphrey Visual Field Analyser) in order to classify the stage of glaucoma, where present.

7.2.3 Optical coherence tomography datasets and image processing

Ten degree scans centred on the ONH were acquired using enhanced depth imaging, and the image datasets were processed and scaled as described in section 2.4.4. Datasets were cropped in the enface direction from 50 μ m prior to the anterior LC surface, then averaged in blocks of 50 μ m. These averaged datasets were then divided into 12 clock-hour type regions using 'ONHseg' macro (version

1.0, N. White, VSBL, Cardiff University) in ImageJ (Figure 7.1). Lamina cribrosa beam coherence and preferred orientation were determined using 'OrientationJ' an ImageJ plugin (version 19.11.2012, R Resakhaniha *et. al*, Biomedical Imaging Group, EPFL, Sweden), as previously described in Rezakhaniha *et al.* (2012).

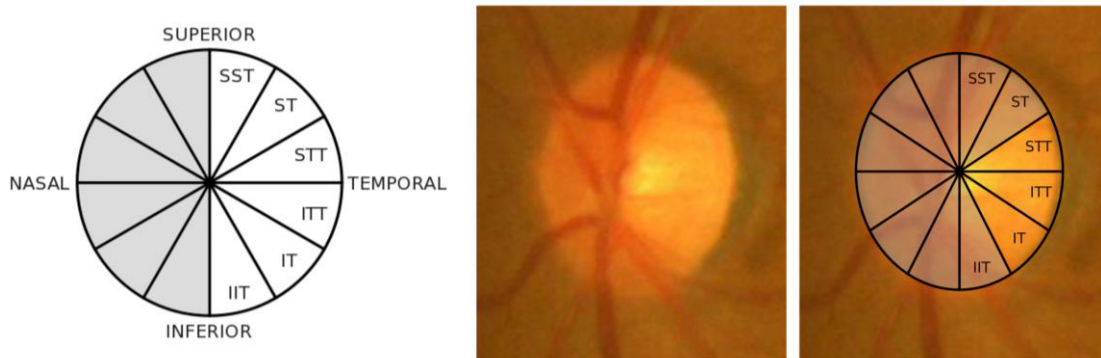


Figure 7.1: Schematic diagram of division of optic nerve head (ONH) regions of a left eye, with nasal side of the ONH in greyscale as the measurements were discarded due to vascular shadowing. (b) Fundus photo of optic nerve head with (c) grid overlay showing regional division. Additionally, in this example the SST, ST and IIT regions were greyed out due to blood vessels within the regions. S = superior; T = temporal; I = inferior. Image repeated from Figure 2.21.

Orientation was defined as the dominant direction of the features within a given region of interest, with an outcome value of between $\pm 90^\circ$. A result of 0° represented the horizontal x-axis, $+90^\circ$ was the vertical y-axis in the superior direction, and -90° depicted the inferior vertical meridian (Figure 7.2).

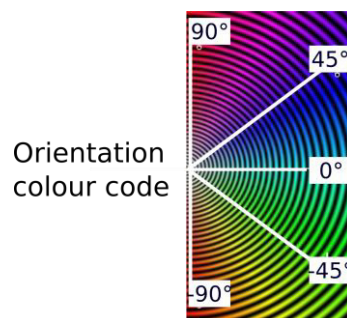


Figure 7.2: Colour code used to represent dominant orientation of LC beams in the OCT datasets.

Coherence was defined as how closely the features within an image were orientated. A coherence of 1 indicated a region where all features within an image were aligned in the same direction, and a

coherence of 0 indicated an image where the features were distributed randomly. Data from the nasal side of the ONH were discarded and temporal regions that contained either blood vessels or vascular shadowing were also excluded from analysis.

OrientationJ was also used to create colour-coded orientation coherence maps for each averaged section of LC to allow visualisation of the areas of the ONH with preferred orientation and higher connective tissue alignment. For the colour-coded maps a 300µm diameter area was considered to create the orientation or coherence colour for each pixel; this was to replicate the 300µm beam size used in the small angle light scattering study by Jones et al. (2015).

7.2.4 Statistical analysis

All statistical analyses were performed in RStudio (version 0.98.1091). LC beam orientation and coherence were examined for each dataset in relation to the depth into the LC, region, and stage of glaucoma. Due to the large inter-subject variability in baseline orientation, changes in orientation (Δ orientation) with respect to the slice above were also examined with respect to depth into ONH. Following the acquisition of data for regional connective tissue fibre orientation and coherence, the glaucoma stage or control status of each ONH (as previously determined in 2.4.6) was unmasked.

In order to determine regional differences in LC connective tissue orientation and coherence, data from each depth slice were considered separately for each glaucoma group and controls. Linear mixed-effects modelling (LMM) was used to determine whether there were regional differences between the 'clock-hour' segments at each depth, with the random (repeated measures) effect (*participant*) being used to account for the fact that data from both eyes were being used. Where regional differences were determined, the R package 'lsmeans' with Tukey post-hoc correction was used to determine within which regions the differences lay. Values were considered significant where $p < 0.01$ and a trend was determined where $p < 0.05$. Similarly, in order to investigate

differences in LC beam orientation and coherence with increasing depth into the LC, each region was considered separately and LMMs with subsequent Tukey post-hoc analysis were applied to discover if there were changes with increasing depth, and where those changes lay. Finally, to assess differences with respect to glaucoma, data were grouped according to region and differences in LC beam coherence and orientation were determined as previously stated. Data from all depths were grouped due to the limited differences with increasing depth.

7.3 Results

7.3.1 Visualisation of lamina cribrosa (LC) beam orientation and coherence in control and glaucoma

Colour-coded plots of LC beam orientation and coherence were created to visualise the data (Figure 7.3). Although there did appear to be depth-related differences in LC beam orientation and coherence, there did *not* appear to be consistent pockets of higher coherence in any particular region. The regional dominant LC beam orientation at each depth of the LC for control and each stage of glaucoma is shown in Table 7.2 while the regional coherence of the LC beams for control and each stage of glaucoma is shown in Table 7.3.

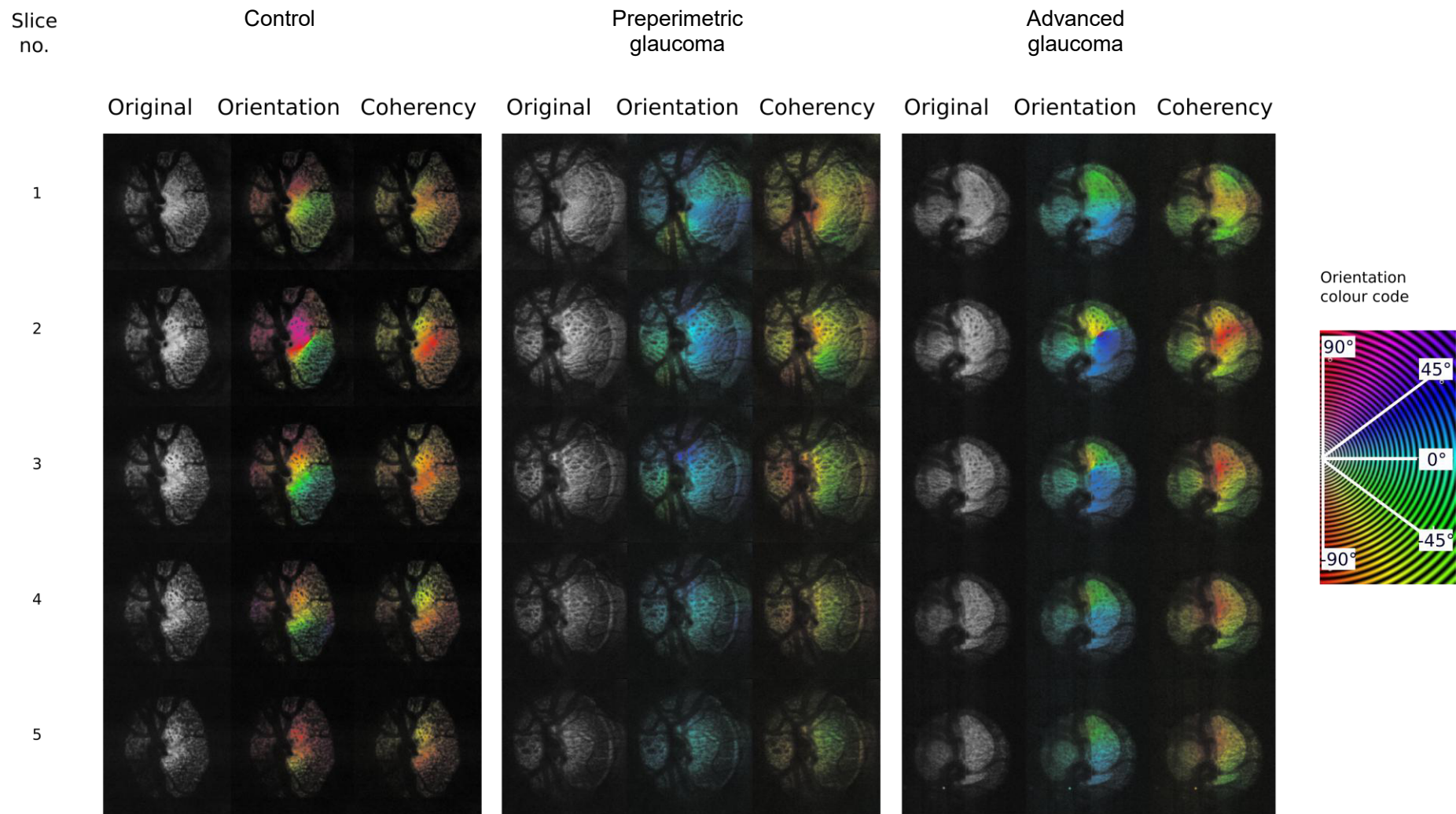


Figure 7.3: Examples of colour coded maps of lamina cribrosa (LC) beam orientation and coherence with increasing depth into the LC for control, early glaucoma and advanced glaucoma. Each slice is 50 μ m averaged.

Depth (slice)	SST orientation		ST orientation		STT orientation		ITT orientation		IT orientation		IIT orientation	
	mean	± SD	mean	± SD	mean	± SD	mean	± SD	mean	± SD	mean	± SD
C	1	10.73 ± 52.83	16.01 ± 62.53	-20.06 ± 31.04	-5.61 ± 42.97	-12.22 ± 46.35	25.12 ± 50.44					
	2	17.42 ± 48.60	24.96 ± 45.11	-11.97 ± 27.20	5.61 ± 34.65	-1.04 ± 39.46	27.36 ± 53.12					
	3	20.89 ± 42.28	11.51 ± 39.31	-12.90 ± 31.98	3.19 ± 43.74	12.82 ± 41.96	6.27 ± 57.60					
	4	-25.95 ± 42.81	-26.86 ± 45.20	-12.60 ± 39.03	8.80 ± 45.71	-16.95 ± 38.06	-27.61 ± 42.91					
	5	13.38 ± 53.27	-29.64 ± 45.01	-20.49 ± 42.66	9.00 ± 44.39	-14.90 ± 43.14	-17.22 ± 47.41					
	6	-35.96 ± 52.03	-8.54 ± 59.54	5.83 ± 50.80	-22.02 ± 44.31	-50.16 ± 40.40	5.43 ± 80.12					
PG	1	- -	-2.02 ± 4.58	-4.99 ± 7.00	8.50 ± 8.90	13.44 ± 17.33	9.62 ± 0.00					
	2	- -	-0.01 ± 22.01	-0.56 ± 3.00	23.89 ± 19.19	4.44 ± 37.99	10.76 ± 0.00					
	3	- -	-22.94 ± 37.66	0.68 ± 10.33	16.94 ± 11.78	7.50 ± 10.39	17.73 ± 0.00					
	4	- -	-27.78 ± 51.39	-3.04 ± 12.13	13.10 ± 17.81	0.21 ± 5.12	9.71 ± 0.00					
	5	- -	-11.37 ± 17.56	-4.63 ± 6.65	3.75 ± 12.05	3.20 ± 4.68	-3.39 ± 0.00					
	6	- -	- -	-10.52 ± 0.00	2.67 ± 0.00	2.47 ± 0.00	- -					
EG	1	-2.87 ± 6.54	17.61 ± 33.42	-1.49 ± 38.10	9.80 ± 28.14	-11.02 ± 32.11	3.27 ± 35.84					
	2	2.58 ± 12.52	8.60 ± 39.57	-16.41 ± 33.78	4.47 ± 34.71	-14.34 ± 30.43	-1.07 ± 39.71					
	3	-0.38 ± 14.21	12.74 ± 40.45	-1.55 ± 33.17	5.14 ± 39.56	2.72 ± 40.27	4.42 ± 39.80					
	4	4.20 ± 10.94	6.32 ± 41.13	4.02 ± 31.49	-2.31 ± 32.79	-15.95 ± 33.50	-8.03 ± 31.78					
	5	8.29 ± 10.66	2.99 ± 35.45	-2.18 ± 22.82	1.89 ± 25.79	7.67 ± 28.87	-3.16 ± 29.25					
	6	4.74 ± 6.94	-0.54 ± 8.71	0.71 ± 4.46	3.75 ± 3.83	2.83 ± 0.00	12.16 ± 16.82					
AG	1	-18.66 ± 6.24	-6.37 ± 28.69	3.52 ± 8.91	3.19 ± 28.63	-3.34 ± 14.48	9.17 ± 25.51					
	2	-20.70 ± 12.66	2.24 ± 11.05	8.88 ± 20.50	6.90 ± 35.23	0.97 ± 10.19	-3.78 ± 8.00					
	3	-25.88 ± 23.70	4.99 ± 35.40	13.94 ± 23.47	11.19 ± 35.13	-0.77 ± 10.48	17.31 ± 31.51					
	4	-21.51 ± 10.79	-16.68 ± 13.41	23.78 ± 37.93	27.76 ± 40.55	-1.90 ± 10.19	2.23 ± 6.38					
	5	-18.79 ± 9.98	-15.37 ± 14.20	-1.51 ± 2.52	2.99 ± 6.65	0.92 ± 7.24	0.86 ± 4.11					

Table 7.2: Dominant lamina cribrosa (LC) beam orientation for each optic nerve head (ONH) region at each depth in the ONH, for control (C) and each stage of glaucoma. For depth, each slice is at 50µm intervals into the LC. Where there is a “-” there was insufficient data available for that region at that depth, due to vascular shadowing from retinal blood vessels. Note that for AG there was no LC data at depth >250µm so no data for slice 6. Abbreviations: PG = preperimetric glaucoma; EG = early glaucoma; AG = advanced glaucoma; S = superior; T, = temporal; I, = inferior.

Depth (slice)	SST coherence		ST coherence		STT coherence		ITT coherence		IT coherence		IIT coherence	
	mean	± SD	mean	± SD	mean	± SD	mean	± SD	mean	± SD	mean	± SD
C	1	0.20 ± 0.10	0.15 ± 0.07	0.13 ± 0.07	0.15 ± 0.07	0.17 ± 0.06	0.20 ± 0.11					
	2	0.20 ± 0.12	0.16 ± 0.10	0.14 ± 0.10	0.16 ± 0.09	0.15 ± 0.07	0.19 ± 0.14					
	3	0.16 ± 0.11	0.14 ± 0.10	0.15 ± 0.09	0.14 ± 0.10	0.12 ± 0.07	0.24 ± 0.13					
	4	0.18 ± 0.06	0.17 ± 0.11	0.13 ± 0.10	0.14 ± 0.10	0.14 ± 0.09	0.24 ± 0.09					
	5	0.17 ± 0.08	0.18 ± 0.07	0.13 ± 0.10	0.15 ± 0.09	0.09 ± 0.05	0.20 ± 0.07					
	6	0.14 ± 0.04	0.19 ± 0.10	0.15 ± 0.12	0.14 ± 0.11	0.07 ± 0.03	0.20 ± 0.09					
PG	1	- -	0.27 ± 0.13	0.18 ± 0.05	0.20 ± 0.10	0.22 ± 0.14	0.36 -					
	2	- -	0.29 ± 0.02	0.17 ± 0.04	0.17 ± 0.10	0.22 ± 0.16	0.38 -					
	3	- -	0.23 ± 0.12	0.14 ± 0.09	0.19 ± 0.11	0.17 ± 0.08	0.28 -					
	4	- -	0.18 ± 0.11	0.13 ± 0.08	0.20 ± 0.12	0.23 ± 0.09	0.24 -					
	5	- -	0.15 ± 0.15	0.15 ± 0.08	0.18 ± 0.07	0.23 ± 0.08	0.27 -					
	6	- -	- -	0.20 ± 0.00	0.29 ± 0.00	0.19 ± 0.00	- -					
EG	1	0.28 ± 0.12	0.22 ± 0.08	0.18 ± 0.06	0.15 ± 0.09	0.17 ± 0.07	0.21 ± 0.10					
	2	0.24 ± 0.12	0.21 ± 0.11	0.16 ± 0.05	0.17 ± 0.08	0.19 ± 0.10	0.24 ± 0.14					
	3	0.25 ± 0.17	0.25 ± 0.07	0.17 ± 0.07	0.17 ± 0.08	0.19 ± 0.12	0.21 ± 0.11					
	4	0.24 ± 0.13	0.19 ± 0.08	0.17 ± 0.07	0.18 ± 0.07	0.19 ± 0.08	0.19 ± 0.08					
	5	0.24 ± 0.07	0.21 ± 0.10	0.17 ± 0.04	0.19 ± 0.07	0.16 ± 0.10	0.19 ± 0.08					
	6	0.21 ± 0.15	0.25 ± 0.17	0.11 ± 0.03	0.24 ± 0.11	0.07 ± 0.00	0.19 ± 0.06					
AG	1	0.35 ± 0.11	0.23 ± 0.05	0.16 ± 0.07	0.20 ± 0.09	0.30 ± 0.11	0.40 ± 0.16					
	2	0.34 ± 0.18	0.38 ± 0.01	0.18 ± 0.04	0.21 ± 0.05	0.29 ± 0.06	0.33 ± 0.11					
	3	0.27 ± 0.17	0.20 ± 0.04	0.20 ± 0.04	0.19 ± 0.05	0.26 ± 0.05	0.23 ± 0.08					
	4	0.27 ± 0.14	0.21 ± 0.07	0.16 ± 0.02	0.23 ± 0.08	0.22 ± 0.06	0.32 ± 0.04					
	5	0.25 ± 0.11	0.24 ± 0.05	0.24 ± 0.05	0.28 ± 0.02	0.25 ± 0.05	0.28 ± 0.02					

Table 7.3: Lamina cribrosa (LC) beam coherence for each optic nerve head (ONH) region at each depth in the ONH, for control (C) and each stage of glaucoma. For depth, each slice is at 50µm intervals into the LC. Where there is a “-” there was insufficient data available for that region at that depth, due to vascular shadowing from retinal blood vessels. Note that for AG there was no LC data at depth >250µm so no data for slice 6. Abbreviations: PG = preperimetric glaucoma; EG = early glaucoma; AG = advanced glaucoma; S = superior; T = temporal; I = inferior.

7.3.2 Regional differences within the lamina cribrosa beam orientation in control and glaucoma

There were no significant differences in the orientation of lamina cribrosa beams between regions at each depth within the ONH, in control eyes or in any of the glaucoma groups.

7.3.3 Regional differences within the lamina cribrosa beam coherence

In control eyes the LC beams were found to have higher coherence, i.e. better alignment, in the IIT region than STT and ITT in slice 2 (IIT > STT $p=0.017$; IIT > ITT $p=0.026$; see Table 7.3), although this did not quite reach statistical significance at $p<0.01$. In slice 6, deeper within the ONH, LC beams

showed a trend to be more aligned in the SST region than both ST and ITT (SST > ST $p=0.018$; SST > ITT $p=0.034$).

In eyes with preperimetric glaucoma there were no significant differences in LC beam coherence between regions at equal depth within the ONH ($p>0.01$). LC beams in eyes with early glaucoma had significantly higher coherence in the SST region (slice 2, 0.24 ± 0.12 ; slice 3, 0.25 ± 0.17) than the STT (slice 2 0.16 ± 0.05 , $p=0.004$; slice 3 0.17 ± 0.07 , $p=0.007$), and higher in SST than the ITT region in slice 2 (0.17 ± 0.08 , $p=0.025$), although this did not quite reach statistical significance.

In slice 1 of eyes with advanced glaucoma, ITT regions had significantly higher LC beam coherence (0.40 ± 0.16) than the STT region (0.16 ± 0.07 , $p=0.001$), and showed a trend in the ST (0.23 ± 0.05 , $p=0.014$) and ITT regions (0.20 ± 0.09 , $p=0.011$). The STT region also had LC beams that were less coherent than in the SST region (0.35 ± 0.11 , $p=0.013$), although this did not quite reach significance at $p<0.01$. A summary of the regional differences in LC beam coherence is shown below (Figure 7.4).

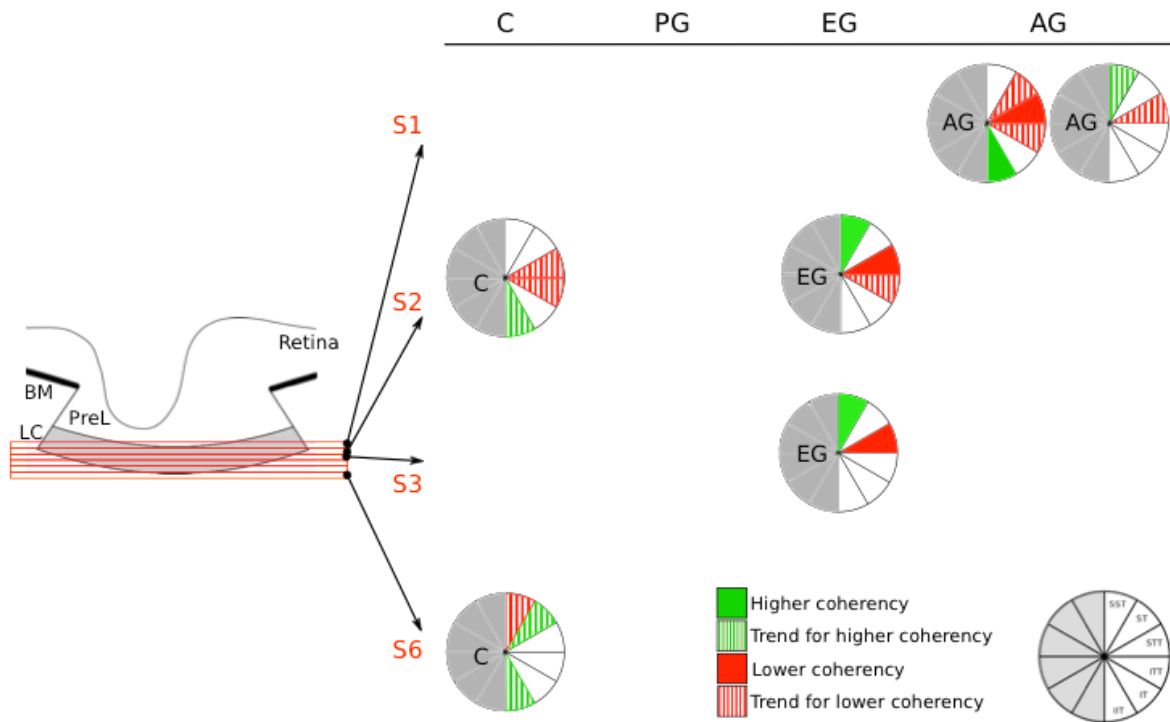


Figure 7.4: Summary of differences in regional lamina cribrosa (LC) beam coherence in the optic nerve head (ONH). Averaged data from 50µm sections (S) at increasing depth into the ONH were analysed in control (C), preperimetric glaucoma (PG), early glaucoma (EG) and advanced glaucoma (AG). Regions highlighted green had higher coherence than regions highlighted red at specified depths in the ONH. Solid colour indicates a significant difference ($p < 0.05$) and striped colour indicates a trend ($p < 0.05$). BM = Bruch’s membrane, PreL = prelamina.

7.3.4 Differences within lamina cribrosa beam orientation at increasing depth

Regional LC beam orientation and changes in orientation with increasing depth into the LC for control and each stage of glaucoma are shown in Figure 7.5. In control eyes and in each stage of glaucoma there were no significant differences in the orientation of LC beams with increasing depth into the LC ($p > 0.01$).

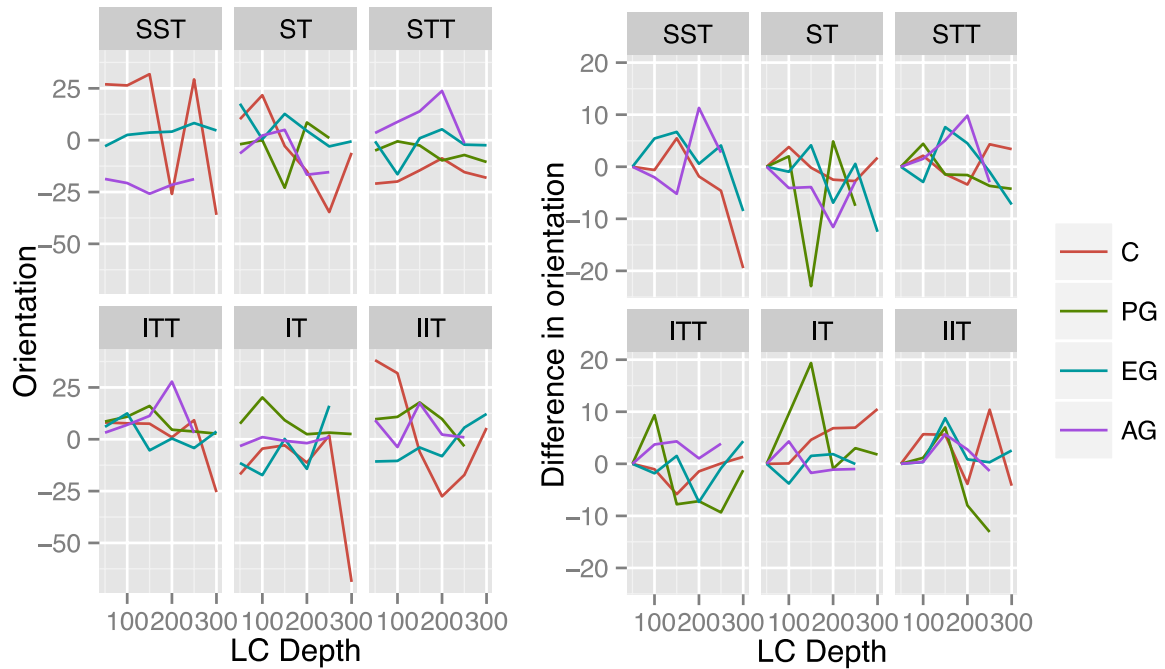


Figure 7.5: Regional lamina cribrosa (LC) beam orientation and change in orientation for each stage of glaucoma with increasing depth into the LC. Each LC depth is the block average of 50 μ m. C = control, PG = preperimetric glaucoma, EG = early glaucoma, AG = advanced glaucoma. S = superior, T = temporal, I = inferior.

7.3.5 Differences in lamina cribrosa beam coherence with increasing depth in the optic nerve head in control and glaucoma

Regional LC beam coherence and changes in coherence for increasing depth into the LC for control and each stage of glaucoma are shown in Figure 7.6.

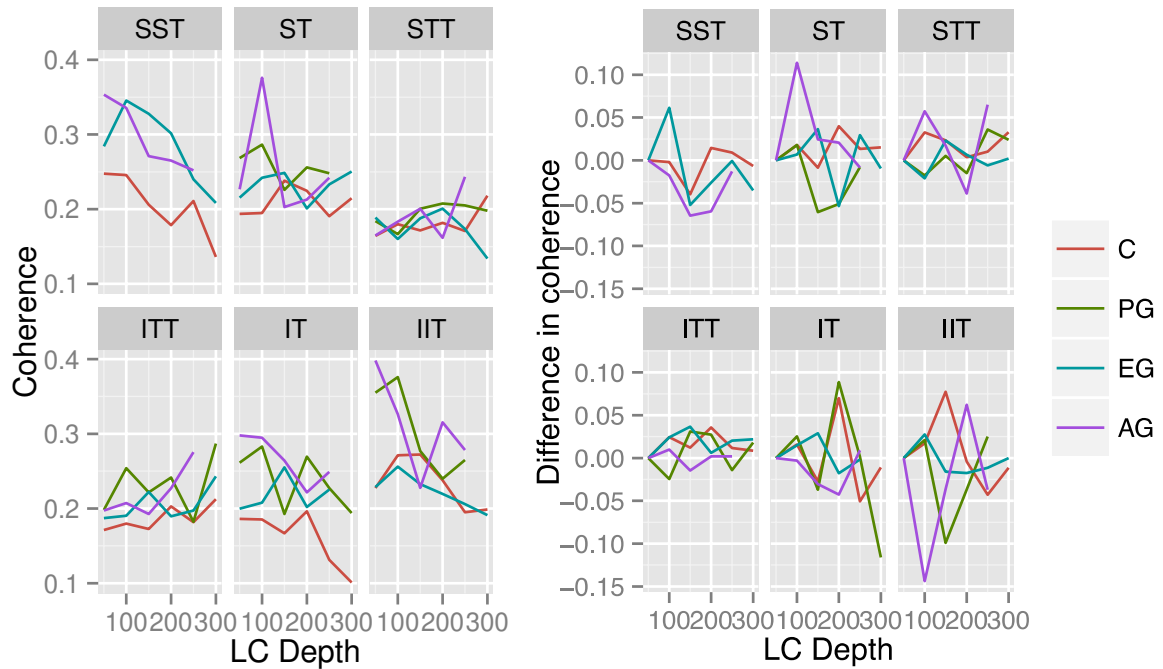


Figure 7.6: Regional lamina cribrosa (LC) beam coherence and change in coherence for each stage of glaucoma with increasing depth into the LC. Each LC depth is the block average of 50µm. C = control, PG = preperimetric glaucoma, EG = early glaucoma, AG = advanced glaucoma, S = superior, T = temporal, I = inferior.

In eyes with advanced glaucoma the LC beams showed a trend to be more coherent, or more closely organised, in slice 2 of the ST region (0.38 ± 0.01) than in slice 1 (0.23 ± 0.05 , $p=0.050$), slice 3 (0.20 ± 0.04 , $p=0.011$), slice 4 (0.21 ± 0.07 , $p=0.017$) and slice 5 (0.24 ± 0.05 , $p=0.025$; Figure 7.7).

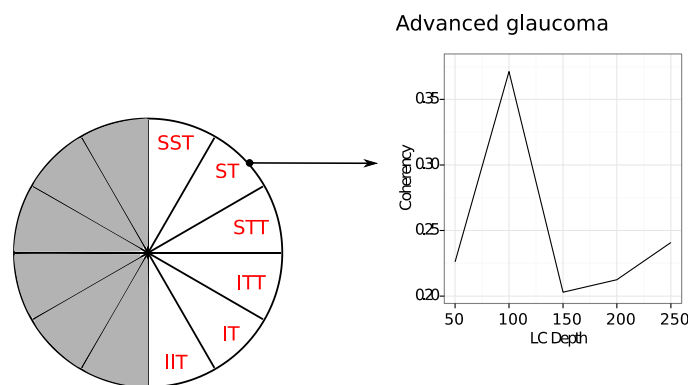


Figure 7.7: Regional differences in lamina cribrosa (LC) beam coherence with increasing depth in the optic nerve head were observed in eyes with advanced glaucoma. Depth is shown in terms of 50µm slices. S = superior, T = temporal, I = inferior.

7.3.6 Differences in lamina cribrosa beam orientation at different stages of glaucoma

In the STT region the average LC beam orientation showed a trend to be higher in the eyes with advanced glaucoma compared to the healthy control group ($p=0.035$; Figure 7.8), although this did not reach statistical significance.

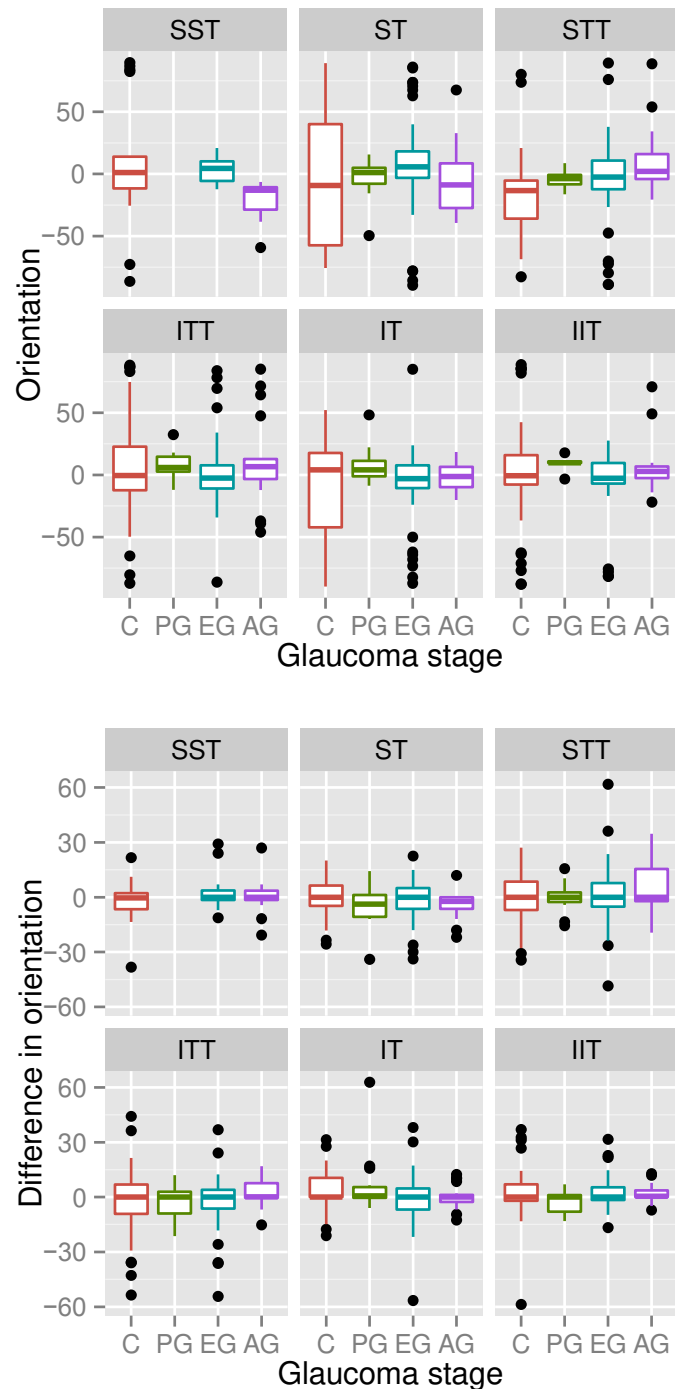


Figure 7.8: Regional lamina cribrosa (LC) beam orientation and difference in orientation for each stage of glaucoma, with outliers represented by black spots. C = control, PG = preperimetric glaucoma, EG = early glaucoma, AG = advanced glaucoma, S = superior, T = temporal, I = inferior.

7.3.7 Differences in lamina cribrosa beam coherence between control and each stage of glaucoma

There were no significant differences in regional LC beam coherence between control and any stage of glaucoma ($p > 0.01$, Figure 7.9). However the advanced glaucoma group showed a trend towards higher coherency in the IT region ($p = 0.047$) compared to the control group.

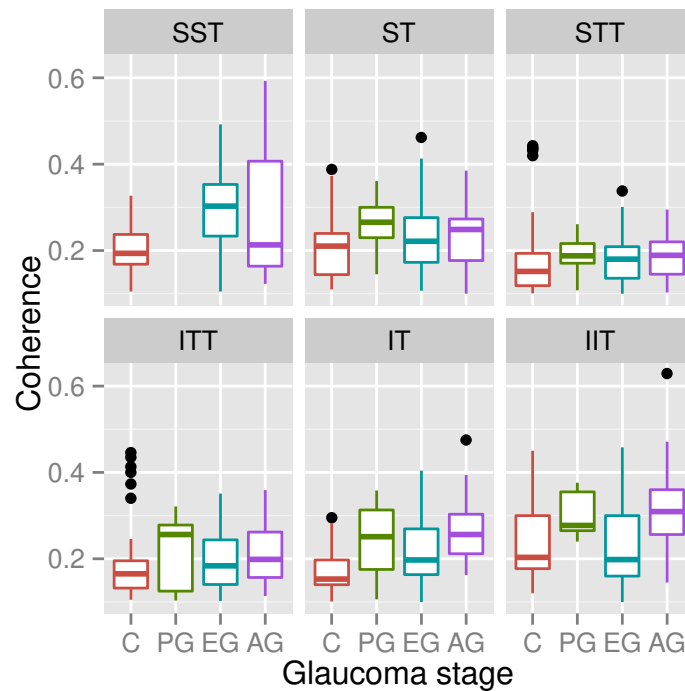


Figure 7.9: Regional lamina cribrosa (LC) beam coherence for each stage of glaucoma, with outliers represented by black spots. There were no significant differences between stages of glaucoma for any region of the LC. C = control, PG = preperimetric glaucoma, EG = early glaucoma, AG = advanced glaucoma, S = superior, T = temporal, I = inferior.

7.3.8 Summary of significant results

The key findings from this study are as follows:

- LC beam coherence was higher in superior and inferior regions than in temporal regions in early and advanced glaucoma.
- There were no significant differences in LC beam coherence or orientation with increasing depth into the LC.

- There were no significant differences in LC beam coherence of orientation between control and glaucoma groups.

7.4 Discussion

The primary aim of this study was to investigate differences in lamina cribrosa (LC) beam coherence and orientation with respect to region, depth within the LC and stage of glaucoma. Regional differences were determined in LC beam coherence in control, early glaucoma and advanced glaucoma, while trends were observed in preperimetric glaucoma. Furthermore, LC beam orientation showed regional differences in preperimetric glaucoma and there were differences with increasing depth into the LC in control eyes. Finally, eyes with advanced glaucoma had LC beams with different orientation in the STT region than control eyes and higher coherence in the IT region compared to control eyes, although these did not quite reach statistical significance.

The inferior and superior poles of the LC are known to contain larger pores and thinner connective tissue than the nasal and the temporal poles (Quigley and Addicks 1981; Radius and Gonzales 1981). The latter is consistent with backwards bowing of the LC as glaucoma advances, more pronounced in the superior and inferior poles (Quigley et al. 1983). More recently, Winkler et al. (2010) determined that the density of collagen was lower in the IT region compared to other regions. It is also proposed that glaucomatous damage to the ONH tends to occur in the IT region first, e.g. focal LC defects or acquired pits of the optic nerve (APONs; Ugurlu et al. 1998; Kiumehr et al. 2012), while greater glaucomatous loss of the neuroretinal rim in the inferior-temporal quadrant has been reported (Jonas et al. 1993; Garway-Heath et al. 1997). The greater level of glaucomatous damage in the inferior-temporal region could be linked to the regional differences in coherence and orientation described in the present study. As IOP increases, there is increased stress on the LC which could induce cell activation, causing remodelling in that region (Yang et al. 2011).

To date there has been limited research done into regional orientation and coherence of beams in the LC in humans, although some work has been done in monkeys (Roberts et al. 2009; Roberts et al. 2010) where considerable regional variation was discovered and an increase in connective tissue volume in early disease was presented. As described previously, the LC is composed of cribriform sheets which form a sieve-like structure that contains pores through which RGC axons pass as they leave the eye. In the past few years technological advances such as adaptive optics have enabled improvements in OCT, SLO and imaging to the point where it is possible to now image and characterise these pores in vivo (Ivers et al. 2011; Lee et al. 2011; Niles et al. 2012). Indeed, Wang et al. (2013) was able to characterise LC pore counts, pore diameter and aspect ratio, as well as LC beam thickness, and found both an increase in LC beam diameter and a decrease in LC pore diameter, when correlated with increasing visual field loss. This suggests that the worsening of glaucomatous disease leads to LC remodelling, which leads to the increase in beam thickness (relating to the pore diameter). Although studies have not yet described LC pore orientation in vivo, there is potential for researchers using devices with enough resolution to begin to investigate LC pores to instead assess LC beam orientation using the same methods.

This premise of the approach taken in this chapter stems from the recent findings of Jones et al. (2015), who, using small angle light scattering in ex vivo human eyes, reported regions of higher CT coherence in the inferior-temporal quadrant of elderly LC compared to young LC, which were further increased with glaucoma. In the present study, LC beams were found to be more aligned in the inferior and superior regions when compared to temporal regions in both control eyes and those with glaucoma. This was particularly apparent in the more anterior slices of eyes with latter stages of glaucoma. One theory is that those regions of increased coherence in the inferior regions of control eyes are more susceptible to IOP-related stress due to their increased alignment. As a result, in these regions, the LC may be less flexible, in turn causing less outwards bowing, which would cause damage to retinal ganglion cell (RGC) axons.

No significant changes in beam coherence with increasing depth into the LC were observed in the present study, although there was a trend for the LC beams in the ST region to have higher coherency than other regions in eyes with advanced glaucoma. Additionally, as described above, eyes with advanced glaucoma showed significantly different LC beam orientation in the IIT and ST regions compared to other regions, and there was a trend for the IT regions to have more coherence in advanced glaucoma compared to control eyes.

The above results suggest that the inferior-temporal quadrant is structurally different to the superior-temporal quadrant. Although the pockets of high beam alignment described by Jones et al. (2015) were not apparent in the current data using 1050nm OCT, there were still orientation and coherence differences in that region compared to others.

7.4.1 Limitations of study

One of the major obstacles of this work was the presence of retinal blood vessels. Previous work in this area is limited, and the majority of existing literature describes techniques performed on ex vivo eyes. Indeed, this study is the first to attempt to recreate these results in in vivo eyes and while this could give interesting insight into changes in the LC beam structure with glaucoma, vascular shadows are currently a major problem. This issue meant that all data from the nasal side of the ONH was discarded immediately after collection, and the remaining data from the temporal LC were carefully examined in order to filter out regions that contained blood vessels or vascular shadows prior to analysis. The regions that had to be most often removed due to vascular shadows were the SST and IIT regions, i.e. those closest to the nasal side of the LC. As an example, of the 47 eyes available 41 were able to have data measured from the STT region, whereas only 11 had visible and useable data in the SST region.

Another limiting factor in this work is the resolution of the OCT device. 10° OCT scans were acquired, which provided a transverse pixel calibration of 5-6 $\mu\text{m}/\text{pixel}$. Given that LC beams have been found to be average $38.1 \pm 1.4 \mu\text{m}$ when viewed in the transverse direction this resolution should be sufficient, however, in an *ex vivo* scanning electron microscopy study, pores in the LC have been reported to have diameter of 10-100 μm (Quigley and Addicks 1981), and so resolving such fine detail in OCT images is made more difficult.

Finally, 10 of the datasets acquired for this study had to be discarded due to poor image quality, mostly due to eye movements during image acquisition. Unlike some of the commercial OCT devices currently available, there is no eye-tracker on the OCT device used in this work. If this technology was available, it is likely fewer datasets would have had to be omitted, which would in turn result in greater numbers and a higher probability of arriving at statistically powerful conclusions.

There is considerable scope for this work to be improved, particularly if vascular shadows could accurately be removed from the OCT images. Although there has been some progression in this area of research (e.g. Girard et al. 2011), as yet the published image analysis algorithms have not been able to make effective inroads into data acquired from the 1050nm OCT device used in this study. Further work, with increased sample size and improvements such as eye tracking and adaptive optics would not only provide more data but would also allow for the analysis of data from the nasal side of the ONH.

6.4.3 Conclusion

Differences have been identified in LC beam coherence and orientation in the inferior-temporal region of the optic nerve head. Although the resolution is not equivalent to that acquired from *ex vivo* imaging, there is sufficient evidence to suggest that the inferior-temporal region is important in

explaining structural changes in the LC, however, further work is required to understand the biomechanics and pathology related to these changes.

Chapter 8:

General discussion

8 Discussion

Glaucoma is a progressive optic neuropathy that causes irreversible vision loss and is the second leading cause of blindness worldwide (Quigley and Broman 2006; Quigley 2011). Glaucoma is characterised by loss of retinal ganglion cells (RGC) and the proposed site of damage is the lamina cribrosa (LC; Minckler 1989; Bellezza et al. 2003), where RGC axonal transport is disrupted, causing subsequent RGC damage and, in turn cell death. Currently, clinical detection of primary open angle glaucoma (POAG) is based upon optic disc changes, visual field loss and an increase in intraocular pressure (IOP; Anderson 2006). Therefore, typically the first time glaucoma is suspected is during a routine eye examination by an optometrist. Subsequently, when detected, a patient is then assessed by an ophthalmologist and there are then several options: the diagnosis is confirmed and the patient is offered treatment; the diagnosis is a different pathology, which is subsequently treated; the eye is healthy and no treatment is required; or the eye is monitored over time to confirm the diagnosis. As the diagnosis of glaucoma is often based on changes during the early stages of the disease, it follows that an observable change is needed to occur before a diagnosis can be confirmed.

It is thought that up to 35% of retinal ganglion cells are required to be affected before there is a detectable visual field loss using perimetry (Kerrigan-Baumrind et al. 2000). Additionally, up to a third of patients with POAG do not initially present with raised IOP (Klein et al. 1992), while only 10% of those with IOP above the recommended 21mmHg (NICE Guidelines 2009) actually have glaucoma (Tielsch et al. 1991). Optic nerve head changes, such as enlargement of the optic cup and notching of the neuroretinal rim (Jonas et al. 1993; Jonas et al. 1999) indicate that RGC loss has already occurred and as glaucomatous damage is irreversible, with current treatments, any vision loss that had transpired up to that point, is permanent. Thus, the ability to diagnose glaucoma at its earliest stages is critical to effective treatment and minimising damage.

Since the introduction of optical coherence tomography (OCT), there have been a number of optical parameters that have shown differences between eyes with glaucoma and healthy control eyes. These include an increase in anterior LC surface depth (Park and Ritch 2011) and changes to the macula ganglion cell complex (consisting of the nerve fibre layer, ganglion cell layer, and inner plexiform layer combined; (Arintawati et al. 2013)). However, not all OCT devices have the capability to classify specific ocular parameters and furthermore, not all published literature is in agreement as to which parameters are worth assessing, e.g. the LC has been shown to become thinner with glaucoma (Lee et al. 2012; Park et al. 2012) whereas other groups have reported LC remodelling as a result of glaucomatous damage, leading to LC thickness *increasing* (Bellezza et al. 2003; Yang et al. 2011). The use of OCT is becoming much more widespread in clinical practice and, as such, a comprehensive investigation into the structural changes that occur, particularly within the ONH and macula, is warranted in order to determine what, if any, parameters can be used as a biomarker of early glaucoma in order to ensure treatment at the earliest stage as well as to determine which optic discs are at risk of disease progression.

As such, the aim of this project was to characterise any structural alterations in the optic nerve head (ONH) and macula that result from glaucoma, in order to identify biomarkers for the earliest stages of the disease.

The specific aims are listed below and will be considered sequentially:

1. *To quantify regional thickness and volume measurements of the inner retinal layers in 3D OCT image datasets of maculae measured at different stages of glaucoma severity, in order to identify a measure of RGC integrity that can be used as a biomarker of early stage glaucomatous disease.*

This first aim was addressed in Chapter 3. In this chapter the thickness and volume of the macula nerve fibre layer (mNFL), ganglion cell layer (GCL) and inner plexiform layer (IPL) were investigated at different stages of glaucoma in order to indirectly determine changes in RGC axons, cell bodies and dendrites, respectively. Previously unreported thinning in the GCL of preperimetric glaucoma patients, in the IPL of early glaucoma patients, and a trend for thickening of the IPL in more advanced glaucoma were discovered. There was also a trend for the GCL to become thicker in advanced glaucoma, although this did not quite reach statistical significance. It is likely that these changes correspond to RGC apoptosis (Quigley et al. 1995), dendritic shrinkage (Weber et al. 1998; Shou et al. 2003; Liu et al. 2010), and remodelling (Weber et al. 1998; Morgan et al. 2006), respectively. These data suggest that the GCL becomes thinner in preperimetric glaucoma, i.e. as a result of RGC cell body shrinkage and death. In turn, the IPL becomes thinner in early glaucoma, i.e. as a result of dendritic shrinkage, while in advanced glaucoma, both layers become thicker (IPL significantly thicker), presumably as a result of RGC remodelling.

Another point of note is the difference between preperimetric and early glaucoma. Eyes with preperimetric glaucoma were found to have ONH changes but no visual field loss, whereas eyes with early glaucoma exhibited early visual field loss. It is interesting to note that there were changes in GCL but they *did not* affect vision however, once the IPL started to thin, i.e. as a result of RGC dendritic changes, there *were* changes in functional vision, perhaps as RGC dendrites were no longer connected with the midretinal cells situated downstream of them in the visual pathway.

The use of the ratio of IPL to GCL thickness was implemented as a way of overcoming, to a degree, the issue of biological variance in the thickness of the inner retinal layers. The IPL:GCL ratio could therefore potentially be a useful biomarker for determining very early stages of glaucoma, before vision loss occurs. In this study, the ratio of IPL to GCL thickness was shown to be larger in eyes with

preperimetric glaucoma (0.96 ± 0.17) than control eyes (0.76 ± 0.11), presumably due to the differing rates at which the IPL and GCL change in response to the causes of glaucoma.

2. *To identify if ONH microstructural parameters alter with age, a major risk factor for glaucoma, and if changes are present to identify whether they are region specific*

The second aim was addressed in Chapter 4. In this chapter, Bruch's membrane opening (BMO) diameter, prelamina depth and thickness, LC depth (and thickness) and nerve fibre layer thickness were investigated in order to determine changes with respect to age, as well as assessing the contribution to changes of other ocular parameters (e.g. axial length and corneal thickness). Significant changes in BMO, the LC, prelamina and peripapillary NFL (pNFL) were observed. Briefly, the BMO diameter in the superior-inferior and ST-IN directions was found to decrease with increasing age, the LC the anterior surface depth showed no significant changes with increasing age, while the posterior LC depth decreased with increasing age and there was a corresponding decrease in LC thickness in regions on the temporal side of the ONH (Figure 8.1). These observations suggest that with increasing age in the healthy eye, the position of the anterior LC surface doesn't change (unlike the backwards bowing that is reported in glaucoma) but the posterior LC surface was closer to the anterior surface, with subsequent LC thinning. However, this could also be an artefact as a function of OCT signal attenuation with increasing age, and so not correspond to actual thinning of the LC. However, in the superior-temporal region, the prelamina depth decreased and the prelamina thickness increased with age.

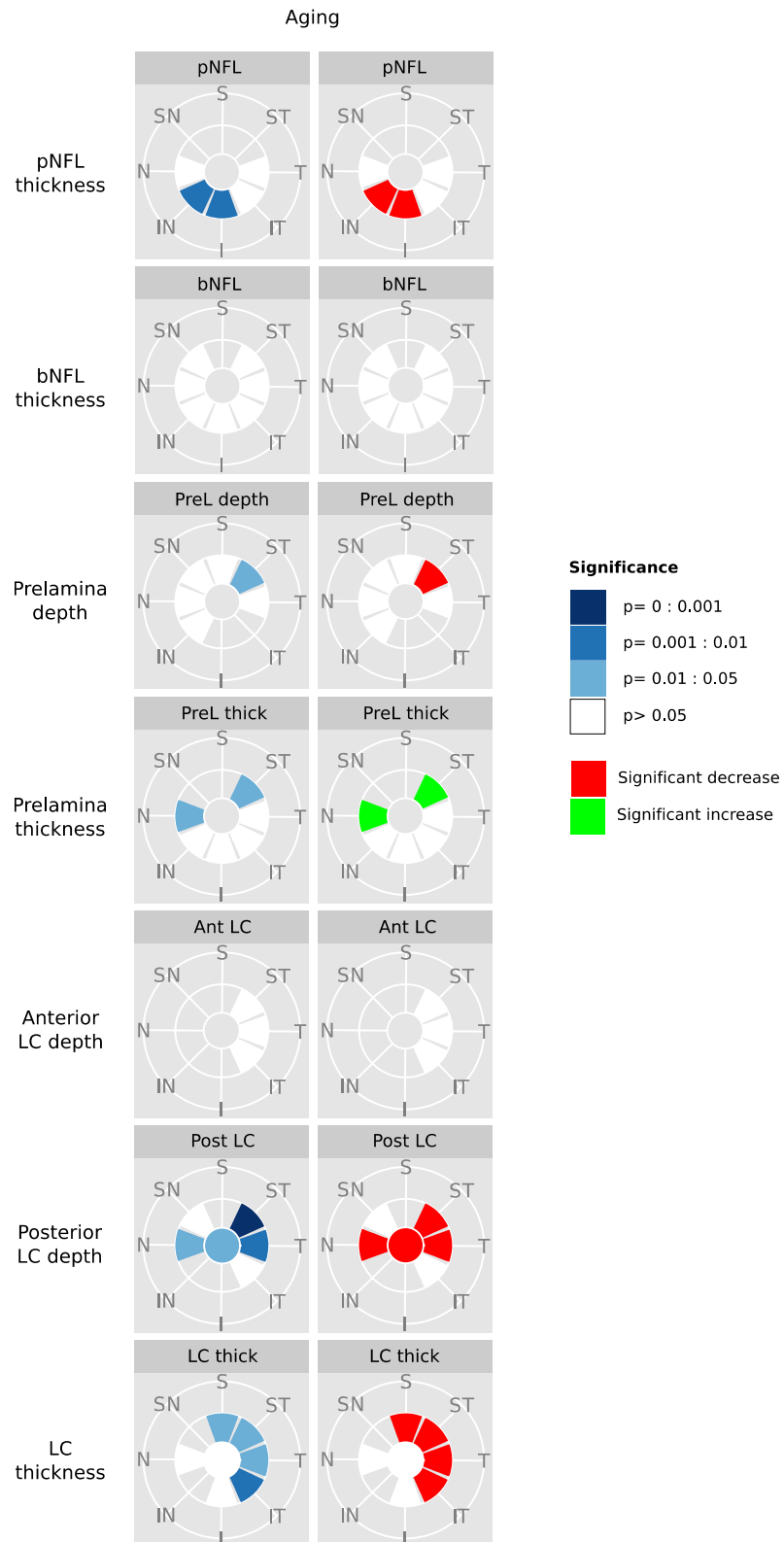


Figure 8.1: Regions of the optic nerve head that were affected as a function of age, using general linear models (GLM). pNFL = peripapillary nerve fibre layer, bNFL = border nerve fibre layer, PreL depth = prelamina depth, PreL thick = prelamina thickness, Ant LC = anterior lamina cribrosa (LC) depth, Post LC = posterior LC depth, LC thick = LC thickness, T = temporal, ST = superior-temporal, S = superior, SN = superior-nasal, N = nasal, IN = inferior-nasal, I = inferior, IT = inferior-temporal. Blue indicates a significant contribution to the GLM, white indicates that age was part of the GLM but not significant. Green t-values = positive effect, red t-values = negative effect.

As part of normal aging, the connective tissue content of the LC changes. An increase in the amount of collagen (Hernandez et al. 1987; Hernandez et al. 1989; Morrison et al. 1989; Albon et al. 1995) causes an increase in the relative stiffness of the LC in older eyes (Albon et al. 2000). Despite this being a study on aging, the oldest eye included was 68 years, and the mean age of the cohort 34 years. As such, it may be the case that some of the changes in the LC observed in this study were a normal part of the aging process (i.e. the anterior LC surface not showing any backwards displacement with increased age due to increased stiffness), whereas others, i.e. posterior LC surface decreasing in depth with age, represented changes from eyes that were older than the mean, but not old enough to be considered elderly.

Additionally, the thickness of the pNFL was shown to decrease with age in the inferior and inferior-nasal regions, which corresponds to reported age-related RGC loss (Dolman et al. 1980; Johnson et al. 1987; Mikelberg et al. 1989; Moya et al. 1999). Finally, the changes at the ONH in this chapter were all determined using statistical modelling that accounted for other ocular parameters. The axial length and refractive error of an eye both contributed to changes in the aging eye, and the importance of including other ocular parameters when assessing changes in the eye was discussed.

3. *To identify those microstructural changes that occur in the ONH at different glaucoma disease stages, i.e. preperimetric, early and advanced glaucoma and to subsequently determine which of those factors best explain the observed changes.*

This third aim was addressed in Chapter 5. In this chapter, regional differences in nerve fibre layer thickness, prelamina depth and thickness, anterior LC depth, and LC thickness were assessed. The differences in preperimetric and early glaucoma compared to control are summarised in (Figure 8.3). In preperimetric glaucoma the pNFL and prelamina became thinner and the prelamina depth increased. Both the prelamina and pNFL consist of RGC axons, and these changes indicate that the

earliest detectable changes in glaucoma are the result of RGC axon loss. In early glaucoma there was a progression in prelamina depth increase and prelamina thinning with more regions affected. Agoumi et al. (2011) reported compression of the prelamina immediately following experimental IOP elevation in human eyes. It is also interesting to note that there was significant bNFL thinning in all regions except nasal and inferior-nasal in early glaucoma compared to control but no changes in preperimetric glaucoma compared to control. Eyes with preperimetric glaucoma, by definition, have no vision loss, whereas eyes with early glaucoma had early visual field changes. Perhaps one explanation is that by the time vision loss occurs, there is sufficient RGC loss to be detected at the bNFL.

There were no significant changes in the LC with preperimetric glaucoma, and few in early glaucoma. Central and nasal LC was thinner in early glaucoma compared to control, and the anterior LC depth was greater, indicating that in the earliest stages of glaucoma, the prelamina is affected first. The posterior LC depth decreased with age, causing the LC to become thinner. In preperimetric and early glaucoma there were no changes in the posterior LC depth. However, as the LC is known to become stiffer with age (Albon et al. 2000), it may be that if the glaucomatous eyes had stiffer LCs such a change in IOP would cause more changes, instead, in the peripapillary sclera, pulling the LC taut but not affecting the thickness and the extra strain on the LC is what caused RGC axonal damage.

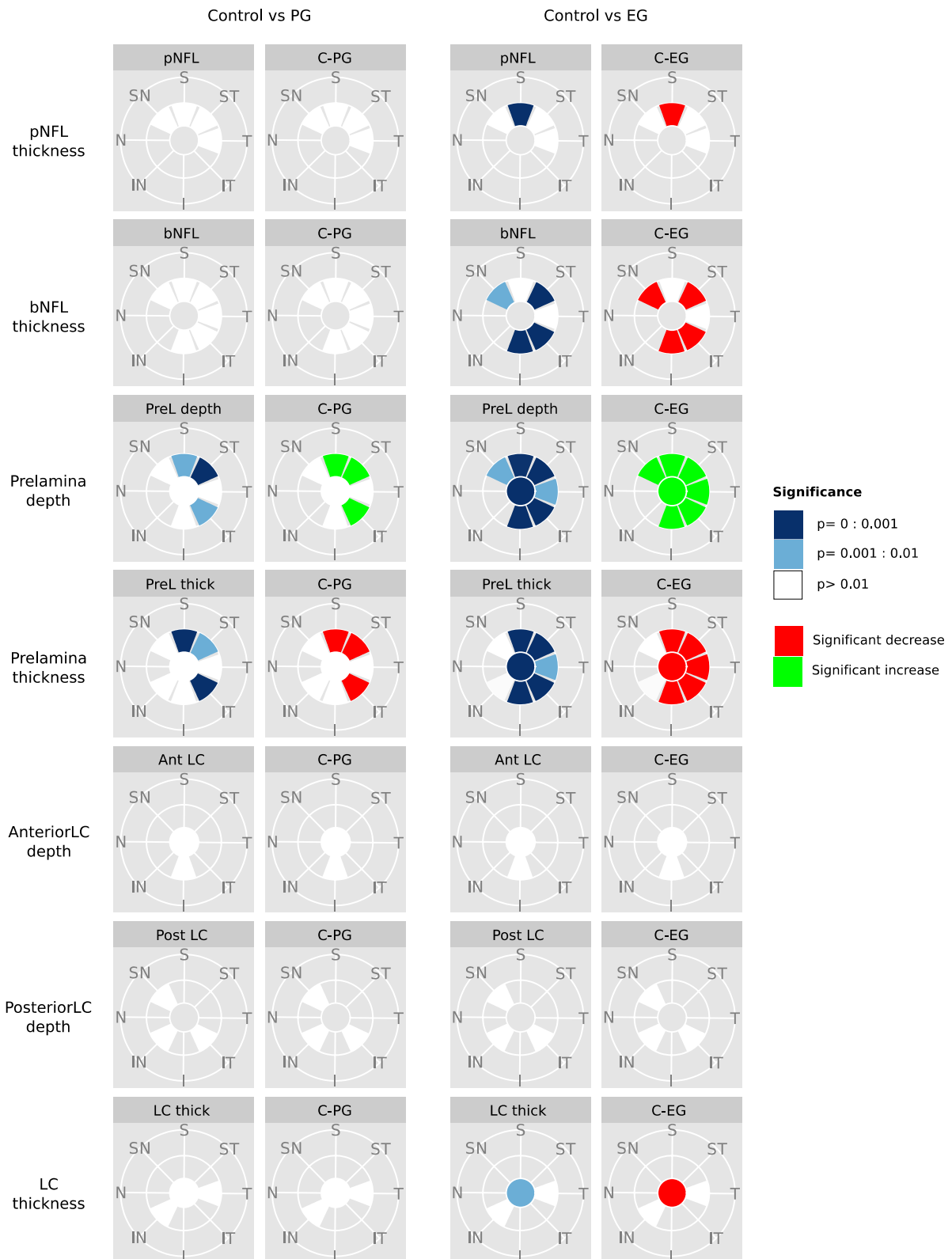


Figure 8.2: Difference between control and preperimetric glaucoma (PG) and early glaucoma (EG) using linear mixed-effects models (LMM). pNFL = peripapillary nerve fibre layer, bNFL = border nerve fibre layer, PreL depth = prelamina depth, PreL thick = prelamina thickness, Ant LC = anterior lamina cribrosa (LC) depth, Post LC = posterior LC depth, LC thick = LC thickness, T = temporal, ST = superior-temporal, S = superior, SN = superior-nasal, N = nasal, IN = inferior-nasal, I = inferior, IT = inferior-temporal. Blue indicates a significant contribution to the GLM, white indicates that *stage of glaucoma* was part of the LLM but not significant, grey indicates that *stage of glaucoma* was not a factor in the optimised LMM.

Sigal et al. (2011) have summarised this relationship between peripapillary sclera and LC using the diagram below (Figure 8.3). If the peripapillary sclera was compliant, then an increase in IOP would lead to posterior displacement of the sclera and expansion of the scleral canal, and the LC would be pulled taut. If the peripapillary sclera was stiff, an increase in IOP would not displace the sclera, the sclera canal would not increase and the LC would displace under the increase in pressure. However, Sigal et al. (2011) also found that under some conditions the LC depth and scleral expansion were not related or showed an inverse relationship. Some models had particularly deep LC or large scleral canal, which they suggested predisposed the ONH to being more sensitive to changes in IOP and, therefore, more susceptible to glaucomatous damage.

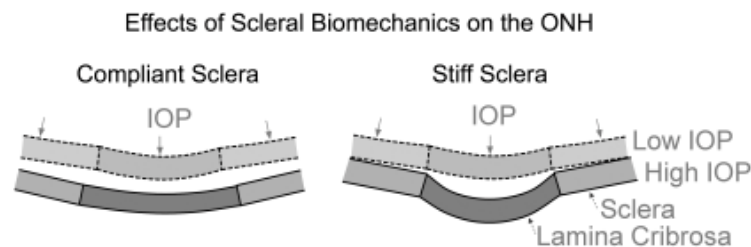


Figure 8.3: Schematic diagram of how deformation of the sclera and lamina cribrosa (LC), may be related. For a compliant sclera, an increase in IOP induces scleral deformation which increases the size of the scleral canal and pulls the LC taut, resulting in a decrease in LC depth. For a stiff sclera, an increase in IOP does little to deform the sclera so there is little scleral canal expansion, and the LC is pushed outwards under the pressure. Taken from (Sigal et al. 2011).

In light of this, the changes present in the bNFL may be due to changes in the insertion region of the LC. If the peripapillary sclera is compliant and stretching the LC taut, then the overlying BMO may shift outwards. Conversely, if the peripapillary sclera is stiff, the LC would be displaced posteriorly, causing a posterior displacement of the insertion regions and possibly a shift in BMO.

The main factors, other than glaucoma, which contributed to changes in NFL, prelamina and LC were axial length, mean spherical refraction (MS), and central corneal thickness (CCT). Axial length and MS are strongly associated with one another: larger eyes have greater levels of myopia and myopia is a known risk factor for glaucoma (Xu et al. 2007). The association between CCT and glaucoma is unclear; previous research has shown no relationship between LC thickness and CCT in healthy eyes

(Jonas and Holbach 2005; Ren et al. 2010; Lee et al. 2012), however, an association between prelamina and LC *depth* and CCT has not been established. From the present study it is clear that, when measuring ONH parameters, CCT, as well as axial length and MS, should be accounted for in the statistical analyses.

4. *To identify and quantify changes in the volume of the optic cup, the prelamina and lamina cribrosa as well as in the area of Bruch's membrane opening (BMO) at different stages of glaucoma.*

The fourth aim was addressed in Chapter 6, in which the volume of the cup was found to increase in each stage of glaucoma compared to control as well as in advanced glaucoma when compared to early glaucoma. Enlargement of the cup is an established biomarker for glaucoma (Quigley and Green 1979; Quigley et al. 1981; Gardiner et al. 2011; Yang et al. 2011). Interestingly, there were no changes in prelamina volume with increasing stage of glaucoma. Indeed an increase in prelamina depth, i.e. corresponding with enlargement of the optic cup and prelamina thinning was observed. The finding that the prelamina volume did *not* increase is interesting and supports a model of scleral canal expansion in glaucoma, which has been indicated by finite element modelling (Norman et al. 2011; Sigal et al. 2011) and experimental monkey glaucoma models (Bellezza et al. 2001; Bellezza et al. 2003) but *not* in human glaucoma before. The data in this thesis supports a hypothesis of prelamina thinning and cup enlargement. The prelamina volume did not change, suggesting there could be scleral canal expansion, and the added volume from this expansion could account for that lost due to enlargement of the cup.

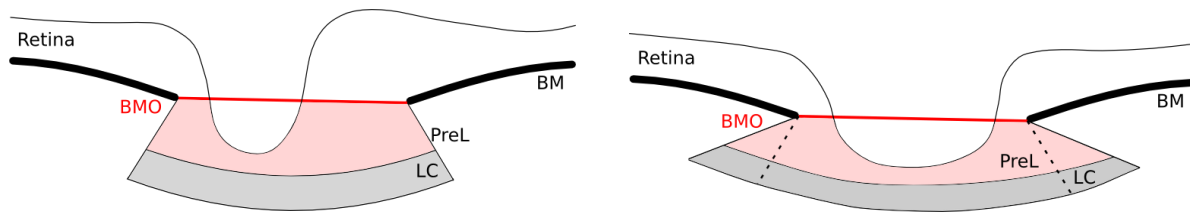


Figure 8.4: Schematic diagram of possible scleral canal expansion in glaucoma. Pink indicate the measured volume of the prelaminar region in (a) control and (b) glaucoma eyes. Dotted line indicates where scleral canal lay prior to expansion. This could explain why there is an increase in cup volume but no change in prelaminar region (PreL) volume with glaucoma. LC = lamina cribrosa, BM = Bruch's membrane, BMO = Bruch's membrane opening.

Additionally, there was no significant change in the volume of the LC but there were non-significant trends between stages of glaucoma, i.e. there was a decrease in LC volume in preperimetric glaucoma compared to control, then an increase in early and advanced glaucoma. This latter increase in volume is consistent with LC thickening and remodelling, as previously shown in monkey models (Yang et al. 2011) and is certainly worthy of follow up investigations.

5. *To investigate and determine whether regional and depth-related differences in LC beam orientation and coherence occurred between healthy and glaucomatous eyes.*

The final aim of this thesis was addressed in Chapter 7, in which the coherence of LC beams was higher in the superior and inferior regions than temporal regions for all stages of glaucoma (Figure 7.4) but at a greater depth into the LC in control eyes. There were no significant differences in LC beam coherence or orientation between control and glaucoma groups, although there was a trend for eyes with advanced glaucoma to have greater LC beam coherence than the other groups in the IIT region. Although, as yet, there is not sufficient data from this study to determine biomarkers for early glaucomatous disease, significant early differences were observed between regions. Orientation of the LC has been shown to be very varied in monkey eyes (Roberts et al. 2009; Roberts et al. 2010), and an *ex vivo* study has shown areas of increased beam coherence in the inferior-temporal LC (Jones et al. 2015). In this thesis there are data to suggest that the inferior-temporal

quadrant is structurally different to the superior-temporal quadrant and further research would allow for more insight into the potential causes of the susceptibility of the inferior temporal LC to glaucomatous damage compared to other regions (Jonas et al. 1993; Garway-Heath et al. 1997; Kiumehr et al. 2012).

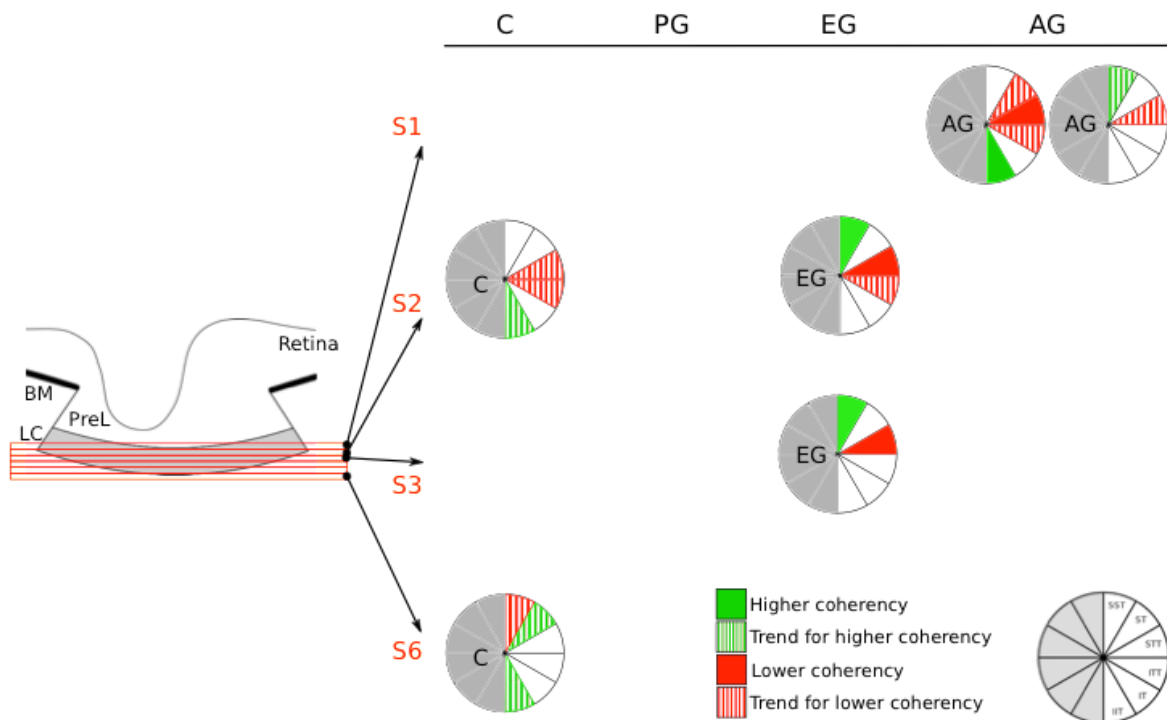


Figure 8.5: Summary of differences in regional lamina cribrosa (LC) beam coherence in the optic nerve head (ONH). Averaged data from 50 μ m sections (S) at increasing depth into the ONH were analysed in control (C), preperimetric glaucoma (PG), early glaucoma (EG), and advanced glaucoma (AG). Regions highlighted green had higher coherence than regions highlighted red at specified depths in the ONH. Solid colour indicates a significant difference ($p < 0.01$) and striped colour indicates a trend ($p < 0.05$). BM = Bruch's membrane, PreL = prelaminar.

8.1 Conclusion

The overall aim of this thesis was to characterise structural alterations in the optic nerve head (ONH) and macula as a result of glaucoma, in order to identify biomarkers for the earliest stages of disease. The inner plexiform layer : ganglion cell layer ratio is one potential biomarker for the earliest stage of glaucoma as it could be used to differentiate between eyes with preperimetric glaucoma and control eyes. An increase in prelaminar depth and prelaminar thinning are also indicative of both preperimetric and early glaucoma. In addition, border nerve fibre layer thickness has potential for

the diagnosis of early glaucoma. Furthermore, it is now apparent that it is critical to consider axial length, refractive error and central corneal thickness when taking measurements of the optic nerve head. Finally, an increase in cup volume with no corresponding change in prelamina volume was found in eyes with glaucoma, supporting a hypothesis of scleral canal expansion in glaucoma.

8.2 Future work

- The primary goal following this study would be to increase the sample size in all groups. This would potentially allow for even greater statistical confidence.
- All the methods described in this thesis would benefit greatly from an image processing technique that could remove vascular shadows from the OCT datasets. Although there has been work done in this area by other groups (Girard et al. 2011; Mari et al. 2013), the algorithms that were published have not yet been successful when used with data from the research OCT device used in this thesis.
- The major limitation of the macula work was the time required to segment the macula datasets. Automated segmentation software is now available and devices such as the Spectralis OCT (Zeiss, Carl Zeiss Meditec Inc.) have the ability to segment the inner plexiform layer and ganglion cell layer independently. As such, it would be interesting to use such a device to corroborate the results found in this thesis and additionally to use automated segmentation software on datasets from the 1050nm research OCT device. In this instance, particular focus would be placed on eyes with moderate and advanced glaucoma in order to further investigate the potential remodelling seen in later disease stages.

- The 2D aging and glaucoma studies and the 3D glaucoma study were performed on 20° OCT scans. The same techniques could be applied to 10° datasets, and the greater magnification would allow more accurate measurements to be performed.
- It would be interesting to further investigate the possible scleral expansion suggested by the 3D glaucoma study by using image enhancement algorithms to improve visibility of LC insertion points and to assess both 2D and 3D datasets.
- The orientation and coherence study would benefit from a greater number of datasets and removal of blood vessel shadows, which would allow for data from the nasal side of the ONH to be assessed. In addition, this study was performed on 10° OCT datasets. These datasets gave better resolution of LC parameters, but were more difficult to acquire as small eye movements during image acquisition left very large artefacts and, as such, a large amount of the data had to be discarded. An eye tracker on the OCT device would negate this and greatly assist with image quality.
- The datasets used for investigating LC beam orientation and coherency could be used to investigate pores in the LC, although further image analysis techniques would need to be developed to achieve this.
- Finally, a statistical model including both the macula and ONH parameters could be created (e.g. using a principle component analysis) in order to determine which parameters are the best predictors for glaucomatous development and progression.

Bibliography

9 Bibliography

A Moura, a L., Raza, a S., Lazow, M. a, De Moraes, C.G. and Hood, D.C. 2012. Retinal ganglion cell and inner plexiform layer thickness measurements in regions of severe visual field sensitivity loss in patients with glaucoma. *Eye* 26(9), pp. 1188–1193.

Agawa, T., Miura, M., Ikuno, Y., Makita, S., Fabritius, T., Iwasaki, T., Goto, H., Nishida, K. and Yasuno, Y. 2011. Choroidal thickness measurement in healthy Japanese subjects by three-dimensional high-penetration optical coherence tomography. *Graefe's Archive for Clinical and Experimental Ophthalmology* 249(10), pp. 1485–1492.

Agoumi, Y., Sharpe, G.P., Hutchison, D.M., Nicoleta, M.T., Artes, P.H. and Chauhan, B.C. 2011. Lamellar and prelaminar tissue displacement during intraocular pressure elevation in glaucoma patients and healthy controls. *Ophthalmology* 118(1), pp. 52–59.

Akaike, H. 1974. A new look at the statistical model identification. *IEEE Transactions on Automatic Control* 19(6).

Alasil, T., Wang, K., Keane, P.A., Lee, H., Baniasadi, N., de Boer, J.F. and Chen, T.C. 2013. Analysis of normal retinal nerve fiber layer thickness by age, sex, and race using spectral domain optical coherence tomography. *Journal of Glaucoma* 22(7), pp. 532–541.

Albon, J., Farrant, S., Akhtar, S., Young, R., Boulton, M.E., Smith, G., Taylor, M., Guggenheim, J. and Morgan, J.E. 2007. Connective tissue structure of the tree shrew optic nerve and associated ageing changes. *Investigative Ophthalmology & Visual Science* 48, pp. 2134–2144.

Albon, J., Karwatowski, W.S., Avery, N., Easty, D.L. and Duance, V.C. 1995. Changes in the collagenous matrix of the aging human lamina cribrosa. *British Journal of Ophthalmology* 79(4), pp. 368–75.

Albon, J., Karwatowski, W.S., Easty, D.L., Sims, T.J. and Duance, V.C. 2000. Age related changes in the non-collagenous components of the extracellular matrix of the human lamina cribrosa. *British Journal of Ophthalmology* 84, pp. 311–317.

Albon, J., Purslow, P.P., Karwatowski, W.S. and Easty, D.L. 2000. Age related compliance of the lamina cribrosa in human eyes. *British Journal of Ophthalmology* 84(3), pp. 318–23.

Anderson, D.R. 1969. Ultrastructure of human and monkey lamina cribrosa and optic nerve head. *Archives of Ophthalmology* 82(6), pp. 800-814

Anderson, D.R. and Hendrickson, A. 1974. The effect of elevated intraocular pressure on axoplasmic transport in the optic nerve of the rhesus monkey. *Investigative Ophthalmology & Visual Science* 13(10), p. 771.

Anderson, D.R., Hoyt, W.F. and Hogan, M.J. 1967. The fine structure of the astroglia in the human optic nerve and optic nerve head. *Transactions of the American Ophthalmological Society* 65, pp. 275–305.

- Anderson, R.S. 2006. The psychophysics of glaucoma: Improving the structure/function relationship. *Progress in Retinal and Eye Research* 25, pp. 79–97.
- Ang, L.P.K., Aung, T., Chua, W.-H., Yip, L.W. and Chew, P.T.K. 2004. Visual field loss from primary angle-closure glaucoma: a comparative study of symptomatic and asymptomatic disease. *Ophthalmology* 111(9), pp. 1636–1640.
- Anton, A., Moreno-Montanes, J., Blazquez, F., Alvarez, A., Martin, B. and Molina, B. 2007. Usefulness of optical coherence tomography parameters of the optic disc and the retinal nerve fiber layer to differentiate glaucomatous, ocular hypertensive, and normal eyes. *Journal of Glaucoma* 16, pp. 1–8.
- Anwar, S., Patel, A., Lee, H., Proudlock, F.A., Cusack, J., and Gottlob, I. 2014. In vivo retinal development using hand held ultra-high resolution spectral domain optical coherence tomography in premature and full term infants. *Investigative Ophthalmology & Visual Science* 55(13), pp. 696.
- Arintawati, P., Sone, T., Akita, T., Tanaka, J. and Kiuchi, Y. 2013. The applicability of ganglion cell complex parameters determined from SD-OCT images to detect glaucomatous eyes. *Journal of Glaucoma* 22(9), pp. 713–718.
- Avery, R.A., Cnaan, A., Schuman, J.S., Chen, C.L., Glau, N.C., Packer, R.J., Quinn, G.E. and Ishikawa, H. 2014. Intra- and inter-visit reproducibility of ganglion cell-inner plexiform layer measurements using handheld optical coherence tomography in children with optic pathway gliomas. *American Journal of Ophthalmology* 158(5), pp. 916–23.
- Avery, R.A., Cnaan, A., Schuman, J.S., Chen, C.L., Glau, N.C., Packer, R.J., Quinn, G.E. and Ishikawa, H. 2014. Reproducibility of circumpapillary retinal nerve fiber layer measurements using handheld optical coherence tomography in sedated children. *American Journal of Ophthalmology* 158(4), pp. 780–787.e1.
- Balazsi, A.G., Rootman, J., Drance, S.M., Schulzer, M. and Douglas, G.R. 1984. The effect of age on the nerve fiber population of the human optic nerve. *American Journal of Ophthalmology* 97(6), pp. 760–766.
- Bandyopadhyay, A.K., Bhattacharya, A., Dan, A.K., Banerjee, B., Biswas, I., Das, S.K. and Bhaduri, G. 2011. A study on central corneal thickness and optic disc size in patients with primary open angle glaucoma. *Journal of the Indian Medical Association* 109(7), pp. 465–468.
- Barrancos, C., Rebolleda, G., Oblanca, N., Cabarga, C. and Munoz-Negrete, F.J. 2014. Changes in lamina cribrosa and prelaminar tissue after deep sclerectomy. *Eye (London, England)* 28(1), pp. 58–65.
- Beck, R.W., Servais, G.E. and Hayreh, S.S. 1987. Anterior ischemic optic neuropathy. IX. Cup-to-disc ratio and its role in pathogenesis. *Ophthalmology* 94, pp. 1503–1508.
- Bellezza, a. J., Rintalan, C.J., Thompson, H.W., Downs, J.C., Hart, R.T. and Burgoyne, C.F. 2003. Deformation of the lamina cribrosa and anterior scleral canal wall in early experimental glaucoma. *Investigative Ophthalmology & Visual Science* 44(2), pp. 623–637.
- Bellezza, A.J., Rintalan, C.J., Thompson, H.W. and Burgoyne, C.F. 2001. Deformation of the lamina cribrosa and scleral canal wall underlies the onset of CSLT-detected ONH surface change in early experimental glaucoma. *Investigative Ophthalmology & Visual Science* 42, pp. S827–S827.

- Bengtsson, B.O. 1980. The alteration and asymmetry of cup and disc diameters. *Acta Ophthalmologica* 58(5), pp. 726–732.
- Bennett, A.G., Rudnicka, A.R. and Edgar, D.F. 1994. Improvements on Littmann method of determining the size of retinal features by fundus photography. *Graefe's Archive for Clinical and Experimental Ophthalmology* 232, pp. 361–367.
- Brezinski, M. 2006. *Optical Coherence Tomography: Principles and Applications*. 1st ed. Elsevier.
- Britton, R.J., Drance, S.M., Schulzer, M., Douglas, G.R. and Mawson, D.K. 1987. The area of the neuroretinal rim of the optic nerve in normal eyes. *American Journal of Ophthalmology* 103(4), pp. 497–504.
- Broman, A.T., Quigley, H.A., West, S.K., Katz, J., Munoz, B., Bandeen-Roche, K., Tielsch, J.M., Friedman, D.S., Crowston, J., Taylor, H.R., Varma, R., Leske, M.C., Bengtsson, B., Heijl, A., He, M. and Foster, P.J. 2008. Estimating the rate of progressive visual field damage in those with open-angle glaucoma, from cross-sectional data. *Investigative Ophthalmology & Visual Science* 49, pp. 66–76.
- Burgoyne, C.F. 2011. A biomechanical paradigm for axonal insult within the optic nerve head in aging and glaucoma. *Experimental Eye Research* 93(2), pp. 120–132.
- Burgoyne, C.F., Downs, J.C., Bellezza, A.J., Suh, J.-K.K.F. and Hart, R.T. 2005. The optic nerve head as a biomechanical structure: a new paradigm for understanding the role of IOP-related stress and strain in the pathophysiology of glaucomatous optic nerve head damage. *Progress in Retinal and Eye Research* 24(1), pp. 39–73.
- Burk, R.O., Rohrschneider, K., Noack, H. and Volcker, H.E. 1992. Are large optic nerve heads susceptible to glaucomatous damage at normal intraocular pressure? A three-dimensional study by laser scanning tomography. *Graefe's Archive for Clinical and Experimental Ophthalmology* 230(6), pp. 552–560.
- Burton, P., Gurrin, L., Sly, P. 1998. Extending the simple linear regression model to account for correlated responses: an introduction to generalized estimating equations and multi-level mixed modelling. *Statistics in Medicine* 17(11), pp. 1261–1291.
- Bussel, I.I., Wollstein, G. and Schuman, J.S. 2014. OCT for glaucoma diagnosis, screening and detection of glaucoma progression. *The British Journal of Ophthalmology* 98(Suppl 2), pp. ii15–ii19.
- Callaway, E.M. 2005. Structure and function of parallel pathways in the primate early visual system. *The Journal of Physiology* 566(Pt 1), pp. 13–19.
- Campbell, I.C., Coudrillier, B. and Ross Ethier, C. 2014. Biomechanics of the posterior eye: a critical role in health and disease. *Journal of Biomechanical Engineering* 136(2), p. 21005.
- NICE Guidelines 2009. *CG85 Glaucoma*. National Institute for Health and Clinical Excellence.
- Carpel, E.F. and Engstrom, P.F. 1981. The normal cup-disk ratio. *American Journal of Ophthalmology* 91(5), pp. 588–597.
- Cavallotti, C., Pacella, E., Pescosolido, N., Tranquilli-Leali, F.M. and Feher, J. 2002. Age-related changes in the human optic nerve. *Canadian Journal of Ophthalmology*. 37(7), pp. 389–394.

- Chauhan, B.C., O'Leary, N., Almobarak, F.A., Reis, A.S.C., Yang, H., Sharpe, G.P., Hutchison, D.M., Nicoleta, M.T. and Burgoyne, C.F. 2013. Enhanced detection of open-angle glaucoma with an anatomically accurate optical coherence tomography-derived neuroretinal rim parameter. *Ophthalmology* 120(3), pp. 535–543.
- Cheng, C.Y., Liu, J.H., Chiang, S.C., Chen, S.J. and Hsu, W.M. 2000. Statistics in ophthalmic research: two eyes, one eye or the mean? *Zhonghua yi xue za zhi = Chinese Medical Journal; Free China ed* 63(12), pp. 885–892.
- Choi, W., Mohler, K.J., Potsaid, B., Lu, C.D., Liu, J.J., Jayaraman, V., Cable, A.E., Duker, J.S., Huber, R. and Fujimoto, J.G. 2013. Choriocapillaris and choroidal microvasculature imaging with ultrahigh speed OCT angiography. *PLoS ONE* 8(12), p. e81499.
- Choma, M., Sarunic, M., Yang, C. and Izatt, J. 2003. Sensitivity advantage of swept source and Fourier domain optical coherence tomography. *Optics Express* 11, pp. 2183–2189.
- Chrysostomou, V., Rezanian, F., Trounce, I.A. and Crowston, J.G. 2013. Oxidative stress and mitochondrial dysfunction in glaucoma. *Current Opinion in Pharmacology* 13(1), pp. 12–5.
- Deleon-Ortega, J.E., Arthur, S.N., McGwin Jr., G., Xie, A., Monheit, B.E., Girkin, C.A., Deleón-Ortega, J.E. and McGwin, G. 2006. Discrimination between glaucomatous and nonglaucomatous eyes using quantitative imaging devices and subjective optic nerve head assessment. *Investigative Ophthalmology & Visual Science* 47(8), pp. 3374–3380.
- Dolman, C.L., McCormick, A.Q. and Drance, S.M. 1980. Aging of the optic nerve. *Archives of Ophthalmology (Chicago, Ill. : 1960)* 98(11), pp. 2053–2058.
- Downs, J.C. 2015. Optic nerve head biomechanics in aging and disease. *Experimental Eye Research* 133, pp. 19–29.
- Downs, J.C., Roberts, M.D. and Burgoyne, C.F. 2008. Mechanical environment of the optic nerve head in glaucoma. *Optometry and Vision Science* 85, pp. 425–435.
- Downs, J.C., Roberts, M.D. and Sigal, I.A. 2011. Glaucomatous cupping of the lamina cribrosa: A review of the evidence for active progressive remodeling as a mechanism. *Experimental Eye Research* 93(2), pp. 133–140.
- Drance, S.M. 1989. Disc hemorrhages in the glaucomas. *Survey of Ophthalmology* 33(5), pp. 331–337.
- Drexler, W., Morgner, U., Kartner, F.X., Pitris, C., Boppart, S.A., Li, X.D., Ippen, E.P. and Fujimoto, J.G. 1999. In vivo ultrahigh-resolution optical coherence tomography. *Optics Letters* 24, pp. 1221–1223.
- Durmus, M., Karadag, R., Erdurmus, M., Totan, Y. and Feyzi Hepsen, I. 2009. Assessment of cup-to-disc ratio with slit-lamp funduscopy, Heidelberg Retina Tomography II, and stereoscopic photos. *European Journal of Ophthalmology* 19, pp. 55–60.
- Ehlers, N., Bramsen, T. and Sperling, S. 1975. Applanation tonometry and central corneal thickness. *Acta Ophthalmologica* 53(1), pp. 34–43.

- Esmaelpour, M., Povazay, B., Hermann, B., Hofer, B., Kajic, V., Kapoor, K., Sheen, N.J.L., North, R. V and Drexler, W. 2010. Three-dimensional 1060-nm OCT: choroidal thickness maps in normal subjects and improved posterior segment visualization in cataract patients. *Investigative Ophthalmology & Visual Science* 51(10), pp. 5260–5266.
- Fan, Q., Teo, Y.Y. and Saw, S.M. 2011. Application of advanced statistics in ophthalmology. *Investigative Ophthalmology & Visual Science* 52(9), pp. 6059–6065.
- Fan, S., Hejkal, J.J., Gulati, V., Galata, S., Camras, C.B. and Toris, C.B. 2011. Aqueous humor dynamics during the day and night in volunteers with ocular hypertension. *Archives of Ophthalmology* 129, pp. 1162–1166.
- Feiner, L. and Piltz-Seymour, J.R. 2003. Collaborative Initial Glaucoma Treatment Study: a summary of results to date. *Current Opinion in Ophthalmology* 14(2).
- Fenolland, J.R., Boucher, C., Mayer, M., Rostene, W., Baudouin, C. and Denoyer, A. 2013. Developments in optical coherence tomography imaging in a rat model of glaucoma. *Investigative Ophthalmology & Visual Science* 54(15), pp. 4833.
- Folio, L.S., Wollstein, G. and Schuman, J.S. 2012. Optical coherence tomography: future trends for imaging in glaucoma. *Optometry and Vision Science* 89(5), pp. E554–E562.
- Forte, R., Cennamo, G.L., Finelli, M.L. and de Crecchio, G. 2009. Comparison of time domain Stratus OCT and spectral domain SLO/OCT for assessment of macular thickness and volume. *Eye (Lond)* 23, pp. 2071–2078.
- Francoz, M., Fenolland, J.-R., Giraud, J.-M., El Chehab, H., Sendon, D., May, F. and Renard, J.-P. 2014. Reproducibility of macular ganglion cell-inner plexiform layer thickness measurement with cirrus HD-OCT in normal, hypertensive and glaucomatous eyes. *British Journal of Ophthalmology* 98(3), pp. 322–328.
- Fujita, Y., Imagawa, T. and Uehara, M. 2000. Comparative study of the lamina cribrosa and the pial septa in the vertebrate optic nerve and their relationship to the myelinated axons. *Tissue Cell* 32(4), pp. 293–301.
- Gaasterland, D., Tanishima, T. and Kuwabara, T. 1978. Axoplasmic flow during chronic experimental glaucoma. 1. Light and electron microscopic studies of the monkey optic nervehead during development of glaucomatous cupping. *Investigative Ophthalmology & Visual Science* 17(9), pp. 838–846.
- Gabriele, M.L., Wollstein, G., Ishikawa, H., Xu, J., Kim, J., Kagemann, L., Folio, L.S. and Schuman, J.S. 2010. Three dimensional optical coherence tomography imaging: Advantages and advances. *Progress in Retinal and Eye Research* 29, pp. 556–579.
- Gardiner, S.K., Johnson, C.A. and Demirel, S. 2011. Cup size predicts subsequent functional change in early glaucoma. *Optometry and Vision Science* 88, pp. 1470–1476.
- Garway-Heath, D.F., Wollstein, G. and Hitchings, R. a 1997. Aging changes of the optic nerve head in relation to open angle glaucoma. *British Journal of Ophthalmology* 81(10), pp. 840–845.

Girard, M.J.A., Tun, T.A., Husain, R., Acharyya, S., Haaland, B.A., Wei, X., Mari, J.M., Perera, S.A., Baskaran, M., Aung, T. and Strouthidis, N.G. 2015. Lamina cribrosa visibility using optical coherence tomography: comparison of devices and effects of image enhancement techniques. *Investigative Ophthalmology & Visual Science* 56(2), pp. 865–874.

Girard, M.J.A.M.J. a, Strouthidis, N.G., Ethier, C.R. and Mari, J.M. 2011. Shadow removal and contrast enhancement in optical coherence tomography images of the human optic nerve head. *Investigative Ophthalmology & Visual Science* 52(10), pp. 7738–7748.

Glynn, R.J. and Rosner, B. 1992. Accounting for the correlation between fellow eyes in regression analysis. *Archives of Ophthalmology* 110(3), pp. 381–387.

Gordon, M.O., Beiser, J.A., Brandt, J.D., Heuer, D.K., Higginbotham, E.J., Johnson, C.A., Keltner, J.L., Miller, J.P., Parrish, R.K.I., Wilson, M.R. and Kass, M.A. 2002. The Ocular Hypertension Treatment Study: baseline factors that predict the onset of primary open angle glaucoma. *Archives of Ophthalmology* 120(6), pp. 714–720; Discussion 829–830.

Greenfield, D.S., Bagga, H. and Knighton, R.W. 2003. Macular thickness changes in glaucomatous optic neuropathy detected using optical coherence tomography. *Archives of Ophthalmology* 121(1), pp. 41–46.

Grytz, R., Sigal, I.A., Ruberti, J.W., Meschke, G. and Downs, J.C. 2012. Lamina cribrosa thickening in early glaucoma predicted by a microstructure motivated growth and remodeling approach. *Mechanics of Materials* 44, pp. 99–109.

Guedes, V., Schuman, J.S., Hertzmark, E., Wollstein, G., Correnti, A., Mancini, R., Lederer, D., Voskanyan, S., Velazquez, L., Pakter, H.M., Pedut-Kloizman, T., Fujimoto, J.G. and Mattox, C. 2003. Optical coherence tomography measurement of macular and nerve fiber layer thickness in normal and glaucomatous human eyes. *Ophthalmology* 110(1), pp. 177–189.

Gupta, V., Gupta, A. and Dogra, M.R. 2004. Introduction to OCT. In: *Optical Coherence Tomography of Macula Diseases*. ATLAS. 1st ed. Taylor and Francis, pp. 3–17.

Hammer, M., Roggan, A., Schweitzer, D. and Muller, G. 1995. Optical properties of ocular fundus tissues--an in vitro study using the double-integrating-sphere technique and inverse Monte Carlo simulation. *Physics in Medicine and Biology* 40(6), pp. 963–978.

Han, I.C. and Jaffe, G.J. 2009. Comparison of spectral- and time-domain optical coherence tomography for retinal thickness measurements in healthy and diseased eyes. *American Journal of Ophthalmology* 147, pp. 847–858.

Harwerth, R.S., Wheat, J.L. and Rangaswamy, N. V. 2008. Age-related losses of retinal ganglion cells and axons. *Investigative Ophthalmology and Visual Science* 49(10), pp. 4437–4443.

Hayreh, S.S. 2001. The blood supply of the optic nerve head and the evaluation of it - Myth and reality. *Progress in Retinal and Eye Research* 20(5), pp. 563–593.

Healey, P.R., Mitchell, P., Smith, W. and Wang, J.J. 1997. Relationship between cup-disc ratio and optic disc diameter: the Blue Mountains Eye Study. *Australian and New Zealand Journal of Ophthalmology* 25 Suppl 1, pp. S99–101.

- Hee, M.R., Izatt, J.A., Swanson, E.A., Huang, D., Schuman, J.S., Lin, C.P., Puliafito, C.A. and Fujimoto, J.G. 1995. Optical coherence tomography of the human retina. *Archives of Ophthalmology* 113, pp. 325–332.
- Heijl, A., Leske, M., Bengtsson, B. and al, et 2002. Reduction of intraocular pressure and glaucoma progression: Results from the early manifest glaucoma trial. *Archives of Ophthalmology* 120(10), pp. 1268–1279.
- Hermann, M.M., Theofylaktopoulos, I., Bangard, N., Jonescu-Cuypers, C., Coburger, S. and Diestelhorst, M. 2004. Optic nerve head morphometry in healthy adults using confocal laser scanning tomography. *British Journal of Ophthalmology* 88(6), pp. 761–765.
- Hernandez, M.R. 2000. The optic nerve head in glaucoma: role of astrocytes in tissue remodeling. *Progress in retinal and eye research* 19(3), pp. 297–321.
- Hernandez, M.R. 1992. Ultrastructural immunocytochemical analysis of elastin in the human lamina cribrosa. Changes in elastic fibers in primary open-angle glaucoma. *Investigative Ophthalmology & Visual Science* 33(10), pp. 2891–2903.
- Hernandez, M.R., Andrzejewska, W.M. and Neufeld, A.H. 1990. Changes in the extracellular matrix of the human optic nerve head in primary open-angle glaucoma. *American Journal of Ophthalmology* 109(2), pp. 180–188.
- Hernandez, M.R., Igoe, F. and Neufeld, A.H. 1986. Extracellular-matrix of the human optic nerve head. *American Journal of Ophthalmology* 102, pp. 139–148.
- Hernandez, M.R., Luo, X.X., Andrzejewska, W. and Neufeld, A.H. 1989. Age-related changes in the extracellular matrix of the human optic nerve head. *American Journal of Ophthalmology* 107(5), pp. 476–484.
- Hernandez, M.R., Luo, X.X., Igoe, F. and Neufeld, A.H. 1987. Extracellular-matrix of the human lamina cribrosa. *American Journal of Ophthalmology* 104, pp. 567–576.
- Hildebrand, G.D. and Fielder, A.R. 2011. Anatomy and physiology of the retina. *Pediatric Retina* pp. 39-64.
- Hirasawa, H., Tomidokoro, A., Araie, M., Konno, S., Saito, H., Iwase, A., Shirakashi, M., Abe, H., Ohkubo, S., Sugiyama, K., Ootani, T., Kishi, S., Matsushita, K., Maeda, N., Hangai, M. and Yoshimura, N. 2010. Peripapillary retinal nerve fiber layer thickness determined by spectral-domain optical coherence tomography in ophthalmologically normal eyes. *Archives of Ophthalmology* 128(11), pp. 1420–1426.
- Hodapp, E., Parrish, R.K.I. and Anderson, D.R. 1993. *Clinical decisions in glaucoma*. St. Louis: The CV Mosby Co.
- Hogan, M., Alvarado, J. and Weddell, J. 1971. *Histology of the human eye: an atlas and textbook*. Philadelphia, USA: WB Saunders.
- Hood, D.C. and Kardon, R.H. 2007. A framework for comparing structural and functional measures of glaucomatous damage. *Progress in Retinal and Eye Research* 26(6), pp. 688–710.

- Hood, D.C., Anderson, S., Rouleau, J., Wenick, A.S., Grover, L.K., Behrens, M.M., Odel, J.G., Lee, A.G., Kardon and R.H. 2008. Retinal nerve fiber structure versus visual field function in patients with ischemic optic neuropathy: A test of a linear model. *Ophthalmology* 115(5), pp. 904–910.
- Hood, D.C., Fortune, B., Arthur, S.N., Xing, D., Salant, J.A., Ritch, R. and Liebmann, J.M. 2008. Blood vessel contributions to retinal nerve fiber layer thickness profiles measured with optical coherence tomography. *Journal of Glaucoma* 17(7), pp. 519–528.
- Hood, D.C. and Raza, A.S. 2011. Method for comparing visual field defects to local RNFL and RGC damage seen on frequency domain OCT in patients with glaucoma. *Biomedical Optics Express* (2), pp. 1097–1105.
- Hood, D.C., Raza, A.S., de Moraes, Carlos G.V., Liebmann, J.M. and Ritch, R. 2013. Glaucomatous damage of the macula. *Progress in Retinal and Eye Research* 32(C), pp. 1–21.
- Hood, D.C., Slobodnick, A., Raza, A.S., de Moraes, C.G., Teng, C.C. and Ritch, R. 2014. Early glaucoma involves both deep local, and shallow widespread, retinal nerve fiber damage of the macular region. *Investigative Ophthalmology & Visual Science* 55(2), pp. 632–49.
- Huang, D., Swanson, E.A., Lin, C.P., Schuman, J.S., Stinson, W.G., Chang, W., Hee, M.R., Flotte, T., Gregory, K., Puliafito, C.A. and Fujimoto, J.G. 1991. Optical coherence tomography. *Science* 254, pp. 1178–1181.
- Inoue, R., Hangai, M., Kotera, Y., Nakanishi, H., Mori, S., Morishita, S. and Yoshimura, N. 2009. Three-dimensional high-speed optical coherence tomography imaging of lamina cribrosa in glaucoma. *Ophthalmology* 116(2), pp. 214–222.
- Ishikawa, H., Stein, D.M., Wollstein, G., Beaton, S., Fujimoto, J.G. and Schuman, J.S. 2005. Macular segmentation with optical coherence tomography. *Investigative Ophthalmology & Visual Science* 46(6), pp. 2012–2017.
- Ivers, K.M., Li, C., Patel, N., Sredar, N., Luo, X., Queener, H., Harwerth, R.S. and Porter, J. 2011. Reproducibility of measuring lamina cribrosa pore geometry in human and nonhuman primates with in vivo adaptive optics imaging. *Investigative Ophthalmology & Visual Science* 52(8), pp. 5473–5480.
- Izatt, J.A. and Choma, M.A. 2008. Theory of optical coherence tomography. In: Drexler, W. and Fujimoto, J. G. eds. *Optical Coherence Tomography: Technology and Applications*. 1st ed. Springer.
- Jeoung, J.W. and Park, K.H. 2010. Comparison of Cirrus OCT and Stratus OCT on the ability to detect localized retinal nerve fiber layer defects in preperimetric glaucoma. *Investigative Ophthalmology & Visual Science* 51(2), pp. 938–945.
- Jia, Y., Wei, E., Wang, X., Zhang, X., Morrison, J.C., Parikh, M., Lombardi, L.H., Gattey, D.M., Armour, R.L., Edmunds, B., Kraus, M.F., Fujimoto, J.G., Huang, D. 2014. Optical coherence tomography angiography of optic disc perfusion in glaucoma. *Ophthalmology* 121(7), pp. 1322–32.
- Johnson, B., Miao, M. and Sadun, A. 1987. Age-related decline of human optic nerve axon populations. *AGE* 10(1), pp. 5–9.

- Johnson, M., Chan, D., Read, A.T., Christensen, C., Sit, A. and Ethier, C.R. 2002. The pore density in the inner wall endothelium of Schlemm's canal of glaucomatous eyes. *Investigative Ophthalmology & Visual Science* 43(9), pp. 2950–2955.
- Johnstone, J., Fazio, M., Rojananuangnit, K., Smith, B., Clark, M., Downs, C., Owsley, C., Girard, M.J.A., Mari, J.M. and Girkin, C.A. 2014. Variation of the axial location of Bruch's membrane opening with age, choroidal thickness, and race. *Investigative Ophthalmology & Visual Science* 55(3), pp. 2004–2009.
- Jonas, J.B., Budde, W.M. and Panda-Jonas, S. 1999. Ophthalmoscopic evaluation of the optic nerve head. *Survey of Ophthalmology* 43(4), pp. 293–320.
- Jonas, J.B., Fernández, M.C. and Naumann, G.O.H. 1991. Correlation of the optic disc size to glaucoma susceptibility. *Ophthalmology* 98(5), pp. 675–680.
- Jonas, J.B., Fernandez, M.C. and Sturmer, J. 1993. Pattern of glaucomatous neuroretinal rim loss. *Ophthalmology* 100(1), pp. 63–68.
- Jonas, J.B., Gusek, G.C. and Naumann, G.O.H. 1988a. Optic disc morphometry in chronic primary open-angle glaucoma - I. Morphometric intrapapillary characteristics. *Graefe's Archive for Clinical and Experimental Ophthalmology* 226(6), pp. 522–530.
- Jonas, J.B., Gusek, G.C. and Naumann, G.O.H. 1988b. Optic disc, cup and neuroretinal rim size, configuration and correlations in normal eyes. *Investigative Ophthalmology & Visual Science* 29, pp. 1151–1158.
- Jonas, J.B. and Hayreh, S.S. 2009. Central corneal thickness and thickness of the lamina cribrosa and Peripapillary Sclera in Monkeys. *Archives of Ophthalmology* 127, pp. 1395–1396.
- Jonas, J.B. and Holbach, L. 2005. Central corneal thickness and thickness of the lamina cribrosa in human eyes. *Investigative Ophthalmology & Visual Science* 46, pp. 1275–1279.
- Jonas, J.B., Jonas, R.A., Jonas, S.B. and Panda-Jonas, S. 2012. Lamina cribrosa thickness correlated with peripapillary sclera thickness. *Acta Ophthalmologica* 90, pp. e248–e250.
- Jonas, J.B., Muller-Bergh, J. a., Schlotzer-Schrehardt, U.M. and Naumann, G.O.H. 1990. Histomorphometry of the human optic nerve. *Investigative Ophthalmology and Visual Science* 31(4), pp. 736–744.
- Jonas, J.B. and Papastathopoulos, K.I. 1996. Optic disc shape in glaucoma. *Graefe's Archive for Clinical and Experimental Ophthalmology* 234 Suppl , pp. S167–73.
- Jonas, J.B., Schmidt, A.M., Mullerbergh, J.A., Schlotzerschrehardt, U.M. and Naumann, G.O.H. 1992. Human optic nerve fibre count and optic disc size. *Investigative Ophthalmology & Visual Science* 33, pp. 2012–2018.
- Jonas, J.B., Schneider, U. and Naumann, G.O.H. 1992. Count and density of human retinal photoreceptors. *Graefe's Archive for Clinical and Experimental Ophthalmology* 230, pp. 505–510.

Jones, H.J., Girard, M.J., White, N., Fautsch, M.P., Morgan, J.E., Ethier, C.R. and Albon, J. 2015. Quantitative analysis of three-dimensional fibrillar collagen microstructure within the normal, aged and glaucomatous human optic nerve head. *Journal of The Royal Society Interface* 12(106).

Kagemann, L., Ishikawa, H., Wollstein, G., Brennen, P.M., Townsend, K.A., Gabriele, M.L. and Schuman, J.S. 2008. Ultrahigh-resolution spectral domain optical coherence tomography imaging of the lamina cribrosa. *Ophthalmic Surg Lasers Imaging* 39, pp. S126–131.

Kanamori, A., Nakamura, M., Escano, M.F.T., Seya, R., Maeda, H. and Negi, A. 2003. Evaluation of the glaucomatous damage on retinal nerve fiber layer thickness measured by optical coherence tomography. *American Journal of Ophthalmology* 135(4), pp. 513–20.

Karakosta, A., Vassilaki, M., Plainis, S., Elfadl, N.H., Tsilimbaris, M., Moschandreas, J. 2012. Choice of analytic approach for eye-specific outcomes: one eye or two? *American Journal of Ophthalmology* 153(3), pp. 571–579.e1.

Keane, P.A., Bhatti, R.A., Brubaker, J.W., Liakopoulos, S., Sadda, S.R. and Walsh, A.C. 2009. Comparison of clinically relevant findings from high-speed Fourier-domain and conventional time-domain optical coherence tomography. *American Journal of Ophthalmology* 148, pp. 242–248.

Keane, P.A. and Sadda, S.R. 2014. Retinal imaging in the twenty-first century: state of the art and future directions. *Ophthalmology* 121(12), pp. 2489–500.

Kee, C., Koo, H., Ji, Y. and Kim, S. 1997. Effect of optic disc size or age on evaluation of optic disc variables. *British Journal of Ophthalmology* 81 (12), pp. 1046–1049.

Keltner, J.L., Johnson, C.A., Quigg, J.M., Cello, K.E., Kass, M.A. and Gordon, M.O. 2000. Confirmation of visual field abnormalities in the Ocular Hypertension Treatment Study. Ocular Hypertension Treatment Study Group. *Arch Ophthalmol* 118, pp. 1187–1194.

Kerrigan-Baumrind, L.A., Quigley, H.A., Pease, M.E., Kerrigan, D.F. and Mitchell, R.S. 2000. Number of ganglion cells in glaucoma eyes compared with threshold visual field tests in the same persons. *Investigative ophthalmology & visual science* 41(3), pp. 741–748.

Kiernan, D.F., Mieler, W.F. and Hariprasad, S.M. 2010. Spectral-domain optical coherence tomography: A comparison of modern high-resolution retinal imaging systems. *American Journal of Ophthalmology* 149(1), pp. 18–31.e2.

Kim, N.R., Hong, S., Kim, J.H., Rho, S.S., Seong, G.J. and Kim, C.Y. 2013. Comparison of macular ganglion cell complex thickness by Fourier-domain OCT in normal tension glaucoma and primary open-angle glaucoma. *Journal of Glaucoma* 22(2), pp. 133–139.

Kim, N.R., Lee, E.S., Seong, G.J., Kim, J.H., An, H.G. and Kim, C.Y. 2010. Structure-function relationship and diagnostic value of macular ganglion cell complex measurement using Fourier-domain OCT in glaucoma. *Investigative Ophthalmology & Visual Science* 51(9), pp. 4646–4651.

Kim, Y., Han, S.B., Park, K.H., Kim, S.H., Kim, S.J., Seong, M., Kim, T.W. and Kim, D.M. 2010. Risk factors associated with optic disc haemorrhage in patients with normal tension glaucoma. *Eye* 24(4), pp. 567–572.

- Kim, Y.J., Kang, M.H., Cho, H.Y., Lim, H.W. and Seong, M. 2014. Comparative study of macular ganglion cell complex thickness measured by spectral-domain optical coherence tomography in healthy eyes, eyes with preperimetric glaucoma, and eyes with early glaucoma. *Japanese Journal of Ophthalmology* 58(3), pp. 244–51.
- Kita, Y., Kita, R., Takeyama, A., Anraku, A., Tomita, G. and Goldberg, I. 2013. Relationship between macular ganglion cell complex thickness and macular outer retinal thickness: A spectral domain-optical coherence tomography study. *Clinical & Experimental Ophthalmology* 41(7), pp.674-82.
- Kiumehr, S., Park, S.C., Dorairaj, S., Teng, C.C., Tello, C., Liebmann, J.M. and Ritch, R. 2012. In vivo evaluation of focal lamina cribrosa defects in glaucoma. *Archives of Ophthalmology* 130, pp. 552–559.
- Klein, B.E.K., Klein, R., Lee, K.E. and Hoyer, C.J. 2006. Does the intraocular pressure effect on optic disc cupping differ by age? *Transactions of the American Ophthalmological Society* 104, pp. 143–148.
- Klein, B.E.K., Klein, R., Sponsel, W.E., Franke, T., Cantor, L.B., Martone, J. and Menage, M.J. 1992. Prevalence of glaucoma - The Beaver Dam Eye Study. *Ophthalmology* 99, pp. 1499–1504.
- Knighton, R.W., Gregori, G., Budenz, D.L. 2012. Variance reduction in a dataset of normal macular ganglion cell plus inner plexiform layer thickness maps with application to glaucoma diagnosis. *Investigative Ophthalmology & Visual Science* 53(7), pp. 3653–3661.
- Kodach, V.M., Kalkman, J., Faber, D.J. and van Leeuwen, T.G. 2010. Quantitative comparison of the OCT imaging depth at 1300 nm and 1600 nm. *Biomedical Optics Express* 1, pp. 176–185.
- Kokotas, H., Kroupis, C., Chiras, D., Grigoriadou, M., Lamnissou, K., Petersen, M.B. and Kitsos, G. 2012. Biomarkers in primary open angle glaucoma. *Clinical Chemistry and Laboratory Medicine: CCLM / FESCC* 0, pp. 1–13.
- Kotecha, A., Izadi, S. and Jeffery, G. 2006. Age-related changes in the thickness of the human lamina cribrosa. *British Journal of Ophthalmology* 90(12), pp. 1531–1534.
- Lalezary, M., Medeiros, F. a, Weinreb, R.N., Bowd, C., Sample, P.A., Tavares, I.M., Tafreshi, A. and Zangwill, L.M. 2006. Baseline optical coherence tomography predicts the development of glaucomatous change in glaucoma suspects. *American Journal of Ophthalmology* 142(4), pp. 576–582.
- Lederer, D.E., Schuman, J.S., Hertzmark, E., Heltzer, J., Velazques, L.J., Fujimoto, J.G. and Mattox, C. 2003. Analysis of macular volume in normal and glaucomatous eyes using optical coherence tomography. *American Journal of Ophthalmology* 135(6), pp. 838–843.
- Lee, E.J., Kim, T.-W.W., Weinreb, R.N., Park, K.H., Kim, S.H. and Kim, D.M. 2011. Visualization of the lamina cribrosa using enhanced depth imaging spectral-domain optical coherence tomography. *American Journal of Ophthalmology* 152(1), pp. 87–95 e1.
- Lee, E.J., Kim, T.-W. and Weinreb, R.N. 2012. Reversal of lamina cribrosa displacement and thickness after trabeculectomy in glaucoma. *Ophthalmology* 119(7), pp. 1359–1366.

Lee, E.J., Kim, T.-W., Weinreb, R.N., Suh, M.H., Kang, M., Park, K.H., Kim, S.H. and Kim, D.M. 2012. Three-dimensional evaluation of the lamina cribrosa using spectral-domain optical coherence tomography in glaucoma. *Investigative Ophthalmology & Visual Science* 53, pp. 198–204.

Lee, E.J., Kim, T.-W., Weinreb, R.N., Suh, M.H. and Kim, H. 2012. Lamina cribrosa thickness is not correlated with central corneal thickness or axial length in healthy eyes. *Graefe's Archive for Clinical and Experimental Ophthalmology*, pp. 847–854.

Lee, J.Y., Hwang, Y.H., Lee, S.M. and Kim, Y.Y. 2012. Age and retinal nerve fiber layer thickness measured by spectral domain optical coherence tomography. *Korean Journal of Ophthalmology* 26(3), pp. 163–168.

Lee, K., Kwon, Y.H., Garvin, M.K., Niemeijer, M., Sonka, M., Abràmoff, M.D. and Abramoff, M.D. 2012. Distribution of damage to the entire retinal ganglion cell pathway: quantified using spectral-domain optical coherence tomography analysis in patients with glaucoma. *Archives of Ophthalmology* 130(9), pp. 1118–26.

Legarreta, J.E., Gregori, G., Punjabi, O.S., Knighton, R.W., Lalwani, G.A., Puliafito, C.A. 2008. Macular thickness measurements in normal eyes using spectral domain optical coherence tomography. *Ophthalmic Surgery, Lasers & Imaging* 39(4 Suppl), pp. S43–9.

Leite, M.T., Rao, H.L., Weinreb, R.N., Zangwill, L.M., Bowd, C., Sample, P.A., Tafreshi, A. and Medeiros, F.A. 2011. Agreement among spectral-domain optical coherence tomography instruments for assessing retinal nerve fiber layer thickness. *American Journal of Ophthalmology* 151(1), pp. 85–92.

Leske, M., Heijl, A., Hussein, M. and al, et 2003. Factors for glaucoma progression and the effect of treatment: The early manifest glaucoma trial. *Archives of Ophthalmology* 121(1), pp. 48–56.

Leske, M.C. 2007. Open-angle glaucoma - an epidemiologic overview. *Ophthalmic Epidemiology* 14(4), pp. 166–172.

Leung, C.K.S., Cheung, C.Y.L., Lin, D., Chi, P.P., Lam, D.S.C. and Weinreb, R.N. 2008. Longitudinal variability of optic disc and retinal nerve fiber layer measurements. *Investigative Ophthalmology and Visual Science* 49(11), pp. 4886–4892.

Lévêque, P., Zéboulon, P., Brasnu, E., Baudouin, C., Labbé, A. 2016. Optic disc vascularization in glaucoma: value of spectral-domain optical coherence tomography angiography. 20(16).

Li, S., Wang, X., Li, S., Wu, G. and Wang, N. 2010. Evaluation of optic nerve head and retinal nerve fiber layer in early and advance glaucoma using frequency-domain optical coherence tomography. *Graefe's Archive for Clinical and Experimental Ophthalmology* 248(3), pp. 429–34.

Lisboa, R., Weinreb, R.N. and Medeiros, F. a 2013. Combining structure and function to evaluate glaucomatous progression: implications for the design of clinical trials. *Current Opinion in Pharmacology* 13(1), pp. 115–22.

Littmann, H. 1988. Determination of the true size of an object on the fundus of the living eye. *Klinische Monatsblätter Fur Augenheilkunde* 192, pp. 66–67.

- Liu, M., Guo, L., Salt, T.E. and Cordeiro, M.F. 2010. Dendritic changes in the retinal ganglion cells in a rat model of experimental glaucoma. *Investigative Ophthalmology & Visual Science* 51(13), p. 5217.
- Makita, S., Fabritius, T., Yasuno, Y. 2008. Quantitative retinal-blood flow measurement with three-dimensional vessel geometry determination using ultrahigh-resolution Doppler optical coherence angiography. *Optics Letters* 33(8), pp. 836–838.
- Mari, J.M., Strouthidis, N.G., Park, S.C. and Girard, M.J. a 2013. Enhancement of lamina cribrosa visibility in optical coherence tomography images using adaptive compensation. *Investigative Ophthalmology & Visual Science* 54(3), pp. 2238–2247.
- Martinez-de-la-Casa, J.M., Cifuentes-Canorea, P., Berrozpe, C., Sastre, M., Polo, V., Moreno-Montanes, J. and Garcia-Feijoo, J. 2014. Diagnostic ability of macular nerve fiber layer thickness using new segmentation software in glaucoma suspects. *Investigative Ophthalmology & Visual Science* 55(12), pp. 8343–8348.
- Medeiros, F.A., Zangwill, L.M., Bowd, C., Vessani, R.M., Susanna, R. and Weinreb, R.N. 2005. Evaluation of retinal nerve fiber layer, optic nerve head, and macular thickness measurements for glaucoma detection using optical coherence tomography. *American Journal of Ophthalmology* 139(1), pp. 44–55.
- Mikelberg, F.S., Drance, S.M., Schulzer, M., Yidegiligne, H.M. and Weis, M.M. 1989. The normal human optic nerve. Axon count and axon diameter distribution. *Ophthalmology* 96(9), pp. 1325–1328.
- Miller, K.M. and Quigley, H.A. 1988. The clinical appearance of the lamina cribrosa as a function of the extent of glaucomatous optic-nerve damage. *Ophthalmology* 95, pp. 135–138.
- Minckler, D.S. 1986. Correlations between anatomic features and axonal transport in primate optic nerve head. *Transactions of the American Ophthalmological Society* 84, pp. 429–452.
- Minckler, D.S. 1989. Histology of optic nerve damage in ocular hypertension and early glaucoma. *Survey of Ophthalmology* 33 Suppl, p. 401.
- Minckler, D.S., McLean, I.W. and Tso, M.O.M. 1976. Distribution of axonal and glial elements in rhesus optic nerve head studied by electron-microscopy. *American Journal of Ophthalmology* 82, pp. 179–187.
- Mitchell, P., Hourihan, F., Sandbach, J. and Wang, J.J. 1999. The relationship between glaucoma and myopia: the Blue Mountains Eye Study. *Ophthalmology* 106(10), pp. 2010–2015.
- Morgan, J.E. 2002. Retinal ganglion cell shrinkage in glaucoma. *Journal of Glaucoma* 11(4), pp. 365–370.
- Morgan, J.E., Datta, A. V, Erichsen, J.T., Albon, J. and Boulton, M.E. 2006. Retinal ganglion cell remodelling in experimental glaucoma. *Advances in Experimental Medicine and Biology* 572, pp. 397–402.
- Morrison, J.C., L'Hernault, N.L., Jerdan, J.A. and Quigley, H.A. 1989. Ultrastructural location of extracellular matrix components in the optic nerve head. *Archives of Ophthalmology* 107, pp. 123–129.

- Moya, F.J., Brigatti, L. and Caprioli, J. 1999. Effect of aging on optic nerve appearance: a longitudinal study. *The British Journal of Ophthalmology* 83(5), pp. 567–572.
- Murdoch, I.E., Morris, S.S., Cousens, S.N. 1998. People and eyes: statistical approaches in ophthalmology. *The British Journal of Ophthalmology* 82(8), pp. 971–973.
- Mwanza, J.-C., Oakley, J.D., Budenz, D.L. and Anderson, D.R.. 2011. Ability of Cirrus HD-OCT optic nerve head parameters to discriminate normal from glaucomatous eyes. *Ophthalmology* 118, pp. 241–U34.
- Mylonas, G., Ahlers, C., Malamos, P., Golbaz, I., Deak, G., Schuetze, C., Sacu, S. and Schmidt-Erfurth, U. 2009. Comparison of retinal thickness measurements and segmentation performance of four different spectral and time domain OCT devices in neovascular age-related macular degeneration. *The British Journal of Ophthalmology* 93(11), pp. 1453–1460.
- Nadler, Z., Wang, B., Schuman, J.S., Ferguson, R.D., Patel, A., Hammer, D.X., Bilonick, R.A., Ishikawa, H., Kagemann, L., Sigal, I.A. and Wollstein, G. 2014. In vivo three-dimensional characterization of the healthy human lamina cribrosa with adaptive optics spectral-domain optical coherence tomography. *Investigative Ophthalmology & Visual Science* 55(10), pp. 6459–6466.
- Niles, P.I., Greenfield, D.S., Sehi, M., Bhardwaj, N., Iverson, S.M. and Chung, Y.S. 2012. Detection of progressive macular thickness loss using optical coherence tomography in glaucoma suspect and glaucomatous eyes. *Eye (London, England)* 26(7), pp. 983–991.
- Norman, R.E., Flanagan, J.G., Rausch, S.M.K., Sigal, I.A., Tertinegg, I., Eilaghi, A., Portnoy, S., Sled, J.G. and Ethier, C.R. 2010. Dimensions of the human sclera: Thickness measurement and regional changes with axial length. *Experimental Eye Research* 90, pp. 277–284.
- Norman, R.E., Flanagan, J.G., Sigal, I. a, Rausch, S.M.K., Tertinegg, I. and Ethier, C.R. 2011. Finite element modeling of the human sclera: influence on optic nerve head biomechanics and connections with glaucoma. *Experimental Eye Research* 93(1), pp. 4–12.
- Ogden, T.E., Duggan, J., Danley, K., Wilcox, M., Minckler, D.S., Doheny, E., Foundation, E., Street, S.P. and Angeles, L. 1988. Morphometry of nerve fiber bundle pores in the optic nerve head of the human. *Experimental Eye Research* 46, pp. 559–568.
- Oliveira, C., Harizman, N., Girkin, C.A., Xie, A., Tello, C., Liebmann, J.M. and Ritch, R. 2007. Axial length and optic disc size in normal eyes. *The British Journal of Ophthalmology* 91(1), pp. 37–39.
- Osborne, N.N., Melena, J., Chidlow, G. and Wood, J.P.M. 2001. A hypothesis to explain ganglion cell death caused by vascular insults at the optic nerve head: possible implication for the treatment of glaucoma. *British Journal of Ophthalmology* 85, pp. 1252–1259.
- Osborne, N.N. and Del Olmo-Aguado, S. 2013. Maintenance of retinal ganglion cell mitochondrial functions as a neuroprotective strategy in glaucoma. *Current Opinion in Pharmacology* 13(1), pp. 16–22.
- Oyama, T., Abe, H. and Ushiki, T. 2006. The connective tissue and glial framework in the optic nerve head of the normal human eye: light and scanning electron microscopic studies. *Archives of Histology and Cytology* 69, pp. 341–356.

Pakravan, M., Parsa, A., Sanagou, M. and Parsa, C.F. 2007. Central corneal thickness and correlation to optic disc size: a potential link for susceptibility to glaucoma. *The British Journal of Ophthalmology* 91(1), pp. 26–28.

Parikh, R.S., Parikh, S.R., Sekhar, G.C., Prabakaran, S., Babu, J.G. and Thomas, R. 2007. Normal age-related decay of retinal nerve fiber layer thickness. *Ophthalmology* 114(5), pp. 921–6.

Park, H.-Y.L., Jeon, S.H. and Park, C.K. 2012. Enhanced depth imaging detects lamina cribrosa thickness differences in normal tension glaucoma and primary open-angle glaucoma. *Ophthalmology* 119, pp. 10–20.

Park, S.B., Sung, K.R., Kang, S.Y., Kim, K.R. and Kook, M.S. 2009. Comparison of glaucoma diagnostic Capabilities of Cirrus HD and Stratus optical coherence tomography. *Archives of Ophthalmology (Chicago, Ill. : 1960)* 127(12), pp. 1603–1609.

Park, S.C., Kiumehr, S., Teng, C.C., Tello, C., Liehmann, J.M., Ritch, R. and Liebmann, J.M. 2012. Horizontal central ridge of the lamina cribrosa and regional differences in laminar insertion in healthy subjects. *Investigative Ophthalmology & Visual Science* 53(3), pp. 1610–1616.

Park, S.C., De Moraes, C.G. V, Teng, C.C., Tello, C., Liebmann, J.M. and Ritch, R. 2012. Enhanced depth imaging optical coherence tomography of deep optic nerve complex structures in glaucoma. *Ophthalmology* 119(1), pp. 3–9.

Park, S.C. and Ritch, R. 2011. High resolution in vivo imaging of the lamina cribrosa. *Saudi Journal of Ophthalmology* 25(4), pp. 363–72.

Pieroth, L., Schuman, J.S., Hertzmark, E., Hee, M.R., Wilkins, J.R., Coker, J., Mattox, C., Pedut-Kloizman, R., Puliafito, C. a, Fujimoto, J.G., Swanson, E. and Pedut-Kloizman, T. 1999. Evaluation of focal defects of the nerve fiber layer using optical coherence tomography. *Ophthalmology* 106(3), pp. 570–9.

Piltz-Seymour, I.R., Grunwald, J.E., Hariprasad, S.M. and DuPont, J. 2001. Optic nerve blood flow is diminished in eyes of primary open-angle glaucoma suspects. *American Journal of Ophthalmology* 132, pp. 63–69.

Povazay, B., Bizheva, K., Hermann, B., Unterhuber, A., Sattmann, H., Fercher, A., Drexler, W., Schubert, C., Ahnelt, P., Mei, M., Holzwarth, R., Wadsworth, W., Knight, J. and Russell, P.S. 2003. Enhanced visualization of choroidal vessels using ultrahigh resolution ophthalmic OCT at 1050 nm. *Optics Express* 11, pp. 1980–1986.

Povazay, B., Hermann, B., Unterhuber, A., Hofer, B., Sattmann, H., Zeiler, F., Morgan, J.E., Falkner-Radler, C., Glittenberg, C., Blinder, S. and Drexler, W. 2007. Three-dimensional optical coherence tomography at 1050 nm versus 800 nm in retinal pathologies: enhanced performance and choroidal penetration in cataract patients. *Journal of Biomedical Optics* 12(4), p. 41211.

Puliafito, C.A., Hee, M.R., Schuman, J.S. and Fujimoto, J.G. 1999. *Optical Coherence Tomography of Ocular Diseases*. 1st ed. United States of America: SLACK Incorporated.

Quigley, H. a. 2011. Glaucoma. *The Lancet* 377(9774), pp. 1367–1377.

Quigley, H.A. 1999. Neuronal death in glaucoma. *Progress in Retinal and Eye Research* 18, pp. 39–57.

- Quigley, H.A. and Addicks, E.M. 1981. Regional differences in the structure of the lamina cribrosa and their relation to glaucomatous optic nerve damage. *Archives of Ophthalmology* 99, pp. 137–143.
- Quigley, H.A., Addicks, E.M., Green, W.R. and Maumenee, A.E. 1981. Optic nerve damage in human glaucoma. II. The site of injury and susceptibility to damage. *Archives of Ophthalmology* 99, pp. 635–649.
- Quigley, H.A. and Broman, A.T. 2006. The number of people with glaucoma worldwide in 2010 and 2020. *British Journal of Ophthalmology* 90, pp. 262–267.
- Quigley, H.A., Brown, A. and Dorman-Pease, M.E. 1991. Alterations in elastin of the optic nerve head in human and experimental glaucoma. *The British Journal of Ophthalmology* 75(9), pp. 552–557.
- Quigley, H.A., Brown, A.E., Morrison, J.D. and Drance, S.M. 1990. The size and shape of the optic disc in normal human eyes. *Archives of Ophthalmology* 108, pp. 51–57.
- Quigley, H.A., Dormanpease, M.E. and Brown, A.E. 1991. Quantitative study of collagen and elastin of the optic-nerve head and sclera in human and experimental monkey glaucoma. *Current Eye Research* 10, pp. 877–888.
- Quigley, H.A., Dunkelberger, G.R. and Green, W.R. 1989. Retinal ganglion cell atrophy correlated with automated perimetry in human eyes with glaucoma. *American Journal of Ophthalmology* 107, pp. 453–464.
- Quigley, H.A. and Green, W.R. 1979. The histology of human glaucoma cupping and optic nerve damage: clinicopathologic correlation in 21 eyes. *Ophthalmology* 86(10), pp. 1803–1830.
- Quigley, H.A., Hohman, R.M., Addicks, E.M., Massof, R.W. and Green, W.R. 1983. Morphologic changes in the lamina cribrosa correlated with neural loss in open-angle glaucoma. *American Journal of Ophthalmology* 95, pp. 673–691.
- Quigley, H.A., Katz, J., Derick, R.J., Gilbert, D. and Sommer, A. 1992. An evaluation of optic disk and nerve fiber layer examinations in monitoring the progression of early glaucoma damage. *Ophthalmology* 99, pp. 19–28.
- Quigley, H.A., Nickells, R.W., Kerrigan, L.A., Pease, M.E., Thibault, D.J. and Zack, D.J. 1995. Retinal ganglion cell death in experimental glaucoma and after axotomy occurs by apoptosis. *Investigative Ophthalmology & Visual Science* 36(5), pp. 774–786.
- Radius, R.L. and Gonzales, M. 1981. Anatomy of the lamina cribrosa in human eyes. *Archives of Ophthalmology* 99, pp. 2159–2162.
- Raza, A.S., Cho, J. and de Moraes, C.V. 2011. Retinal ganglion cell layer thickness and local visual field sensitivity in glaucoma. *Archives of Ophthalmology* 129(12), pp. 1529–1536.
- Reis, A.S.C., O’Leary, N., Stanfield, M.J., Shuba, L.M., Nicolela, M.T. and Chauhan, B.C. 2012. Laminal displacement and prelaminar tissue thickness change after glaucoma surgery imaged with optical coherence tomography. *Investigative Ophthalmology & Visual Science* 53(9), pp. 5819–5826.

Ren, R., Li, B., Gao, F., Li, L., Xu, X., Wang, N. and Jonas, J.B. 2010. Central corneal thickness, lamina cribrosa and peripapillary scleral histomorphometry in non-glaucomatous Chinese eyes. *Graefe's Archive for Clinical and Experimental Ophthalmology* 248(11), pp. 1579–1585.

Ren, R., Wang, N., Li, B., Li, L., Gao, F., Xu, X. and Jonas, J.B. 2009. Lamina cribrosa and peripapillary sclera histomorphometry in normal and advanced glaucomatous Chinese eyes with various axial length. *Investigative Ophthalmology & Visual Science* 50, pp. 2175–2184.

Repka, M.X. and Quigley, H.A. 1989. The effect of age on normal human optic nerve fiber number and diameter. *Ophthalmology* 96(1), pp. 26–32.

Rezakhaniha, R., Aghianniotis, A., Schrauwen, J.T.C., Griffa, A., Sage, D., Bouten, C.V.C., van de Vosse, F.N., Unser, M. and Stergiopoulos, N. 2012. Experimental investigation of collagen waviness and orientation in the arterial adventitia using confocal laser scanning microscopy. *Biomechanics and Modeling in Mechanobiology* 11(3-4), pp. 461–473.

Rho, C.R., Park, H.-Y.L., Lee, N.Y. and Park, C.K. 2012. Clock-hour laminar displacement and age in primary open-angle glaucoma and normal tension glaucoma. *Clinical and Experimental Ophthalmology* 40(4), pp. E183–E189.

Roberts, M.D., Grau, V., Grimm, J., Reynaud, J., Bellezza, A.J., Burgoyne, C.F. and Downs, J.C. 2009. Remodeling of the connective tissue microarchitecture of the lamina cribrosa in early experimental glaucoma. *Investigative Ophthalmology & Visual Science* 50(2), pp. 681–690.

Roberts, M.D., Liang, Y., Sigal, I.A., Grimm, J., Reynaud, J., Bellezza, A., Burgoyne, C.F. and Downs, J.C. 2010. Correlation between local stress and strain and lamina cribrosa connective tissue volume fraction in normal monkey eyes. *Investigative Ophthalmology & Visual Science* 51(1), pp. 295–307.

Savastano, M.C., Minnella, A.M., Tamburrino, A., Giovinco, G., Ventre, S. and Falsini, B. 2014. Differential vulnerability of retinal layers to early age-related macular degeneration: Evidence by SD-OCT segmentation analysis. *Investigative Ophthalmology & Visual Science* 55(1), pp. 560–566.

Schiefer, U., Papageorgiou, E., Sample, P.A., Pascual, J.P., Selig, B., Krapp, E. and Paetzold, J. 2010. Spatial pattern of glaucomatous visual field loss obtained with regionally condensed stimulus arrangements. *Investigative Ophthalmology & Visual Science* 51(11), pp. 5685–5689.

Schmitt, J.M. 1999. Optical Coherence Tomography (OCT): A Review. *Selected Topics in Quantum Electronics, IEEE Journal of* 5, pp. 1205–1215.

Schuman, J.S., Hee, M.R., Arya, A. V., Pedut-Kloizman, T., Puliafito, C.A., Fujimoto, J.G. and Swanson, E.A. 1995. Optical coherence tomography: a new tool for glaucoma diagnosis. *Current Opinion in Ophthalmology* 6, pp. 89–95.

Sekhar, G.C., Prasad, K., Dandona, R., John, R.K. and Dandona, L. 2001. Planimetric optic disc parameters in normal eyes: a population-based study in South India. *Indian Journal of Ophthalmology* 49(1), pp. 19–23.

Shou, T., Liu, J., Wang, W., Zhou, Y. and Zhao, K. 2003. Differential dendritic shrinkage of alpha and beta retinal ganglion cells in cats with chronic glaucoma. *Investigative Ophthalmology and Visual Science* 44(7), pp. 3005–3010.

- Sigal, I. a and Ethier, C.R. 2009. Biomechanics of the optic nerve head. *Experimental Eye Research* 88(4), pp. 799–807.
- Sigal, I.A., Flanagan, J.G. and Ethier, C.R. 2005. Factors influencing optic nerve head biomechanics. *Investigative Ophthalmology & Visual Science* 46(11), pp. 4189–4199.
- Sigal, I.A., Flanagan, J.G., Tertinegg, I. and Ethier, C.R. 2010. 3D morphometry of the human optic nerve head. *Experimental Eye Research* 90, pp. 70–80.
- Sigal, I.A., Yang, H., Roberts, M.D., Grimm, J.L., Burgoyne, C.F., Demirel, S. and Downs, J.C. 2011. IOP-Induced Lamina cribrosa deformation and scleral canal expansion: Independent or related? *Investigative Ophthalmology & Visual Science* 52, pp. 9023–9032.
- Sihota, R., Gupta, V., Tuli, D., Sharma, A., Sony, P. and Srinivasan, G. 2007. Classifying patterns of localized glaucomatous visual field defects on automated perimetry. *Journal of Glaucoma* 16(1), pp. 146–152.
- Sihota, R., Sony, P., Gupta, V., Dada, T. and Singh, R. 2005. Comparing glaucomatous optic neuropathy in primary open angle and chronic primary angle closure glaucoma eyes by optical coherence tomography. *Ophthalmic and Physiological Optics* 25, pp. 408–415.
- Silver, F.H., Horvath, I. and Foran, D.J. 2002. Mechanical implications of the domain structure of fiber-forming collagens: comparison of the molecular and fibrillar flexibilities of the alpha1-chains found in types I-III collagen. *Journal of Theoretical Biology* 216(2), pp. 243–254.
- Sommer, A., Katz, J., Quigley, H.A., Miller, N.R., Robin, A.L., Richter, R.C. and Witt, K.A. 1991. Clinically detectable nerve fiber atrophy precedes the onset of glaucomatous field loss. *Archives of Ophthalmology* 109, pp. 77–83.
- Spaide, R.F., Koizumi, H. and Pozonni, M.C. 2008. Enhanced depth imaging spectral-domain optical coherence tomography. *American Journal of Ophthalmology* 146, pp. 496–500.
- Spaide, R.F., Klancnik, J.M., Cooney, M.J. 2015. Retinal vascular layers imaged by fluorescein angiography and optical coherence tomography angiography. *JAMA Ophthalmology* 133(1), pp. 45–50.
- Strouthidis, N.G. and Girard, M.J. a 2013. Altering the way the optic nerve head responds to intraocular pressure—a potential approach to glaucoma therapy. *Current Opinion in Pharmacology* 13(1), pp. 83–9.
- Strouthidis, N.G., Grimm, J., Williams, G.A., Cull, G. a, Wilson, D.J. and Burgoyne, C.F. 2010. A comparison of optic nerve head morphology viewed by spectral domain optical coherence tomography and by serial histology. *Investigative Ophthalmology & Visual Science* 51(3), pp. 1464–1474.
- Strouthidis, N.G., Yang, H., Fortune, B., Downs, J.C. and Burgoyne, C.F. 2009. Detection of optic nerve head neural canal opening within histomorphometric and spectral domain optical coherence tomography data sets. *Investigative Ophthalmology & Visual Science* 50, pp. 214–223.

Sung, K.R., Na, J.H. and Lee, Y. 2012. Glaucoma diagnostic capabilities of optic nerve head parameters as determined by Cirrus HD optical coherence tomography. *Journal of Glaucoma* 21(7), pp. 498–504.

Sung, K.R., Wollstein, G., Bilonick, R.A., Townsend, K.A., Ishikawa, H., Kagemann, L., Noecker, R.J., Fujimoto, J.G. and Schuman, J.S. 2009. Effects of age on optical coherence tomography measurements of healthy retinal nerve fiber layer, macula, and optic nerve head. *Ophthalmology* 116(6), pp. 1119–1124.

Susanna Jr., R. 1983. The lamina cribrosa and visual field defects in open-angle glaucoma. *Canadian Journal of Ophthalmology* 18, pp. 124–126.

Tan, O., Chopra, V., Lu, A.T.-H., Schuman, J.S., Ishikawa, H., Wollstein, G., Varma, R. and Huang, D. 2009. Detection of macular ganglion cell loss in glaucoma by Fourier-domain optical coherence tomography. *Ophthalmology* 116(12), pp. 2305–2314.e1–e2.

Tan, O., Li, G., Lu, A.T.-H., Varma, R. and Huang, D. 2008. Mapping of macular substructures with optical coherence tomography for glaucoma diagnosis. *Ophthalmology* 115(6), pp. 949–956.

Tarabishy, A.B., Alexandrou, T.J. and Traboulsi, E.I. 2007. Syndrome of myelinated retinal nerve fibers, myopia, and amblyopia: A review. *Survey of Ophthalmology* 52, pp. 588–596.

Terai, N., Spoerl, E., Pillunat, L.E., Kuhlisch, E., Schmidt, E. and Boehm, A.G. 2011. The relationship between central corneal thickness and optic disc size in patients with primary open-angle glaucoma in a hospital-based population. *Acta Ophthalmologica* 89(6), pp. 556–559.

Tezel, G., Trinkaus, K. and Wax, M.B. 2004. Alterations in the morphology of lamina cribrosa pores in glaucomatous eyes. *British Journal of Ophthalmology* 88, pp. 251–256.

Tham, Y.-C., Cheung, C.Y., Koh, V.T., Cheng, C.-Y., Sidhartha, E., Strouthidis, N.G., Wong, T.Y. and Aung, T. 2013. Relationship between ganglion cell-inner plexiform layer and optic disc/retinal nerve fibre layer parameters in non-glaucomatous eyes. *British Journal of Ophthalmology* 97(12), pp. 1592–1597.

Tielsch, J.M., Katz, J., Singh, K., Quigley, H.A., Gottsch, J.D., Javitt, J. and Sommer, A. 1991. A population-based evaluation of glaucoma screening - The Baltimore Eye Survey. *American Journal of Epidemiology* 134, pp. 1102–1110.

Tomita, G., Nyman, K., Raitta, C. and Kawamura, M. 1994. Interocular asymmetry of optic disc size and its relevance to visual field loss in normal-tension glaucoma. *Graefe's Archive for Clinical and Experimental Ophthalmology* 32(5), pp. 290–296.

Tong, A.Y., El-Dairi, M., Maldonado, R.S., Rothman, A.L., Yuan, E.L., Stinnett, S.S., Kupper, L., Cotten, C.M., Gustafson, K.E., Goldstein, R.F., Freedman, S.F., Toth, C.A. 2014. Evaluation of optic nerve development in preterm and term infants using handheld spectral-domain optical coherence tomography. *Ophthalmology* 121(9), pp. 1818–26.

Tsai, C.S., Ritch, R., Shin, D.H., Wan, J.Y. and Chi, T. 1992. Age-related decline of disc rim area in visually normal subjects. *Ophthalmology* 99(1), pp. 29–35.

Ugurlu, S., Weitzman, M., Nduaguba, C. and Caprioli, J. 1998. Acquired pit of the optic nerve: a risk factor for progression of glaucoma. *American Journal of Ophthalmology* 125, pp. 457–464.

Unterhuber, A., Povazay, B., Hermann, B., Sattmann, H., Chavez-Pirson, a and Drexler, W. 2005. In vivo retinal optical coherence tomography at 1040 nm - enhanced penetration into the choroid. *Optics Express* 13(9), pp. 3252–3258.

Varma, R., Bazzaz, S. and Lai, M. 2003. Optical tomography-measured retinal nerve fiber layer thickness in normal Latinos. *Investigative Ophthalmology & Visual Science* 44(8), pp. 3369–3373.

Vrabec, F. 1976. Glaucomatous cupping of the human optic disk: a neuro-histologic study. *Graefe's Archive for Clinical and Experimental Ophthalmology* 198(3), pp. 223–234.

Wang, B., Nevins, J.E., Nadler, Z., Wollstein, G., Ishikawa, H., Bilonick, R. a., Kagemann, L., Sigal, I. a., Grulkowski, I., Liu, J.J., Kraus, M., Lu, C.D., Hornegger, J., Fujimoto, J.G. and Schuman, J.S. 2013. In vivo lamina cribrosa micro-architecture in healthy and glaucomatous eyes as assessed by optical coherence tomography. *Investigative Ophthalmology & Visual Science* e 54(13), pp. 8270–8274.

Wang, Y., Nelson, J., Chen, Z., Reiser, B., Chuck, R. and Windeler, R. 2003. Optimal wavelength for ultrahigh-resolution optical coherence tomography. *Optics Express* 11, pp. 1411–1417.

Weber, A.J., Kaufman, P.L. and Hubbard, W.C. 1998. Morphology of single ganglion cells in the glaucomatous primate retina. *Investigative Ophthalmology & Visual Science* 39(12), pp. 2304–2320.

Wilczek, M. 1947. The lamina cribrosa and its nature. *British Journal of Ophthalmology* 31, pp. 551–565.

Winkler, M., Jester, B., Nien-Shy, C., Massei, S., Minckler, D.S., Jester, J. V and Brown, D.J. 2010. High resolution three-dimensional reconstruction of the collagenous matrix of the human optic nerve head. *Brain Research Bulletin* 81(2-3), pp. 339–348.

Wojtkowski, M., Leitgeb, R., Kowalczyk, A., Bajraszewski, T. and Fercher, A.F. 2002. In vivo human retinal imaging by Fourier domain optical coherence tomography. *Journal of Biomedical Optics* 7(3), pp. 457–463.

Wollstein, G., Schuman, J.S., Price, L.L., Aydin, A., Beaton, S.A., Stark, P.C., Fujimoto, J.G. and Ishikawa, H. 2004. Optical coherence tomography (OCT) macular and peripapillary retinal nerve fiber layer measurements and automated visual fields. *American Journal of Ophthalmology* 138(2), pp. 218–225.

Wong, I.Y.H., Wong, a C.M. and Chan, C.W.N. 2010. Relationship between age and peripapillary retinal nerve fibre layer thickness: an optical coherence tomography study. *Hong Kong Medical Journal* 16(4), pp. 265–268.

Wu, Z., Xu, G., Weinreb, R.N., Yu, M. and Leung, C.K.S.S. 2015. Optic nerve head deformation in glaucoma: A prospective analysis of optic nerve head surface and lamina cribrosa surface displacement. *Ophthalmology* 122(7), pp. 1–13.

Xu, L., Wang, Y., Wang, S., Wang, Y. and Jonas, J.B. 2007. High myopia and glaucoma susceptibility: The Beijing Eye Study. *Ophthalmology* 114, pp. 216–220. A

Yang, H., Williams, G., Downs, J.C., Sigal, I.A., Roberts, M.D., Thompson, H. and Burgoyne, C.F. 2011. Posterior (outward) migration of the lamina cribrosa and early cupping in monkey experimental glaucoma. *Investigative Ophthalmology & Visual Science* 52, pp. 7109–7121.

Yoshikawa, M., Akagi, T., Hangai, M., Ohashi-Ikeda, H., Takayama, K., Morooka, S., Kimura, Y., Nakano, N. and Yoshimura, N. 2014. Alterations in the neural and connective tissue components of glaucomatous cupping after glaucoma surgery using swept-source optical coherence tomography. *Investigative Ophthalmology and Visual Science* 55(1), pp. 477–484.

Zawadzki, R.J., Jones, S.M., Olivier, S.S., Zhao, M., Bower, B.A., Izatt, J.A., Choi, S., Laut, S. and Werner, J.S. 2005. Adaptive-optics optical coherence tomography for high-resolution and high-speed 3D retinal in vivo imaging. *Optics Express* 13(21), pp. 8532–8546.

Zeimer, M., Gutfleisch, M., Heimes, B., Spital, G., Lommatzsch, A. and Pauleikhoff, D. 2015. Association between changes in macular vasculature in optical coherence tomography- and fluorescein- angiography and distribution of macular pigment in type 2 idiopathic macular telangiectasia. *Retina* 35(11).

Zhang, Y., Rha, J., Jonnal, R. and Miller, D. 2005. Adaptive optics parallel spectral domain optical coherence tomography for imaging the living retina. *Optics Express* 13(12), pp. 4792–4811.

Zhu, D., Reznik, C., Chen, C.L., Wang, R. and Puliafito, C. 2015. Evaluation of optic disc perfusion in normal-tension glaucoma patients by optical coherence tomography angiography. *Investigative Ophthalmology & Visual Science* 56(7), p. 2745.

Zingirian, M., Calabria, G. and Gandolfo, E. 1979. The nasal step in normal and glaucomatous visual fields. *Canadian journal of ophthalmology* 14(2), pp. 88–94.

Appendix

Appendix 1: Examples of participant consent form and information

Example consent form for participants in the study

Study Number: Version 2.1 (14.01.2013)

Patient Identification Number for this trial:



CONSENT FORM: PATIENTS

Title of Project: High Resolution Optical Coherence Tomography in Healthy and Glaucomatous Optic Nerves

Name of Researchers: Professor James Morgan
Professor Rachel North
Dr Julie Albon

Please
initial box

1. I confirm that I have read and understand the information sheet dated (Version 2.1: 14.01.2013) for the above study. I have had the opportunity to consider the information, ask questions and have had these answered satisfactorily.
2. I understand that my participation is voluntary and that I am free to withdraw at any time without giving any reason, without my medical care or legal rights being affected.
3. I understand that relevant sections of my medical notes and data collected during the study may be looked at by individuals from Cardiff University, or from the NHS Trust, where it is relevant to my taking part in this research. I give permission for these individuals to have access to my records.
4. I understand that my General Practitioner (GP) will be informed of my participation in the study.
5. I agree to take part in the above study

Name of participant

Date

Signature

Name of person taking consent

Date

Signature

- Please tick this box if you wish to receive a paper summary of the research findings at the end of the study.

Example participant information sheet

University Hospital of Wales
Cardiff and Vale NHS Trust
Heath Park
Cardiff CF14 4XW
Tel: 029-20743222

School of Optometry & Vision Sciences
Maindy Road
Cardiff University
Cardiff CF24 4LU
Tel: 029-20874374

Project Title:**High Resolution Optical Coherence Tomography (UHR-OCT) in Glaucoma**

Principal Investigator: Professor James Morgan

PATIENT INFORMATION SHEET

You are being invited to take part in a research study. Before you decide to take part, it is important for you to understand why the research is being done and what it will involve. Please take time to read the following information carefully.

- Part 1 tells you the purpose of this study and what will happen to you if you take part.
- Part 2 gives you more detailed information about the conduct of the study.

Ask us if there is anything that is not clear or if you would like more information. Take time to decide whether or not you wish to take part.

PART 1

1. What is the purpose of the study?

The study is being carried out to understand the early changes in glaucoma, an eye disease, which remains one of the commonest causes of vision loss in the UK. In glaucoma, the pressure in the eye is usually increased which can damage the nerve that connects the eye with the brain (the optic nerve). If this pressure is not reduced then vision can be lost.

The treatment of glaucoma has advanced greatly in recent years with the development of treatments for the reduction of eye pressure, which have been shown to reduce or stop the progression of this disease. Therefore, the earlier the disease is detected, the earlier treatment can start to prevent visual loss. At present, doctors often rely on detecting loss of the visual field to diagnose and treat this condition. Using a new technology (UHR-OCT eye imaging) we may be able to diagnose and treat glaucoma before it has caused any detectable visual loss.

2. Why have we approached you to take part in this study?

You will have been approached to participate in this study either as a patient with possible glaucoma or as a healthy volunteer. You will have a number of tests that will allow us to see if you have early glaucoma by comparing your eyes with those of healthy volunteers. We aim to include 500 participants like you.

3. Do you have to take part?

It is entirely up to you to decide whether or not to take part. If you do, you will be given this information sheet to keep and be asked to sign a consent form. You are still free to withdraw at any time and without giving a reason. A decision to withdraw at any time, or a decision not to take part, will not, in any way affect the standard of care you receive.

4. What will happen if you do decide to take part in the study?

If you agree to participate you will have a normal assessment for glaucoma which will include checking your eyes, eye pressures, your field of vision and take some pictures of the inside of the eye at the medical illustration department at University Hospital of Wales. Participants with glaucoma will have an abnormality in one or more of these tests. The pictures with the new technology will be taken at the School of Optometry and Vision Sciences, Cardiff University. You will also have your pupils dilated and the imaging will take up to 45 minutes. You will be asked to attend the University once initially and possibly for a follow-up appointment one year later to see if your optic nerve is changing. You will receive your regular treatment as required regardless of the study.

If we see any changes in the optic nerve as a result of the study, your eye doctor will be informed so that any changes in treatment can be made.

5. Will you be paid for taking part in the study?

We do not offer any payment for taking part in the study. However we will cover any reasonable travel expenses associated with taking part.

6. What is the procedure that is being tested?

We are testing a new method, called Ultra-High Resolution Optical Coherence Tomography (UHR-OCT), of taking pictures of the back of the eye. UHR-OCT can provide images of the eye at very high resolution that we should be able to detect the earliest signs of glaucoma damage. We hope

that this will be able to pick changes at the changes suggestive of glaucoma before it starts to affect your eyesight. In order to do this we have to also take images from healthy volunteers.

7. What are the side effects of any imaging when taking part?

The imaging device has been used as a diagnostic tool with an established safety record and there are no potential side effects known. The laser light used to take the pictures of the back of the eye is harmless and is below internationally recognised (ANSI) standards for light exposure. Overall the degree of light exposure is less than experienced during the standard photography performed routinely.

If you have any concerns, do feel free to ask any questions regarding the risk.

8. What are the possible benefits of taking part?

We cannot promise the study will help you but the information we acquire will provide us with further information of various changes occurring at a microscopic level, which is not visible with standard photographic techniques presently available. We hope that the results from this study will help us detect the earliest signs of glaucoma – or of progressive glaucoma. The earlier we start treating patients with glaucoma, the greater our chances that we will be able to prevent damage.

9. What will happen to my routine care?

If you are currently receiving treatment or are being monitored at the hospital, you will continue to receive your appointments as before.

10. What happens when the research study stops?

The photographic procedure will stop after a one year of follow-up but if we plan to extend the study you will be informed about it in due course. If during the course of the study you develop worsening of the glaucoma in either eye then appropriate treatment shall be provided.

11. Will my taking part in the study be kept confidential?

Yes, all the information collected about you during the course of the research will be kept strictly confidential. You shall only be identified by a code number to ensure confidentiality.

12. Contact Details for further information:

Principal Investigator: Professor JE Morgan
Professor in Ophthalmology
Hon Consultant Ophthalmologist
School of Optometry and Vision Sciences
Cardiff University
CF10 3NB, UK
Office: 029 20876344
Secretary: 029 20743222
Fax: 029 20874859

If you would like to participate in this study, please contact: **Ms Beth Flynn, Optometrist and Post-graduate Researcher, School of Optometry and Vision Sciences, Cardiff University** to discuss the study and arrange an appointment.

Telephone: 029 20876471

This completes Part 1 of the Information Sheet. If the information in Part 1 has interested you and you are considering participation, please continue to read the additional information in Part 2 before making any decision.

PART 2**13. What if relevant new information becomes available?**

If new information becomes available during the course of study your research doctor will tell you about it and discuss whether you want to or should continue in the study. We stress that any changes in your participation in the study will not affect the care you currently receive.

14. What will happen if I don't want to carry on with the study?

If you withdraw from the study we will use the data collected up to your withdrawal and your care will continue as required.

15. What if there is a problem?

If you have a concern about any aspect of this study, you should ask to speak with the researchers who will do their best to answer your questions.

16. Involvement of the General Practitioner/Family doctor (GP)

Your GP will be notified regarding your condition if you have a type of glaucoma and treatment you require. The GP of volunteers with normal eye examinations will not be informed unless requested by the study participant.

17. What will happen to the results of the research study?

The work will be presented at the various national and international meetings (for example the American Association of Ophthalmologists or meeting relating to Biomedical Imaging Technologies) as required. Results of general interest to Glaucoma patients will be communicated through publications sponsored by the Glaucoma Society. The full results of the study will also be made available through peer-reviewed publications. In all these presentations, the identity of the study participants will remain confidential.

A summary of the results will be sent at the conclusion of the study to any participant who requests it.

18. Who is organising and funding the research?

Cardiff University will act as sponsors of this study. The School of Optometry and Vision Sciences, Cardiff University will fund transport costs.

19. Who has reviewed the study?

The study has been reviewed and approved by CaRRS (the Cardiff & Vale Research Review Service), at the NHS Research and Development Office, University Hospital of Wales, Cardiff and the South East Wales Research Ethics Committee.

Appendix II: Regional thickness and volume of the inner retinal layers

Regional volume of inner retinal layers for control and each stage of glaucoma

Retinal layer volume	R1		R2		R3		R4		R5		R6		R7		R8		R9		R10		R11		R12		R13		Total		
	Mean	± SD	Mean	± SD																									
GCC	C	0.53	0.16	0.54	0.17	0.56	0.17	0.54	0.15	0.29	0.09	0.29	0.09	0.29	0.09	0.29	0.09	0.07	0.02	0.07	0.02	0.07	0.02	0.07	0.02	0.03	0.01	3.59	1.11
	PG	0.45	0.16	0.45	0.18	0.48	0.18	0.46	0.16	0.25	0.09	0.25	0.09	0.25	0.09	0.25	0.09	0.06	0.02	0.06	0.02	0.06	0.02	0.06	0.02	0.02	0.01	3.05	1.14
	EG	0.38	0.10	0.38	0.10	0.40	0.10	0.40	0.11	0.21	0.06	0.21	0.06	0.21	0.06	0.21	0.06	0.05	0.01	0.05	0.01	0.05	0.01	0.05	0.01	0.02	0.01	2.58	0.71
	AG	0.43	0.12	0.43	0.13	0.42	0.15	0.42	0.14	0.23	0.07	0.24	0.07	0.24	0.07	0.23	0.07	0.06	0.01	0.06	0.02	0.05	0.02	0.05	0.02	0.02	0.01	2.90	0.89
mNFL	C	0.26	0.15	0.28	0.16	0.29	0.16	0.27	0.16	0.14	0.08	0.15	0.09	0.14	0.09	0.14	0.08	0.03	0.02	0.04	0.02	0.04	0.02	0.03	0.02	0.02	0.01	1.79	1.06
	PG	0.21	0.14	0.21	0.15	0.22	0.15	0.21	0.14	0.11	0.07	0.11	0.07	0.11	0.07	0.11	0.07	0.03	0.02	0.03	0.02	0.03	0.02	0.03	0.02	0.01	0.01	1.37	0.90
	EG	0.17	0.09	0.17	0.09	0.18	0.09	0.19	0.10	0.10	0.05	0.10	0.05	0.10	0.05	0.10	0.05	0.02	0.01	0.02	0.01	0.02	0.01	0.02	0.01	0.01	0.01	1.18	0.61
	AG	0.18	0.06	0.18	0.06	0.16	0.05	0.16	0.05	0.09	0.03	0.10	0.03	0.10	0.03	0.10	0.03	0.03	0.01	0.02	0.01	0.02	0.01	0.02	0.01	0.01	0.00	1.19	0.38
GCL	C	0.15	0.03	0.15	0.03	0.15	0.03	0.15	0.03	0.08	0.02	0.08	0.02	0.08	0.02	0.08	0.02	0.02	0.00	0.02	0.00	0.02	0.00	0.02	0.00	0.01	0.00	1.02	0.19
	PG	0.12	0.03	0.12	0.04	0.13	0.04	0.13	0.03	0.07	0.02	0.07	0.02	0.07	0.02	0.07	0.02	0.02	0.01	0.02	0.01	0.02	0.00	0.02	0.00	0.01	0.00	0.88	0.28
	EG	0.11	0.02	0.11	0.02	0.12	0.02	0.11	0.02	0.06	0.01	0.06	0.01	0.06	0.01	0.06	0.01	0.01	0.00	0.01	0.00	0.01	0.00	0.01	0.00	0.01	0.00	0.75	0.15
	AG	0.13	0.03	0.13	0.03	0.13	0.03	0.13	0.03	0.07	0.02	0.07	0.02	0.07	0.02	0.07	0.02	0.02	0.00	0.02	0.00	0.02	0.00	0.02	0.00	0.01	0.00	0.89	0.20
IPL	C	0.11	0.02	0.11	0.02	0.12	0.02	0.12	0.02	0.06	0.01	0.06	0.01	0.06	0.01	0.06	0.01	0.01	0.00	0.02	0.00	0.02	0.00	0.01	0.00	0.01	0.00	0.78	0.16
	PG	0.12	0.03	0.12	0.03	0.12	0.03	0.12	0.02	0.07	0.02	0.07	0.02	0.07	0.02	0.07	0.02	0.02	0.00	0.02	0.00	0.02	0.00	0.02	0.00	0.01	0.00	0.80	0.18
	EG	0.10	0.02	0.10	0.02	0.10	0.02	0.10	0.02	0.05	0.01	0.05	0.01	0.05	0.01	0.05	0.01	0.01	0.00	0.01	0.00	0.01	0.00	0.01	0.00	0.00	0.00	0.65	0.15
	AG	0.11	0.02	0.11	0.02	0.11	0.02	0.11	0.02	0.06	0.01	0.06	0.01	0.06	0.01	0.06	0.01	0.02	0.00	0.02	0.00	0.01	0.00	0.01	0.00	0.01	0.00	0.77	0.15

Figure 0.1: Regional volume of inner retinal layers for each stage of glaucoma. GCC = ganglion cell complex, mNFL = macula nerve fibre layer, GCL = ganglion cell layer, IPL = inner plexiform layer, C = control, PG = preperimetric glaucoma, EG = early glaucoma, AG = advanced glaucoma.

Regional thickness of inner retinal layers for control and each stage of glaucoma

Retinal layer thickness	R1		R2		R3		R4		R5		R6		R7		R8		R9		R10		R11		R12		R13		Total		
	Mean	± SD	Mean	± SD																									
GCC	C	146.	42.1	150.	44.3	150.	46.6	146.	44.0	147.	42.7	147.	43.0	147.	42.6	147.	42.4	145.	41.6	149.	45.3	152.	46.5	148.	43.3	154.	50.2	148.	42.9
		87	4	48	9	99	7	83	7	83	5	95	0	55	4	42	5	32	8	95	2	78	3	08	7	72	1	00	3
	PG	117.	42.0	120.	43.6	118.	42.8	114.	41.1	117.	40.4	117.	40.5	117.	40.3	117.	40.2	117.	40.4	117.	40.1	117.	41.0	116.	41.6	121.	43.9	117.	40.4
		15	5	61	3	07	6	10	3	68	2	68	9	54	7	56	4	12	5	60	4	42	5	92	4	54	8	61	5
EG	95.6	20.6	95.6	19.4	96.7	21.6	97.3	22.6	96.1	19.5	96.1	19.8	95.9	19.8	95.9	19.5	95.3	23.6	93.1	17.4	96.6	18.0	98.8	23.6	96.0	22.6	95.9	19.6	
	6	0	8	6	7	0	7	6	2	2	1	7	2	2	4	0	0	4	8	9	4	7	1	3	3	5	3	3	
AG	115.	33.9	115.	36.4	107.	35.5	108.	33.5	113.	35.5	113.	35.1	114.	34.9	114.	35.2	118.	32.3	118.	39.4	109.	43.8	110.	33.2	111.	39.5	114.	35.4	
	18	9	29	4	77	8	42	0	42	3	62	6	50	1	28	6	27	2	07	1	98	3	16	9	05	5	02	1	
mNFL	C	73.2	40.8	76.9	42.1	77.8	44.0	73.5	42.4	73.5	41.4	73.6	41.4	73.3	41.2	73.2	41.2	73.3	40.3	74.3	44.0	76.4	44.5	75.4	40.7	82.2	46.3	73.7	41.4
		5	4	6	2	7	0	5	3	8	3	9	8	7	7	9	7	9	2	6	7	1	1	1	6	6	3	8	8
	PG	54.5	35.0	56.8	37.6	54.5	35.7	52.8	34.9	52.9	32.9	53.0	33.1	52.7	32.7	52.7	32.6	51.8	31.8	52.2	31.7	53.2	33.0	52.8	34.0	55.4	34.8	52.7	32.7
		2	7	7	4	1	3	0	7	3	9	1	4	9	5	0	2	4	3	2	0	8	6	8	6	9	3	6	3
EG	42.8	20.8	41.7	18.9	44.1	20.6	45.9	22.6	43.1	19.6	43.2	20.2	42.9	20.1	42.9	19.5	42.7	23.9	40.3	16.6	43.6	17.7	46.1	24.9	43.7	23.3	43.0	19.8	
	5	4	6	5	2	9	0	7	7	0	3	3	9	5	5	6	5	3	2	3	8	3	4	1	5	5	1	4	
AG	52.7	19.3	52.2	21.4	46.8	21.5	47.9	19.4	50.8	20.9	51.2	20.5	51.8	20.4	51.4	20.7	56.4	18.9	54.2	23.7	46.6	28.9	48.8	19.0	47.2	22.5	51.3	20.7	
	0	4	7	8	8	2	3	0	1	2	0	8	7	2	7	5	1	1	3	0	8	8	9	4	2	8	8	4	
GCL	C	41.9		42.0		41.2		41.1		42.3		42.3		42.2		42.2		40.7		43.5		43.8		41.0		41.2		42.3	
		4	7.18	7	6.75	3	5.76	9	6.38	3	6.70	0	6.70	5	6.83	7	6.83	7	7.97	6	7.48	3	6.18	1	6.50	1	7.64	2	6.78
	PG	146.	42.1	150.	44.3	150.	46.6	146.	44.0	147.	42.7	147.	43.0	147.	42.6	147.	42.4	145.	41.6	149.	45.3	152.	46.5	148.	43.3	154.	50.2	148.	42.9
		87	4	48	9	99	7	83	7	83	5	95	0	55	4	42	5	32	8	95	2	78	3	08	7	72	1	00	3
EG	117.	42.0	120.	43.6	118.	42.8	114.	41.1	117.	40.4	117.	40.5	117.	40.3	117.	40.2	117.	40.4	117.	40.1	117.	41.0	116.	41.6	121.	43.9	117.	40.4	
	15	5	61	3	07	6	10	3	68	2	68	9	54	7	56	4	12	5	60	4	42	5	92	4	54	8	61	5	
AG	95.6	20.6	95.6	19.4	96.7	21.6	97.3	22.6	96.1	19.5	96.1	19.8	95.9	19.8	95.9	19.5	95.3	23.6	93.1	17.4	96.6	18.0	98.8	23.6	96.0	22.6	95.9	19.6	
	6	0	8	6	7	0	7	6	2	2	1	7	2	2	4	0	0	4	8	9	4	7	1	3	3	5	3	3	
IPL	C	115.	33.9	115.	36.4	107.	35.5	108.	33.5	113.	35.5	113.	35.1	114.	34.9	114.	35.2	118.	32.3	118.	39.4	109.	43.8	110.	33.2	111.	39.5	114.	35.4
		18	9	29	4	77	8	42	0	42	3	62	6	50	1	28	6	27	2	07	1	98	3	16	9	05	5	02	1
	PG	73.2	40.8	76.9	42.1	77.8	44.0	73.5	42.4	73.5	41.4	73.6	41.4	73.3	41.2	73.2	41.2	73.3	40.3	74.3	44.0	76.4	44.5	75.4	40.7	82.2	46.3	73.7	41.4
		5	4	6	2	7	0	5	3	8	3	9	8	7	7	9	7	9	2	6	7	1	1	1	6	6	3	8	8
EG	54.5	35.0	56.8	37.6	54.5	35.7	52.8	34.9	52.9	32.9	53.0	33.1	52.7	32.7	52.7	32.6	51.8	31.8	52.2	31.7	53.2	33.0	52.8	34.0	55.4	34.8	52.7	32.7	
	2	7	7	4	1	3	0	7	3	9	1	4	9	5	0	2	4	3	2	0	8	6	8	6	9	3	6	3	
AG	42.8	20.8	41.7	18.9	44.1	20.6	45.9	22.6	43.1	19.6	43.2	20.2	42.9	20.1	42.9	19.5	42.7	23.9	40.3	16.6	43.6	17.7	46.1	24.9	43.7	23.3	43.0	19.8	
	5	4	6	5	2	9	0	7	7	0	3	3	9	5	5	6	5	3	2	3	8	3	4	1	5	5	1	4	

Figure 0.2: Regional mean thickness of inner retinal layers for each stage of glaucoma. GCC = ganglion cell complex, mNFL = macula nerve fibre layer, GCL = ganglion cell layer, IPL = inner plexiform layer, C = control, PG = preperimetric glaucoma, EG = early glaucoma, AG = advanced glaucoma

Regional inner plexiform layer : macula nerve fibre layer and inner plexiform layer : ganglion cell layer ratios

Retinal layer ratio	R1		R2		R3		R4		R5		R6		R7		R8		R9		R10		R11		R12		R13		Total		
	Mean	± SD	Mean	± SD																									
IPL : mNFL	C	0.63	0.41	0.60	0.41	0.61	0.40	0.64	0.40	0.63	0.40	0.63	0.40	0.64	0.40	0.64	0.41	0.62	0.42	0.67	0.46	0.61	0.37	0.57	0.34	0.53	0.36	0.63	0.40
	PG	0.75	0.40	0.76	0.42	0.78	0.41	0.78	0.42	0.78	0.39	0.78	0.39	0.78	0.39	0.78	0.39	0.79	0.40	0.79	0.40	0.77	0.40	0.79	0.46	0.72	0.36	0.78	0.38
	EG	0.71	0.39	0.73	0.41	0.69	0.42	0.66	0.40	0.69	0.39	0.70	0.39	0.70	0.39	0.70	0.39	0.73	0.39	0.73	0.41	0.69	0.43	0.67	0.38	0.74	0.49	0.70	0.39
	AG	0.67	0.31	0.69	0.32	0.74	0.31	0.72	0.30	0.70	0.31	0.69	0.30	0.69	0.31	0.69	0.31	0.64	0.31	0.69	0.36	0.79	0.30	0.68	0.25	0.69	0.22	0.69	0.31
IPL : GCL	C	0.76	0.11	0.75	0.11	0.77	0.10	0.78	0.10	0.76	0.11	0.76	0.11	0.76	0.11	0.76	0.11	0.77	0.10	0.74	0.10	0.75	0.11	0.77	0.13	0.76	0.15	0.76	0.11
	PG	0.96	0.17	0.97	0.19	0.97	0.19	0.98	0.18	0.96	0.17	0.96	0.17	0.96	0.17	0.96	0.17	0.95	0.16	0.97	0.20	0.96	0.19	0.94	0.19	0.92	0.16	0.96	0.17
	EG	0.87	0.17	0.86	0.18	0.87	0.16	0.87	0.14	0.87	0.17	0.87	0.17	0.87	0.17	0.87	0.17	0.86	0.17	0.87	0.18	0.87	0.18	0.86	0.15	0.87	0.15	0.87	0.17
	AG	0.88	0.11	0.88	0.12	0.91	0.13	0.91	0.12	0.89	0.12	0.89	0.12	0.89	0.11	0.89	0.12	0.87	0.11	0.87	0.12	0.91	0.19	0.90	0.13	0.86	0.14	0.89	0.12

Figure 0.3: Regional ratio of inner plexiform layer (IPL) : macula nerve fibre layer (mNFL) and IPL : ganglion cell layer (GCL) for each stage of glaucoma. C = control, PG = preperimetric glaucoma, EG = early glaucoma, AG = advanced glaucoma.

Appendix III: Regional differences in the inner retinal layers in glaucoma

Differences in thickness of the ganglion cell complex between control and glaucoma

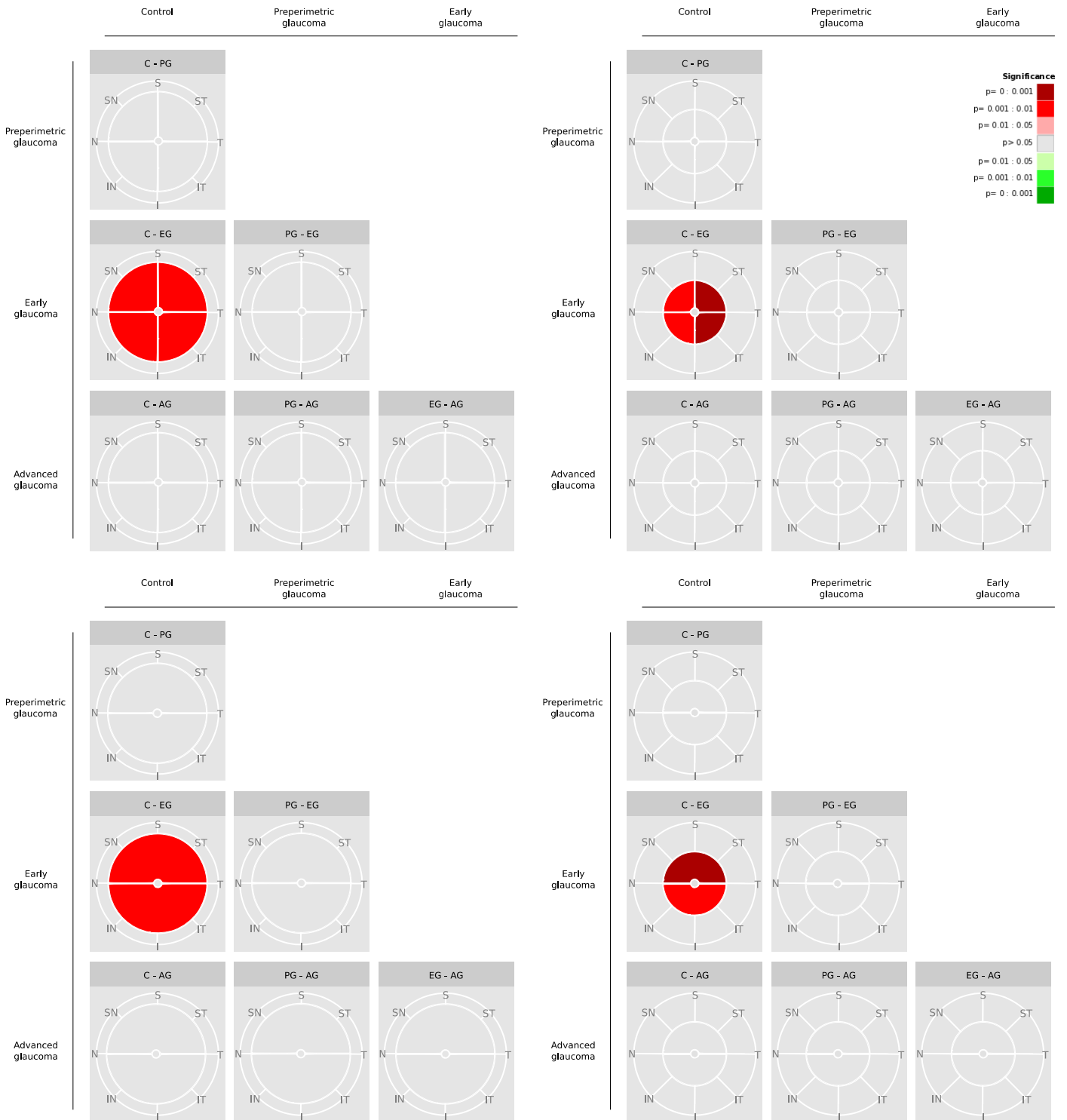


Figure 0.1: Differences in ganglion cell complex (GCC) thickness between control (C) and preperimetric glaucoma (PG), early glaucoma (EG) and advanced glaucoma (AG). Red indicates GCC thinning with increasing glaucoma stage, green indicates GCC thickening with increasing glaucoma stage.

Differences in volume of the ganglion cell complex between control and glaucoma

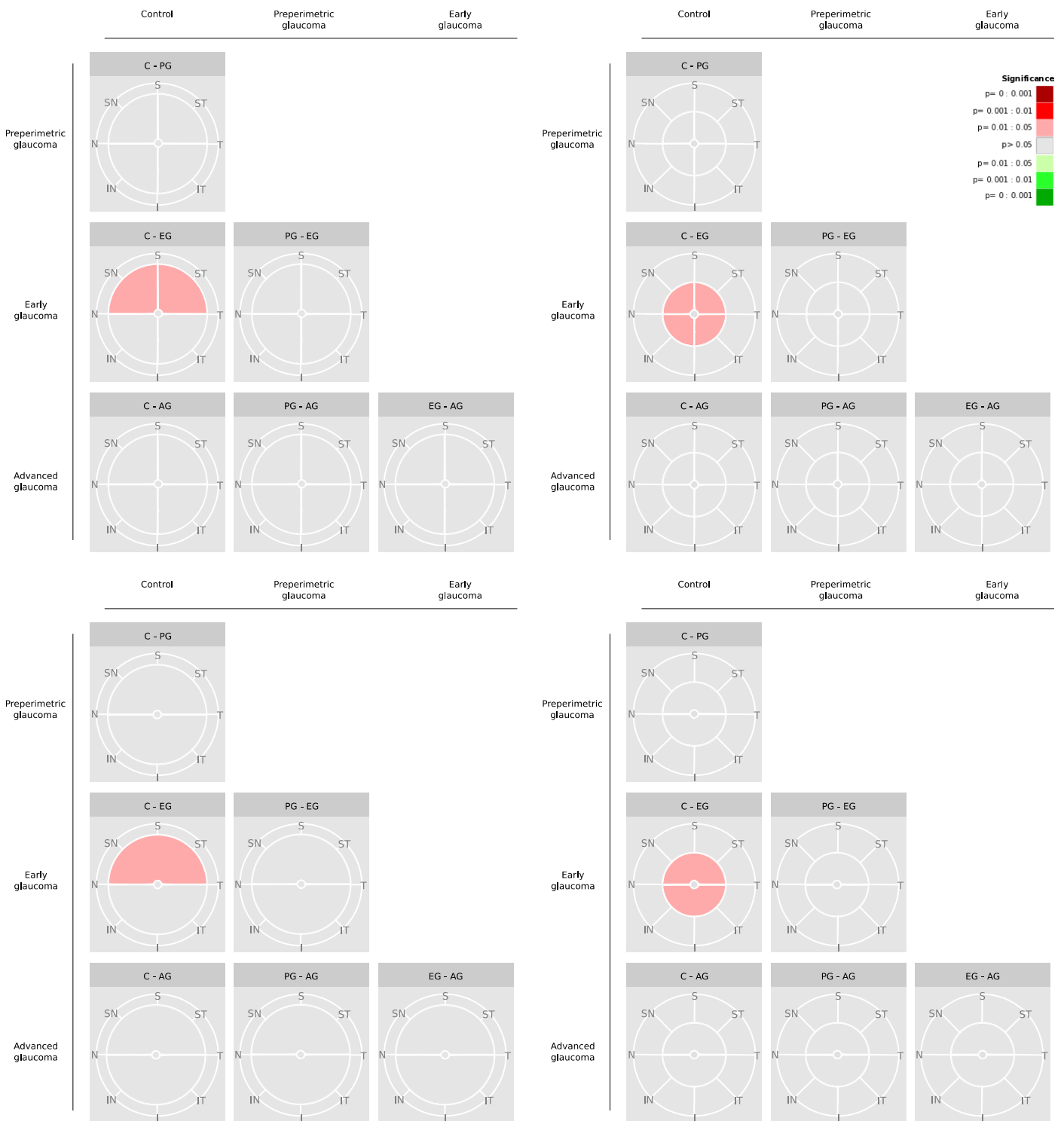


Figure 0.2: Differences in ganglion cell complex (GCC) volume between control (C) and preperimetric glaucoma (PG), early glaucoma (EG) and advanced glaucoma (AG). Red indicates GCC volume decrease with increasing glaucoma stage, green indicates GCC volume increase with increasing glaucoma stage.

Differences in thickness of the macula nerve fibre layer between control and glaucoma

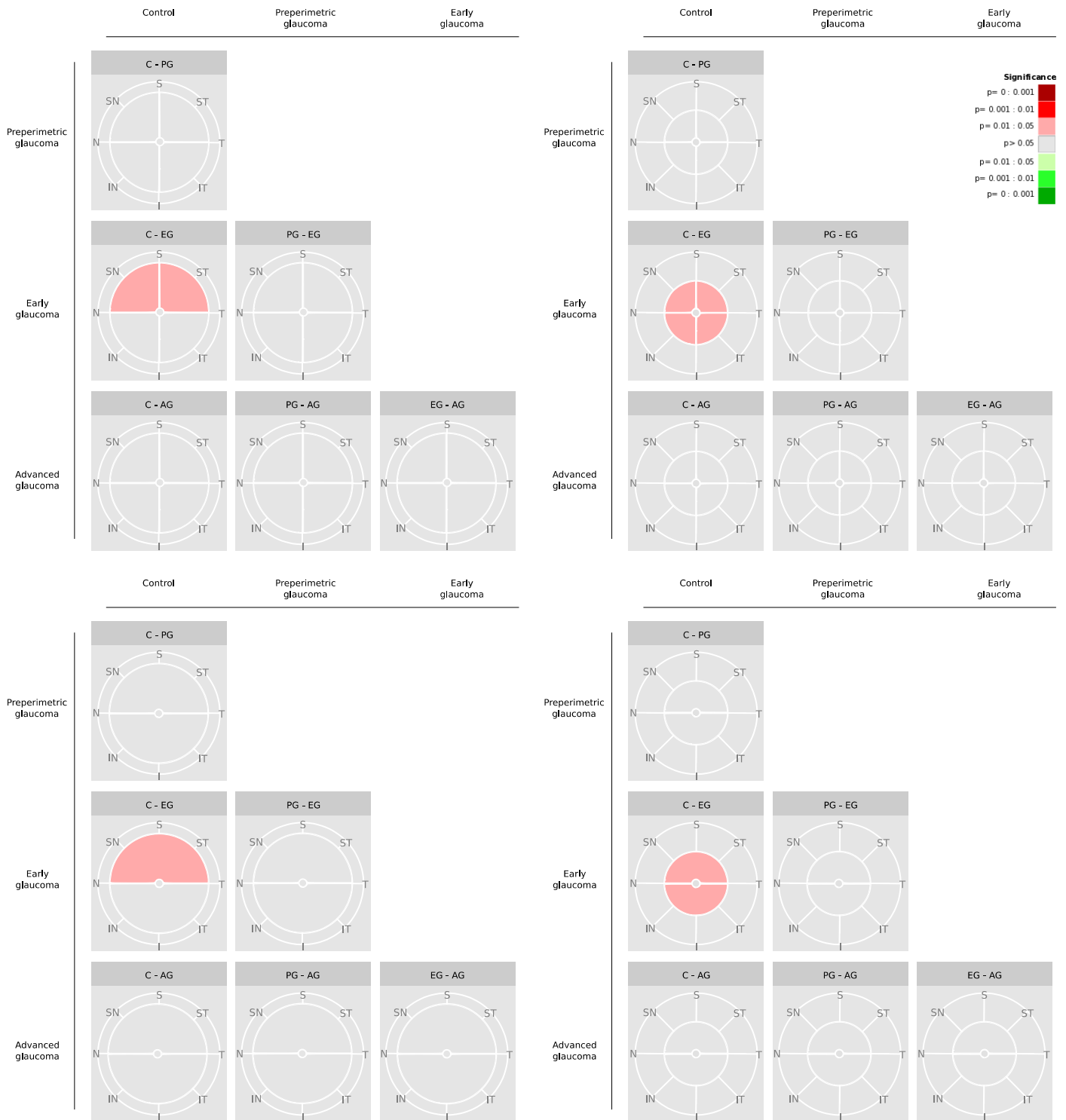


Figure 0.3: Differences in macula nerve fibre layer (mNFL) thickness between control (C) and preperimetric glaucoma (PG), early glaucoma (EG) and advanced glaucoma (AG). Red indicates mNFL thinning with increasing glaucoma stage, green indicates mNFL thickening with increasing glaucoma stage.

Differences in thickness of the ganglion cell layer between control and glaucoma

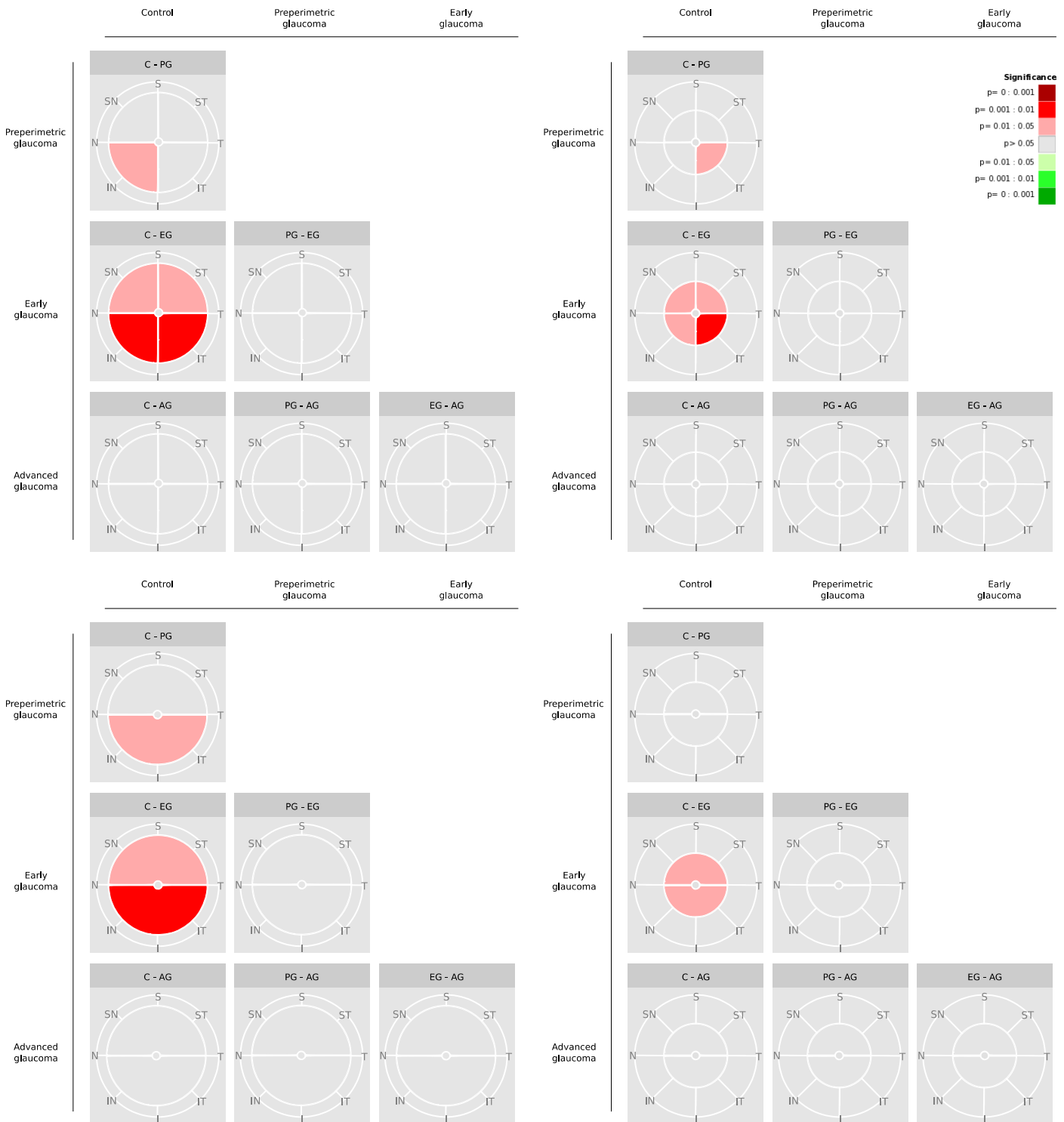


Figure 0.4: Differences in ganglion cell layer (GCL) thickness between control (C) and preperimetric glaucoma (PG), early glaucoma (EG) and advanced glaucoma (AG). Red indicates GCL thinning with increasing glaucoma stage, green indicates GCL thickening with increasing glaucoma stage.

Differences in volume of the ganglion cell layer between control and glaucoma

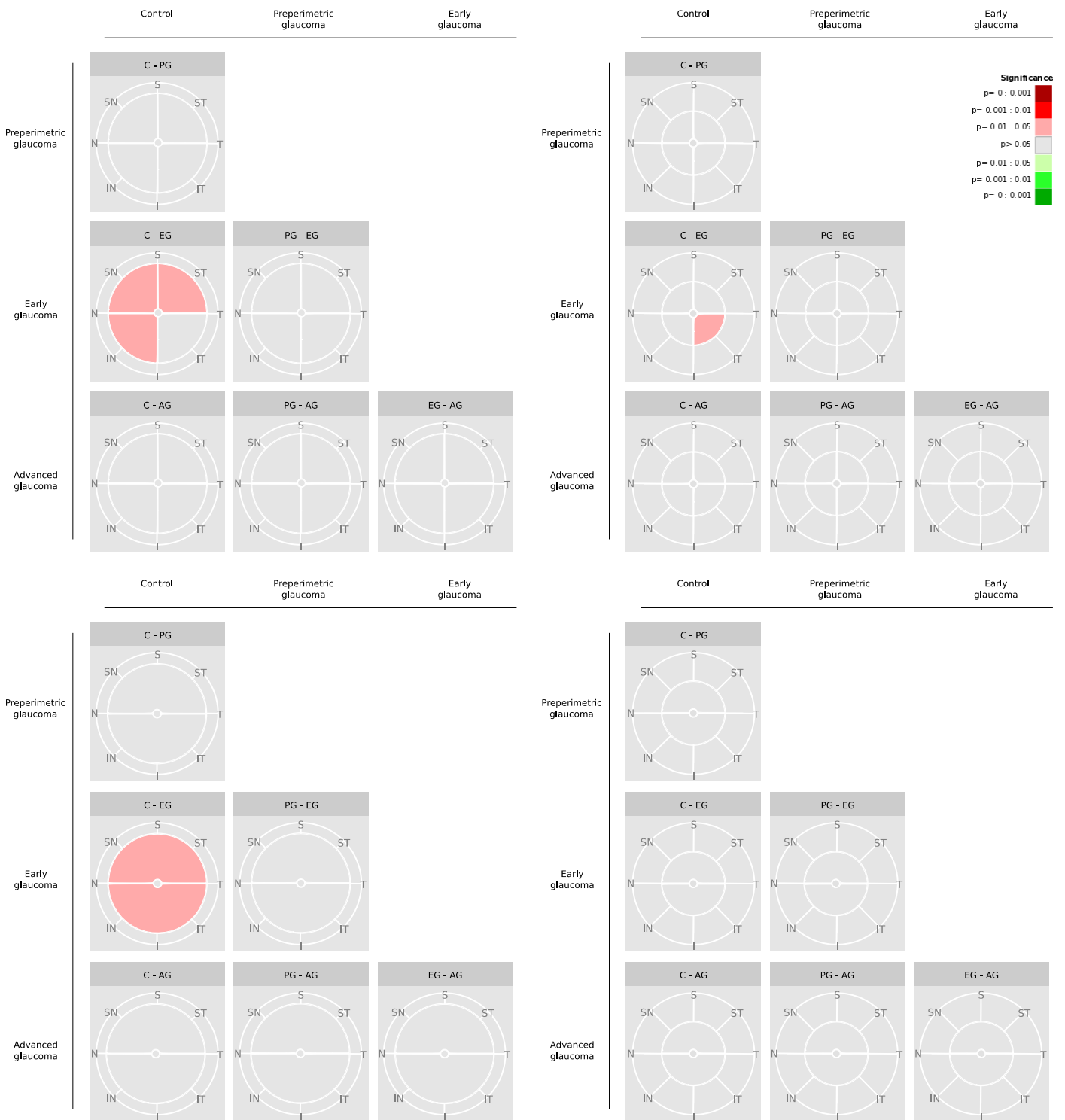


Figure 0.5: Differences in ganglion cell layer (GCL) volume between control (C) and preperimetric glaucoma (PG), early glaucoma (EG) and advanced glaucoma (AG). Red indicates GCL volume decrease with increasing glaucomatous stage, green indicates GCL volume increase with increasing glaucoma stage.

Differences in thickness of the inner plexiform layer between control and glaucoma

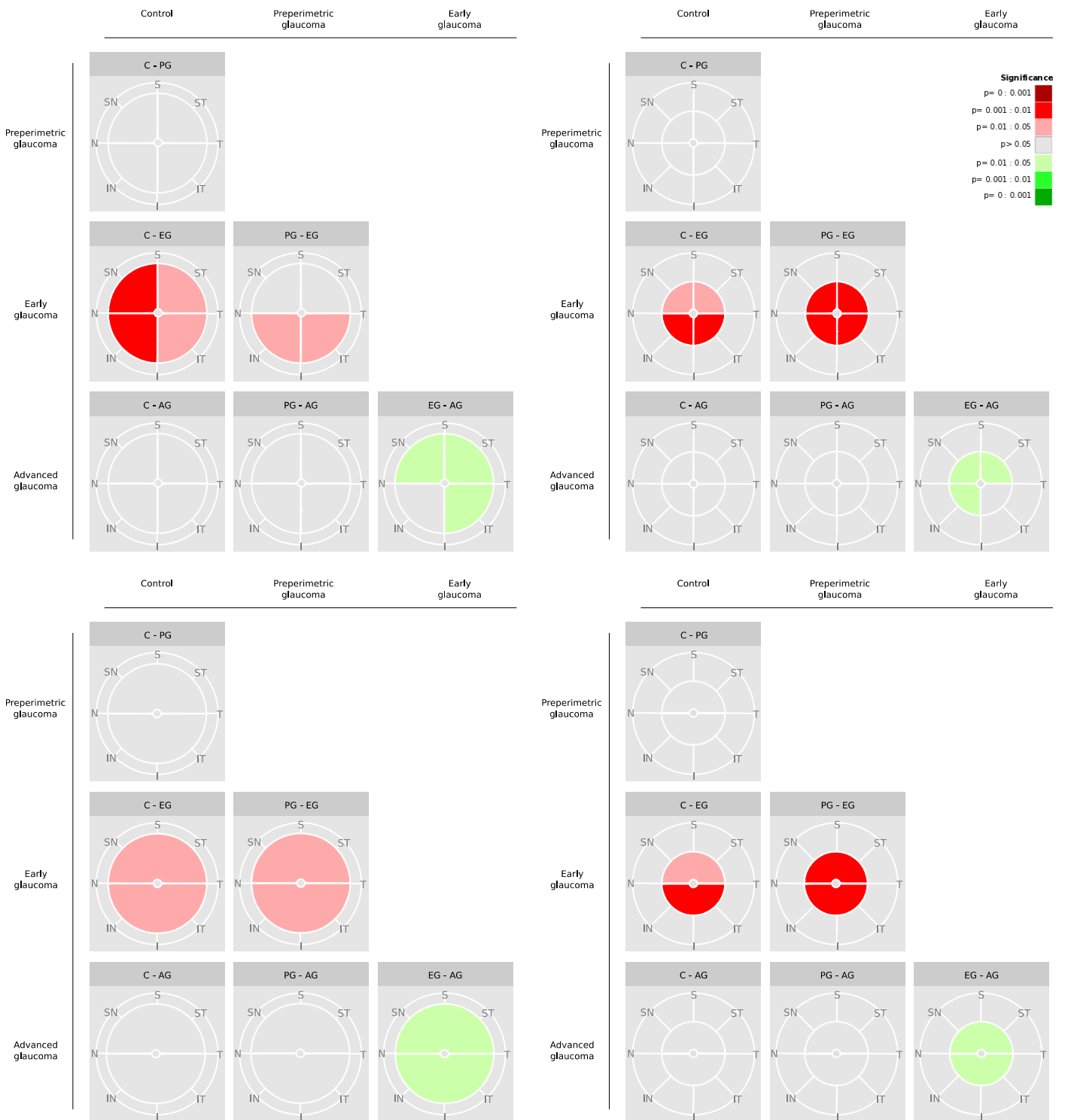


Figure 0.6: Differences in inner plexiform layer (IPL) thickness between control (C) and preperimetric glaucoma (PG), early glaucoma (EG) and advanced glaucoma (AG). Red indicates IPL thinning with increasing glaucoma stage, green indicates IPL thickening with increasing glaucoma stage.

Differences in volume of the inner plexiform layer between control and glaucoma

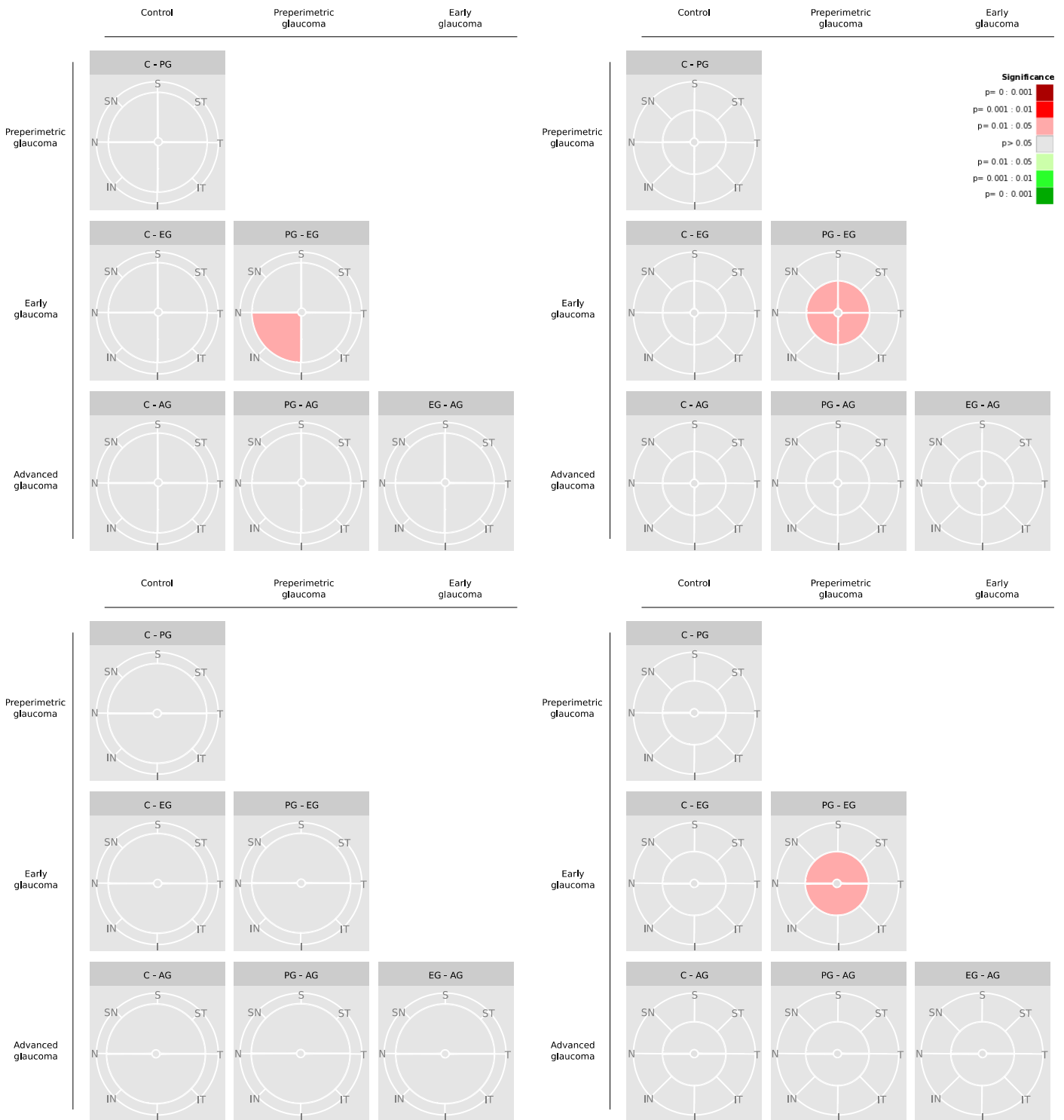


Figure 0.7: Differences in inner plexiform layer (IPL) volume between control (C) and preperimetric glaucoma (PG), early glaucoma (EG) and advanced glaucoma (AG). Red indicates IPL volume decrease with increasing glaucoma stage, green indicates IPL volume increase with increasing glaucoma stage.

Differences in inner plexiform layer : ganglion cell layer ratio between control and glaucoma

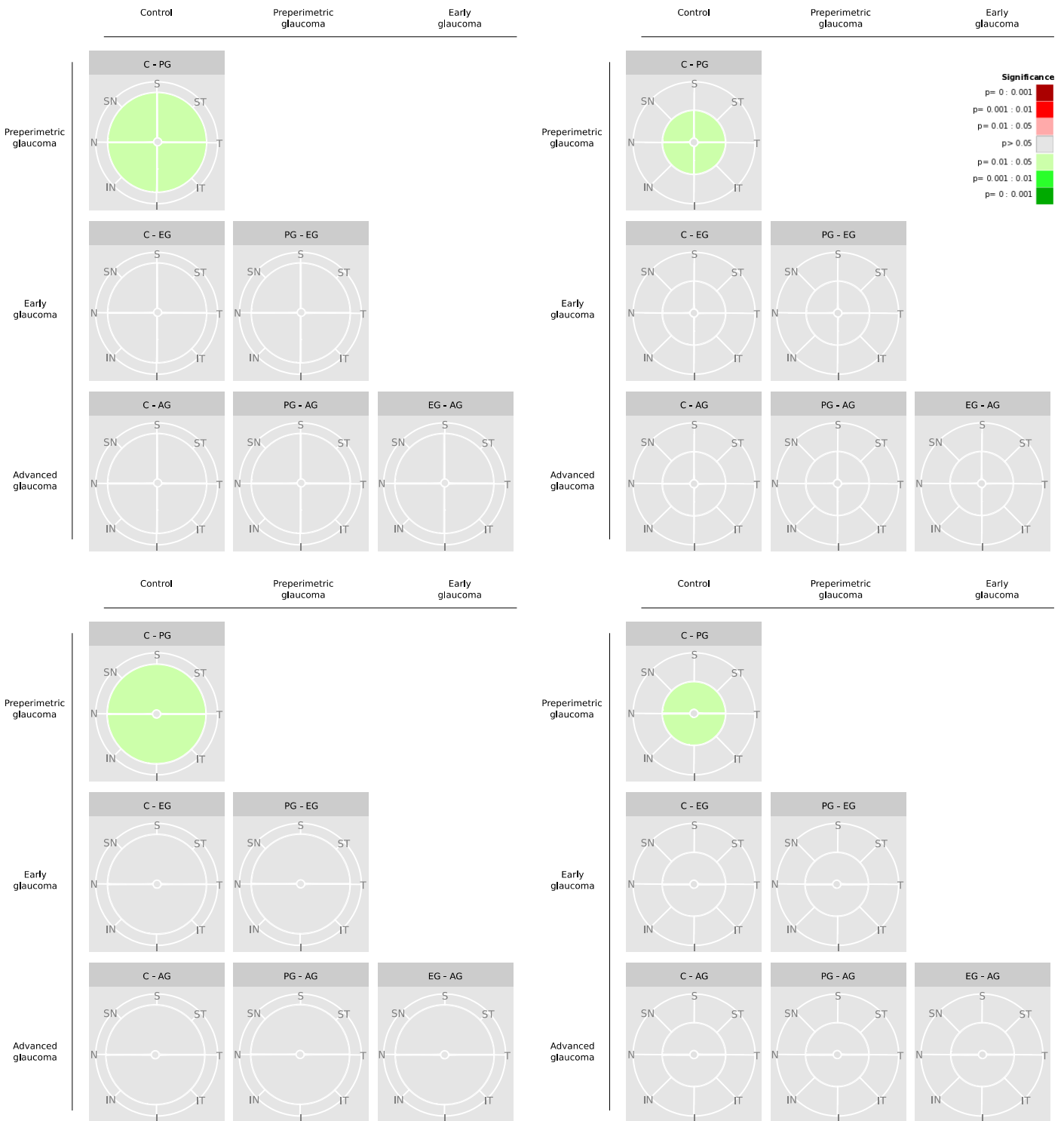


Figure 0.8: Differences in inner plexiform layer : ganglion cell layer (IPL:GCL) ratio between control (C) and preperimetric glaucoma (PG), early glaucoma (EG) and advanced glaucoma (AG). Red indicates a decrease in IPL:GCL ratio with increasing glaucoma stage, green indicates an increase in IPL:GCL ratio with increasing glaucoma stage.

Differences in volume of the macula nerve fibre layer between control and glaucoma

There were no statistically significant differences in regional mNFL volume between control or any stage of glaucoma, for any of the grouped regions examined.

Differences in inner plexiform layer : macula nerve fibre layer ratio between control and glaucoma

There were no statistically significant differences in regional IPL:mNFL ratio between control and any stage of glaucoma, for any of the grouped regions examined.

Appendix IV: Published abstracts and conferences

Oral presentations

- **Flynn BE**, Mortlock KE, Abid M, Rakebrandt F, Fergusson JR, White N, Drexler W, Morgan JE, North RV, Albon J. Quantification of change in the ganglion cell layer and inner plexiform layer in the glaucomatous macula. Presented at United Kingdom and Eire Glaucoma Society, Bristol, UK, 27 Nov 2014.
- **Flynn BE**, Mortlock KE, Fergusson JR, White N, Morgan JE, North RV, Albon J. *In vivo* analysis of the pores in the human lamina cribrosa using long wavelength optical coherence tomography. Presented at British Congress of Optometry and Vision Sciences, Bradford, UK, 3-4 September 2012. **
- **Flynn BE**, North RV, Albon J. Imaging the healthy and glaucomatous human optic nerve head with ultrahigh resolution optical coherence tomography. Presented at Speaking of Science Conference, Cardiff, UK, 3 April 2012

Poster presentations

- **Flynn BE**, Mortlock KE, Fergusson JR, White N, Morgan JE, North RV, Albon J. Analysis of the glaucomatous optic nerve head using 1050nm OCT. Presented at Association for Research in Vision and Ophthalmology, Orlando, FL, USA, 4-8 May 2014 **
- **Flynn BE**, Mortlock KE, Abid M, Rakebrandt F, Fergusson JR, White N, Morgan JE, North RV, Albon J. Analysis of the inner retina in glaucomatous and healthy subjects using 1050nm OCT datasets. Presented at Optometry Tomorrow, York, UK, 16-17 March 2014

- **Flynn BE**, Mortlock KE, Abid M, Rakebrandt F, Fergusson JR, White N, Morgan JE, North RV, Albon J. Analysis of the inner retinal layers in glaucoma using 1050nm OCT. at the Bristol Vision Institute (BVI) Young Researchers' Colloquium, Cardiff, UK, 28 June 2013
- North RV, Mortlock KE, **Flynn BE**, Fergusson JR, White N, Drexler W, Morgan JE, Albon J. Lamina cribrosa pore analysis in glaucomatous human optic nerve heads *in vivo*. Presented at Association for Research in Vision and Ophthalmology, Seattle, WA, USA, 5-9 May 2013 **
- **Flynn BE**, Mortlock KE, Fergusson JR, White N, Morgan JE, North RV, Albon J. OCT analysis of the human lamina cribrosa *in vivo*. Presented at Cardiff Institute of Tissue Engineering and Repair Conference, Cardiff, UK, 20-21 September 2012
- Mortlock KE, **Flynn BE**, Tumlinson A, Fergusson JR, Povazay, B, Drexler W, Morgan JE, North RV, Albon J. Three dimensional (3D) segmentation of normal and glaucomatous optic nerve heads in 1050nm optical coherence tomography (OCT) datasets. Presented at Association for Research in Vision and Ophthalmology, Fort Lauderdale, FL, USA, 6-9 May 2012 **

** = Published abstract